USING COMPOUND-SPECIFIC ISOTOPE ANALYSIS (CSIA) AND FATE AND TRANSPORT MODELING TO QUANTIFY THE MASS CONTRIBUTION OF COMINGLED CHLORINATED ETHENE PLUMES

by

Jason Everett Shiflet

A dissertation submitted to the faculty of
The University of North Carolina at Charlotte
in partial fulfillment of the requirements
for the degree of Doctor of Philosophy in
Infrastructure and Environmental Systems

Charlotte

2016

Approved by:

_____
Dr. Craig Allan

_____
Dr. Anne Jefferson

_____
Dr. Paul Philp

_____
Dr. David Vinson

_____
Dr. James Amburgey

_____
Dr. Milind Khire

ABSTRACT

JASON EVERETT SHIFLET. Using Compound-Specific Isotope Analysis (CSIA) and fate and transport modeling to quantify the mass contribution of comingled chlorinated ethene plumes. (Under the direction of DR. CRAIG ALLAN)

Chlorinated solvents are present in soil and groundwater at thousands of sites across the United States. Resolving the remedial and fiscal responsibility of multiple potentially responsible parties at sites containing comingled chlorinated ethene plumes can be both scientifically and legally challenging. Presented herein is a case study describing the development of a framework by which compound-specific isotope analysis (CSIA) is combined with traditional investigative techniques within a three-dimensional (3D) reactive transport model.

The study site, located in central Oklahoma, is composed of a 60m thick sequence of both fine-grained and coarse-grained matrices with three saturated zones separated by semi-confining and confining layers making up the six major hydrostratigraphic units, overlying the primary drinking water aquifer for this region. Work is focused on a comingled multi-species chlorinated ethene contaminant plume discovered throughout the hydrostratigraphic units in the late 1980's, emanating from three primary source locations.

The investigation included traditional techniques, such as evaluation and synthesis of historical data, various field measurements (e.g., hydraulic gradient using pressure transducers, dye traces, and in situ permeability), and aqueous sampling for the measurement of chlorinated solvent concentrations. Compound-specific isotope analysis (CSIA) data collection and analysis was also performed to provide insight into

biotransformation characteristics of contaminant plume(s) by revealing how the chlorinated ethenes have changed (i.e., fractionated) during subsurface migration.

The vast historical site data developed following traditional investigative techniques and CSIA data were integrated into a modern 3D reactive transport model. Iterative simulations of potential source concentrations and isotopic ratios at suspected source locations were performed using a calibrated “base case” model representing a best fit for observed concentration and isotopic data, which allowed for the approximation of quantitative contributions from multiple source areas, specifically that ~75% of the contaminant mass observed at a central point within the site domain originated from a source area to the east and ~25% of the contaminant mass originated from a source areas to northeast. The synergistic relationship of traditional investigation techniques and innovative CSIA provide valuable data necessary for understanding contaminant sites. Traditional techniques allow researchers to understand contaminant concentration history, source locations, and subsurface hydraulics. CSIA provides insight into biotransformation characteristics of contaminant plume(s) by revealing how the chlorinated ethenes have changed (i.e., fractionated) during subsurface migration. These two techniques are not often combined and neither, used independently, allows for the quantification of contaminant sources within comingled contaminant plumes. When these two techniques are integrated into a three-dimensional reactive transport model, it is believed contaminant characteristics of present-day and future conditions may be more clearly understood. Results of this study indicate that traditional characterization techniques combined with CSIA can be used to establish a framework for modeling comingled plumes, thus providing a fundamental approach for source differentiation.

This represents a novel approach to determining contaminant remediation responsibility at sites with complex comingled contaminant plumes.

DEDICATION

In life, we seek to realize the gifts of faith, hope, and love. And when we find the greatest of these, we should cling to it with every ounce of our being. This work is dedicated to those with whom I share the gift of love. Especially for my wife Becca, I am eternally grateful; this work would not have been possible without her steadfast support, unwavering grace, and deep dedication. She has carried my heart, in her heart, encouraging me along the way to achieve my dreams. Together, we've enjoyed raising three beautiful children, Will, Evan, and Sarah Layton. I hope they will proudly use this work to inspire their own education as they seek their personal endeavors.

To my parents, Clifford and Teresa, and my sister Jennifer, thank you for the gifts of opportunity and encouragement. You have always inspired me to believe in myself and to trust in my abilities. I am proud to honor you and all of your sacrifices with this work.

To my extended family and friends, thank you for supporting my wife and children during this adventure. The extensive fieldwork and hours sitting at my laptop took me away from my household and your support helped alleviate the stress. I also appreciate all of the kind words of encouragement, along the way.

ACKNOWLEDGEMENTS

This research was funded through small business innovative research (SBIR) grants from the United State Air Force (USAF) awarded to Zapata Incorporated (ZAPATA) of Charlotte, North Carolina in July 2006 and October 2007 (Contract numbers FA8103-06-C-0198 and FA8103-08-C-0005). The author was the Principal Investigator for ZAPATA and led the investigations from July 2006 through January 2010.

Numerous USAF personnel provided oversight and guidance during investigation planning phases and field activities, including Sara Wakelam-Sayler, Jason Flaming and Scott Bowen at Tinker Air Force Base. Dr. Bill Langley, Dr. Eric Klingel, Benjamin Shivar, P.G., Clay Perry, Nathan Reel, and Dr. Brian Zapata, of ZAPATA, supported various aspects of planning, data collection, and reporting to the USAF. Manual and Karen Zapata and Mary Richards, of ZAPATA, graciously provided financial support and encouragement for the entirety of my doctoral academic work.

This research spanned over many years, and brought together a diverse group of committee members, including Dr. Craig Allan, Dr. David Vinson, Dr. James Amburgey, and Dr. Milind Khire from the University of North Carolina Charlotte, Dr. Anne Jefferson from Kent State University, and Dr. R. Paul Philp from the University of Oklahoma. Throughout the research and during the manuscript development, the committee provided academic inspiration, clear guidance and thoughtful suggestions to help improve my understanding of the subject matter and the way in which I communicate that understanding. These advisors were integral in my ability to complete this work and their contribution is sincerely appreciated.

TABLE OF CONTENTS

LIST OF TABLES

LIST OF FIGURES

LIST OF ABBREVIATIONS

3D	three-dimensional
AFB	Air Force Base
AQ	aquiclude
ASL	above sea level
°C	degrees celsius
C	carbon
Cl	chlorine
cis-DCE	*cis*-1,2 dichloroethene
COC	contaminant of concern
CSIA	Compound-Specific Isotope Analysis
DNAPL	dense non-aqueous phase liquid
DO	dissolved oxygen
Eth	ethene
EPA	Environmental Protection Agency
GC-MS	gas chromatograph-mass spectroscopy
GCqMS	gas chromatograph-quadrupole mass spectroscopy
GIS	Geographic Information System
GML	Gauss-Marquardt-Levenburg
GWMU	Groundwater Waste Management Unit
H	hydrogen
HSU	hydrostratigraphic unit
ID	identification

IRMS	Isotope Ratio Mass Spectrometry
ITRC	Interstate Regulatory & Technology Council
IWTP	Industrial Waste Treatment Plant
K	hydraulic conductivity
LCL	lower confining layer
LLSZ	lower-lower saturated zone
LSZ	lower saturated zone
m	meter(s)
MDL	method detection limit
mg/L	milligrams per liter
mL	milliliter
MO	Missouri
MSL	meters above sea level
MW	monitoring well
mV	millivolts
na	not analyzed
NAD	North American Datum
NAPL	non-aqueous phase liquid
NCDC	National Climatic Data Center
nd	non-detect
NPL	National Priority List
NTU	nephelometric turbidity units
OK	Oklahoma

ORP	oxidation-reduction potential
OU	Oklahoma University
PC	personal computer
PCE	tetrachloroethylene
PEST	parameter estimation
P.G.	Professional Geologist
Pgr	Garber Formation (Permian)
Phy	Hennessey Formation (Permian)
PZ	production zone
Qal	Alluvium (Holocene)
RCRA	Resource Conservation and Recovery Act
RFI	RCRA Facility Investigation
RL	reporting limit
RMS	root mean square
ROD	Record of Decision
SAIC	Science Applications International Corporation
SBIR	Small Business Innovative Research
TAFB	Tinker Air Force Base
TCE	trichloroethylene
trans-DCE	*trans*-1,2-dichloroethylene
UCL	upper confining layer
µg/L	micrograms per liter
US	United States

USACE	United States Army Corps of Engineers
USAF	United States Air Force
USGS	United States Geological Survey
USZ	upper saturated zone
UTM	Universal Transverse Mercator
VC	vinyl chloride
VOCs	volatile organic compounds
V-PDB	Vienna Pee Dee Belemnite
ZAPATA	Zapata Incorporated

CHAPTER 1: BACKGROUND AND HISTORY

1.1. Introduction

Chlorinated solvents are common soil and groundwater contaminants, because of their pervasive use in industrial, military and commercial (e.g., dry-cleaning) facilities since the 1920's. In 2004, the United States (US) Environmental Protection Agency (EPA) identified more than 75,000 soil and groundwater-contaminated sites within the US and estimated that number of sites would grow to over 300,000 by 2015. Cleanup costs for those sites are expected to range from $170 to $250 billion through the year 2030 [1]. Widespread use, improper disposal methods of waste solvent, and relatively high solubility and density of chlorinated ethenes allow for persistence in groundwater and greatly enhances the probability that dissolved chlorinated ethene plumes will exist in groundwater away from their original source locations.

Current standard practices for evaluating subsurface contamination typically involves soil and groundwater collection and analysis for total volatile organic compounds (VOCs) concentrations. In some cases, the contaminant source is unclear, particularly if the contaminant has been in the environment for a considerable length of time or site records are missing. Contaminated sites can be further complicated by the possibility of multiple sources of contamination, multiple contaminant releases, or by biodegradation of contaminants (see FIGURE 1-1).

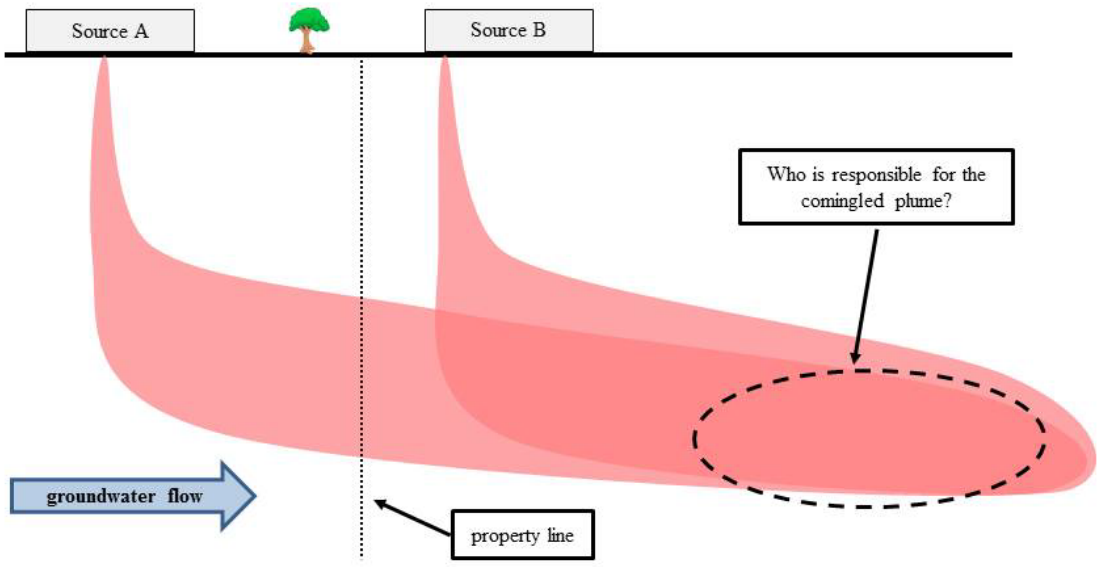

FIGURE 1-1: Conceptual site model
Conceptual schematic illustrating two sources, Source A and Source B, contributing identical contaminants (e.g., PCE) to the subsurface, where those individual plumes merge down-gradient into a comingled plume.

Using total concentration data, it is often difficult to properly assign remediation responsibility for subsurface impacts by multiple sources of the same contaminant. From a fiduciary perspective, being able to ascertain whether contamination at a site was caused by and is, therefore, the responsibility of a site owner is important. In these cases, site owners have a burden to determine whether contamination is their sole responsibility or if another entity has contributed to the contamination. Multiple-source mixed contamination is complicated and cleanup responsibility is often difficult to prove. In this study, focus is placed specifically on a subgroup of chlorinated compounds among VOCs; namely the chlorinated ethene compounds, including tetrachloroethylene (PCE), trichloroethylene (TCE), *cis-/trans*-1,2-dichloroethylene (*cis*-DCE/*trans*-DCE) and vinyl chloride (VC) along with ethene (Eth).

Some researchers and consultants have integrated compound-specific isotope analyses (CSIA) of chlorinated ethenes into their investigative practices. CSIA has proved to be an important tool for providing reliable indicators for chlorinated ethenes that have been transformed, particularly by reductive dechlorination processes. Researchers have used CSIA data in one and two dimensional reactive transport models to quantitatively evaluate source-plume relationships [2, 3]. However, CSIA data have not yet been incorporated into a three-dimensional (3D) reactive fate and transport model to quantify mass contribution of multiple sources to a single plume. Integration of CSIA into a 3D reactive fate and transport model will vastly improve the comprehensive understanding of both movement and transformation of chlorinated ethenes in the subsurface.

Herein, a framework for integration of CSIA along with standard chemical and hydraulic information into a 3D reactive fate and transport model is presented. Chlorinated ethene concentrations and compound-specific isotope data, along with other traditional field measurements are coupled into a reactive finite element fate and transport model. Based primarily on computing limitations, a simulation of 20 years is evaluated (see FIGURE 1-2). The simulation period corresponds approximately to 1988 – 2008; data used in this study were collected in 2008 and used as a comparison for modeling results. It is assumed that contaminant mass began seeping into the subsurface from multiple source locations within several years of the activation of the installation in March 1942 and that those contributions were generally similar in quantity and rate for several decades. Light and heavy carbon isotopes of chlorinated ethenes (PCE to VC) and ethene, based on estimated mass contributions from observed historical concentration

data, are modeled independently; results are then combined to approximate contaminant concentrations for comparison. Adjustments in source concentrations over numerous simulations and the resulting modeled contaminant concentrations provide insight on the contribution of multiple sources to the comingled plume.

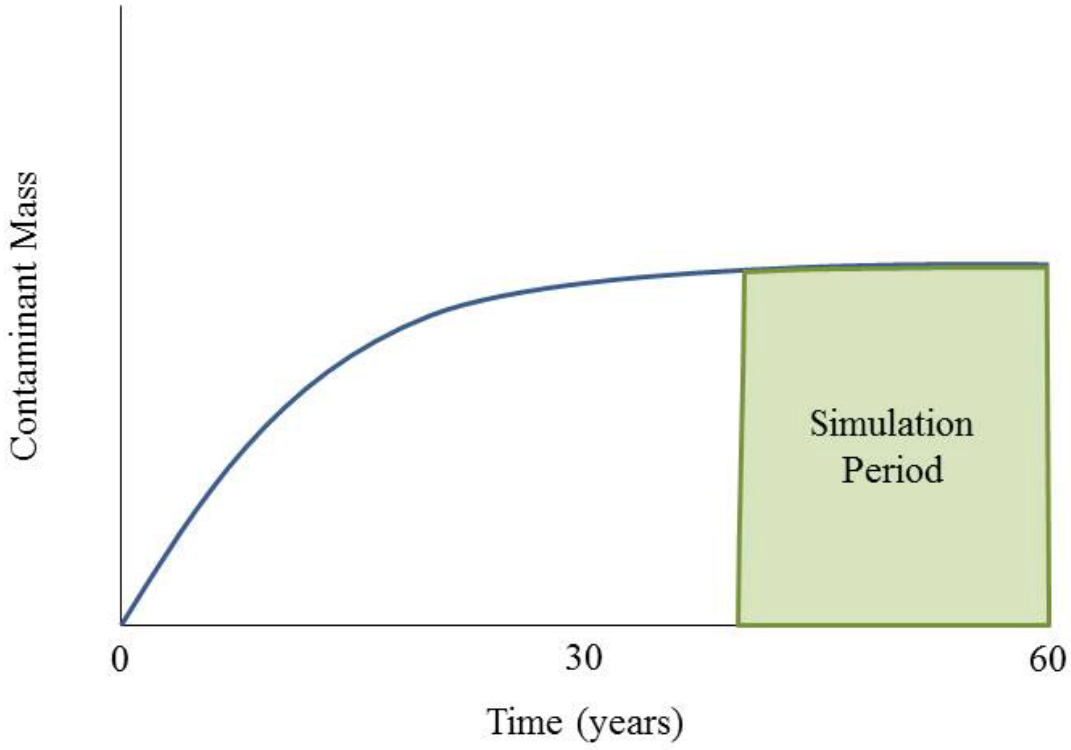

FIGURE 1-2: Conceptual reactive fate and transport simulation period
Illustrates the 20 year simulation used in this study, beginning in 1988 and ending in 2008 (when data collection occurred). This assumes the estimated initial source concentration contribution into the subsurface occurred approximately 40 years prior to simulation, in the late 1940s, six years after the installation was officially activated.

Numerous researchers have evaluated isotopic characteristics of chlorinated compounds in subsurface in microcosms [4-7] and at the field-scale [7-14]. Previous researchers have focused efforts on using isotopes to identify mass reduction by

transformation [15-20], distinguishing between various transformations [21, 22], estimating rates of transformation[23-28] and attributing plume mass to a source [8, 14, 29, 30]. Separate source area locations, complex subsurface conditions, variable transformation and comingled contaminant plumes of similar parent contaminants at this study site present a unique set of conditions favorable for investigation. The objective is to provide a framework for quantifying mass contribution of comingled chlorinated ethene plumes using a combination of chemical, physical and CSIA techniques to parameterize a three dimensional reactive transport model. This represents a novel approach to determining contaminant remediation responsibility by utilizing a combination of CSIA and three-dimensional modeling to extend beyond traditional total concentration evaluation, isotopic characterization or fate and transport modeling alone.

Within the last decade, researchers have focused efforts on integrating dual isotope analyses of specific compounds, like ^{37}Cl included in chlorinated ethenes, while overcoming problems associated with the significant abundance of polychlorinated molecules containing the heavy chlorine isotope. Hunkeler et al. (2009) developed and modeled a framework that combined the carbon-chlorine dual isotope analysis to describe the expected isotope fractionation patterns through primary effects at dechlorinating C-Cl bonds during transformation of chlorinated compounds. They demonstrated several important factors in that research but, the two pertinent factors relevant to this work are that 1) chlorine isotope trends can be simulated by reproducing the average independent behavior of both light and heavy isotopes and 2) chlorine isotope values of a reaction product cannot be more negative than the initial value of its precursor, provided that secondary isotope effects are absent [31]. They note for sites where TCE is encountered

with significantly more negative carbon isotope values than PCE, observers may have concluded that TCE is a degradation product of PCE. However, when carbon-chlorine dual isotope data are coupled, they demonstrate that conclusion can be ruled out and that TCE must be a co-contaminant or a product from another source.

Recent development of online δ^{37}Cl-CSIA methods using gas chromatography-quadrupole mass spectrometry (GCqMS) now allows for rapid and accurate ^{37}Cl measurements at concentrations relevant to field samples [32, 33]. Wiegert et al. (2012) employed the 2D-CSIA method at a field site to measure extent of biodegradation, quantify mass removal along a transect, and determine detailed assessment of source and fate [34]. Jin et al. (2013) developed a quantitative modeling approach to simultaneously consider evolution of combined carbon-chlorine isotopologues, in particular where mass-transfer limitations (e.g., physical and biochemical transformation processes) affect the observed isotopic values [35]. They suggest the approach could be extended to reactive transport models of contaminant fate in groundwater systems.

In more recent work, Kuder et al. (2013) combined carbon, chlorine, and hydrogen isotopes into a "3D-CSIA" approach to present (among other things) evidence of secondary Cl isotope effects, which should be considered when CSIA is used in numerical modeling of field sites [36]. In their work, they performed a detailed assessment of degradation mechanisms and associated isotope fractionation mechanisms during reductive dechlorination of TCE to ethene on a mixed culture microcosm containing *Dehalococcoides*. They further note that discriminating between reductive dechlorination by the activity of bacteria genus *Dehalococcoides* from alternative

transformation mechanisms (e.g., aerobic degradation) will provide valuable insight in developing and validation of conceptual site models for specific sites.

Lutz and Van Breukelen (2014) developed a stable isotope sources and sinks (SISS) model using a linear stable isotope mixing model and the Rayleigh equation, to analyze how and to what extent source apportionment and quantification of in situ degradation are feasible in the presence of both mixing of sources and degradation [37]. Modeling two sources and one reaction pathway with SISS, they demonstrate that using dual-element CSIA provides unequivocal source apportionment and enables quantification of extent of degradation, but note that validation using reactive transport modeling and to actual field data would be a necessary next step.

1.2. Chlorinated Ethene Chemistry

1.2.1.1. Chlorinated Ethenes

Chlorinated ethenes have commonly been used as industrial solvents. In general, these chemicals are dense non-aqueous phase liquids (DNAPLs), meaning that they are "heavier" than water and if exposed to groundwater, will generally sink within the aquifer. Generally, the liquids are clear and non-flammable. Tetrachloroethene (PCE), trichloroethene (TCE), *cis*- and *trans*-1,2 dichloroethene (*cis/trans*-DCE), and vinyl chloride (VC) compose the group of chlorinated ethenes included in this research along with ethene (C_2H_4); these are collectively referred to as contaminants of concern (COCs) herein. Each of the chemicals contain covalent carbon bonds central to the molecule and differ in the number of chlorine and hydrogen atoms completing the molecule; PCE (C_2Cl_4), TCE (C_2HCl_3), DCE ($C_2H_2Cl_2$) and VC (C_2H_3Cl). All are known or suspected carcinogens. Pankow and Cherry (1996) report literature solubility (the maximum

amount of the chemical to dissolve in water at equilibrium) for PCE, TCE, *cis*-DCE, *trans*-DCE, and VC at 25ºC as 200 mg/L, 1,100 mg/L, 6,300 mg/L, 3,500 mg/L, and 8,800 mg/L, respectively [38]. The organic carbon-water partition coefficients, which defines the distribution of chlorinated ethene mass between the sorbed and aqueous phases, also decreases as the level of chlorination decreases [39]. Thus, the less-chlorinated ethenes are more soluble and less susceptible to adsorption than the previous compounds in the sequence, meaning those compounds are more likely to be present in the dissolved phase and are more mobile.

1.2.1.2. Degradation Pathway

Once chlorinated ethenes are exposed to the environment, they generally follow one of two primary degradation pathways. Under aerobic conditions, they do not readily degrade and can persist with their only movement governed by physical hydrologic processes [8]. Under anaerobic conditions, they are sequentially reduced primarily through microbial reductive dechlorination (see FIGURE 1-3). Generally, microorganisms catalyze these reactions, where hydrogen is the electron donor (which is oxidized) and the chlorinated ethene is the electron acceptor. These reactions (or degradation pathways) progressively strip away chloride ion away from reactants, leading to a series of less chlorinated products.

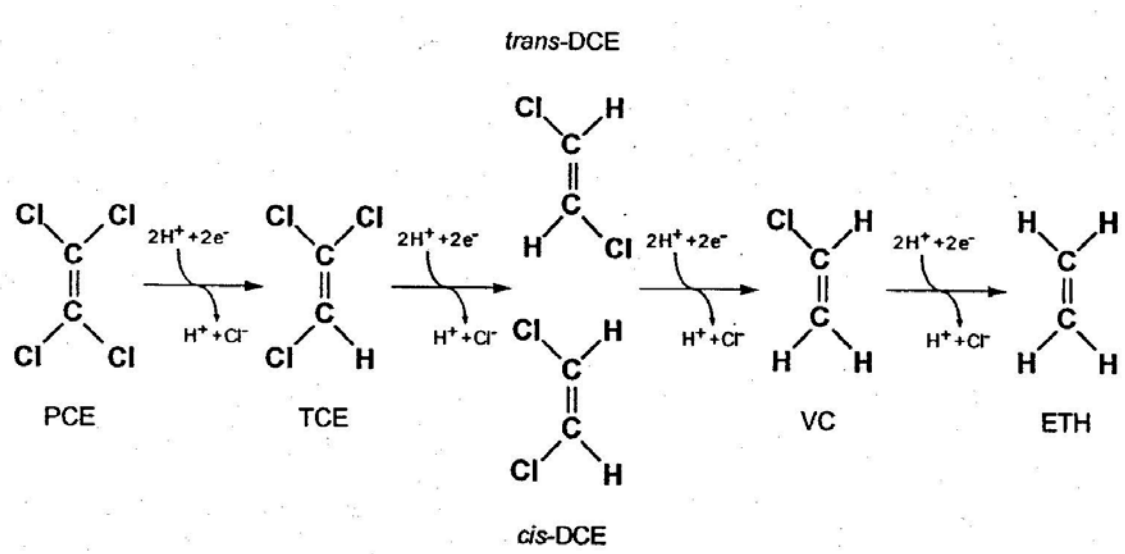

FIGURE 1-3: Reductive dechlorination sequence
This figure illustrates sequential reduction of PCE to ethene by anaerobic reductive dechlorination [39].

For TCE, this involves the sequential reduction of TCE to DCE (primarily *cis*-1,2 Dichloroethene, but *trans*-1,2 Dichloroethene and 1,1-Dichloroethene have also been observed), followed by conversion of DCE to VC and finally VC to ethene [24]. Essentially, each of the products differs from the reactant in that it has one less chlorine atom, which has been replaced by one hydrogen atom.

1.2.1.3. Elemental Isotopes

Each elemental component (C, Cl and H) of the chlorinated ethene has varying isotopic constituents. Isotopes are various forms of an element that contain the same number of protons in the nucleus but a varying number of neutrons, and therefore differing atomic mass. For chlorinated ethenes, ^{13}C, ^{37}Cl and ^{2}H isotopes are the predominant isotopic variants of ^{12}C, ^{35}Cl and ^{1}H, respectively. Elemental isotopes can be accurately measured using Gas Chromatograph/Isotope Ratio Mass Spectrometry (GC/IRMS), a commercially available analysis tool. The GC/IRMS can analyze the

isotopic ratios of individual compounds, even when they are present in complex mixtures and in low abundances. Generally, the element isotopic variation of a compound is expressed as a ratio (using the δ notation) of the less abundant isotope to the more abundant isotope. The isotopic concentration variations are small and thus are expressed as parts per thousand or per mil (‰)[40]. For example, in chlorinated ethenes the carbon isotopic ratio could be expressed as follows:

$$\delta^{13}C(‰) = \left(\left(\frac{\left(\frac{^{13}C}{^{12}C} \right)_{sample}}{\left(\frac{^{13}C}{^{12}C} \right)_{std}} \right) - 1 \right) \times 1000$$

This ratio is reported relative to a standard. For carbon, the standard is Vienna Pee Dee Belemnite (V-PDB), which has a ^{13}C:^{12}C ratio of 0.0112372 and has a $\delta^{13}C$ defined as 0 ‰. Therefore, samples with a negative $\delta^{13}C$ value are considered depleted in the "heavier" ^{13}C isotope (e.g., ^{13}C:^{12}C ratio of 0.0109 has a δ13C of -30‰). The $\delta^{13}C$ of manufactured (i.e., "fresh") TCE has been measured by numerous researchers and generally has a mean $\delta^{13}C$ value around -30.6 ‰; FIGURE 1-4 illustrates the range and mean of several manufactured chlorinate ethenes [41]. Increasingly negative $\delta^{13}C$ values (e.g., -40 ‰) are considered to be lighter with respect to initial $\delta^{13}C$ values, while less negative $\delta^{13}C$ values (e.g., -20 ‰) are considered to be heavier with respect to initial $\delta^{13}C$ values.

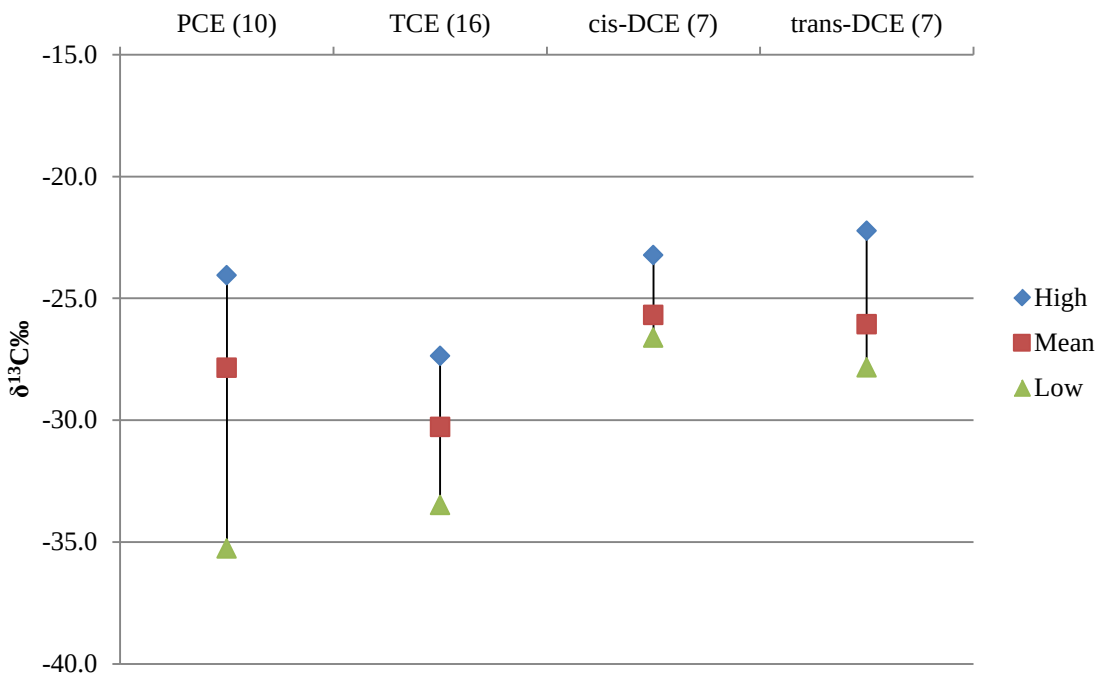

FIGURE 1-4: Range and mean of manufactured chlorinated ethenes
Minimum, maximum, and mean carbon isotope ratio of chlorinated hydrocarbons from different manufacturers and production batches measured to date. The number in parentheses following each compound name indicates the number of samples analyzed for that compound [41].

1.2.1.4. Kinetic Isotope Fractionation

Theoretically, isotope fractionation is caused by isotope exchange reactions and by mass-dependent differences in the rates of certain chemical reactions and physical processes (e.g., diffusion, sorption, volatilization, and microbial respiration). Isotope exchange reactions progress from some initial state or isotopic ratio toward equilibrium. Fractionation will continue toward equilibrium as the chemical reactions are balanced [42]. The kinetic isotope fractionation factor (α) between two compounds (the reactant, r and the product, p) is calculated using the following equations, where R_r is the isotope ratio of the available reactant, R_p is the isotope ratio of the product formed at this R_r and

$\delta^{13}C$ represents the stable isotope ratio ($^{13}C/^{12}C$) of the compounds r and p, respectively [41, 43]:

$$\alpha = \left(\frac{R_r}{R_p} \right) = \left(\frac{1000 + \delta^{13}C_r}{1000 + \delta^{13}C_p} \right)$$

For chlorinated ethenes at the molecular level, carbon bonds are held together with covalent bonds, while carbon-chlorine bonds and carbon-hydrogen bonds are ionic. ^{13}C forms a stronger bond with chlorine than does ^{12}C; the heavier carbon isotope increases the mass of the molecule thereby decreasing its vibrational energy [42]. In the reductive dechlorination reaction, more energy is required to break ^{13}C bonds than that required to break ^{12}C bonds, leading to differing reaction rates. The reaction rate difference between ^{12}C and ^{13}C results in a partitioning of the lighter isotopes to the products (^{13}C-depleted) as compared to the initial reactant. For example, TCE with an initial $\delta^{13}C$ value of -30 ‰ will biodegrade to DCE with a $\delta^{13}C$ value < -30 ‰ (e.g., -40 ‰). The kinetic fractionation factor (α) can also be represented as an enrichment factor (ε), as described in the following equation [41]:

$$\varepsilon = 1000(\alpha - 1)$$

The isotopic fractionation effect imparted on a residual reactant (e.g., TCE) is more pronounced in the positive $\delta^{13}C$‰ direction when the product (e.g., *cis*-DCE) is removed from the system (e.g., physical processes) and the magnitude of isotopic

fractionation increases with each dechlorination. For chlorinated ethenes, mass-dependent differences do not account for large isotope fractionation. Physical processes only affect isotopic values in that they may mobilize contaminants with varying isotopic compositions across a site through dispersion and advection, resulting in an apparent mixing of isotopically-different contaminants. Physical processes themselves do not involve isotopic fractionation greater than ±0.5 ‰ [24].

1.2.1.5. Rayleigh Distillation Model

For the purposes of theoretical background, the Rayleigh distillation model describes changes in the isotope ratio as reactions progress, which can be used to evaluate the extent of biodegradation of chlorinated ethenes; generally, some may think this approach is not applicable to field sites because dilution and dispersion is often important at the field scale. According to that model, the isotope ratio of the product is related to its original isotope ratio (assuming a constant α) by the following equation [41]:

$$R = R_0 f^{(\alpha-1)}$$

where R is the measured ratio, R_o is the initial ratio, f is fraction remaining and α is the kinetic isotope fractionation factor. For TCE, this equation can be re-written as follows [44]:

$$(\alpha - 1)\ln f = \ln\left(\frac{\left(\frac{\delta^{13}C_{sample}}{1000}\right)+1}{\left(\frac{\delta^{13}C_{initial}}{1000}\right)+1}\right)$$

When the initial TCE isotope composition ($\delta^{13}C_{TCEo}$) is known (or assumed), the current TCE isotopic composition ($\delta^{13}C_{TCE}$) is measured and the fraction of TCE remaining (*f*) is calculated (from reactant/product concentrations), a least-squares linear regression of a plot of ln *f* versus ln ((($\delta^{13}C_{TCE}$/1000)+1)/(($\delta^{13}C_{TCEo}$/1000)+1)) yields a line with a slope of α-1 [15]. Using a similar equation:

$$\left(\frac{R}{R_1}\right) = \left(\frac{C}{C_1}\right)^{\left(1/(\alpha-1)\right)}$$

where α is the kinetic isotope fractionation factor, R is the isotope ratio and C is the reactant concentration (R_1 and C_1 are initial), Scott, et al. demonstrated that kinetic isotope effects estimated from the slope (linear regression of 1/(α-1)) of the line ln (R) versus ln (C) over time, where R is plotted on the y axis and C is plotted on the x axis, were accurate and precise, meaning 95% confidence intervals for α cover the true value approximately 95% of the time. Theoretically, the line should pass through the origin [43]. The enrichment factor (discussed above) equals the slope of the line, following the Rayleigh distillation model when $\delta^{13}C$ of a reactant is plotted versus the fraction of the reactant remaining (*f*) [15].

Hunkeler et al. (2008), in disagreement with the intuitive assumptions noted at the beginning of this section, case studies (reported between 2002 and 2006) that have shown a significant number of sites do have field data that fit the Rayleigh model, indicating

potentially that biodegradation or abiotic transformation are significant processes controlling contaminant concentrations. [41].

1.2.1.6. Transformation Indicators

Isotopic ratios have the potential to differentiate between contaminant concentration decreases due to chemical transformation and those caused by physical processes, such as sorption, dissolution, and volatilization. As previously described, chemical transformation mechanisms preferentially consume isotopically lighter molecules of the reactant during the reaction process. The result of transformation includes a depleted (i.e., lighter) less-chlorinated product and an enriched (i.e., heavier) residual reactant. For example, as PCE (with an initial conceptual $\delta^{13}C$ = -32 ‰) undergoes reductive dechlorination, the resulting compounds include an isotopically lighter product, TCE (with a conceptual $\delta^{13}C$ = -36 ‰), and an isotopically heavier residual reactant PCE (with a conceptual $\delta^{13}C$ = -28 ‰). Furthermore, if the reductive dechlorination degradation process proceeds to completion (i.e., PCE to ethene), ethene will have a final ^{13}C isotopic composition that is equal to the initial ^{13}C isotopic composition of source chlorinated ethene [15]. For chlorinated ethenes, physical processes (e.g., volatilization, dissolution, diffusion, and sorption) alone do not produce isotopic fractionation greater than ±0.5 ‰ for carbon [24, 41, 45]. Physical processes only appear to affect isotopic values in that they may mobilize contaminants with varying isotopic compositions [e.g., non-transformed TCE (depleted) vs. transformed TCE (enriched)] across a site resulting in an apparent mixing of contaminants and their isotopic signature.

Under anaerobic conditions, chlorinated ethenes will biodegrade, resulting in significant positive $\delta^{13}C$ isotopic compositional shifts of each of the residual reactants, as the lighter isotope bonds are broken [41]. In their 2005 publication, Christ et al. provide an excellent review of microbial dechlorination processes that can occur in the subsurface [46]. Included in that summary are 1) Organisms capable of metabolic reductive dechlorination (i.e., chlororespiration, a process in which chlorinated compounds serve as a metabolic electron acceptor for energy generation) have been observed and these organism populations are generally strict anaerobes; 2) In some cases (e.g., the presence and activity of *Dehalococcoides* species strain BAV1 or KB-1), chlororespiration can lead to efficient dechlorination to ethene and achieve complete detoxification; 3) Chlororespiration investigations have been performed in the presence of non-aqueous-phase PCE; and 4) Nielsen and Keasling (1999) demonstrated complete reductive dechlorination (e.g., ethene formation) at saturated PCE concentrations in batch systems with a dechlorinating microbial culture enriched by contaminated groundwater.

Chlororespiring microbial populations are highly competitive hydrogen users in anaerobic environments and can outcompete methanogens, acetogens, and sulfate-reducing populations for this electron donor, as long as reductive dechlorination is not limited by the concentration or bioavailability of the chlorinated electron acceptor (e.g., PCE) [47].

From a biological perspective, there are three main conditions that must be satisfied to support optimum reductive dechlorination; a) the organisms capable of chlororespiration have to be present and active, b) sufficient nutrients must be available

for the organisms to thrive, and c) competing organisms must not significantly interfere with biogeochemical processes.

In an ideal case, various strains of *Dehalococcoides* species (including the strain BAV1) are naturally occurring in the subsurface. These microbial populations are capable of operating in a range of conditions and can completely transform PCE to ethene [48]. The species not only have to be present and capable, but they have to be active.

To be active, the organisms have to have an electron donor source and acceptor. Under reducing conditions, chlorinated ethenes can be sequentially dechlorinated by halorespiration or cometabolic processes [49]. In some cases, various amendment substrates, such as lactate and molasses, can be injected into the subsurface to act as an electron donor sources. To proliferate, these organisms also favor relatively neutral pH and temperatures near 20°C [50].

It has been reported that biological dechlorination activity increased aqueous phase total chlorinated ethene concentrations by about a factor of five [51]. In that paper, Yang and McCarty (2000) report that dechlorinating organisms can withstand concentrations of total chlorinated ethenes in solution that exceed saturation concentrations of PCE on a molar basis. Specifically, PCE and TCE dehalogenation can be obtained at saturation concentrations of >0.9mM and up to 2.26mM, respectively. According to their work, the high concentrations very near a DNAPL inhibited the activity of other organisms, such as methanogens, that could potentially compete with dechlorinators for hydrogen.

Specific metabolic pathways of transformation are complex and can vary with the microbial type, the contaminant type, and other environmental conditions (e.g., pH,

dissolved oxygen, etc.). Generally, microbial metabolism requires a source of carbon, an electron donor and acceptor, nutrients, suitable temperature and pH, and other environmental conditions. An ITRC report (2005) summarizes the three major biodegradation pathways for chlorinated ethenes as follows: 1) Contaminant is an electron acceptor – contaminant is reduced by microbes but not used as a carbon source; 2) Contaminant is an electron donor – contaminant is oxidized by microbes (obtains energy and organic carbon from contaminant); and 3) Co-metabolism – an enzyme or other factor used by microbes for some other purpose fortuitously destroys the contaminant while providing no benefit to the microbe [50].

Dehalogenation is a broad term that describes the replacement of a halogen (Cl, Br, etc.) on an organic molecule by a hydrogen atom. Hydrogenolysis, a term commonly used in chlorinated ethene reduction literature, describes the process by which one chlorine atom is replaced by one hydrogen atom. The term's usage appears to be rather synonymous with reductive dechlorination. Hydrogenolysis is thought to be the primary reaction pathway occurring at a site undergoing microbially-mediated reductive dechlorination.

Hunkeler et al. (2008) summarize from numerous publications site-specific enrichment factors (ε) that have been observed under a variety of redox conditions, along differing degradation pathways, and with varying bacterial consortiums as follows: PCE ε ranges from -0.42 to -8.8 (α ranges were not reported); TCE α ranges from 0.9975 to 0.9771 and ε ranges from -2.5 to -22.9; *cis*-DCE α ranges from 0.9859 to 0.9789 and ε ranges from -14.1 to -21.1; and VC α ranges from 0.9785 to 0.9689 and ε ranges from -

21.5 to -31.1 [41]. Ideally, the fractionation factor should be determined at the site through laboratory experimentation using site-specific microcosms [14].

Potential indicators useful in determining the nature and extent of TCE contamination and the "baseline" degradation potential of a site include various natural attenuation parameters (biological and chemical), physical processes (gradient, dispersion, volatilization, etc.) and source, reactant and product isotopic compositions and concentrations. Understanding physical processes at a site is critical for developing an effective fate-and-transport model.

Through sample collection and analysis, the total concentrations (and mole fraction) of PCE, TCE, DCE, VC and ethene can be determined, providing some information about the degradation of the source contaminant. The concentrations of the transformation products relative to the apparent source may help delineate the amount of degradation that has occurred.

1.3. Site History

In 1983, high concentrations of dissolved-phase chlorinated ethenes were discovered in two Tinker Air Force Base (AFB) water supply wells (TABLE 1-1) [52]. Solvent waste pits in Building 3001 were identified as likely source areas [53]. Another three source areas were identified at the IWTP; those included a waste pit, two blending tanks, and sludge drying beds [53]. Sources at Building 3001 contributed contaminants directly to the USZ while the IWTP sources contributed contaminants to the LSZ. Results from soil samples collected in the immediate vicinity of these source areas confirm the presence of these chlorinated ethenes in the vadose zone [53]. High

concentrations were again observed in follow-on investigations, prior to installation of a large-scale remediation system [54].

TABLE 1-1: Maximum concentrations of select chlorinated ethenes (1983 to 1993)

Hydro-stratigraphic Unit	PCE_{max} (µg/L)	TCE_{max} (µg/L)	*trans*-DCE_{max} (µg/L)	VC_{max} (µg/L)
USZ	5,300	330,000	2,100	23
LSZ	4,600	30,000	1,400	830
LLSZ	550	80,000	160	22

Notes: *cis*-DCE was not typically reported in historical data.
Abbreviations/symbols: USZ, upper saturated zone; LSZ, lower saturated zone; LLSZ, lower-lower saturated zone; µg/L, micrograms per liter; PCE, tetrachloroethylene; TCE, trichloroethylene; *trans*-DCE, *trans*-1,2-dichloroethylene;VC, vinyl chloride

On November 12, 1984, a major fire began on the roof of the north end of Building 3001, damaging about one third of the building's approximately 2.2 million square feet [55]. According to verbal communication with site personnel, massive amounts of water were used to extinguish the fire, which likely flush chlorinated ethenes into the subsurface.

During early investigations at this site, a groundwater mound was observed under the north end of Building 3001 [53]. It is speculated that the mound exists, in part, because storm drains that collect water from the roof of Building 3001 convey those water into the shallow subsurface. The USZ water table was also altered by improper well construction and deterioration of annular seals over time may have allowed for "short-circuiting" vertical movement of dissolved-phase chlorinated ethenes from upper to lower hydrostratigraphic units. Many of those wells have been abandoned and replaced by properly constructed telescoping wells. The severity of vertical movement of contaminants is dependent upon the degree and timing of short-circuiting and the vertical

gradient, which was determined to have a mean value of 0.68 downward between the USZ and LSZ at 14 nested monitoring well locations in February 2009.

Between 1993 and 1994, a pump-and-treat remediation system consisting of 16 vertical extraction wells and three horizontal extraction wells was installed at the northern end of Building 3001 and operated for ten years. During the operation of groundwater extraction wells, steep cones of depression were recorded by water level measurements and portions of the USZ were dewatered. The groundwater remediation system affected steady-state migration, degradation and mass flux of chlorinated ethenes by removing mass in vapor or aqueous phase, altering migration pathways vertically and horizontally, interrupting or slowing anaerobic degradation by moving oxygen from the USZ to the LSZ and LLSZ, enhancing diffusion from the NAPL phase to the aqueous phase by increasing the concentration gradient between the NAPL phase and the dissolved phase of chlorinated ethenes, and enhancing vinyl chloride aerobic degradation in the USZ. The pump-and-treat system was shut down in April 2004 and has not operated since. In the years following the shutdown of the pump and treat system, the potentiometric surfaces returned to their natural pre-pump and treat state.

Potentiometric surfaces measured in 1989 were compared with groundwater elevation data collected in 2008; little differences were observed in the USZ (i.e., the groundwater mound under Building 3001 returned), LSZ and LLSZ (data not shown). Thus, it is believed that groundwater flow documented in 2008 represents a return to natural flow conditions that existed in 1989 prior to the start of the pump-and-treat system.

CHAPTER 2: HYDROGEOLOGY, HYDRAULICS, AND FLOW MODEL

2.1. Setting

The project site is located in the northeastern corner of Tinker Air Force Base (TAFB), an active industrial military site, which is located east of Oklahoma City, Oklahoma. Chlorinated ethenes were detected in soil, sediment and groundwater at numerous locations at the site in the late 1980s. Numerous potential sources of chlorinated ethenes have been identified across the northeastern portion of TAFB, hereafter referred to as the northeast quadrant. This study focuses on two source areas that are separated by several hundred meters; an industrial wastewater treatment plant (IWTP) along Soldier Creek, in the northeast corner of the site, and aircraft maintenance and repair degreasing pits in the northern end of Building 3001 (the large building west of the IWTP; FIGURE 2-1).

Both Building 3001 and IWTP source areas are suspected to contribute PCE and TCE from industrial processes to the subsurface. Since the late 1980's, approximately 1,400 monitoring wells have been installed and >10,000 soil, sediment and groundwater samples have been collected and analyzed for numerous organic and inorganic parameters. Chemical analytical data from across the study site indicate the presence of large chlorinated ethene plumes; these plumes originate from each of the source areas and appear to have comingled in a deep aquifer under Building 3001. However, the nature and extent of contribution of each is unknown.

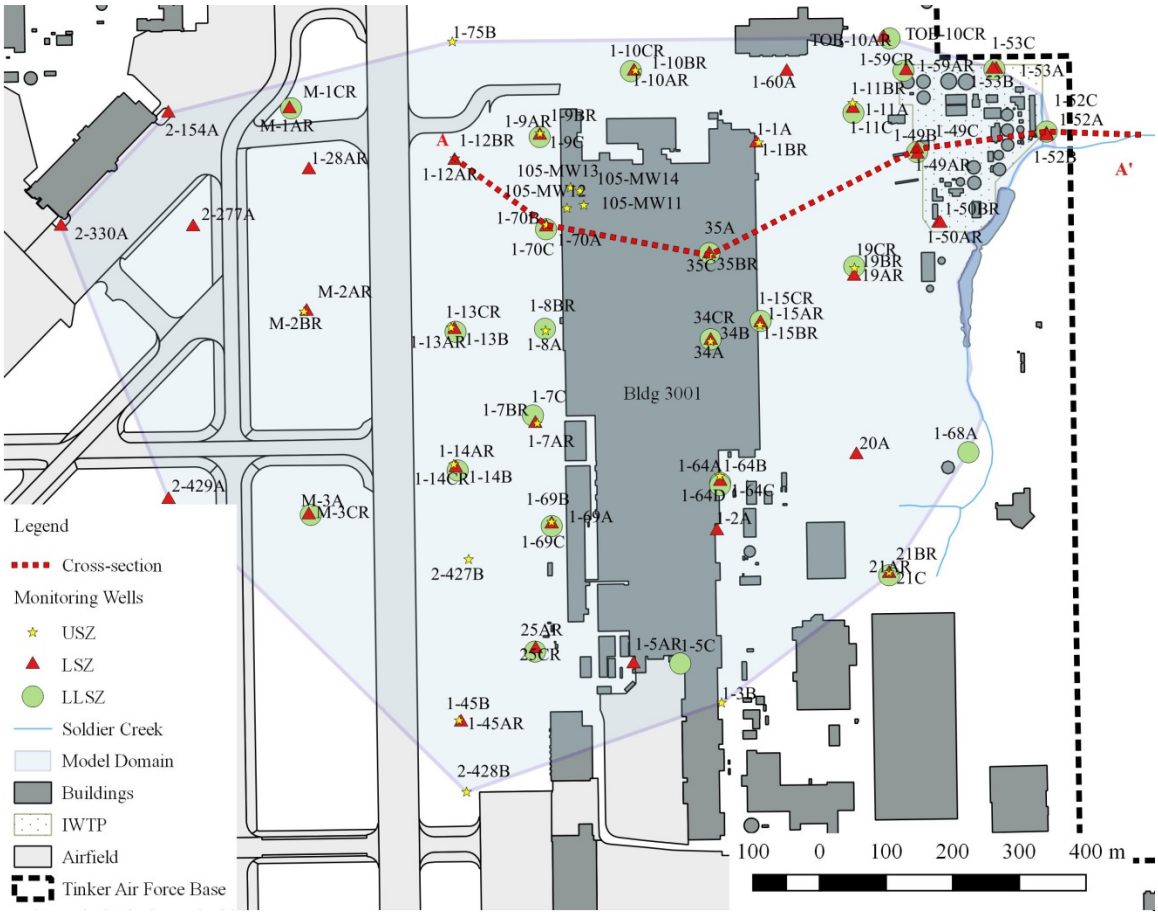

FIGURE 2-1: Monitoring well locations
Map illustrating the location of monitoring wells used in this study; monitoring wells discussed in the text are labeled. Wells symbols correspond to the hydrostratigraphic unit in which the well is screened. The IWTP is located in the top right corner of the model domain. Cross section A-A' is designated by a dashed line.

There are multiple funding mechanisms responsible for providing the resources necessary to characterize and remediate various portions of the site; military funds often cannot be transferred across remediation accounts within the DoD organization. While much is known about the site and attempts have been made to remediate the various source locations, it has continued to be difficult to assign the responsibility of the chlorinated ethene plumes to specific source areas, which makes finding appropriate funding difficult.

2.2. Geology and Hydrogeology

The study area geology (see FIGURE 2-2) consists of the Permian-age Hennessey Formation in the southern and western part of the site, which conformably overlies the Permian Garber Formation, a relatively transmissive unit in the Central Oklahoma aquifer [56]. The Hennessey is assumed to be a confining unit above the Garber. Building 3001 sits on a slight topographic divide which is oriented north-south. Bedrock formations dip to the southwest by approximately 0.5 degrees.

FIGURE 2-2: Geology of the study area
Map illustrating the geologic units present in the study area. The Hennessey Formation (Phy) is present at the surface, across most of the model domain. Permian-age Garber Formation (Pgr) is exposed along Soldier Creek, where the Hennessey Formation (Phy) has been eroded.

The Hennessey Formation consists of clays and clayey silts that are interbedded with thin, clayey sand layers, ranging from 0 to 18.3 meters thick across TAFB [57]. The

lower member of the Hennessey Formation is composed of red-brown blocky shales and mudstones with a few thin beds of very fine-grained sandstone and ranges in thickness from 0 to 12.2 meters in the Building 3001 area. The Hennessey Formation is present in the south and west part of the Building 3001 area and absent east and north of Building 3001 where it has been eroded. The Hennessey Formation is an unconfined aquifer. The Fairmont Shale component of the Hennessey Formation is an aquitard when it is present as a unit containing large amounts of mudstone and cemented siltstone [58].

The Garber Formation is composed of lenticular and interbedded sandstone, shale, and siltstone ranging from 43 to 49 meters thick in the Building 3001 area. Sandstone units are variably well consolidated and well to poorly cemented and friable. Shale beds within the Garber Formation beneath the Building 3001 area vary greatly in thickness and are discontinuous over short distances. The upper Garber Formation is unconfined and exposed on the eastern and northern portion of the Building 3001 area, and is marginally unconfined and overlain by the Hennessey under the southern part of Building 3001. On the western side of the Building 3001 area, the Garber Formation is confined and overlain by the Hennessey Formation aquitard. On the north and east side of Building 3001 except in the area of Soldier Creek (where shale units have been removed by erosion), the upper shale units of the Garber Formation act as an aquitard [59].

Five major hydrostratigraphic units were established at the study site above the production zone (PZ), the primary drinking water aquifer for this region (FIGURE 2-3). Those units are based on measured groundwater elevations and lithologic logs and include an upper saturated zone (USZ); the upper confining layer (UCL); a lower saturated zone (LSZ); a lower confining layer (LCL); and a lower-lower saturated zone

(LLSZ). In the western and southern portion of the study area, the USZ acts as a water-table aquifer, with an unsaturated zone thickening to the west. Separating the USZ from the LSZ, except where erosion has occurred, is a discontinuous series of shale and mudstone from the upper Garber Formation. The PZ is a confined unit underlying the LLSZ and is separated from overlying zones by a shale unit within the Garber Formation.

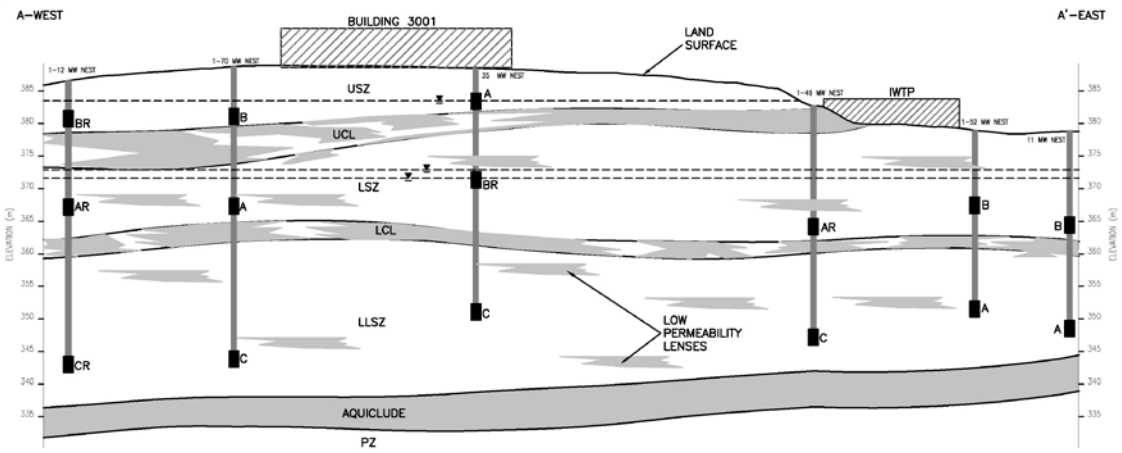

FIGURE 2-3: Conceptual cross-section of the study area
Hydrostratigraphic units (HSU) include the upper saturated zone (USZ), the lower saturated zone (LSZ), the lower-lower saturated zone (LLSZ) and the production zone (PZ). HSUs are separated by semi-confining and confining layers including the upper confining layer (UCL), the lower confining layer (LCL) and the lower-lower confining layer (LLCL) or aquiclude. Monitoring well clusters are typically nested with screens installed at various depths. Low permeability shale lenses and layers are illustrated in gray. Vertical scale is exaggerated approximately 10X.

Potentiometric data from 1984 to 1992 were evaluated for each of the primary aquifer zones. The primary groundwater flow trend observed in the USZ is directed by a groundwater mound that exists underneath Building 3001, thus creating a southeastern groundwater flow on the eastern side of Building 3001 and a southwest groundwater flow on the western side. The cause of the groundwater mound is unknown but, it has been suggested that drainage from the roof and interior of Building 3001 may artificially

mound water beneath the building. The dominant groundwater flow trend for the LSZ and LLSZ throughout the project area is to the southwest. East of Building 3001 in the area of East Soldier Creek, the LSZ is a water table aquifer until it reaches the western boundary of Building 3001 where it becomes a confined aquifer. According to Tinker AFB geologists in personal communication, the transition from water table aquifer to confined aquifer in the LSZ shifts back and forth, east to west, depending on infiltration rates and dewatering (from remedial activities) rates. The effect of that shift, at times, is an observed apparent unsaturated zone can just beneath the UCL. Pumping tests were conducted by the United States Army Corps of Engineers in 1990 and Parsons in 1995 to determine hydrogeologic properties of the USZ, LSZ and LLSZ; those data are summarized in TABLE 2-1 [54, 60]. Falling head in situ permeability tests were conducted at 12 monitoring wells screened in varying hydrostratigraphic units in February 2009 to validate ranges of hydraulic conductivity (K) values.

TABLE 2-1: Hydrogeologic properties of the USZ, LSZ and LLSZ

Hydro-stratigraphic Unit	T (m^2/day)	S	K_h (cm/sec)	K_v (cm/sec)
USZ	3.8 – 34.4	1E-4 – 1E-2	3.5E-4	n/a
LSZ	21.37 – 464	9E-5 – 1.3E-1	3.5E-4 – 3.7E-3	1.2E-7 – 1.3E-4
LLSZ	26 – 111.5	7.4E-5 – 8.4E-4	2.7E-4 – 5.5E-3	1.5E-7 – 1.06E-5

Abbreviations/symbols: USZ, upper saturated zone; LSZ, lower saturated zone; LLSZ, lower-lower saturated zone; T, transmissivity; m^2/day, square meters per day; S, storativity; K_h, horizontal hydraulic conductivity; cm/sec, centimeters per second; K_v, vertical hydraulic conductivity.

2.3. Historical Site Data Evaluation

Following an evaluation of established monitoring well locations, it was determined that 833 of approximately 1,400 monitoring wells present in the northeast

quadrant of Tinker Air Force Base exist in the study area. Those monitoring wells are screened at various depths with varying screen lengths. Since the late 1980's, those wells have been sampled at varying frequencies for numerous analytes. Monitoring wells were eliminated from the data set based on two initial criteria; screen lengths not equal to 3 m and wells lacking reported chlorinated ethene results between 2004 and 2007. From the remaining monitoring wells, a subset of monitoring wells that were nested with screens located in the USZ, LSZ and LLSZ were preferentially selected. A total of 101 monitoring wells were used during this investigation (FIGURE 2-1).

2.4. Data Collection Methods

Our framework for quantifying mass contribution of comingled chlorinated ethene plumes using a three dimensional reactive transport model includes traditional site characterization techniques coupled with non-traditional investigative techniques, such as CSIA. In development of that framework, a multi-pronged approach was completed, including (1) evaluation, synthesis, and reduction of historical data, (2) performance of field tests to evaluate hydraulic properties of the subsurface (e.g., pressure transducer studies, fluorescent dye trace studies and in-situ permeability studies), (3) refinement of a conceptual site model, and (4) aqueous sampling and analysis. Combined, these activities allowed us to develop a framework and supporting data for quantifying mass contribution of comingled chlorinated ethene plumes using a three dimensional reactive transport model.

2.4.1. Pressure Transducer Deployment

Groundwater elevations are measured across the study site along with groundwater sample collection as part of a base-wide annual sampling program managed

by the USAF. According to sampling records, historical groundwater elevation measurements were collected over a period of several days. For this study, groundwater elevation data were collected across the study site in one day and potentiometric surfaces were simultaneously monitored over a longer period of time to evaluate barometric effects, infiltration, and potential pumping scenarios on hydraulic gradient for accurate representation within the three-dimensional model.

To accurately record hydraulic head for representation within the hydrogeologic model layers, Level Troll® 700 pressure transducers were placed in 18 monitoring wells from July 16, 2008 to September 15, 2008. Transducers were placed in six monitoring well nests; each well nest contained a well screened in the USZ, LSZ and LLSZ (representing the three primary model layers). The six well nests were the 1-10, 1-11, 1-64, 1-69, 21 and 34 nests (see FIGURE 2-4). Groundwater elevations were measured prior to transducer placement and used as a reference to calibrate the recorded pressure data. The internal clocks of all transducers were synchronized. Data were recorded every 15 minutes (beginning on the hour following deployment) and stored on the internal flash drive of the device. Data were downloaded on August 26, 2008 and September 15, 2008.

Raw data files were imported into Microsoft Excel and combined into a single file. Corrected elevation data from each of the pressure transducers were synchronized according to the associated timestamps. Data collected before 8:00 a.m. on July 17, 2008 and after 12:00 p.m. on September 15, 2008 were deleted, resulting in a comprehensive synchronized data set for all monitoring wells between those dates.

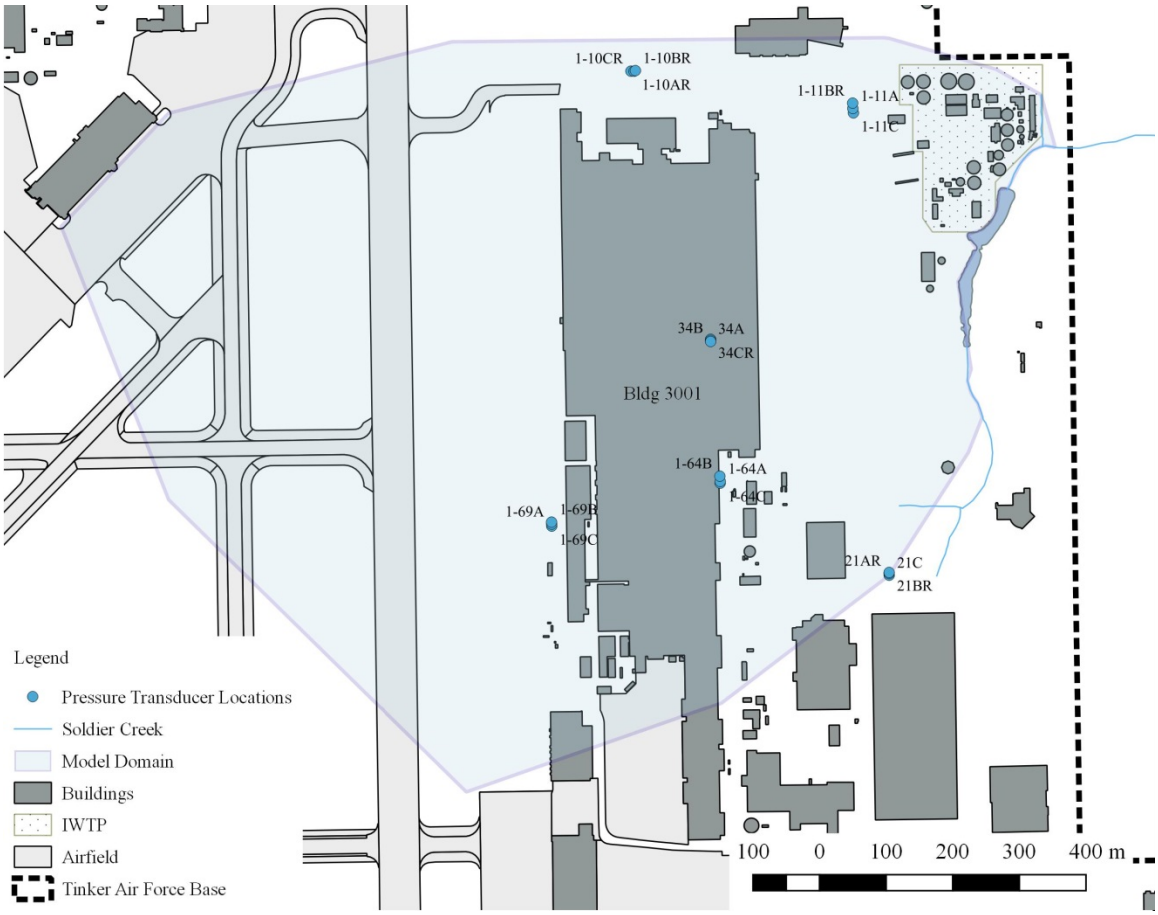

FIGURE 2-4: Pressure transducer monitoring well placement
Pressure transducers were installed in six monitoring well nests, each with a well in the USZ, LSZ, and LLSZ from July 16, 2008 to September 15, 2008.

The simultaneous, real-time data record of flow dynamics within the study area provided the data necessary to assign dimensions to the model layers to accurately represent individual potentiometric surfaces and horizontal and vertical gradients within the model by avoiding problems with data collection time delays, human error, and verification of hydraulic head data. Additionally, the transducer network provided information related to barometric effects, infiltration, and various pumping scenarios on hydraulic gradient at the study site.

2.4.2. *In-situ* Permeability Tests

To determine the hydraulic conductivity (K) of distinct subsurface horizons under in-situ conditions, in-situ permeability tests were conducted at nine monitoring wells, three in each of the USZ, LSZ and LLSZ, between February 4, 2009 and February 6, 2009. In-situ permeability tests were conducted at three additional wells on April 6, 2009. Level Troll 700 pressure transducers were lowered into the wells and placed about one meter below the water level within each well. After allowing approximately 20 minutes for the water level to equilibrate and stabilize, the pressure transducer pressure reading was reset to zero and data logging was initiated. Data were recorded every 15 seconds. A slug-in (or falling head) method was used by instantaneously adding approximately 10 gallons of potable water to the well by pouring two five gallon buckets of water through a large-mouth funnel. Data were recorded until the artificial fluctuation of the water level (measured by the pressure reading achieving a reading of zero) stabilized at the original water level. Data were downloaded to a PC for further processing. Hydraulic conductivity values were calculated using the Hvorslev method [61].

2.4.3. Fluorescent Dye Traces

Preliminary analysis of vertical and horizontal hydraulic gradients indicated flow paths from Building 3001 and the IWTP may merge in the subsurface. However, the nature of merging flow paths is unclear. Three fluorescent dye convergent traces were performed to evaluate potential horizontal and vertical migration of contaminants originating at Building 3001 and the IWTP [62]. Background sampling for interference dyes were conducted over a one-month period prior to dye introduction to assist in

fluorescent dye selection and calibration of analytical instruments. Background sampling consisted of suspending wire screen packets containing 4.25g of laboratory-grade activated coconut shell carbon in the middle of the screened interval of select monitoring wells; these carbon samplers adsorb dye cumulatively while in place. Following a two-week adsorption period, carbon packets were exchanged with fresh packets and a 50mL grab water sample was collected using a dedicated Teflon® bailer for each monitoring well. A second background sampling event was completed immediately prior to introducing fluorescent dyes.

Seventeen pounds of eosine mixture was introduced into monitoring wells 105-MW1 and 105-C2 and 10.76 lbs. of fluorescein mixture into monitoring wells 1-52A, 1-52B, 1-53A and 1-53B on July 17, 2008 to simulate contaminant releases in the USZ and LSZ, respectively. At both locations, dyes were composed of a mixture of 75% dye and 25% deionized water. The insides of well riser casings were wetted with potable water before dye introduction. Following dye introduction, multiple well volumes of potable water were added to each well to flush the dye into the formation. Carbon packets were exchanged and water samples were collected on two to three-week intervals for a total of six exchange events (approximately 15 weeks) following dye introduction. Selected packets were analyzed until a dye was reported in the sample, at which point archived samples within the pathway of the dye plume were analyzed to determine the extent and approximate timing of the dye migration.

Ten pounds of fluorescein mixture was introduced into monitoring well 105-MW14 on February 6, 2009 as a second simulation of contaminant release in the USZ. The dye composition and introduction procedure was similar to that previously described.

Concurrent with dye introduction at 105-MW14, approximately 107 gallons and 27 gallons of potable water were added to monitoring wells 105-MW1 and 105-C2, respectively. This water was added to provide an additional flush to the previous trace. Sample events were performed on a subset of the initial eosine dye trace network for a total of six exchange events following dye introduction.

2.4.4. Aqueous Sampling and Analysis

Groundwater samples were collected from ten existing monitoring wells from December 6 to December 11, 2006 as part of a preliminary site investigation. An extensive sampling event was completed from June 18 to June 23, 2008 by collecting groundwater samples from 89 existing monitoring wells. Sample locations were based primarily on previous sampling results indicating the presence of chlorinated ethenes, the horizontal spread of wells within the model domain and elevations of screened intervals with respect to hydrostratigraphic units. Based on groundwater velocities determined by previous studies and preliminary data collection, temporal sampling was less important than completely understanding the spatial variation of plume concentrations. Distance from an inferred source was used as a proxy for time, thereby eliminating the need for repetitive sampling.

All but one of the monitoring wells used in this study have dedicated tubing and stainless-steel pumps. Each well was purged prior to sample collection to remove stagnant water from the existing tubing and pump and increase the likelihood that samples collected were representative of local groundwater quality and dissolved chlorinated ethenes in the aquifer at the well screen. Purging was conducted until water quality parameters (i.e., dissolved oxygen, pH, specific conductance, oxidation-reduction

potential and temperature) stabilized. A YSI-556 flow-through cell was incorporated in-line with the sampling device to determine when field parameters had stabilized. Groundwater stabilization parameters are provided below, in TABLE 2-2. All down-hole tubing was Teflon lined. Immediately following completion of purging, sample containers were filled through the pump and Teflon tubing.

Once stabilization was achieved, unfiltered samples were collected in 40ml glass vials with Teflon-lined caps, pre-preserved with hydrochloric acid for chemical and isotopic analysis. Samples were packed in ice and kept below 4°C until they were analyzed. Groundwater samples submitted to Prism Laboratories, Inc. for chemical analysis were analyzed for a subset of VOCs (i.e., PCE, TCE, *cis*-DCE, *trans*-DCE and VC) by EPA Method 8260B and for ethene by EPA Method 8015 [63, 64]. Groundwater samples were analyzed at the University of Oklahoma for $\delta^{13}C$ for the corresponding subset of VOCs and ethene. Stable-isotope analysis was accomplished using a combined gas-chromatograph-isotope-ratio mass-spectrometer (GC/IRMS) system following published analytical procedures for chlorinated ethane [22, 64]. This system permits determination of the isotopic composition of individual components in very complex mixtures.

TABLE 2-2: Groundwater sampling stabilization parameters

Well ID	pH	Temperature (°C)	Specific Conductance (µS/cm)	Dissolved Oxygen (mg/L)	Turbidity (NTUs)	ORP (mV)
21BR			Data Not Recorded			
34A	7.62	23.96	0.810	3.70	3.34	60.1
35A	7.42	23.16	1.289	0.97	5.34	34.4
1-3B	7.10	22.66	1.899	1.69	1.43	-7.0
1-4B	7.26	22.80	0.772	2.43	1.50	75.1
1-7BR	7.28	23.40	0.794	0.28	16.4	3.0
1-8BR	7.60	23.66	0.762	4.12	3.45	4.3
1-9BR	6.75	20.41	0.605	0.74	1.79	51.0

Well ID	pH	Temperature (°C)	Specific Conductance (µS/cm)	Dissolved Oxygen (mg/L)	Turbidity (NTUs)	ORP (mV)
1-12BR	7.34	21.42	0.607	0.37	3.56	-12.2
1-13B	7.20	20.44	0.621	2.83	3.11	29.0
1-14B	7.08	19.92	2.090	2.53	2.44	-32.6
1-15BR	7.46	24.49	1.295	1.20	51.5	48.3
1-45B	6.89	22.85	3.046	0.33	2.42	-47.0
1-64B	7.05	23.27	0.771	0.35	0.65	36.9
1-69B	7.11	26.22	0.357	0.36	36.3	2.6
1-70B	7.29	23.08	1.266	0.38	1.22	-14.6
1-75B	7.43	24.14	0.589	0.55	5.05	-10.0
2-427B	7.39	27.76	1.35	0.33	33.9	-43
2-428B	7.13	24.86	1.594	0.31	6.18	-20.7
105-MW11	7.16	22.25	0.877	2.62	>1000	88.2
105-MW12	7.21	23.03	1.252	1.23	210	100.0
105-MW13	7.17	25.54	1.311	3.09	113.0	88.6
105-MW14	7.08	22.83	0.639	0.57	41.1	82.4
M-2BR	7.05	21.01	1.338	0.44	4.05	15.8
M-3			Data Not Recorded			
19AR	6.88	23.90	0.794	1.28	24.0	50.3
20A	6.79	22.11	0.594	0.97	12.0	32.0
21AR	8.36	23.95	0.244	2.14	5.66	48.8
22DR	7.10	18.85	0.784	0.41	8.62	44.5
25AR	7.58	21.73	0.808	1.32	26.4	53.8
34B	7.33	21.92	1.054	1.25	14.30	63.1
35BR	7.08	21.41	0.865	1.63	54.4	44.2
1-1A	6.92	21.88	1.032	2.16	6.53	91.20
1-2A	7.26	23.07	0.884	2.67	26.4	45.9
1-5AR	7.72	24.97	0.585	0.47	0.41	-7.5
1-7AR	7.12	22.73	0.630	3.32	2.90	72.8
1-11A	7.02	22.25	1.001	0.44	7.35	0.0
1-12AR	8.07	24.14	0.499	0.58	5.33	-23.8
1-13AR	7.43	21.30	0.550	2.60	3.17	1.0
1-14AR	6.98	20.08	0.761	0.49	0.84	15.7
1-15AR	7.11	21.19	0.677	0.27	1.01	9.4
1-28AR	7.21	20.60	0.677	2.21	111.0	77.6
1-45AR	7.52	21.49	0.756	0.87	31.2	-28.9
1-49AR	7.03	21.36	0.710	0.26	0.67	-8.9
1-49B	6.79	25.71	0.844	1.03	0.17	24.4
1-50AR	6.89	22.21	0.751	0.39	3.95	102.9
1-50BR	7.07	22.68	0.543	0.79	0.00	23.8
1-59AR	6.99	23.27	1.037	0.42	6.93	15.1
1-60A	7.02	22.19	0.907	2.21	9.11	55.9
1-64A	7.03	24.04	1.003	2.11	49.9	63.1
1-69A	7.42	23.03	0.236	2.38	3.03	28.2
1-70A	6.32	24.66	0.641	2.42	2.19	35.0
2-154A	6.98	23.32	0.197	0.36	9.26	-88.0
2-277A	7.65	22.08	0.627	0.60	13.80	-62.3
2-330A	7.46	22.65	0.781	0.51	2.05	5.8
2-429A	7.61	19.78	0.435	0.27	3.02	-142.0
M-1AR	7.02	20.46	0.847	0.87	18.0	49.6
M-2AR	7.63	20.33	0.195	0.60	24.1	67.5
M-3A	7.22	18.84	1.065	3.87	0.36	73.1
TOB-10AR	7.65	25.20	0.371	3.71	4.65	108.0
19CR	7.16	22.49	0.629	1.13	3.32	23.7

Well ID	pH	Temperature (°C)	Specific Conductance (µS/cm)	Dissolved Oxygen (mg/L)	Turbidity (NTUs)	ORP (mV)
25CR	7.33	20.80	0.543	3.87	6.18	13.9
34CR	7.26	20.84	0.577	0.42	8.26	0.0
35C	7.00	20.90	0.694	0.53	17.4	-11.8
1-5C	7.64	23.74	0.616	0.40	0.49	85.5
1-7C	8.52	20.90	0.506	2.34	2.60	62.8
1-7D	7.37	22.10	0.418	1.88	43.5	59.9
1-8A	7.10	24.59	0.713	2.49	1.73	16.5
1-9C	7.46	20.11	0.536	2.59	1.01	21.7
1-10CR	7.13	20.68	0.607	2.89	20.7	83.6
1-11C	7.08	21.15	1.013	1.44	133	35.0
1-12CR	Data Not Recorded					
1-13CR	7.19	19.44	0.196	0.55	4.00	-96.5
1-14CR	7.67	19.73	0.351	4.71	11.10	-0.5
1-15CR	7.26	22.69	0.660	0.82	3.91	39.6
1-49C	9.00	26.11	0.328	1.71	11.2	-45.2
1-52C	7.25	21.75	0.539	2.30	3.60	0.7
1-53C	7.20	22.15	0.719	0.33	54.4	-5.1
1-59CR	7.21	21.94	0.682	0.59	13.10	34.3
1-60CR	7.28	20.48	0.788	0.50	4.79	58.3
1-64C	7.08	22.13	0.638	1.10	19.70	-76.4
1-64D	8.15	21.75	0.294	3.19	6.05	30.0
1-68A	7.20	20.95	0.612	0.60	1.05	0.7
1-69C	7.07	22.80	0.650	1.04	23.1	12.8
1-69D	7.29	23.20	0.448	3.88	0.00	-13.1
1-70C	7.31	24.78	0.423	3.28	1.75	22.6
M-1CR	7.44	20.91	0.466	4.42	0.54	55.7
M-3CR	7.45	20.95	0.556	4.59	348	75.5
TOB-10CR	7.36	21.02	0.657	0.48	7.62	57.40

Abbreviations/symbols: °C, degrees Celsius; (µS/cm), microsiemens per centimeter; mg/L, milligrams per Liter; NTUs, nephelometric turbidity units; mV, millivolts.

CHAPTER 3: DATA COLLECTION RESULTS

3.1. Introduction

The project site (and three dimensional volume) is large and the subsurface conditions are complex. For purposes of simplification, various datasets were arranged in terms of horizontal and vertical relevance. Generally, concentration and isotope data are presented herein with respect to the mid-screen elevation of the associated monitoring well from which samples originate.

3.2. Potentiometric Surface

Pressure transducer data were grouped according to aquifer zones USZ, LSZ and LLSZ, based on head measurements. Average water level elevations in USZ monitoring wells range from 383.5 m to 381.5 m above sea level. Average water level elevations in LSZ monitoring wells range from 370 m to 367.5 m above sea level. Average water level elevations in LLSZ monitoring wells range from 369.5 m to 366.5 m above sea level.

These time series data were plotted against elevation to provide a visual representation of water table fluctuations over the course of the study (data not shown). National Climatic Data Center (NCDC) hourly precipitation data (http://www.ncdc.noaa.gov/) from the time period of the study from Station ID KTIK at Tinker Air Force Base were plotted along with pressure transducer data. Two monitoring wells in the USZ, 1-69B and 21BR, appear to be hydraulically connected to surface water flow; peak water elevation increases correspond to heavy rainfall events.

These water level elevation increases can also be seen in monitoring wells screened in the LSZ, 1-69A (faintly) and 21AR. Aside from those two well clusters, water level elevations remain relatively flat over the course of this study. Monitoring wells screened in the LLSZ appear not to be impacted by short-term rainfall events.

3.2.1. Steady-State vs. Transient Flow

The pressure transducer data were grouped according to aquifer zones USZ, LSZ and LLSZ. These time series data were plotted against elevation to provide a visual representation of water table fluctuations over the course of the study. NOAA daily precipitation data from the time period of the study were obtained electronically from the NOAA website (http://www.srh.noaa.gov/oun/climate/) and plotted along with the pressure transducer data. Two monitoring wells in the USZ, 1-69B and 21BR, appear to be hydraulically connected to surface water flow; peak water elevation increases correspond to heavy rainfall events. These water level elevation increases can also be seen in monitoring wells screened in the LSZ, 1-69A (faintly) and 21AR. Aside from those two well clusters, the water level elevations remain relatively flat over the course of this study. Monitoring wells screened in the LLSZ appear not to be impacted by short-term rainfall events. Average water level elevations in USZ monitoring wells range from approximately 383.5 m to 381.5 m above sea level. Average water level elevations in LSZ monitoring wells range from approximately 370 m to 367.5 m above sea level. Average water level elevations in LLSZ monitoring wells range from approximately 369.5 m to 366.5 m ft above sea level.

3.3. Fluorescent Dye Traces

Eosine dye introduced into monitoring wells 105-MW1 and 105-C2 on July 16, 2008 was not detected in carbon packet samples or grab water samples. According to lithologic logs and well construction records, 105-MW1 is screened from 8.5 m to 11.6 m below grade (bg), 105-C2 is screened from 6.1 m to 9.1 m bg, and both wells are installed in a sand unit [65]. Based on the modest resistance to adsorption onto inorganic aquifer substrate, the injection point screen intervals, and the high dye-to-water ratio, it was expected dye would migrate out into the USZ and possibly down into the LSZ. No eosine dye was detected in adjacent wells during the monitoring period, suggesting that there was no or very slow vertical or horizontal movement of eosine dye from release points. While these results are somewhat confounding, it is possible the eosine dye traveled along a preferential pathway that is not encountered by another well or may have settled into abandoned subsurface piping. Subsequent drilling activities conducted in late 2009 encountered eosine dye in the USZ about 8 m south of 105-C2 yielding an approximate travel rate of greater than 0.016 m/day.

Results of the Fluorescein dye trace initiated at the IWTP indicate 1) fast advection in the LSZ, 2) preferential flow paths, and 3) vertical movement from the LSZ to the LLSZ. Fluorescein dye introduced into monitoring wells 1-52A, 1-52B, 1-53A and 1-53B on July 17, 2008 was detected in carbon packet samples and grab water samples in the LSZ, LLSZ, and Soldier Creek (FIGURE 3-1). Confirmed dye detections are noted in two ways, first dye arrival and peak dye arrival. Peak dye arrival is determined by reviewing average daily concentration for each sampling period.

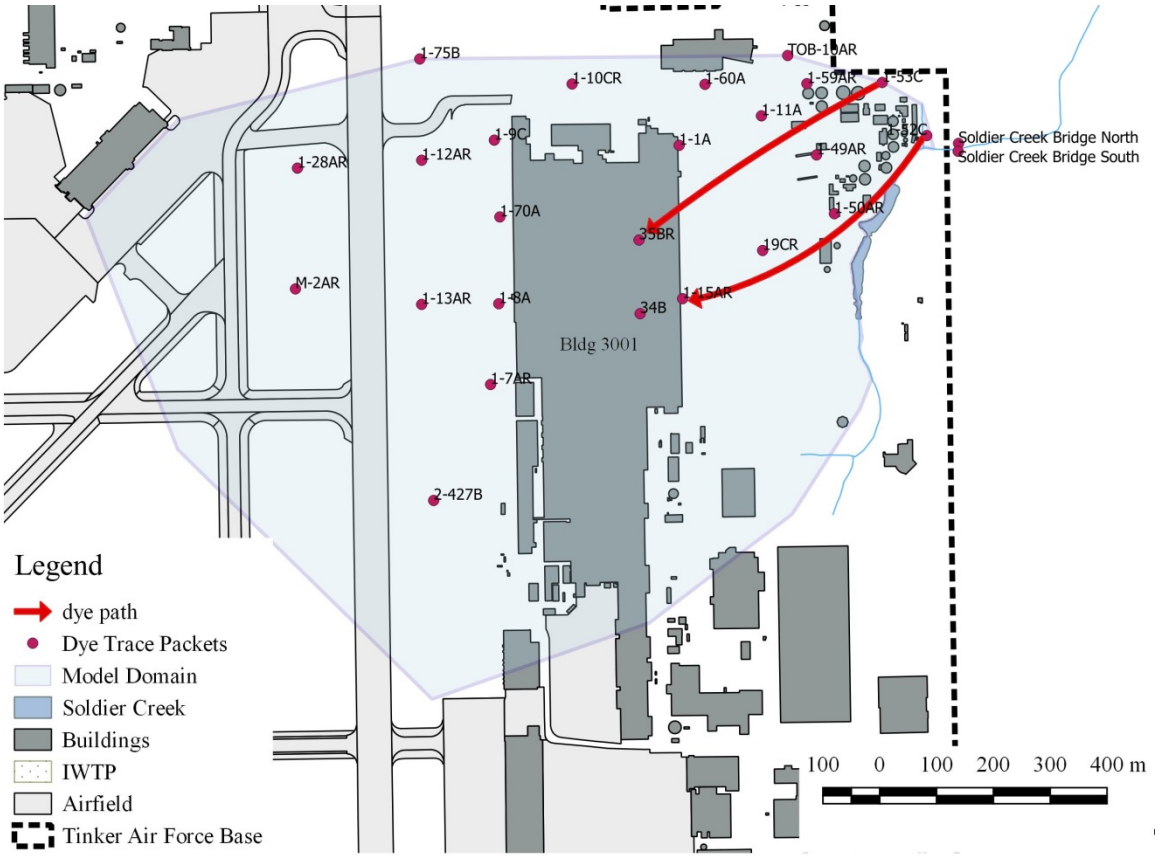

FIGURE 3-1: IWTP fluorescein dye trace result
Fluorescein was introduced into monitoring wells 1-52A, 1-52B, 1-53A, and 1-53B. Dye was detected only in five monitoring wells 1-1A (LSZ), 1-50AR (LSZ), 1-15AR (LSZ), 1-15CR (LLSZ), and 35BR (LSZ). Possible preferential flow paths are illustrated using dashed lines. Note that the groundwater mound present in the USZ does not impact the dye trace in the LSZ.

Estimated mean travel rates of the peak concentration is calculated by dividing the distance from dye introduction points to sampling stations by the number of days since the dye was introduced. Mean travel rates indicated by the fluorescein trace range from 2.9 to 78 m/day. Notably, fluorescein was detected at 35BR (screened in the LSZ) in 7 days and at nearby wells 1-1A, 1-15AR (and 1-15CR) at 20 days and 44 days, respectively. This result was surprising not only because of the apparent rapid travel rate but, also because fluorescein was never detected at monitoring wells 1-11A, 1-49B, 1-49AR, or 19AR (wells are located between the northerly and southerly possible dye flow

routes). It is speculated the lack of dye detection may be due to the locations of those well screens, potential preferential pathways, original drainage paths, and/or less permeable lithology at screened intervals. Fluorescein was also detected at 1-50AR (screened in the LSZ) in 72 days. Fluorescein dye was not detected west of 35BR. Lack of further detection is common at large sites when dye concentrations decrease over large distances and long time periods. These data indicate the likely presence of preferential pathways within the LSZ. Possible flow lines are illustrated on FIGURE 3-1. Fluorescein dye detections in 1-52C and 1-53C indicate vertical groundwater movement with mean travel rates of 0.55 and 0.32 m/day, respectively.

After a lack of eosine detections under Building 3001 and favorable fluorescein results across the site, a second dye trace was conducted at Building 3001 using fluorescein dye. This was done to determine if lack of detections was related to the use of eosine dye, which can sometimes adhere to fine matrices and is therefore less conservative compared to fluorescein. The dye was introduced at monitoring well 105-MW14. Fluorescein dye was detected at three locations during the dye trace event; monitoring wells 1-1A, 35BR and 35C. However, these detections are considered background because the results are not greater than ten times the background concentrations (i.e., those dye concentrations detected in carbon packets and groundwater samples collected before dye introduction). Based on groundwater data and discussions with Tinker AFB personnel familiar with the site, the fluorescein dye detected at these locations is thought to be from the initial fluorescein dye trace initiated at the IWTP. Therefore, fluorescein dye derived from the second dye trace was not detected at any sampling location during the dye trace event. Field measurements confirmed the depth of

the screened interval at monitoring well 105-MW14; from those measurements, it was determined the well is screened in the confining unit between the lower and upper perched aquifer of the USZ. This indicates that no movement of the fluorescein dye trace occurred, which is similar to the eosine dye trace results.

3.4. Chemical Analytical Results

Various chlorinated ethenes were detected in all of the monitoring wells sampled in 2008. A summary of constituent concentrations detected in groundwater samples collected in 2008 is listed in TABLE 3-1. Non-bolded values indicate the analyte was analyzed for, but not detected above the level of the associated laboratory reporting limit (RL). The laboratory method detection limit (MDL) is indicated along with the "<" symbol. Bold concentration values indicate the analyte was detected above the level of the associated reporting limit. Values reported along with "J" indicate the analyte was positively identified. However, the associated numerical value is an approximate concentration of the analyte in the sample. Total concentration values include only those analytes with concentrations detected above the level of the associated RL; values reported as "--" indicates none of the analytes were detected above the RL. Concentration data were contoured in open source software QGIS.

In the USZ, total chlorinated ethene concentrations were highest at the northern end of Building 3001. Chlorinated ethenes were reported at 23 of 25 monitoring wells and total chlorinated ethene concentrations ranged from 4.23 µg/L to 66,520 µg/L at M-2BR and 1-70B, respectively. In the LSZ, total chlorinated ethene concentrations were somewhat evenly distributed across the site. Chlorinated ethenes were reported at 33 of 35 monitoring wells and total chlorinated ethene concentrations ranged from 1.5 µg/L to

3,880 µg/L at 21AR and 2-277A, respectively. In the LLSZ, total chlorinated ethene concentrations were somewhat evenly distributed across the site with the exception of two "hotspots" at monitoring wells 35C and 1-8A. Chlorinated ethenes were reported at all 28 monitoring wells and total chlorinated ethene concentrations ranged from 0.72 µg/L to 5,098.2 µg/L at 1-13CR and 35C, respectively.

TABLE 3-1: Concentrations of chlorinated ethenes at selected wells, 2008

	Concentration (µg/L)[1,2,3]						
Location	**PCE**	**TCE**	***cis*-DCE**	***trans*-DCE**	**VC**	**Ethene**	**~Total Mass[4]**
USZ							
21BR	<0.12	<0.073	<0.054	<0.066	<0.28	<0.182	--
34A	**160**	**4400**	**15**	<1.3	<5.5	<0.182	4575
35A	**19**	**69**	**5.6**	<0.066	<0.28	<0.182	94
1-3B	**1**	**4.4**	<0.054	<0.066	<0.28	<0.182	5
1-4B	**5.6**	<0.073	<0.054	<0.066	<0.28	<0.182	6
1-7BR	**12**	**1200**	**140**	<0.66	<2.8	<0.182	1352
1-8BR	**98**	**200**	**23**	<0.066	<0.28	<0.182	321
1-9BR	**1.3**	**4.9**	**6.0**	<0.066	<0.28	<0.182	12
1-12BR	<2.4	**3800**	**680**	<1.3	<5.5	<0.182	4480
1-13B	**480**	**48**	**160**	**0.59**	<0.28	<0.182	689
1-14B	<0.12	<0.073	<0.054	<0.066	<0.28	<0.182	--
1-15BR	**1.3**	**24**	**0.72**	<0.066	<0.28	<0.182	26
1-45B	<1.2	**1800**	**2500**	**8.5**	**19**	**2.9**	4328
1-64B	**0.52**	**43**	**5.1**	**1.3**	<0.28	<0.182	502
1-69B	<0.12	**1.6**	**6.2**	<0.066	**2.7**	<0.182	11
1-70B	**5100**	**59000**	**2300**	**120**	<28	<0.182	66520
1-75B	<0.12	**120**	**23**	<0.066	<0.28	<0.182	143
2-427B	<0.6	**260**	**40**	<0.33	<1.4	<0.182	300
2-428B	**140**	**220**	**37**	<0.33	<1.4	<0.182	397
105-MW11	**4100**	**34000**	**2300**	**260**	<55	<0.182	40660
105-MW12	**5500**	**46000**	**1800**	<26	<110	<0.182	53300
105-MW13	**410**	**3800**	**580**	**75**	<5.5	<0.182	4865
105-MW14	**450**	**3000**	**200**	**37**	<11	<0.182	3687
M-2BR	**0.72**	**2.9**	**0.61**	<0.066	<0.28	<0.182	4

[1] Non-bolded values indicate the analyte was analyzed for, but not detected above the level of the associated laboratory reporting limit (RL). The laboratory method detection limit (MDL) is indicated along with the "<" symbol.
[2] Bold concentration values indicate the analyte was detected above the level of the associated reporting limit.
[3] Values reported along with "J" indicate the analyte was positively identified. However, the associated numerical value is an approximate concentration of the analyte in the sample.
[4] Total concentration values include only those analytes with concentrations detected above the level of the associated RL; values reported as "--" indicates none of the analytes were detected above the RL.

Location	Concentration (µg/L)[1,2,3]						
	PCE	**TCE**	***cis*-DCE**	***trans*-DCE**	**VC**	**Ethene**	**~Total Mass[4]**
M-3	**6.5**	**3.3**	**1.4**	<0.066	<0.28	<0.182	11
LSZ							
19AR	**70**	**1800**	**1000**	**4.5**	**15**	<0.182	2890
20A	<0.12	**25**	**0.68**	<0.066	<0.28	<0.182	26
21AR	<0.12	**1.5**	<0.054	<0.066	<0.28	<0.182	2
22DR	<0.12	**11**	**17**	<0.066	<0.28	<0.182	28
25AR	<0.12	**240**	**5.6**	<0.066	<0.28	<0.182	246
34B	**47**	**2000**	**10**	<0.66	<2.8	<0.182	2057
35BR	**270**	**1800**	**170**	<0.66	<2.8	<0.182	2240
1-1A	**88**	**300**	**35**	<0.066	**0.63**	<0.182	424
1-2A	**1.8**	**44**	**5**	<0.066	<0.28	<0.182	51
1-5AR	<0.12	**3**	**0.92**	<0.066	<0.28	<0.182	4
1-7AR	<0.12	<0.073	<0.054	<0.066	<0.28	<0.182	--
1-11A	**22**	**16**	**29**	<0.066	**2.5**	<0.182	70
1-12AR	<0.12	**1.6**	<0.054	<0.066	<0.28	<0.182	2
1-13AR	**72**	**2600**	**56**	<1.3	<5.5	<0.182	2728
1-14AR	**0.59**	**140**	**27**	**1.4**	<0.28	<0.182	169
1-15AR	**23**	**120**	**150**	**3.1**	**48**	**3.36**	344
1-28AR	**5.2**	**1800**	**160**	**6.2**	<2.8	<0.182	1971
1-45AR	<0.12	**2.8**	**2.1**	<0.066	<0.28	<0.182	5
1-49AR	**11**	**32**	**83**	**1**	**19**	**0.532J**	146
1-49B	**5.2**	**2.4**	**2.9**	<0.066	<0.28	<0.182	11
1-50AR	**10**	**61**	**110**	**2.2**	**51**	**0.613J**	234
1-50BR	<0.12	**1.9**	**2.1**	<0.066	<0.28	<0.182	4
1-59AR	**3.0**	**1.9**	**12**	<0.066	**1.9**	<0.182	19
1-60A	**96**	**53**	**36**	<0.066	<0.28	<0.182	185
1-64A	**4.7**	**1100**	**120**	**11**	<1.4	<0.182	1236
1-69A	<0.12	**14**	<0.054	<0.066	<0.28	<0.182	14
1-70A	**15**	**310**	**27**	**0.55**	**6.2**	<0.182	359
2-154A	<0.12	**13**	**2.3**	<0.066	<0.28	<0.182	15
2-277A	<2.4	**3500**	**380**	<1.3	<5.5	<0.182	3880
2-330A	<0.6	**320**	**40**	<0.33	<1.4	<0.182	360
2-429A	<0.6	**330**	**440**	**3.9**	<1.4	<0.182	774
M-1AR	**3.1**	**320**	**49**	<0.33	<1.4	<0.182	372
M-2AR	<0.12	**26**	**1.6**	<0.066	<0.28	<0.182	28
M-3A	**7.3**	**1400**	**420**	**6.2**	<2.8	<0.182	1834
TOB-10AR	<0.12	<0.073	<0.054	<0.066	<0.28	<0.182	--
LLSZ							
19CR	**0.76**	**95**	**96**	**2.9**	**13**	**0.282J**	208
25CR	**0.86**	**33**	**5.1**	**0.85**	<0.28	<0.182	40
34CR	**1.7**	**38**	**26**	<0.066	**3.8**	<0.182	70
35C	**1600**	**690**	**2500**	**8.2**	**300**	**7.28**	5098
1-5C	**0.57**	**6.1**	**2.5**	<0.066	<0.28	<0.182	9
1-7C	<0.12	**15**	**12**	<0.066	<0.28	<0.182	27
1-7D	<0.12	**10**	**4.5**	<0.066	<0.28	<0.182	15
1-8A	**140**	**4100**	**590**	**5.3**	<2.8	<0.182	4835
1-9C	<0.12	**3.6**	**2.6**	<0.066	<0.28	<0.182	6
1-10CR	**2.9**	**4.1**	**2.3**	<0.066	<0.28	<0.182	9
1-11C	**110**	**180**	**130**	**2.1**	**3.1**	<0.182	425

Location	Concentration (µg/L)[1,2,3]						
	PCE	TCE	*cis*-DCE	*trans*-DCE	VC	Ethene	~Total Mass[4]
1-13CR	<0.12	**0.72**	<0.054	<0.066	<0.28	<0.182	1
1-14CR	<0.12	**6.8**	**1.4**	<0.066	<0.28	<0.182	8
1-15CR	**4.7**	**40**	**31**	<0.066	<0.28	<0.182	76
1-49C	**25**	**130**	**120**	**6.5**	**16**	**0.42 J**	298
1-52C	<0.12	**2.2**	**1.6**	<0.066	<0.28	<0.182	4
1-53C	<0.12	**0.74**	**0.61**	<0.066	<0.28	<0.182	1
1-59CR	**0.92**	**7.0**	**5.3**	<0.066	<0.28	<0.182	13
1-60CR	**66**	**71**	**120**	**1**	**4.4**	<0.182	262
1-64C	**1.3**	**17**	**3.9**	<0.066	<0.28	<0.182	22
1-64D	<0.12	**12**	**0.6**	<0.066	<0.28	<0.182	13
1-68A	<0.12	**2.8**	**1.6**	<0.066	<0.28	<0.182	4
1-69C	**1.4**	**78**	**6.8**	**0.94**	<0.28	<0.182	87
1-69D	<0.12	**5.4**	**1.9**	<0.066	<0.28	<0.182	7
1-70C	**1.5**	**39**	**13**	**0.56**	<0.28	<0.182	54
M-1CR	<0.12	**80**	**13**	<0.066	<0.28	<0.182	93
M-3CR	<0.6	**340**	**52**	**7.7**	<1.4	<0.182	400
TOB-10CR	<0.12	**2.1**	**1.4**	<0.066	<0.28	<0.182	4

Abbreviations/symbols: µg/L, micrograms per liter; PCE, tetrachloroethylene; TCE, trichloroethylene; *cis*-DCE, *cis*-1,2-dichloroethylene; *trans*-DCE, *trans*-1,2-dichloroethylene;VC, vinyl chloride

3.4.1.1. Upper Saturated Zone Summary

Total chlorinated ethene concentrations were highest at the northern end of Building 3001 near the 105 source. Chlorinated ethenes were reported at 23 of 25 monitoring wells and total chlorinated ethene concentrations ranged from 4.23 µg/L to 66,520 µg/L at M-2BR and 1-70B, respectively (FIGURE 3-2). PCE was detected in 18 of 25 groundwater samples, ranging from 0.52 µg/L to 5,500 µg/L (FIGURE 3-3). TCE was detected in 22 of 25 groundwater samples, ranging from 1.6 µg/L to 59,000 µg/L (FIGURE 3-4). *cis*-DCE was detected in 21 of 25 groundwater samples, ranging from 0.61 µg/L to 2,500 µg/L (FIGURE 3-5). VC was detected in 2 of 25 groundwater samples at 2.7 µg/L and 19 µg/L (FIGURE 3-6); high chlorinated ethene concentrations at some monitoring wells resulted in high reporting limits, which is the case for VC at

numerous locations (e.g., 105 source area monitoring wells). Ethene was detected in one groundwater sample at 2.9 µg/L (FIGURE 3-7).

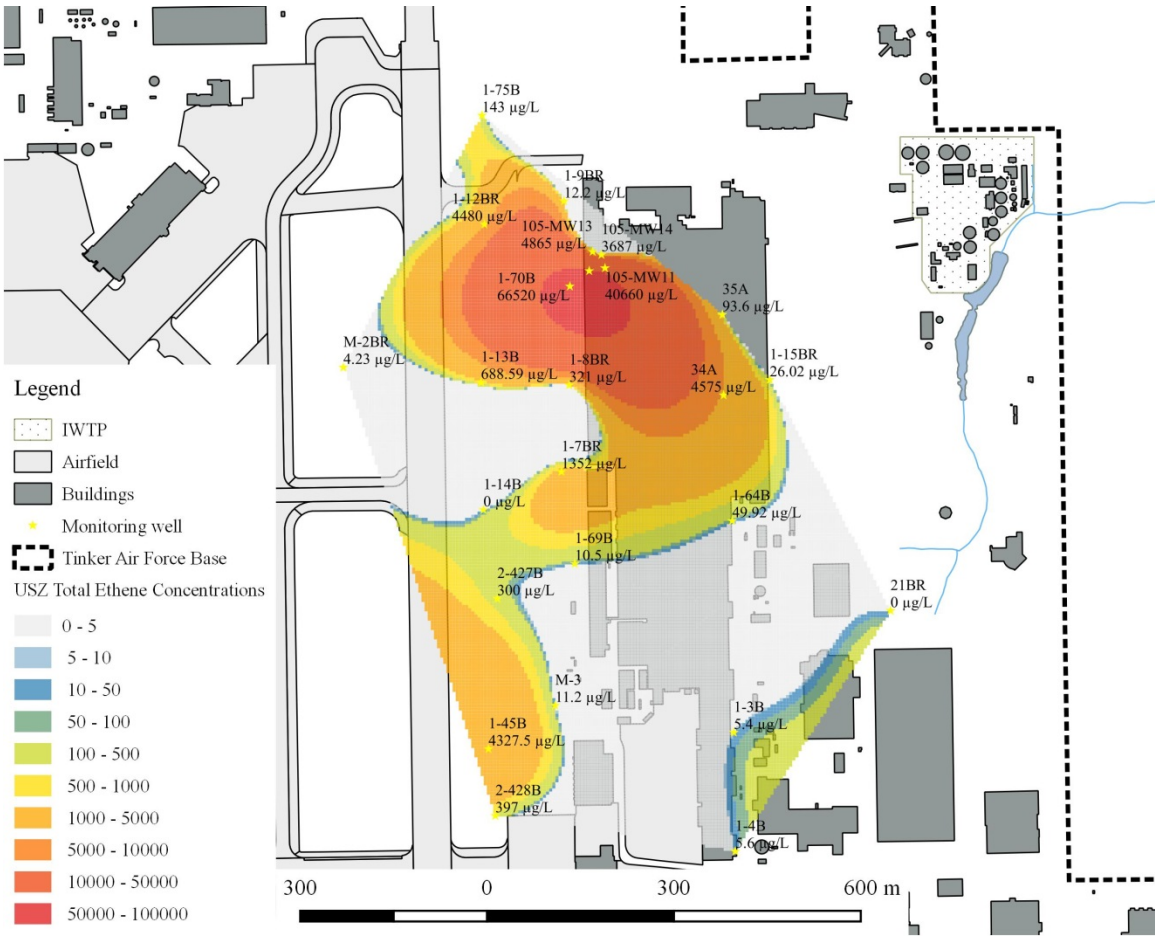

FIGURE 3-2: Total chlorinated ethene concentrations in the USZ, 2008
This figure illustrates the sum of measured chlorinated ethene concentrations in micrograms per liter.

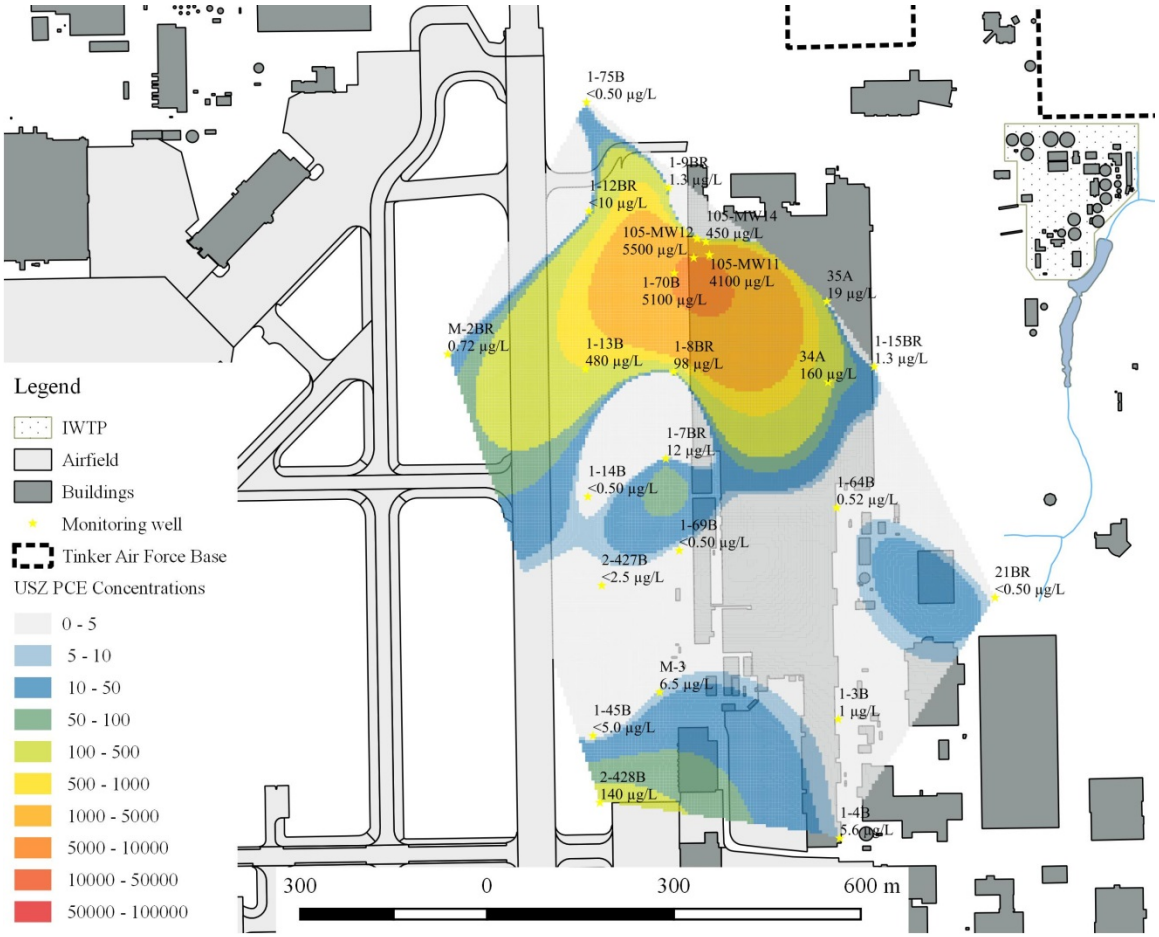

FIGURE 3-3: PCE concentrations in the USZ, 2008
This figure illustrates the measured PCE concentrations in micrograms per liter.

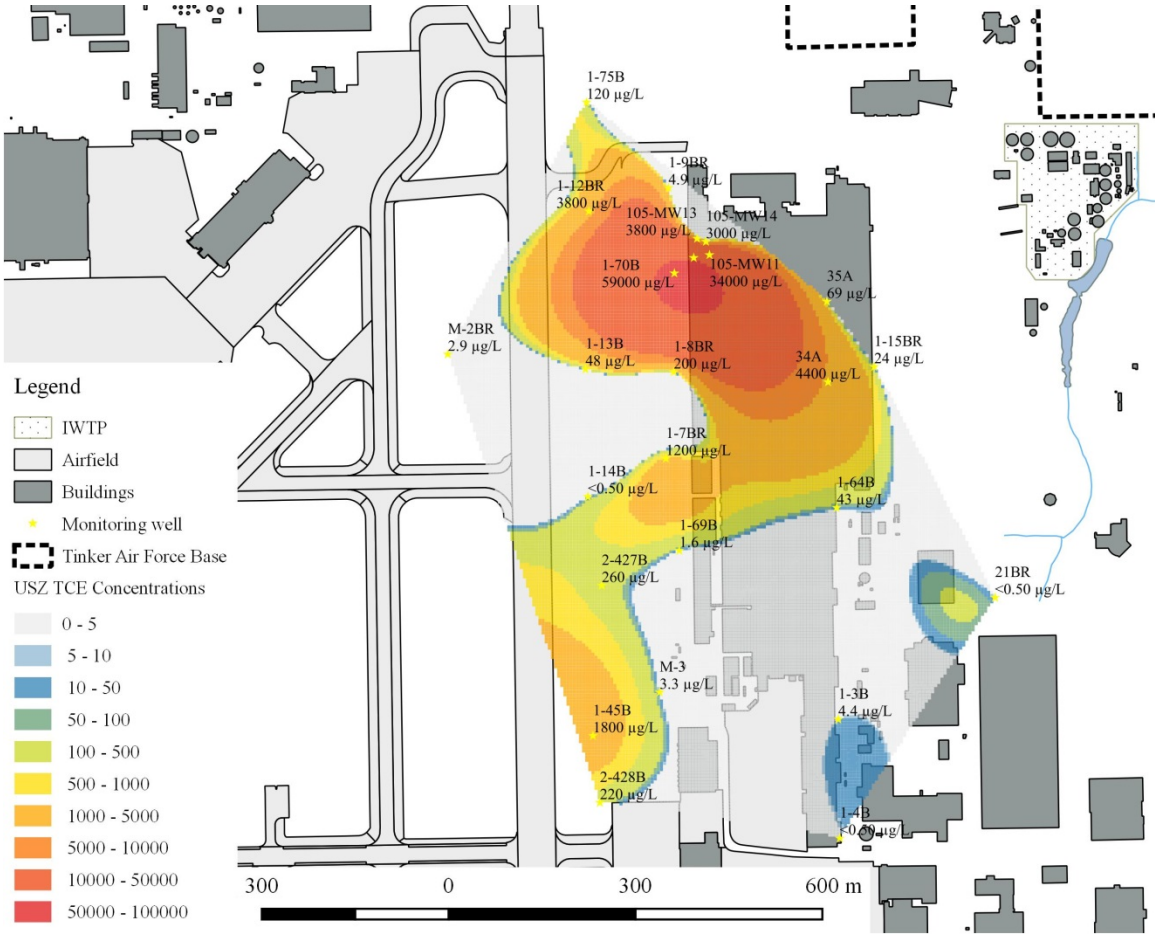

FIGURE 3-4: TCE concentrations in the USZ, 2008
This figure illustrates the measured TCE concentrations in micrograms per liter.

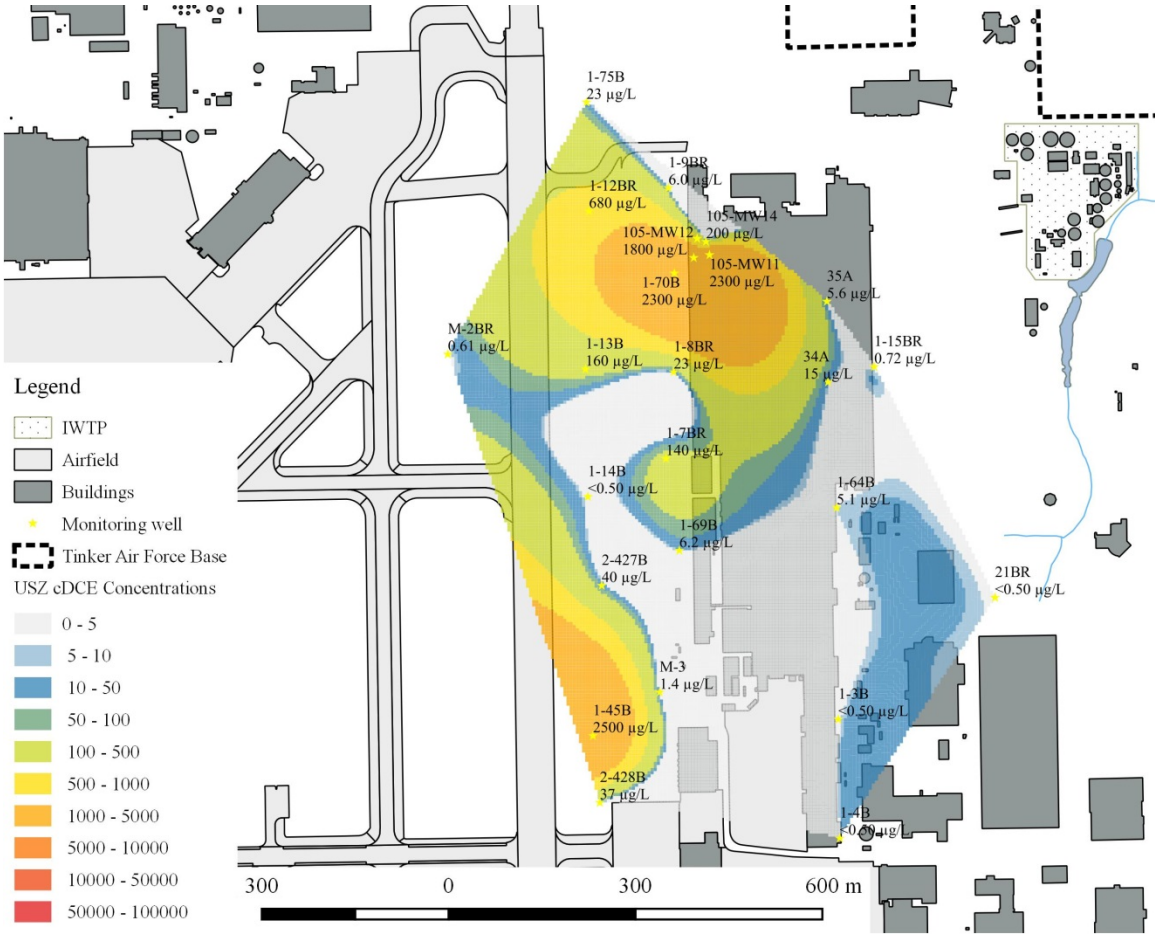

FIGURE 3-5: *cis*-DCE concentrations in the USZ, 2008
This figure illustrates the measured *cis*-DCE concentrations in micrograms per liter.

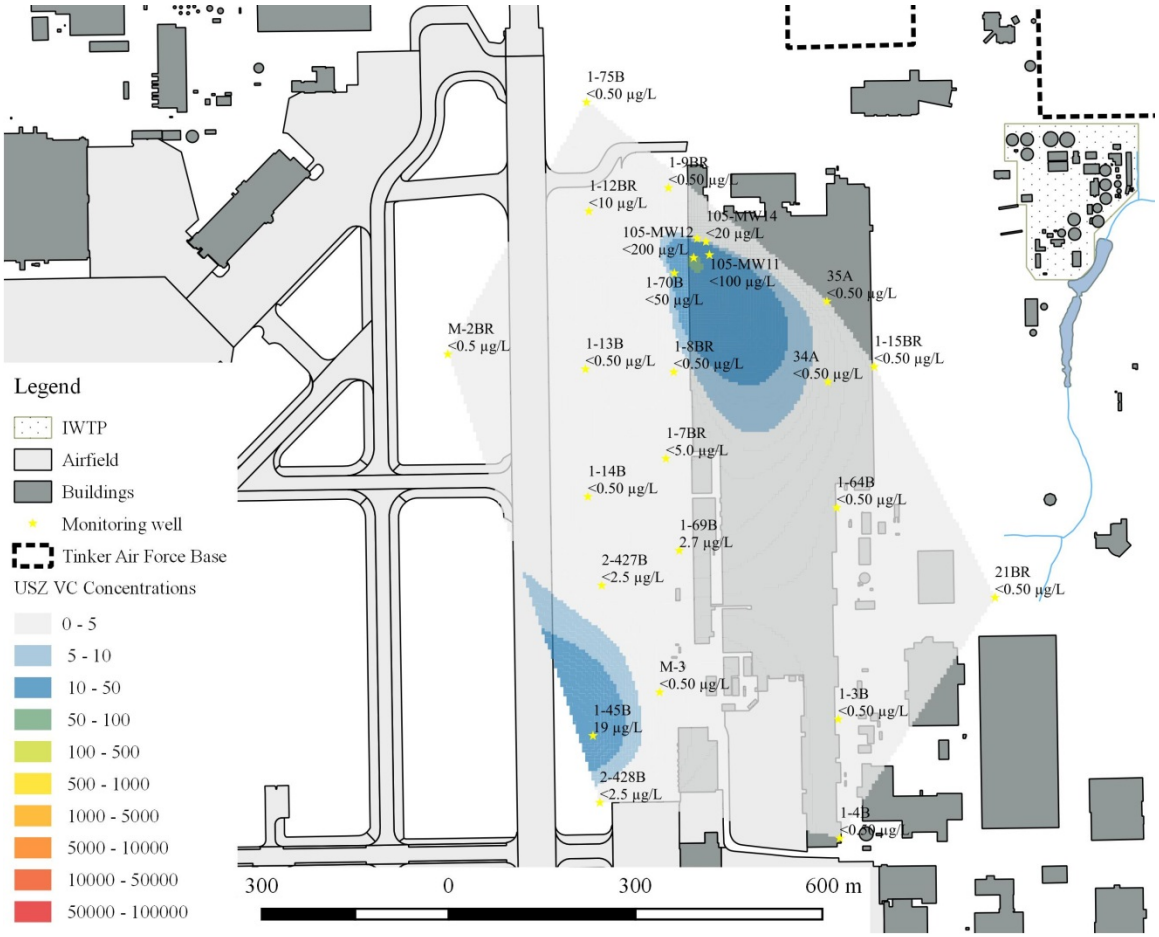

FIGURE 3-6: VC concentrations in the USZ, 2008
This figure illustrates the measured VC concentrations in micrograms per liter.

FIGURE 3-7: Ethene concentrations in the USZ, 2008
This figure illustrates the measured ethene concentrations in micrograms per liter.

3.4.1.1. Lower Saturated Zone Summary

Total chlorinated ethene concentrations were somewhat evenly distributed across the site. Chlorinated ethenes were reported at 33 of 35 monitoring wells and total chlorinated ethene concentrations ranged from 1.5 µg/L to 3,880 µg/L at 21AR and 2-277A, respectively (FIGURE 3-8). PCE was detected in 19 of 35 groundwater samples, ranging from 0.59 µg/L to 270 µg/L (FIGURE 3-9). TCE was detected in 33 of 35 groundwater samples, ranging from 1.5 µg/L to 3,500 µg/L (FIGURE 3-10). *cis*-DCE was detected in 30 of 35 groundwater samples, ranging from 0.68 µg/L to 1,000 µg/L (FIGURE 3-11). VC was detected in 8 of 35 groundwater samples, ranging from 0.63

µg/L to 51 µg/L (FIGURE 3-12). Ethene was detected in 3 of 35 groundwater samples, ranging from 0.532 J µg/L to 3.36 µg/L (FIGURE 3-13).

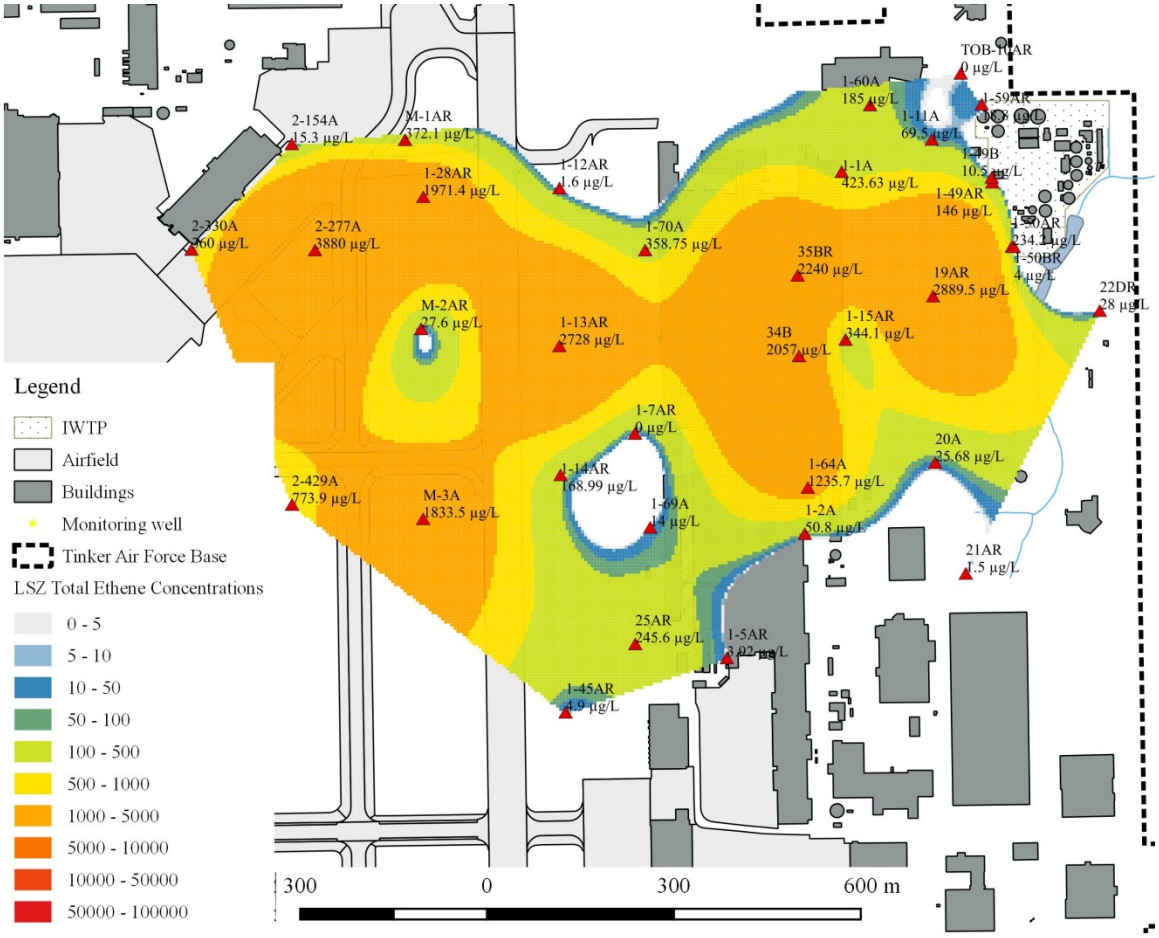

FIGURE 3-8: Total chlorinated ethene concentrations in the LSZ, 2008
This figure illustrates the sum of measured chlorinated ethene concentrations in micrograms per liter.

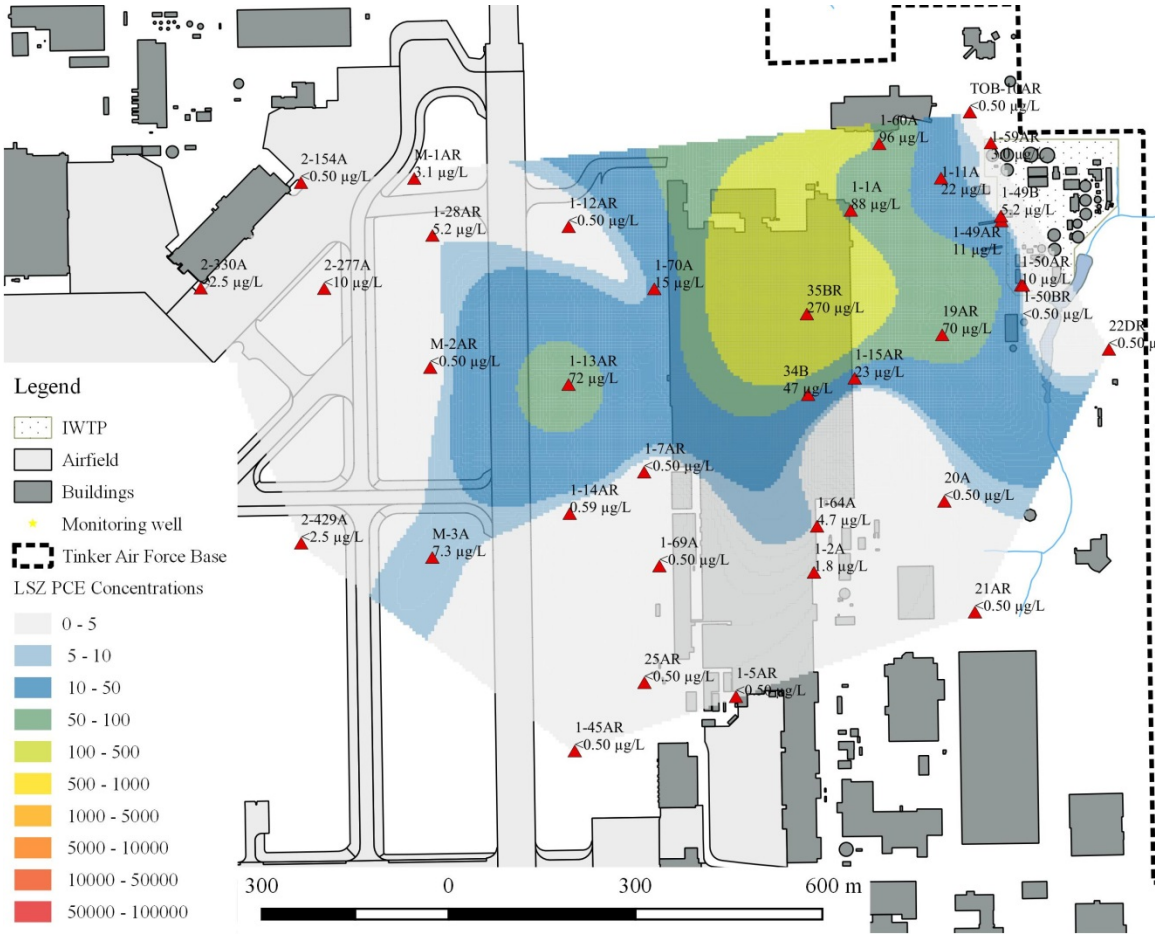

FIGURE 3-9: PCE concentrations in the LSZ, 2008
This figure illustrates the measured PCE concentrations in micrograms per liter.

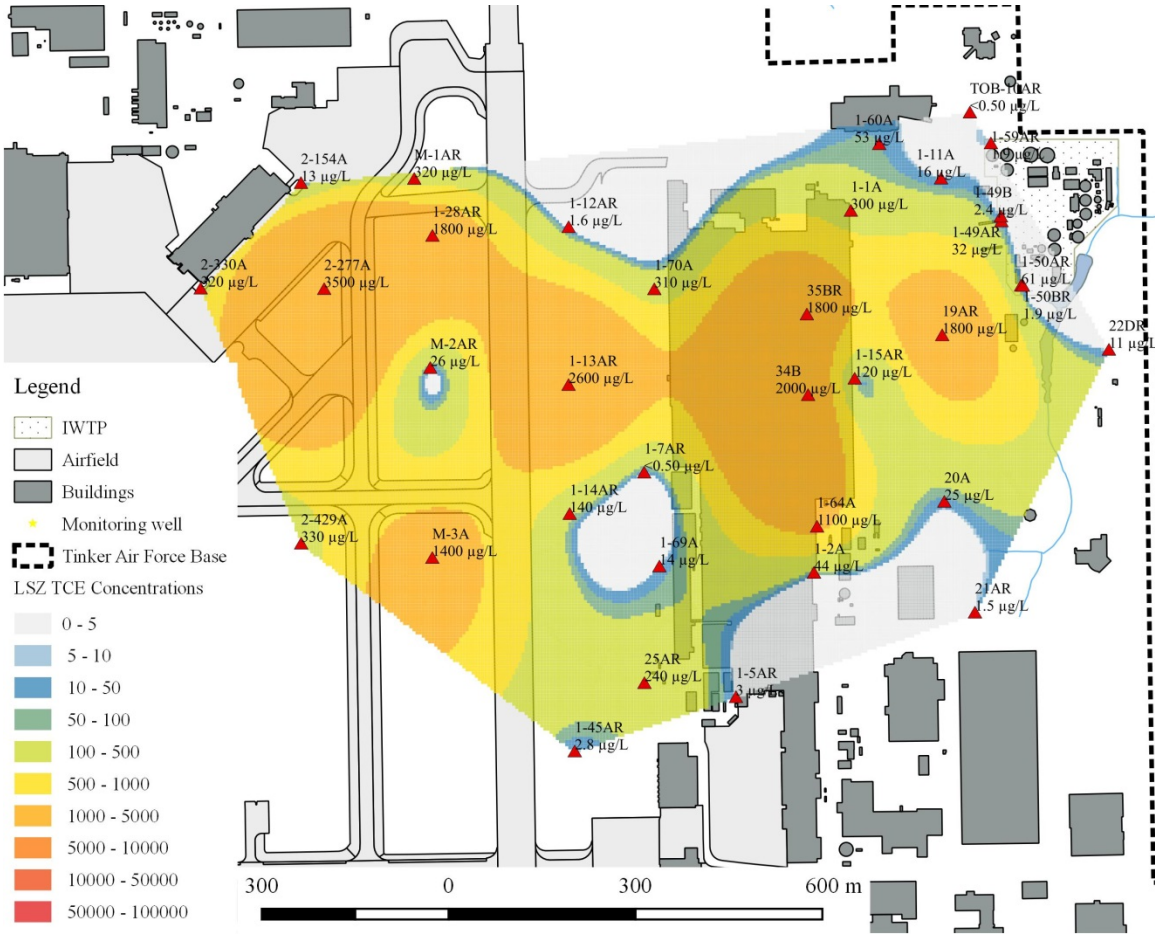

FIGURE 3-10: TCE concentrations in the LSZ, 2008
This figure illustrates the measured TCE concentrations in micrograms per liter.

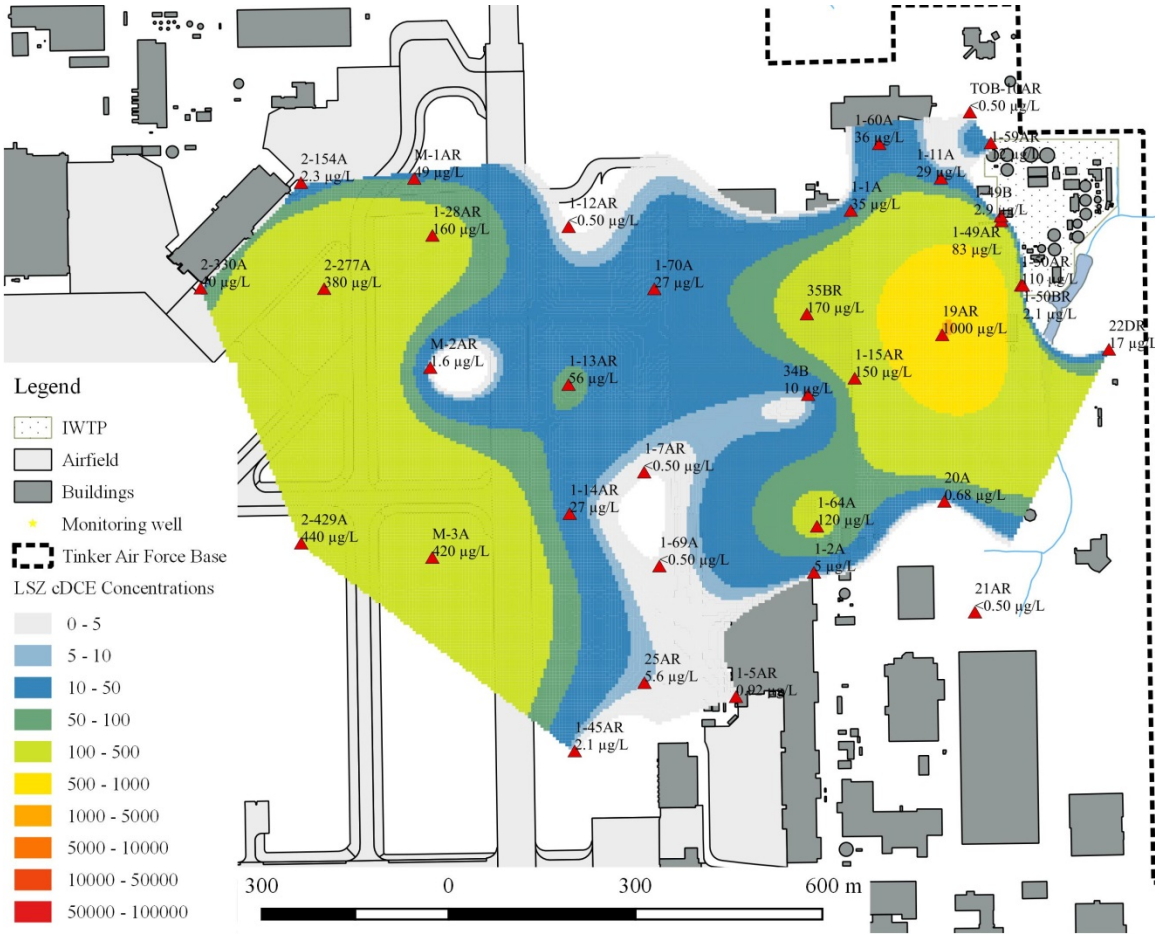

FIGURE 3-11: *cis*-DCE concentrations in the LSZ, 2008
This figure illustrates the measured *cis*-DCE concentrations in micrograms per liter.

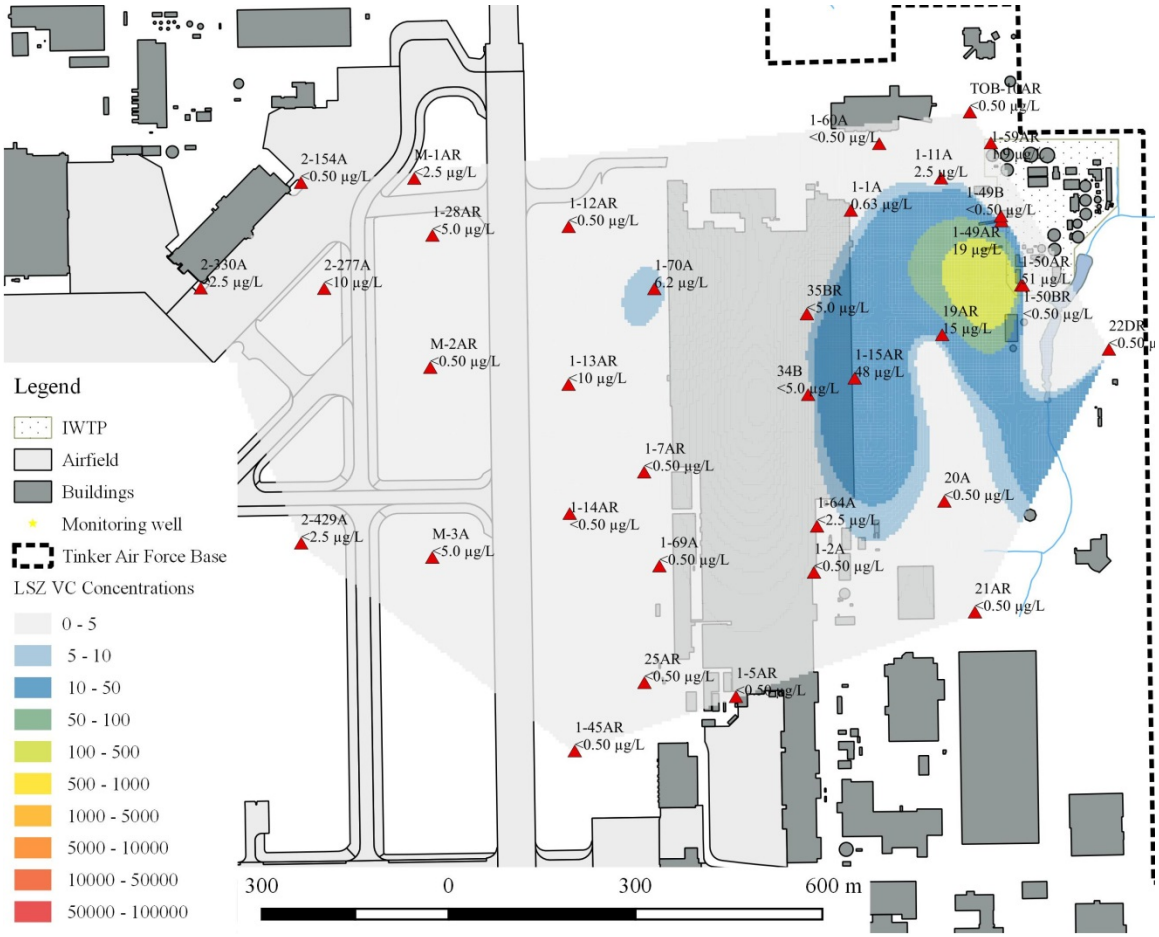

FIGURE 3-12: VC concentrations in the LSZ, 2008
This figure illustrates the measured VC concentrations in micrograms per liter.

FIGURE 3-13: Ethene concentrations in the LSZ, 2008
This figure illustrates the measured ethene concentrations in micrograms per liter.

3.4.1.1. Lower-lower Saturated Zone Summary

Total chlorinated ethene concentrations were somewhat evenly distributed across the site with the exception of two "hotspots" at 35C and 1-8A. Chlorinated ethenes were reported at all 28 monitoring wells and total chlorinated ethene concentrations ranged from 0.72 µg/L to 5,098.2 µg/L at 1-13CR and 35C, respectively (FIGURE 3-14). PCE was detected in 15 of 28 groundwater samples, ranging from 0.57 µg/L to 1,600 µg/L (FIGURE 3-15). TCE was detected in all 28 groundwater samples, ranging from 0.72 µg/L to 4,100 µg/L (FIGURE 3-16). *cis*-DCE was detected in 27 of 28 groundwater samples, ranging from 0.6 µg/L to 2,500 µg/L (FIGURE 3-17). VC was detected in 6 of

28 groundwater samples, ranging from 3.1 µg/L to 300 µg/L (FIGURE 3-18). Ethene was detected in 3 of 28 groundwater samples, ranging from 0.282 J µg/L to 7.28 µg/L (FIGURE 3-19).

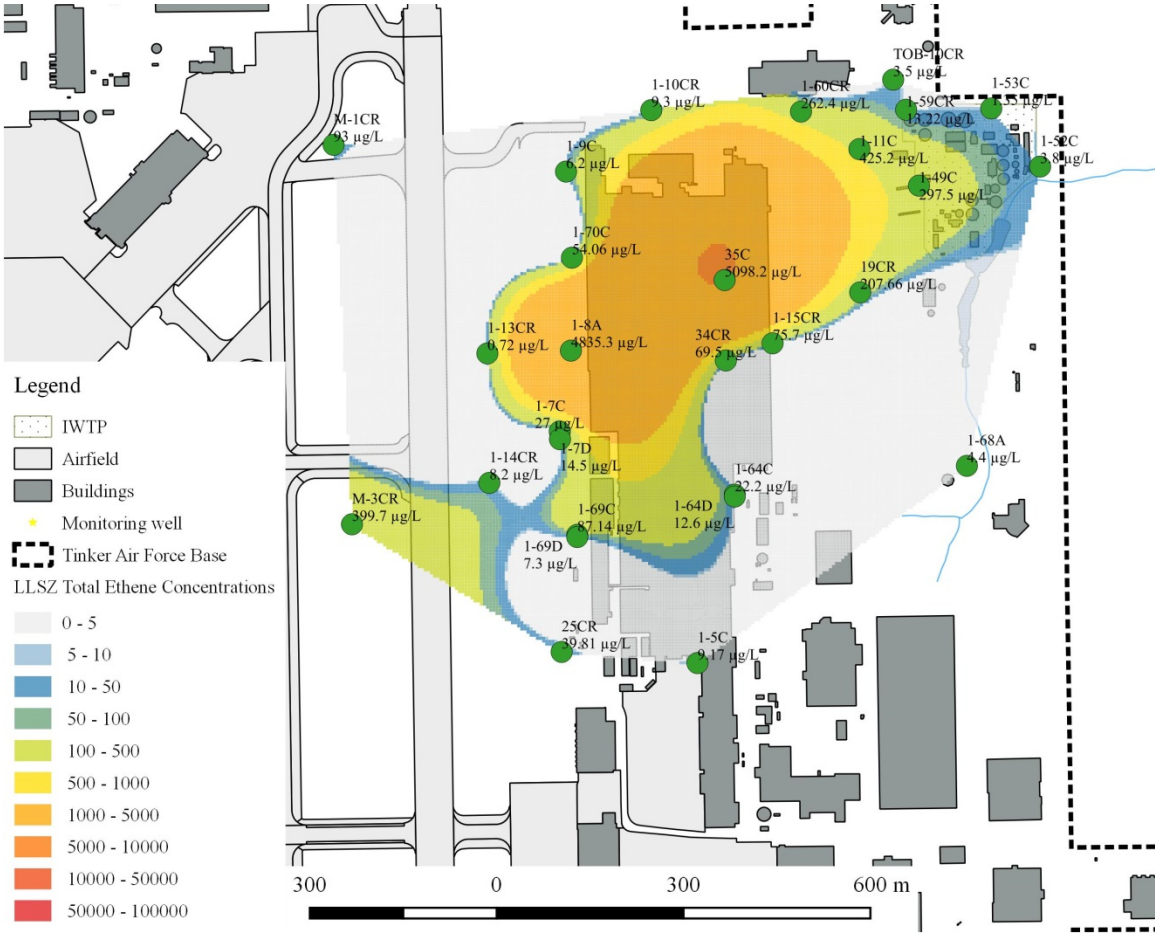

FIGURE 3-14: Total chlorinated ethene concentrations in the LLSZ, 2008
This figure illustrates the sum of measured chlorinated ethene concentrations in micrograms per liter.

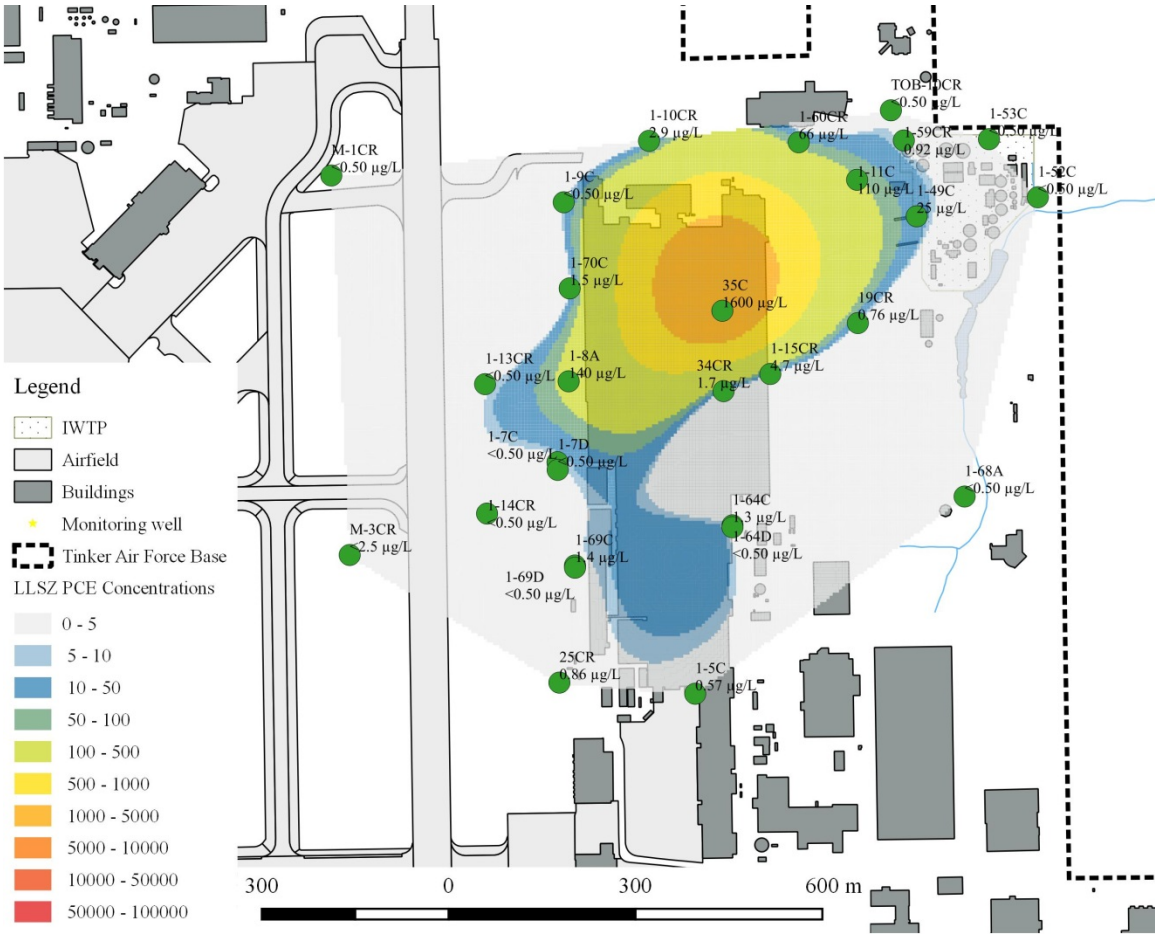

FIGURE 3-15: PCE concentrations in the LLSZ, 2008
This figure illustrates the measured PCE concentrations in micrograms per liter.

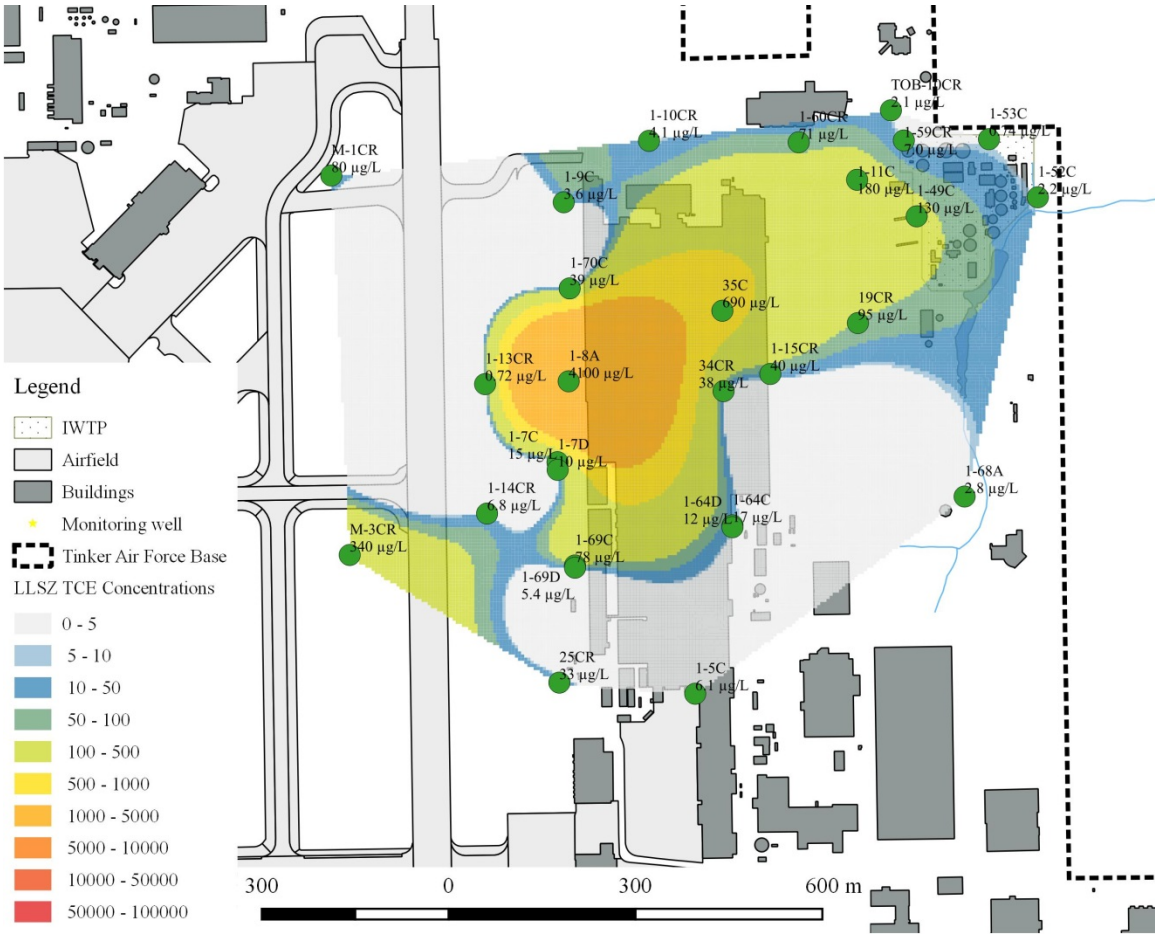

FIGURE 3-16: TCE concentrations in the LLSZ, 2008
This figure illustrates the measured TCE concentrations in micrograms per liter.

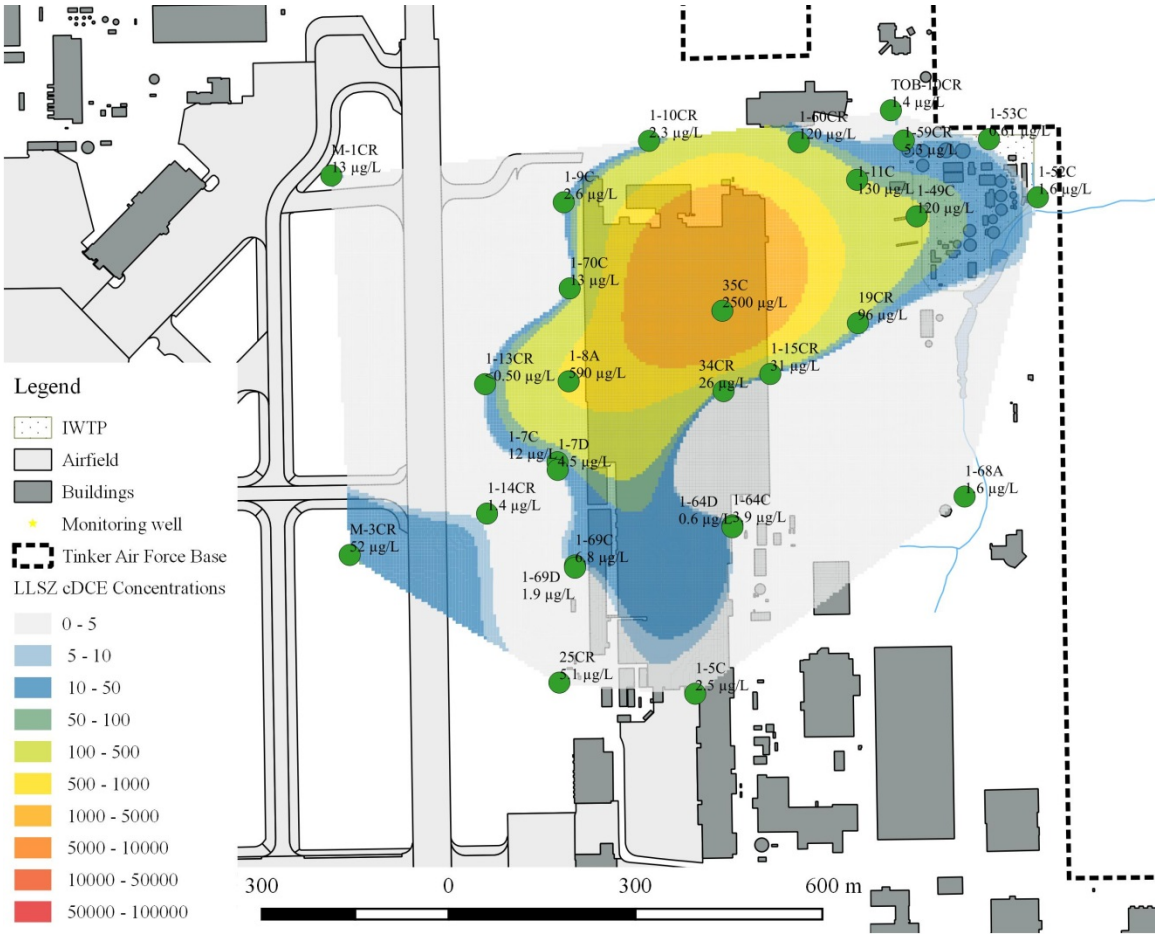

FIGURE 3-17: *cis*-DCE concentrations in the LLSZ, 2008
This figure illustrates the measured *cis*-DCE concentrations in micrograms per liter.

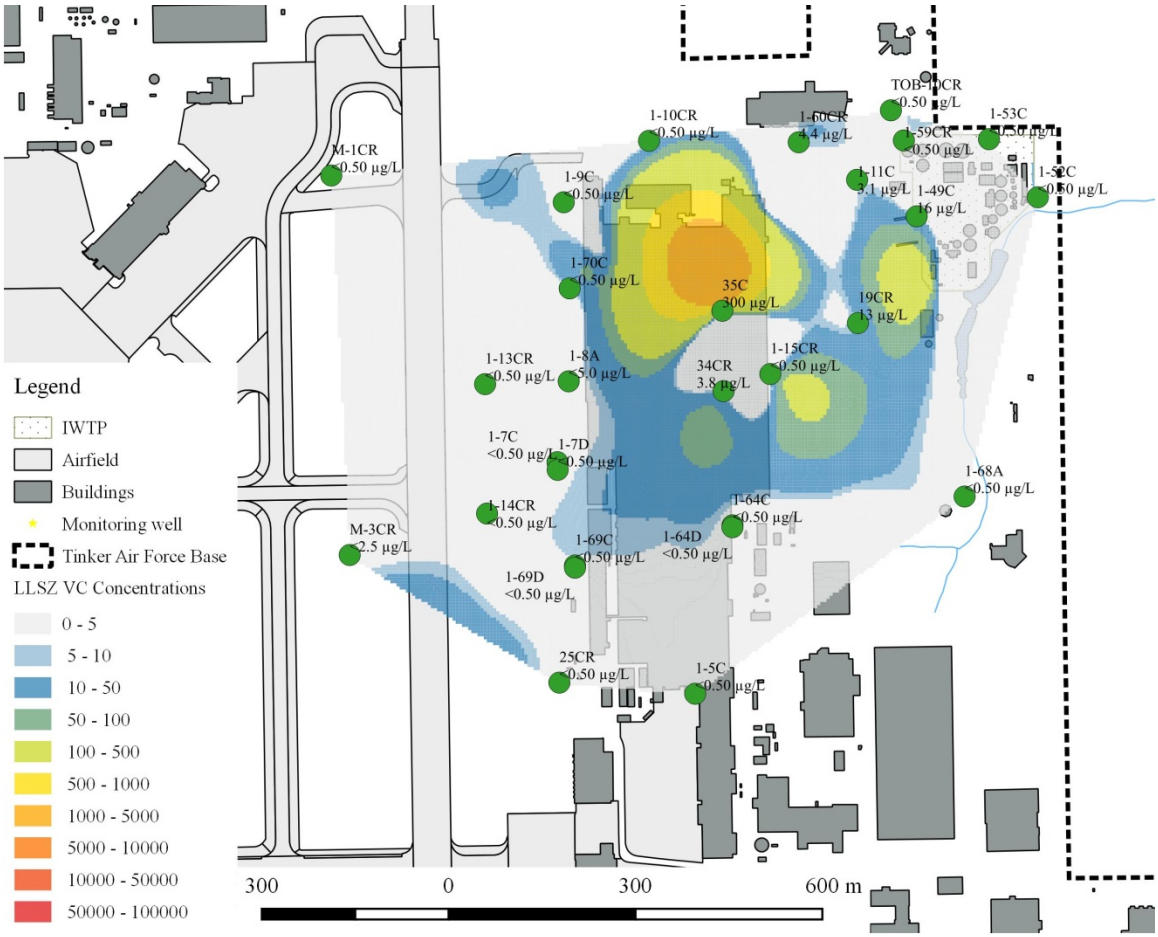

FIGURE 3-18: VC concentrations in the LLSZ, 2008
This figure illustrates the measured VC concentrations in micrograms per liter.

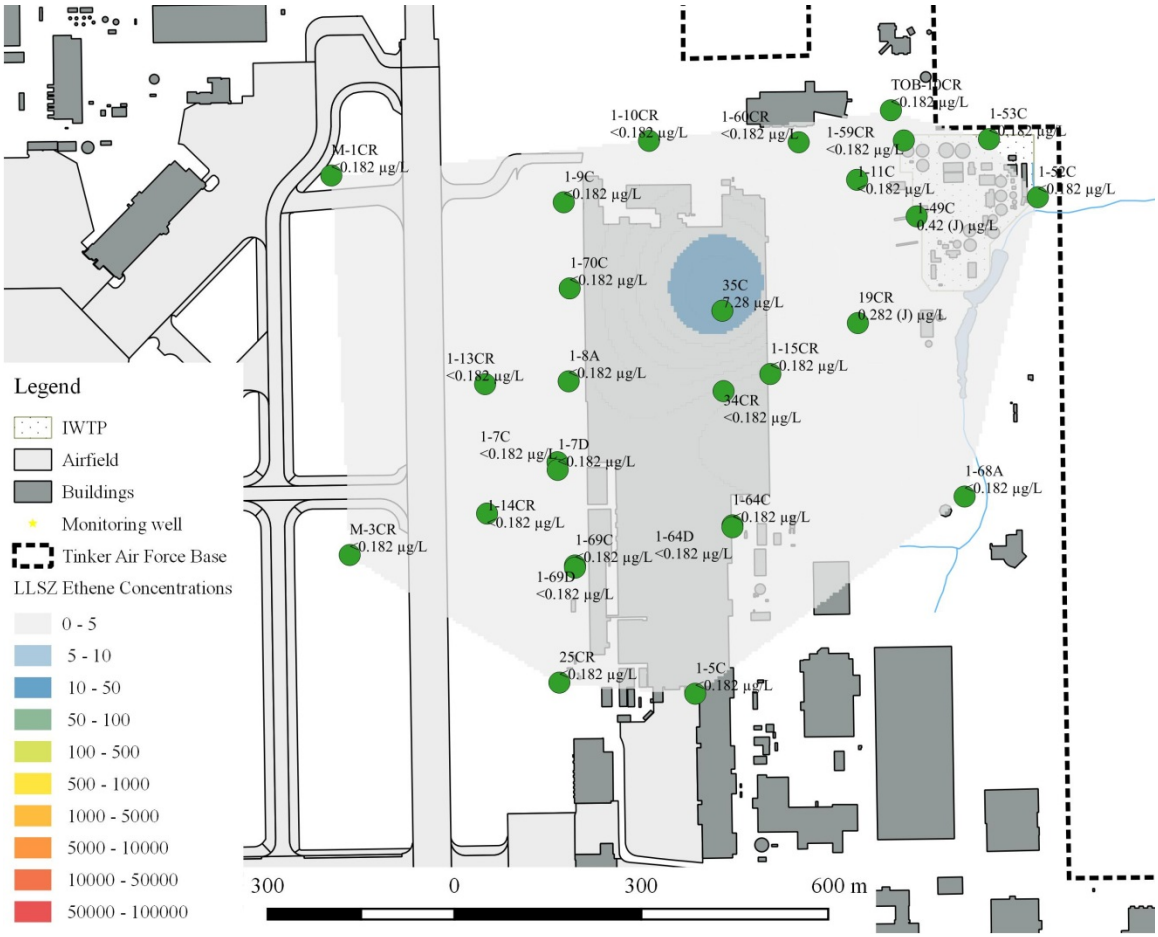

FIGURE 3-19: Ethene concentrations in the LLSZ, 2008
This figure illustrates the measured ethene concentrations in micrograms per liter.

3.4.2. Chlorinated Ethene Concentration Trends

Based on a comparison of reported concentrations from the late 1980's to those from samples collected in 2006 and 2008, the remediation pumping from 1994 to 2004 appears to have removed or redistributed the chlorinated ethene mass from or within the USZ, LSZ, and LLSZ under Building 3001; it's also possible some natural remediation occurred, as well. Ten monitoring wells were sampled in 2006 and 2008; three are screened in the USZ, four are screened in the LSZ and three are screened in the LLSZ. The concentrations between the sampling events varied across the site with some

increases or decreases in concentration, although generally, not by an order of magnitude. Those data are provided in TABLE 3-2.

A subset of chemical analytical results were selected from groundwater samples collected in 1988 and 1989, prior to operation of the pump-and-treat system, for comparison to samples collected in 2006 and 2008. Total chlorinated ethene mass appears to have decreased by an order of magnitude in the USZ near monitoring well nests 34 and 35 but, remained about the same near monitoring well nest 1-70. In the LSZ, mass appears to have decreased by an order of magnitude at monitoring well nest 1-70 but, to a lesser extent at monitoring well nests 34 and 35. In the LLSZ, mass appears to have significantly decreased at monitoring well nests 1-70 and 34 but, has increased by an order of magnitude at monitoring well nest 35.

TABLE 3-2: Historical chlorinated ethene concentrations at select monitoring wells

			Concentration (µg/L)[6,7,8,9]					
Year	**Well ID[5]**	**Aquifer Zone**	**PCE**	**TCE**	***cis*-DCE**	***trans*-DCE**	**VC**	**~Total Mass[10]**
1988	34A	USZ	<25	**310,000**	nm	nm	<50	**310,000**
1989			<6,300	**230,000**	nm	<5,000	<13,000	**230,000**
2006			**89 J**	**3,900**	<11	<7.0	<35	**3,989**
2008			**160**	**4,400**	**15**	<1.3	<5.5	**4,575**
1988	33A	USZ	<2,500	**72,000**	nm	<2,500	<5,000	**52,000**
1989			<5,000	**186,913**	nm	<5,000	<10,000	**150,000**
2006	1-70B		**7,700**	**51,000**	**1,800**	<28	<140	**60,500**
2008			**5,100**	**59,000**	**2,300**	**120**	<28	**66,520**
1988	1-15B	USZ	<5	**200**	nm	**36**	<10	**236**
1989			nm	nm	nm	nm	nm	nm

[5] Monitoring wells 1-15B, 1-15A, 1-15C, 34C and 35B were replaced between 1989 and 2006. Replacement monitoring wells are identified with a "R" following the well identification.
[6] Non-bolded values indicate the analyte was analyzed for, but not detected above the level of the associated laboratory reporting limit (RL). The laboratory method detection limit (MDL) is indicated along with the "<" symbol.
[7] Bold concentration values indicate the analyte was detected above the level of the associated RL.
[8] Values reported along with "J" indicate the analyte was positively identified. However, the associated numerical value is an approximate concentration of the analyte in the sample.
[9] Ethene was measured only in 2008, thus it was excluded from this table.
[10] Total concentration values include only those analytes with concentrations detected above the level of the associated RL.

Year	Well ID[5]	Aquifer Zone	Concentration (µg/L)[6,7,8,9] PCE	TCE	*cis*-DCE	*trans*-DCE	VC	~Total Mass[10]
2006	1-15BR		nm	nm	nm	nm	nm	nm
2008			**1.3**	**24**	**0.72**	<0.066	<0.28	**26**
1988	35A	USZ	<31	**940**	nm	**60**	<63	**1,006**
1989			<31	**1,149**	nm	**88**	<63	**1,237**
2006			nm	nm	nm	nm	nm	nm
2008			**19**	**69**	**5.6**	<0.066	<0.28	**94**
1988	34B	LSZ	<500	**11,000**	nm	<500	<1,000	**11,000**
1989			**26**	**3,377**	nm	**96**	<200	**3,499**
2006			nm	nm	nm	nm	nm	nm
2008			**47**	**2,000**	**10**	<0.66	<2.8	**2,057**
1988	33B	LSZ	**510**	**7,100**	nm	<250	<500	**7,610**
1989			**570**	**9,100**	nm	<310	<630	**9,670**
2006	1-70A		**13**	**510**	**76**	<0.70	**17 J**	**616**
2008			**15**	**310**	**27**	**0.55**	**6.2**	**359**
1988	1-15A	LSZ	<25	**670**	nm	**41**	<50	**711**
1989			nm	nm	nm	nm	nm	nm
2006	1-15AR		nm	nm	nm	nm	nm	nm
2008			**23**	**120**	**150**	**3.1**	**48**	**344**
1988	35B	LSZ	<250	**2,600**	nm	<250	<500	**7,350**
1989			<250	**9,465**	nm	**234**	<500	**6,740**
2006	35BR		**290**	**1,800**	**160**	<7.0	<35	**2,250**
2008			**270**	**1,800**	**170**	<0.66	<2.8	**2,240**
1988	34C	LLSZ	**25**	**680**	nm	**56**	<50	**761**
1989			**6**	**132**	nm	**53**	**3**	**194**
2006	34CR		nm	nm	nm	nm	nm	nm
2008			**1.7**	**38**	**26**	<0.066	**3.8**	**70**
1988	33C	LLSZ	<250	**3,900**	nm	<250	<500	**3,900**
1989			**5**	**454**	nm	<17	<33	**459**
2006	1-70C		nm	nm	nm	nm	nm	nm
2008			**1.5**	**39**	**13**	**0.56**	<0.28	**54**
1988	1-15C	LLSZ	<5	**180**	nm	**21**	<10	**201**
1989			nm	nm	nm	nm	nm	nm
2006	1-15CR		nm	nm	nm	nm	nm	nm
2008			**4.7**	**40**	**31**	<0.066	<0.28	**76**
1988	35C	LLSZ	<13	**300**	nm	<13	<25	**300**
1989			<13	**314**	nm	**181**	<25	**495**
2006			nm	nm	nm	nm	nm	nm
2008			**1,600**	**690**	**2,500**	**8.2**	**300**	**5,098**

Abbreviations/symbols: µg/L, micrograms per liter; PCE, tetrachloroethylene; TCE, trichloroethylene; *cis*-DCE, *cis*-1,2-dichloroethylene; *trans*-DCE, *trans*-1,2-dichloroethylene; VC, vinyl chloride; nm, not measured

Three monitoring wells in the USZ were sampled in 2006 and 2008; 34A, 1-70B, and 2-428B (TABLE 3-3). At monitoring well 34A, PCE increased from 89 J µg/L to 160 µg/L, TCE increased from 3,900 µg/L to 4,400 µg/L, *cis*-DCE was detected at 15

μg/L (previously non-detect), *trans*-DCE and VC were not detected, and ethene was not measured in 2006 and not detected in 2008. At monitoring well 1-70B, PCE decreased from 7,700 μg/L to 5,100 μg/L, TCE increased from 51,000 μg/L to 59,000 μg/L, *cis*-DCE increased from 1,800 μg/L to 2,300 μg/L, *trans*-DCE was detected at 120 μg/L (previously non-detect), VC was not detected, and ethene was not measured in 2006 and not detected in 2008. At monitoring well 2-428B, PCE decreased from 530 μg/L to 140 μg/L, TCE decreased from 1,000 μg/L to 220 μg/L, *cis*-DCE decreased from 120 μg/L to 37 μg/L, *trans*-DCE and VC were not detected, and ethene was not measured in 2006 and not detected in 2008.

TABLE 3-3: Chlorinated ethane concentration[11,12,13] and isotopic values[14,15] comparison

Well ID	Date	PCE	TCE	*cis*-DCE	*trans*-DCE	VC	Ethene
34A	2006	**89 J**	**3,900**	<11	<7.0	<35	NM
(USZ)		-29.9	-25.6	-23.5	nm	na	na
	2008	**160**	**4,400**	**15**	<1.3	<5.5	<0.182
		-29.5	-26.3	-24.8	nm	na	na
1-70B	2006	**7,700**	**51,000**	**1,800**	<28	<140	NM
(USZ)		-30.4	-23.2	-22.9	nm	-21.9	-24.2
	2008	**5,100**	**59,000**	**2,300**	**120**	<28	<0.182
		-30.8	-24.5	-24.3	nm	-19.5	na
2-428B	2006	**530**	**1,000**	**120**	<7.0	<35	NM
(USZ)		-24.8	-22.4	-21.2	nm	na	na
	2008	**140**	**220**	**37**	<0.33	<1.4	<0.182
		-25.2	-23.1	-22.4	nm	na	na
19AR	2006	**97**	**1,800**	**1,100**	<0.70	**11 J**	NM
(LSZ)		-25.9	-24.1	-23.6	nm	-31.8	na

[11] Non-bolded values indicate the analyte was analyzed for, but not detected above the level of the associated laboratory reporting limit (RL). The laboratory method detection limit (MDL) is indicated along with the "<" symbol.

[12] Bold concentration values indicate the analyte was detected above the level of the associated reporting limit.

[13] Values reported along with "J" indicate the analyte was positively identified. However, the associated numerical value is an approximate concentration of the analyte in the sample.

[14] The average standard deviations of replicate analysis for PCE, TCE, cis-DCE, VC and ethene were 0.3 ‰, 0.2 ‰, 0.2 ‰, 0.3 ‰, and 0.1 ‰, respectively.

[15] Isotopic results reported as "na" indicate the peak was not acquired, meaning the compound peak was below detection limit for isotopic analysis. Isotopic results reported as "nm" indicate they were not measured.

Well ID	Date	PCE	TCE	*cis*-DCE	*trans*-DCE	VC	Ethene
	2008	**70**	**1,800**	**1,000**	**4.5**	**15**	<0.182
		-27.1	-24.6	-24.9	nm	-29.4	na
1-70A (LSZ)	2006	**13**	**510**	**76**	<0.70	**17 J**	NM
		-30.6	-23.5	-21.4	nm	-19.0	-24.2
	2008	**15**	**310**	**27**	**0.55**	**6.2**	<0.182
		-30.9	-24.0	-22.2	nm	-19.5	-20.7
35BR (LSZ)	2006	**290**	**1,800**	**160**	<7.0	<35	NM
		-27.6	-25.2	-24.8	nm	-16.1	na
	2008	**270**	**1,800**	**170**	<0.66	<2.8	<0.182
		-27.5	-25.9	-26.4	nm	-14.7	na
1-1A (LSZ)	2006	**74**	**270**	**24**	<0.70	<3.5	NM
		-30.0	-25.5	-21.1	nm	-15.3	na
	2008	**88**	**300**	**35**	<0.066	**0.63**	<0.182
		-30.9	-26.3	-21.7	nm	-16.8	na
1-8A (LLSZ)	2006	**120**	**2,200**	**140**	<7.0	<35	NM
		-27.7	-23.8	-24.1	nm	na	na
	2008	**140**	**4,100**	**590**	**5.3**	<2.8	<0.182
		-27.8	-24.9	-25.6	nm	na	na
1-49C (LLSZ)	2006	**16**	**160**	**120**	<0.70	8.4 J	NM
		-27.9	-17.8	-15.4	nm	-23.1	-24.6
	2008	**25**	**130**	**120**	**6.5**	**16**	**0.42 J**
		-28.0	-18.3	-16.5	nm	-24.3	na
19CR (LLSZ)	2006	**50**	**540**	**98**	<0.70	**6.4 J**	NM
		-30.4	-22.5	-17.3	nm	-20.4	-20.2
	2008	**0.76**	**95**	**96**	**2.9**	**13**	**0.282 J**
		na	-18.8	-17.9	nm	-19.8	-20.0

Abbreviations/symbols: µg/L, micrograms per liter; $\delta^{13}C$ (‰), isotopic ratio of ^{13}C permil; PCE, tetrachloroethylene; TCE, trichloroethylene; *cis*-DCE, *cis*-1,2-dichloroethylene; *trans*-DCE, *trans*-1,2-dichloroethylene;VC, vinyl chloride

Four monitoring wells in the LSZ were sampled in 2006 and 2008; 19AR, 1-70A, 35BR, and 1-1A (TABLE 3-3). At monitoring well 19AR, PCE decreased from 97 µg/L to 70 µg/L, TCE remained stable at 1,800 µg/L, *cis*-DCE decreased from 1,100 µg/L to 1,000 µg/L, *trans*-DCE was detected at 4.5 µg/L (previously non-detect), VC increased from 11 J µg/L to 15 µg/L, and ethene was not measured in 2006 and not detected in 2008. At monitoring well 1-70A, PCE increased from 13 µg/L to 15 µg/L, TCE decreased from 510 µg/L to 310 µg/L, *cis*-DCE decreased from 76 µg/L to 27 µg/L, *trans*-DCE was detected at 0.55 µg/L (previously non-detect), VC decreased from 17 J µg/L to 6.2 µg/L, and ethene was not measured in 2006 and not detected in 2008. At

monitoring well 35BR, PCE decreased from 290 μg/L to 270 μg/L, TCE remained stable at 1,800 μg/L, *cis*-DCE increased from 160 μg/L to 170 μg/L, *trans*-DCE and VC were not detected, and ethene was not measured in 2006 and not detected in 2008. At monitoring well 1-1A, PCE increased from 74 μg/L to 88 μg/L, TCE increased from 270 μg/L to 300 μg/L, *cis*-DCE increased from 24 μg/L to 35 μg/L, *trans*-DCE was not detected, VC was detected at 0.63 μg/L (previously non-detect), and ethene was not measured in 2006 and not detected in 2008.

Three monitoring wells in the LLSZ were sampled in 2006 and 2008; 1-8A, 1-49C, and 19CR (TABLE 3-3). At monitoring well 1-8A, PCE increased from 120 μg/L to 140 μg/L, TCE increased from 2,200 μg/L to 4,100 μg/L, *cis*-DCE increased from 140 μg/L to 590 μg/L, *trans*-DCE was detected at 5.3 μg/L (previously non-detect), VC was not detected, and ethene was not measured in 2006 and not detected in 2008. At monitoring well 1-49C, PCE increased from 16 μg/L to 25 μg/L, TCE decreased from 160 μg/L to 130 μg/L, *cis*-DCE remained stable at 120 μg/L, *trans*-DCE was detected at 6.5 μg/L (previously non-detect), VC increased from 8.4 J μg/L to 16 μg/L, and ethene was not measured in 2006 and was detected at 0.42 J μg/L in 2008. At monitoring well 19CR, PCE decreased from 50 μg/L to 0.76 μg/L, TCE decreased from 540 μg/L to 95 μg/L, *cis*-DCE decreased from 98 μg/L to 96 μg/L, *trans*-DCE was detected at 2.9 μg/L (previously non-detect), VC increased from 6.4 J μg/L to 13 μg/L, and ethene was not measured in 2006 and was detected at 0.282 μg/L in 2008.

3.4.3. Chlorinated Ethene Mole Fractions

Constituent concentrations for PCE, TCE, *cis*-DCE, *trans*-DCE, VC and ethene from each monitoring well sampled in 2008 were converted to mole fractions to evaluate

relative chlorinated ethene contribution of each constituent to total molar concentration of chlorinated ethenes at each monitoring well location. Constituent concentrations reported as non-detect or less than the analytical method detection limit (<MDL) were converted to one half the MDL value for calculation purposes. Concentration and mole fraction data for select monitoring wells are graphically illustrated on FIGURE 3-20 through FIGURE 3-22.

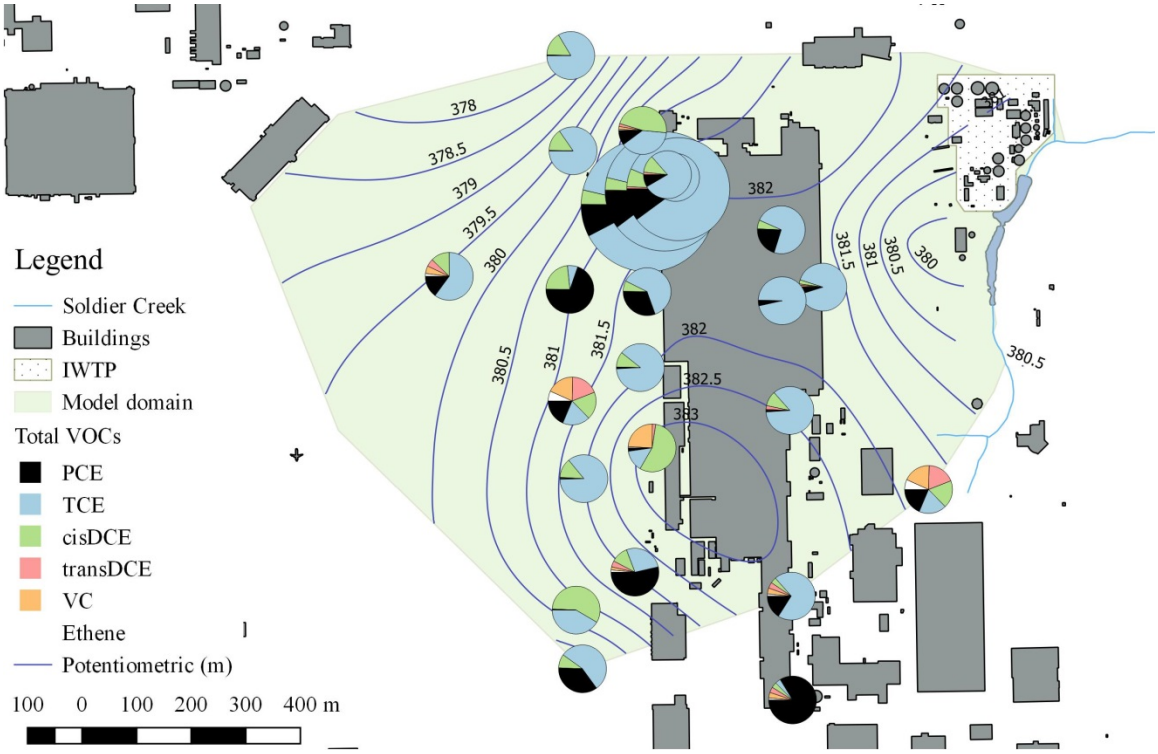

FIGURE 3-20: USZ potentiometric surface and chlorinated ethene composition, 2008
Map illustrating groundwater potentiometric surfaces and chlorinated ethene composition in the USZ within the study area. The pie chart size approximates the range of the total chlorinated ethene concentration in µg/L and relative concentrations of those constituents at select monitoring wells. Potentiometric surfaces are contoured at 0.5 m intervals. The USZ does not exist at the IWTP.

TCE is the primary chlorinated ethene, based on mole fraction, across the site and within all aquifer units. In the USZ, TCE makes up an estimated 70% of chlorinated

ethenes in all but 6 out of 24 locations, where PCE and *cis*-DCE contribute a significant fraction. In the LSZ, TCE is similarly dominant at all locations except in 11 out of 33 locations, where *cis*-DCE, and to a lesser degree PCE, contributes a significant fraction. In the LLSZ, TCE and *cis*-DCE contribute rather evenly to make up the majority of chlorinated ethene mass at all locations except 1-13CR, where VC and ethene contribute a significant fraction. The prevalence of *cis*-DCE at monitoring well 1-9BR suggests unique location-specific transformation conditions may exist. Likewise, the high molar concentration of PCE at 1-13B may suggest a location-specific source contribution.

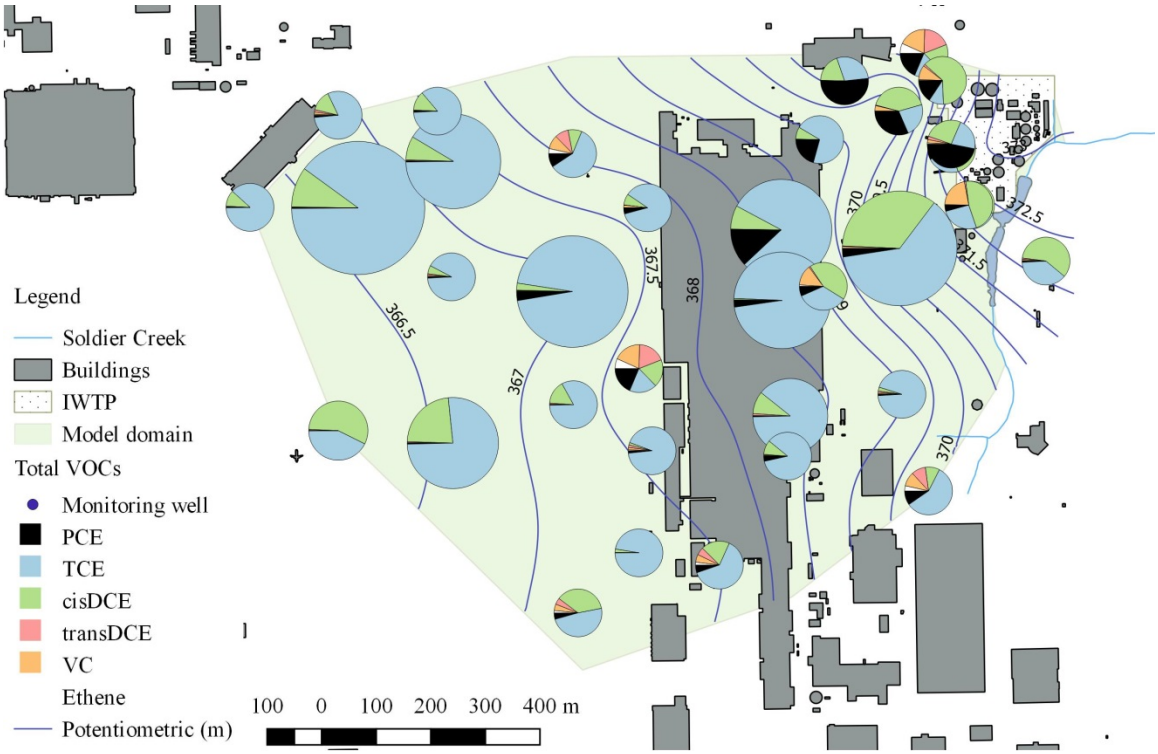

FIGURE 3-21: LSZ potentiometric surface and chlorinated ethene composition, 2008
Map illustrating groundwater potentiometric surfaces and chlorinated ethene composition in the LSZ within the study area. The pie chart size approximates the range of the total chlorinated ethene concentration in µg/L and relative concentrations of those constituents at select monitoring wells. Potentiometric surfaces are contoured at 0.5 m intervals.

Chlorinated ethenes associated with the IWTP appear to have experienced greater transformation processes in the LSZ than those originating from Building 3001. In the LSZ, *cis*-DCE represents a significant portion of chlorinated ethene concentration at monitoring wells located east of Building 3001. Underneath and to the west of Building 3001, TCE is the most prevalent chlorinated ethene species, except at monitoring well 1-12AR. PCE contributes significant mass at monitoring wells 1-49B, 1-11A, 1-1A, and 35BR, which indicates a significant portion of original source contaminant is still present at those locations. In the LLSZ, *cis*-DCE and TCE appear to be the most prevalent chlorinated ethene species. Ethene is also present at a much greater molar concentration than in the USZ or LSZ. These data suggest that transformation may be occurring across the study area. Interestingly, PCE contributes a significant portion of mass at monitoring wells 35C, 1-11C, 1-10CR and 1-60CR, which is somewhat unexpected for the LLSZ, where greater transformation would be anticipated. These data may represent vertical migration of original source contaminant (via poor well conditions or unknown pathways) from the USZ and LSZ.

Constituent concentrations for PCE, TCE, *cis*-DCE, *trans*-DCE, VC and ethene from each monitoring well were converted to mole fractions to evaluate relative chlorinated ethene contribution of each constituent to total molar concentration of chlorinated ethenes at each monitoring well location. Constituent concentrations reported as non-detect or <MDL were converted to one half the MDL value for calculation purposes. Those data are illustrated on FIGURE 3-23 through FIGURE 3-25.

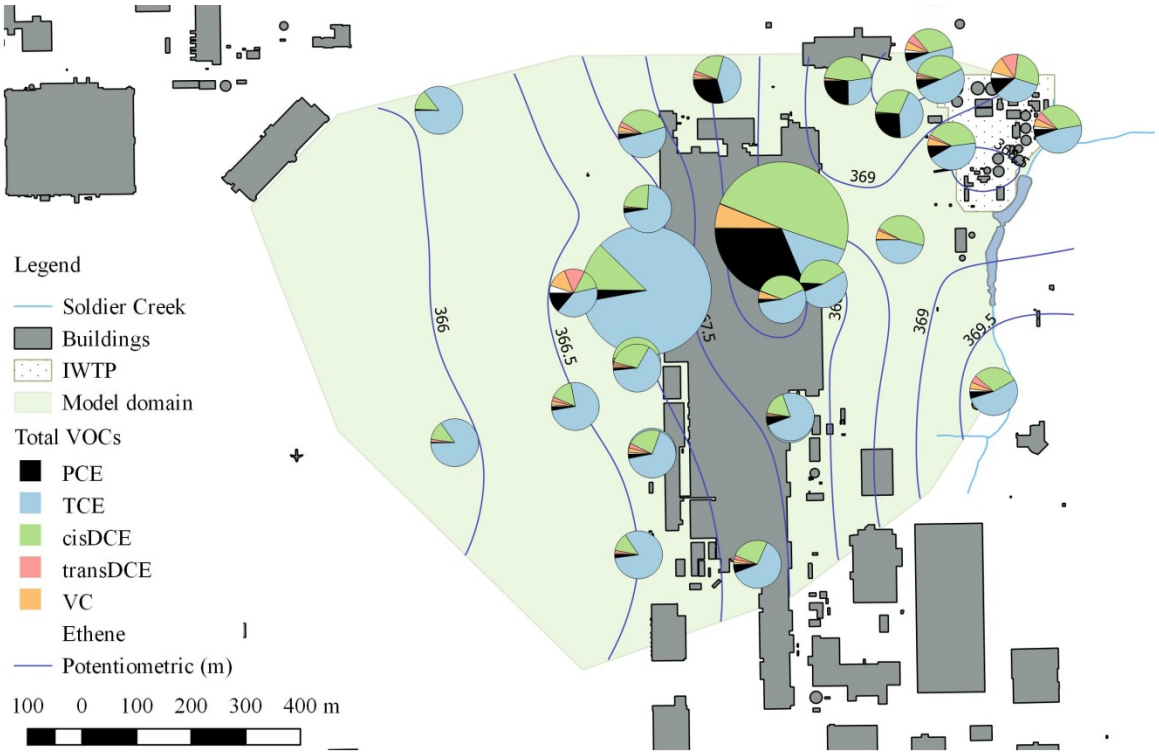

FIGURE 3-22: LLSZ potentiometric surface and chlorinated ethene composition, 2008
Map illustrating groundwater potentiometric surfaces and chlorinated ethene composition in the LLSZ within the study area. The pie chart size approximates the range of the total chlorinated ethene concentration in µg/L and relative concentrations of those constituents at select monitoring wells. Potentiometric surfaces are contoured at 0.5 m intervals.

TCE is the primary chlorinated ethene, based on mole fraction, across the site and within all aquifer units. In the USZ, TCE makes up an estimated 70% of the chlorinated ethenes at all locations except 1-4B, 1-9BR, 1-13B, 1-14B, 1-45B, 1-69B and M-3, where PCE and *cis*-DCE contribute a significant fraction. In the LSZ, TCE is similarly dominant at all locations except 22DR, 1-11A, 1-15AR, 1-49AR, 1-49B, 1-50AR, 1-50BR, 1-59AR, and 1-60A, where *cis*-DCE (and to a lesser degree PCE) contributes a significant fraction. In the LLSZ, TCE and *cis*-DCE contribute rather evenly to make up the majority of the chlorinated ethene mass at all locations except 1-13CR, where ethene contributes a significant fraction.

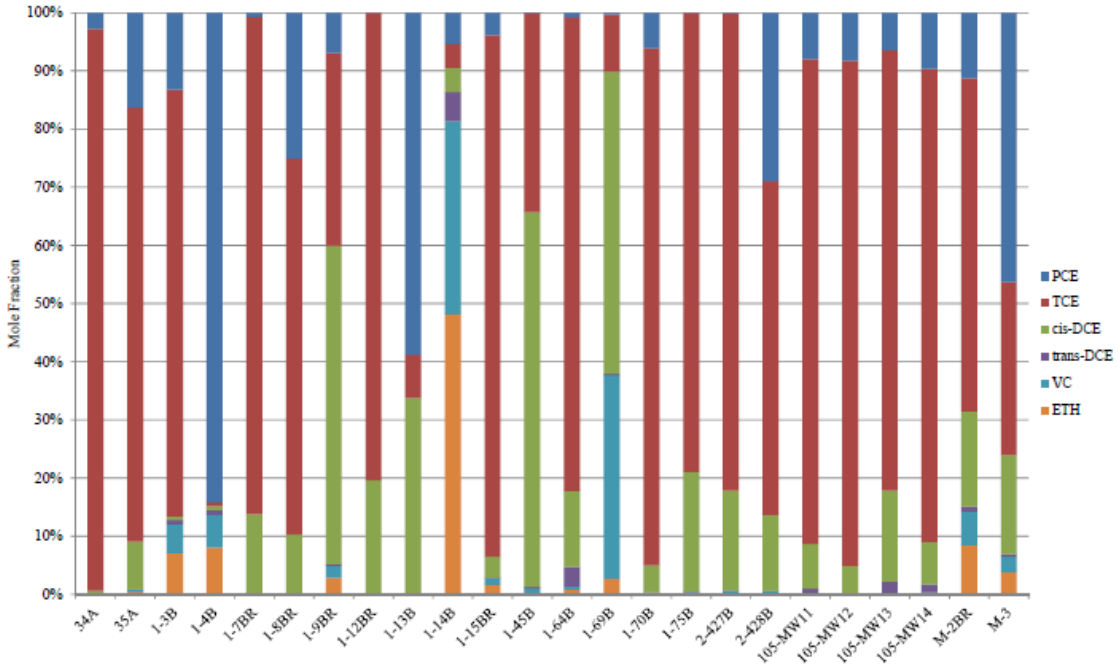

FIGURE 3-23: Mole fraction of chlorinated ethenes in the USZ, 2008

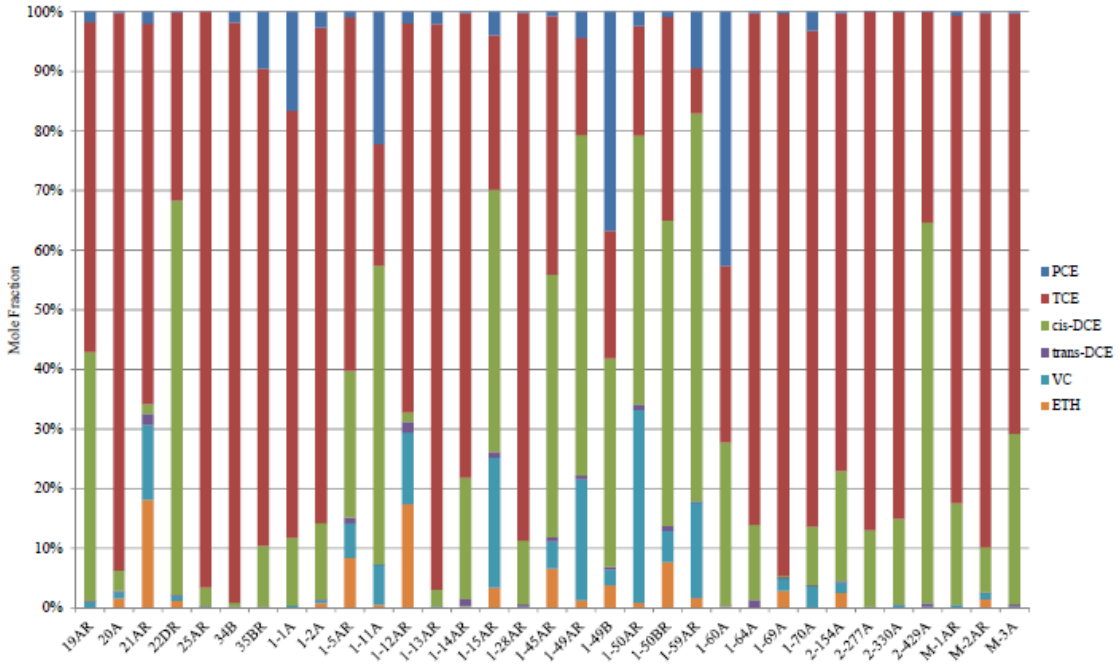

FIGURE 3-24: Mole fraction of chlorinated ethenes in the LSZ, 2008

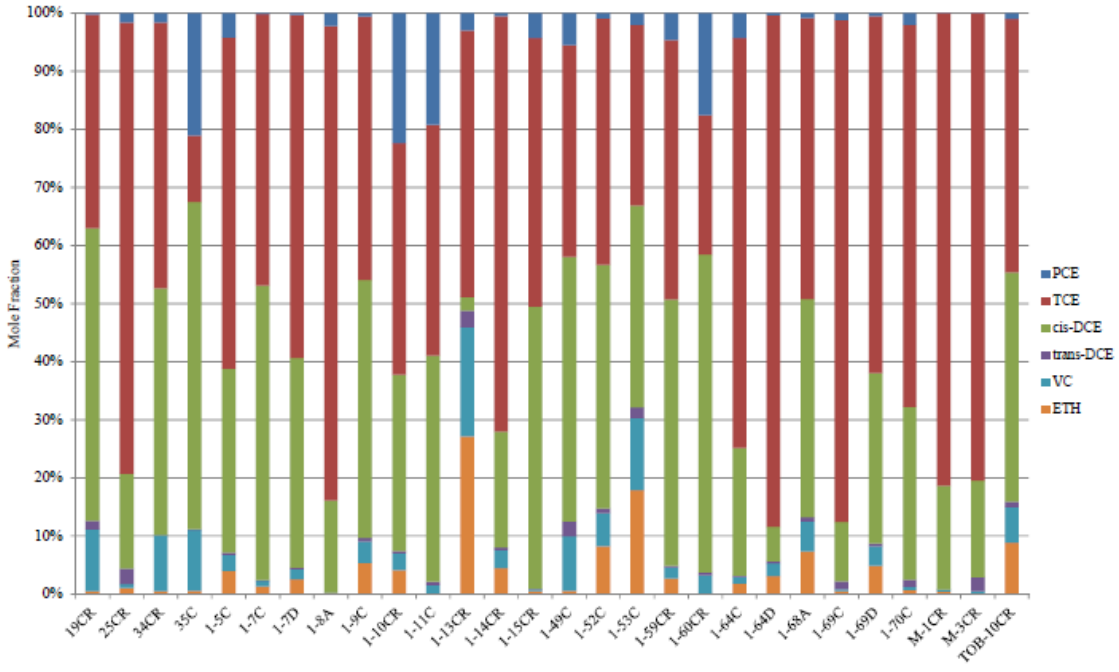

FIGURE 3-25: Mole fraction of chlorinated ethenes in the LLSZ, 2008

As noted above, concentration and mole fraction data for select monitoring wells (i.e., a subset of wells within the model domain) are graphically illustrated on FIGURE 3-20, FIGURE 3-21, and FIGURE 3-22. Data are illustrated in this manner to highlight the significance of the molar concentrations of the chlorinated ethene species. In the USZ, TCE is the most prevalent chlorinated ethene present at many of the monitoring wells, particularly at the 105 and 34 source areas. The distribution of chlorinated ethene species at monitoring well 1-9BR, particularly the prevalence of *cis*-DCE, suggests unique location-specific transformation conditions may exist. Likewise, the high molar concentration of PCE at 1-13B may suggest a location-specific source contribution. In the LSZ, *cis*-DCE represents a significant portion of chlorinated ethene concentration at monitoring wells located east of Building 3001. Underneath and to the west of Building 3001, TCE is the most prevalent chlorinated ethene species, except at monitoring well 1-12AR. These data suggest that chlorinated ethenes associated with the IWTP may have

experienced greater transformation processes in the LSZ. Notably, PCE contributes significant mass at monitoring wells 1-49B, 1-11A, 1-1A, and 35BR. In the LLSZ, *cis*-DCE (and to a lesser extent TCE) appears to be the most significant chlorinated ethene species. Ethene is also present at a much greater molar concentration than in the USZ or LSZ. These data suggest that transformation may be occurring across the model domain. Interestingly, PCE contributes a significant portion of mass at monitoring wells 35C and 1-11C, along with monitoring wells 1-10CR and 1-60CR (data shown on FIGURE 3-22), which is somewhat unexpected for the LLSZ and may represent vertical migration (via poor well conditions or unknown pathway) from the USZ and LSZ.

3.5. Compound-Specific Isotope Analysis (CSIA)

Isotopic ratios were determined for various chlorinated ethenes in many of the monitoring wells sampled in 2008. Reported concentrations for *trans*-DCE for all samples were too low for isotopic analysis. A summary of constituent stable isotope values measured in groundwater samples collected in June 2008 is listed in TABLE 3-4. Isotopic results reported as “na” indicate the peak was not acquired, meaning the compound peak was below detection limit for isotopic analysis. Total isotopic results reported as “nd” indicate the value was not determined. In this study, the standard deviation of replicate analysis for PCE was up to 0.7 ‰, for TCE up to 0.8 ‰, for *cis*-DCE up to 0.5 ‰, for VC up to 0.6 ‰, and for ethene up to 0.1 ‰. Average standard deviation of replicate analysis for PCE, TCE, *cis*-DCE, VC and ethene were 0.3 ‰, 0.2 ‰, 0.2 ‰, 0.3 ‰, and 0.1 ‰, respectively. The average standard deviation of each analyte is assumed to be a “typical” expected analytical precision.

TABLE 3-4: $\delta^{13}C$ of chlorinated ethenes at selected wells, 2008

Location	$\delta^{13}C$ (‰)[16,17]					
	PCE	**TCE**	***cis*-DCE**	***trans*-DCE**	**VC**	**Ethene**
USZ						
21BR	na	na	na	na	na	na
34A	-29.5	-26.3	-24.8	na	na	na
35A	-31.6	-24.3	-27.5	na	na	na
1-3B	na	-24.4	na	na	na	na
1-4B	-22.3	na	na	na	na	na
1-7BR	-28.5	-21.5	-14.9	na	na	na
1-8BR	-25.9	-24.0	-23.9	na	na	na
1-9BR	na	-24.3	-24.2	na	na	na
1-12BR	na	-23.8	-25.0	na	-9.7	na
1-13B	-26.6	-24.4	-17.8	na	na	na
1-14B	na	na	na	na	na	na
1-15BR	-28.3	-25.5	na	na	na	na
1-45B	na	-20.2	-25.5	na	-37.9	-19.7
1-64B	na	-21.6	-23.9	na	na	na
1-69B	na	-25.7	-16.3	na	-2.9	-18.2
1-70B	-30.8	-24.5	-24.3	na	-19.5	na
1-75B	na	-23.9	-22.2	na	na	na
2-427B	na	-22.3	-20.2	na	na	na
2-428B	-25.2	-23.1	-22.4	na	na	na
105-MW11	-30.8	-23.8	-24.9	na	-20.6	na
105-MW12	-27.8	-24.9	-24.7	na	-22.8	na
105-MW13	-30.1	-23.6	-23.1	na	-13.7	na
105-MW14	-31.0	-24.0	-24.4	na	-16.7	na
M-2BR	na	-21.4	na	na	na	na
M-3	na	na	na	na	na	na
MIN	-31.6	-26.3	-27.5	-	-37.9	-19.7
MEAN	-28.3	-23.7	-22.8	-	-18.0	-19.0
MAX	-22.3	-20.2	-14.9	-	-2.9	-18.2
STD DEV	2.74	1.53	3.36	-	10.3	1.06
LSZ						
19AR	-27.1	-24.6	-24.9	na	-29.4	na
20A	na	-23.3	na	na	na	na
21AR	na	na	na	na	na	na
22DR	na	-16.7	-13.2	na	na	na
25AR	na	-23.5	-21.5	na	na	na
34B	-29.5	-26.0	-25.6	na	na	na
35BR	-27.5	-25.9	-26.4	na	-14.7	na
1-1A	-30.9	-26.3	-21.7	na	-16.8	na
1-2A	-28.6	-24.2	-23.1	na	na	na
1-5AR	na	-23.5	na	na	na	na
1-7AR	na	na	na	na	na	na
1-11A	-31.1	-25.9	-20.4	na	-15.9	na
1-12AR	na	-23.6	na	na	na	na
1-13AR	-33.1	-23.9	-23.1	na	na	na

[16] The average standard deviations of replicate analysis for PCE, TCE, *cis*-DCE, VC and ethene were 0.3 ‰, 0.2 ‰, 0.2 ‰, 0.3 ‰, and 0.1 ‰, respectively.

[17] Isotopic results reported as "na" indicate the peak was not acquired, meaning the compound peak was below detection limit for isotopic analysis. Reported concentrations for *trans*-DCE for all samples were too low for isotopic analysis.

Location	$\delta^{13}C$ (‰)[16,17]					
	PCE	**TCE**	***cis*-DCE**	***trans*-DCE**	**VC**	**Ethene**
1-14AR	na	-24.4	-23.3	na	na	na
1-15AR	-27.7	-20.1	-22.1	na	-27.1	-27.9
1-28AR	-32.5	-24.8	-24.6	na	na	na
1-45AR	na	-19.6	-14.8	na	na	na
1-49AR	-29.1	-21.3	-22.2	na	-28.9	-26.6
1-49B	-31.9	-27.2	-24.7	na	na	na
1-50AR	-27.4	-19.8	-21.9	na	-28.8	-20.4
1-50BR	na	na	-20.1	na	na	na
1-59AR	-24.3	-21.9	-19.3	na	-9.0	na
1-60A	-32.6	-26.4	-25.6	na	na	na
1-64A	-26.6	-22.9	-22.1	na	-19.2	na
1-69A	na	-24.7	na	na	na	na
1-70A	-30.9	-24.0	-22.2	na	-19.5	-20.7
2-154A	na	-24.2	-22.8	na	na	na
2-277A	na	-24.0	-24.8	na	-27.1	na
2-330A	na	-23.7	-24.7	na	na	na
2-429A	na	-23.9	-24.9	na	-36.2	na
M-1AR	-30.3	-24.1	-24.2	na	na	na
M-2AR	na	-23.7	-18.6	na	na	na
M-3A	-28.2	-26.4	-23.7	na	na	na
TOB-10AR	na	na	na	na	na	na
MIN	-33.1	-27.2	-26.4	-	-36.2	-27.9
MEAN	-29.4	-23.7	-22.4	-	-22.7	-23.9
MAX	-24.3	-16.7	-13.2	-	-9.0	-20.4
STD DEV	2.42	2.29	3.07	-	7.96	3.91
LLSZ						
19CR	na	-18.8	-17.9	na	-19.8	-20.0
25CR	na	-24.1	-22.8	na	na	na
34CR	-26.2	-19.9	-19.0	na	-18.2	-22.4
35C	-27.3	-26.3	-26.5	na	-33.7	-32.1
1-5C	na	-21.2	-23.6	na	na	na
1-7C	na	-21.1	-19.2	na	na	na
1-7D	na	-23.3	-23.8	na	na	na
1-8A	-27.8	-24.9	-25.6	na	na	na
1-9C	na	-21.2	-22.7	na	na	na
1-10CR	na	-16.7	-16.1	na	na	na
1-11C	-30.9	-24.5	-21.0	na	-19.1	na
1-13CR	na	na	na	na	na	na
1-14CR	na	-24.6	-24.0	na	na	na
1-15CR	-27.6	-18.9	-19.7	na	na	na
1-49C	-28.0	-18.3	-16.5	na	-24.3	na
1-52C	na	-19.0	-25.2	na	na	na
1-53C	na	na	na	na	na	na
1-59CR	-29.5	-20.8	-20.6	na	na	na
1-60CR	-30.7	-24.1	-22.4	na	-20.4	na
1-64C	na	-23.7	-19.5	na	na	na
1-64D	na	-23.3	na	na	na	na
1-68A	na	-17.5	-17.5	na	na	na
1-69C	na	-24.3	-21.4	na	na	na
1-69D	na	-24.9	-24.6	na	na	na
1-70C	-28.7	-23.0	-22.3	na	na	na
M-1CR	na	-23.6	-24.4	na	na	na

Location	$\delta^{13}C$ (‰)[16,17]					
	PCE	**TCE**	***cis*-DCE**	***trans*-DCE**	**VC**	**Ethene**
M-3CR	na	-25.7	-25.3	na	na	na
TOB-10CR	na	-16.1	na	na	na	na
MIN	-30.9	-26.3	-26.5	-	-33.7	-32.1
MEAN	-28.5	-21.9	-21.7	-	-22.6	-24.8
MAX	-26.2	-16.1	-16.1	-	-18.2	-20.0
STD DEV	1.58	2.96	3.02	-	5.84	6.41

Abbreviations/symbols: $\delta^{13}C$ (‰), isotopic ratio of ^{13}C permil; PCE, tetrachloroethylene; TCE, trichloroethylene; *cis*-DCE, *cis*-1,2-dichloroethylene; *trans*-DCE, *trans*-1,2-dichloroethylene;VC, vinyl chloride

3.5.1.1. Upper Saturated Zone Summary

Total chlorinated ethene isotopic values were most depleted at the northern end of Building 3001. PCE $\delta^{13}C$ isotopic values were determined for 13 of 25 groundwater samples, ranging from -22.3 ‰ to -31.6 ‰ (FIGURE 3-29). TCE $\delta^{13}C$ isotopic values were determined for 21 of 25 groundwater samples, ranging from -20.2 ‰ to -26.3 ‰ (FIGURE 3-30). *cis*-DCE $\delta^{13}C$ isotopic values were determined for 18 of 25 groundwater samples, ranging from -14.9 ‰ to -27.5 ‰ (FIGURE 3-31). VC $\delta^{13}C$ isotopic values were determined for 8 of 25 groundwater samples, ranging from -2.9 ‰ to -37.9 ‰ (FIGURE 3-32). Ethene $\delta^{13}C$ isotopic values were determined for 2 of 25 groundwater samples at -18.2 ‰ and -19.7 ‰ (FIGURE 3-33).

Three monitoring wells were sampled in 2006 and 2008; 34A, 1-70B, and 2-428B (TABLE 3-3). At monitoring well 34A, PCE $\delta^{13}C$ was slightly enriched from -29.9 ‰ to -29.5 ‰, TCE $\delta^{13}C$ was depleted from -25.6 ‰ to -26.3 ‰, *cis*-DCE $\delta^{13}C$ was depleted from -23.5 ‰ to -24.8 ‰, and VC and ethene were not detected. At monitoring well 1-70B, PCE $\delta^{13}C$ was slightly depleted from -30.4 ‰ to -30.8 ‰, TCE $\delta^{13}C$ was depleted from -23.2 ‰ to -24.5 ‰, *cis*-DCE $\delta^{13}C$ was depleted from -22.9 ‰ to -24.3 ‰, VC $\delta^{13}C$ was enriched from -21.9 ‰ to -19.5 ‰, and ethene $\delta^{13}C$ was not detected in 2008

(reported at -24.2 ‰ in 2006). At monitoring well 2-428B, PCE $\delta^{13}C$ was slightly depleted from -24.8 ‰ to -25.2 ‰, TCE $\delta^{13}C$ was depleted from -22.5 ‰ to -23.1 ‰, *cis*-DCE $\delta^{13}C$ was depleted from -21.2 ‰ to -22.4 ‰, and VC and ethene were not detected.

3.5.1.2. Lower Saturated Zone Summary

PCE $\delta^{13}C$ isotopic values were determined for 18 of 35 groundwater samples, ranging from -24.3 ‰ to -33.1 ‰ (FIGURE 3-34). TCE $\delta^{13}C$ isotopic values were determined for 31 of 35 groundwater samples, ranging from -16.7 ‰ to -27.2 ‰ (FIGURE 3-35). *cis*-DCE $\delta^{13}C$ isotopic values were determined for 28 of 35 groundwater samples, ranging from -13.2 ‰ to -26.4 ‰ (FIGURE 3-36). VC $\delta^{13}C$ isotopic values were determined for 12 of 35 groundwater samples, ranging from -9.0 ‰ to -36.2 ‰ (see FIGURE 3-37). Ethene $\delta^{13}C$ isotopic values were determined for 4 of 35 groundwater samples, ranging from -20.4 ‰ to -27.9 ‰ (FIGURE 3-38).

Four monitoring wells were sampled in 2006 and 2008; 19AR, 1-70A, 35BR, and 1-1A (TABLE 3-3). At monitoring well 19AR, PCE $\delta^{13}C$ was depleted from -25.9 ‰ to -27.1 ‰, TCE $\delta^{13}C$ was depleted from -24.1 ‰ to -24.6 ‰, *cis*-DCE $\delta^{13}C$ was depleted from -23.6 ‰ to -24.9 ‰, VC $\delta^{13}C$ was enriched from -31.8 ‰ to -29.4 ‰, and ethene $\delta^{13}C$ was not detected. At monitoring well 1-70A, PCE $\delta^{13}C$ was slightly depleted from -30.6 ‰ to -30.9 ‰, TCE $\delta^{13}C$ was depleted from -23.5 ‰ to -24.0 ‰, *cis*-DCE $\delta^{13}C$ was depleted from -21.4 ‰ to -22.2 ‰, VC $\delta^{13}C$ was depleted from -19.0 ‰ to -19.5 ‰, and ethene $\delta^{13}C$ was enriched from -24.2 ‰ to -20.7 ‰. At monitoring well 35BR, PCE $\delta^{13}C$ was slightly enriched from -27.6 ‰ to -27.5 ‰, TCE $\delta^{13}C$ was depleted from -25.2 ‰ to

-25.9 ‰, *cis*-DCE $\delta^{13}C$ was depleted from -24.8 ‰ to -26.4 ‰, VC $\delta^{13}C$ was enriched from -16.1 ‰ to -14.7 ‰, and ethene $\delta^{13}C$ was not detected. At monitoring well 1-1A, PCE $\delta^{13}C$ was depleted from -30.0 ‰ to -30.9 ‰, TCE $\delta^{13}C$ was depleted from -25.5 ‰ to -26.3 ‰, *cis*-DCE $\delta^{13}C$ was depleted from -21.1 ‰ to -21.7 ‰, VC $\delta^{13}C$ was depleted from -15.3 ‰ to -16.8 ‰, and ethene $\delta^{13}C$ was not detected.

3.5.1.3. Lower-lower Saturated Zone Summary

PCE $\delta^{13}C$ isotopic values were determined for 9 of 28 groundwater samples, ranging from -26.2 ‰ to -30.9 ‰ (FIGURE 3-39). TCE $\delta^{13}C$ isotopic values were determined for 26 of 28 groundwater samples, ranging from -16.1 ‰ to -26.3 ‰ (FIGURE 3-40). *cis*-DCE $\delta^{13}C$ isotopic values were determined for 24 of 28 groundwater samples, ranging from -16.1 ‰ to -26.5 ‰ (FIGURE 3-41). VC $\delta^{13}C$ isotopic values were determined for 6 of 28 groundwater samples, ranging from -18.2 ‰ to -33.7 ‰ (FIGURE 3-42). Ethene $\delta^{13}C$ isotopic values were determined for 3 of 28 groundwater samples, ranging from -20.0 ‰ to -32.1 ‰ (FIGURE 3-43).

Three monitoring wells were sampled in 2006 and 2008; 1-8A, 1-49C, and 19CR (TABLE 3-3). At monitoring well 1-8A, PCE $\delta^{13}C$ was slightly depleted from -27.7 ‰ to -27.8 ‰, TCE $\delta^{13}C$ was depleted from -23.8 ‰ to -24.9 ‰, *cis*-DCE $\delta^{13}C$ was depleted from -24.1 ‰ to -25.6 ‰, and VC $\delta^{13}C$ and ethene $\delta^{13}C$ were not detected. At monitoring well 1-49C, PCE $\delta^{13}C$ was slightly depleted from -27.9 ‰ to -28.0 ‰, TCE $\delta^{13}C$ was depleted from -17.8 ‰ to -18.3 ‰, *cis*-DCE $\delta^{13}C$ was depleted from -15.4 ‰ to -16.5 ‰, VC $\delta^{13}C$ was depleted from -23.1 ‰ to -24.3 ‰, and ethene $\delta^{13}C$ was not detected in 2008 (reported at -24.6 ‰ in 2006). At monitoring well 19CR, PCE $\delta^{13}C$ was

not detected in 2008 (reported as -30.4 ‰ in 2006), TCE $\delta^{13}C$ was enriched from -22.5 ‰ to -18.8 ‰, *cis*-DCE $\delta^{13}C$ was depleted from -17.3 ‰ to -17.9 ‰, VC $\delta^{13}C$ was enriched from -20.4 ‰ to -9.8 ‰, and ethene $\delta^{13}C$ was slightly enriched from -20.2 ‰ to -20.0 ‰.

When selecting a source isotopic value for comparison of site data, there are three general approaches; those include selecting values from literature sources, selecting the most negative isotopic value of the constituent of interest, or selecting a conservative estimate based on, isotopic values at monitoring wells with highest constituent concentration, which may be indicative of source values [41]. The last of the three approaches was chosen, and PCE and TCE values were selected based on isotopic values at locations with high concentrations reported in the northern end of Building 3001. A source isotopic value for PCE of -30.8 ‰ was chosen from 105-MW11. A source isotopic value for TCE of -24.9 ‰ was chosen from 105-MW12. These source values are within the range of -23‰ to -37‰ for PCE and -22‰ to -34‰ for TCE reported in the literature [41]. Despite the concern that TCE may have, in theory, evolved from PCE or may be a mixture of dechlorinated PCE and manufactured TCE, it is assumed the high concentrations of TCE >4,000 µg/L represent residual original TCE from the degreasing processes.

In the USZ, chlorinated ethene isotopic values were most depleted at the northern end of Building 3001, particularly around the cluster of monitoring wells near 105-MW14 and at monitoring well 35A. Twenty-five groundwater samples were collected from monitoring wells screened the USZ. Compound-specific isotopic values ($\delta^{13}C$) ranged from -22.3 ‰ to -31.6 ‰ (in 13 samples) for PCE, -20.2 ‰ to -26.3 ‰ (in 21

samples) for TCE, -14.9 ‰ to -27.5 ‰ (in 18 samples) for *cis*-DCE, -2.9 ‰ to -37.9 ‰ (in 8 samples) for VC, and -18.2 ‰ and -19.7 ‰ (in two samples) for ethene.

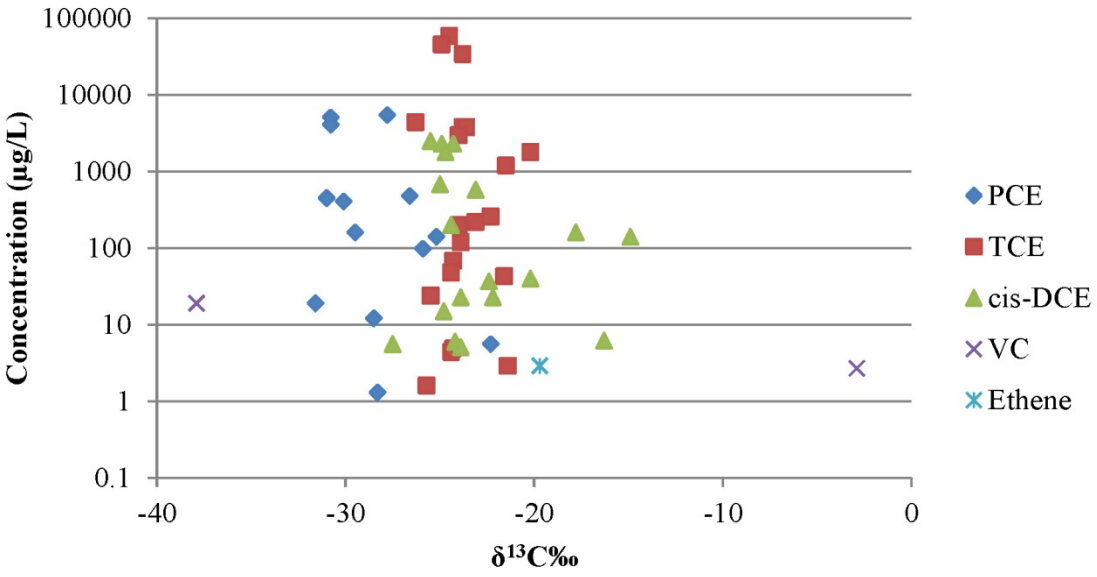

FIGURE 3-26: Chlorinated ethene concentrations vs. isotopes for the USZ, 2008
Illustrates chlorinated ethene concentrations in µg/L compared to the corresponding isotopic value, expressed as δ^{13}C‰. Data collected in 2008.

In the LSZ, chlorinated ethene isotopic values were most depleted underneath the IWTP compared to those underneath Building 3001, particularly at monitoring wells 1-11A, 1-49AR, and 19AR. One apparent exception is that consistently depleted values are reported near monitoring well 35BR. Thirty-five groundwater samples were collected from monitoring wells screened the LSZ. Compound-specific isotopic values (δ^{13}C) ranged from-24.3 ‰ to -33.1 ‰ (in 18 samples) for PCE, -16.7 ‰ to -27.2 ‰ (in 31 samples) for TCE, -13.2 ‰ to -26.4 ‰ (in 28 samples) for *cis*-DCE, -9.0 ‰ to -36.2 ‰ (in 12 samples) for VC, and -20.4 ‰ to -27.9 ‰ (in 4 samples) for ethene.

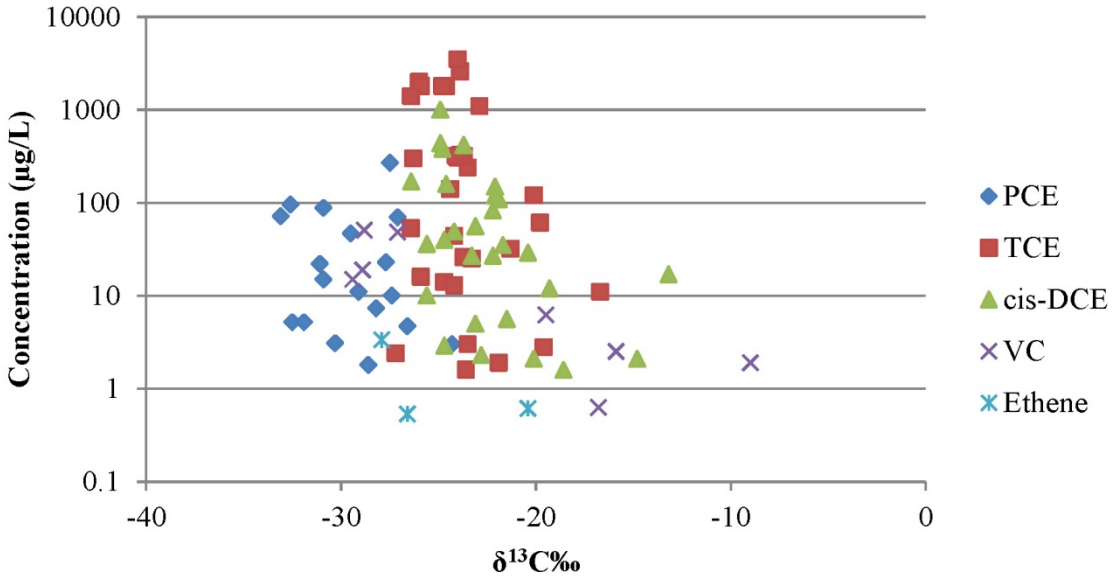

FIGURE 3-27: Chlorinated ethene concentrations vs. isotopes for the LSZ, 2008
Illustrates chlorinated ethene concentrations in µg/L compared to the corresponding isotopic value, expressed as δ^{13}C‰. Data collected in 2008.

In the LLSZ, chlorinated ethene isotopic values are generally consistent across the site. Twenty-eight groundwater samples were collected from monitoring wells screened the LLSZ. Compound-specific isotopic values (δ^{13}C) ranged from -26.2 ‰ to -30.9 ‰ (in 9 samples) for PCE, -16.1 ‰ to -26.3 ‰ (in 26 samples) for TCE, -16.1 ‰ to -26.5 ‰ (in 24 samples) for *cis*-DCE, -18.2 ‰ to -33.7 ‰ (in six samples) for VC, and -20.0 ‰ to -32.1 ‰ (in three samples) for ethene.

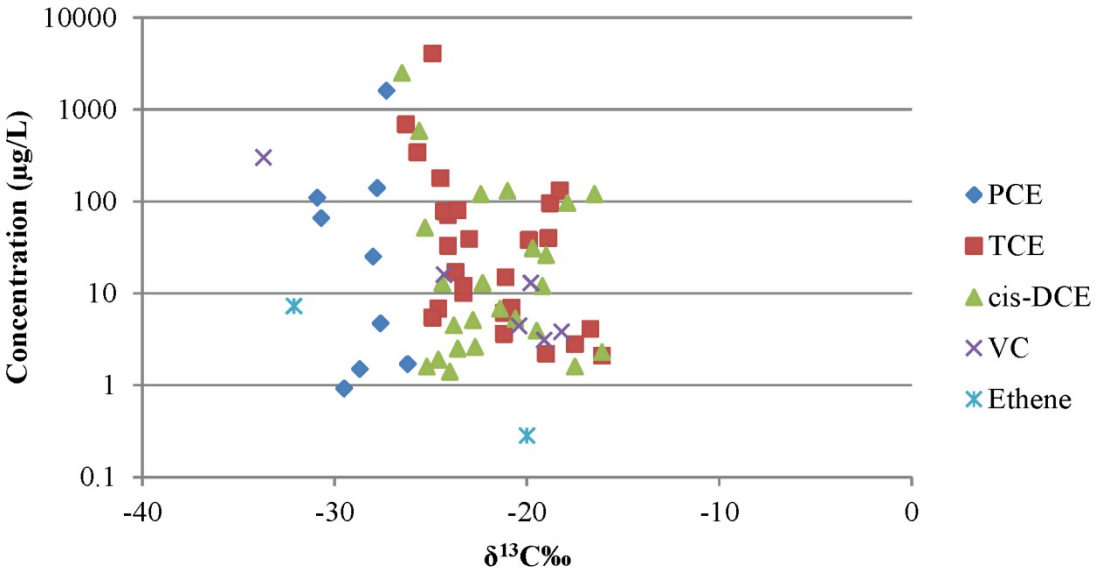

FIGURE 3-28: Chlorinated ethene concentrations vs. isotopes for the LLSZ, 2008 Illustrates chlorinated ethene concentrations in µg/L compared to the corresponding isotopic value, expressed as $\delta^{13}C‰$. Data collected in 2008.

It is clear based on the presence of transformation products and apparent isotopic enrichment that degradative processes are occurring within the project site subsurface. However, some isotopic data indicate little degradation may be occurring at some locations. Separating an isotopic mixture of the apparent same constituent (e.g., TCEsource and TCEdegraded) requires a comprehensive understanding of the fractionation processes and subsurface geochemical conditions and hydraulic flow dynamics.

While non-degradative process can cause minor isotopic shifts, enrichment primarily occurs when chlorinated ethenes degrade. For highly chlorinated hydrocarbons such as PCE and TCE, little biodegradation occurs as long as oxygen is present and the oxidation-reduction (redox) potential is elevated [41]. Thus, the relevance of biodegradation can be evaluated in part by characterizing redox conditions. Researchers have compared isotope enrichment factors for aerobic and anaerobic degradation of

chlorinated ethenes and have reported greater enrichment factors (i.e., similar to those measured at this site) for microbially-mediated anaerobic reductive dechlorination [48, 66, 67]. Thus, it can be assumed reductive dechlorination is occurring where large fractionation and appropriate redox indicators are observed.

When evaluating degradation using CSIA, it is preferable to collect samples from target wells over a period of four to seven months to determine the isotopic fractionation behavior and then sample annually for a few years to evaluate the long-term behavior and stability of the plume[41]. However, when groundwater velocities are low, a spatial approach can be used in lieu of a temporal approach. The study site has low groundwater velocities except in some locations where preferential flow is evident, which indicates that spatial isotopic variation is as useful an indicator as temporal variation. In other words, horizontal and vertical isotopic variation across the site (see FIGURE 3-29 through FIGURE 3-43) is taken at face value and assumed that observed isotopic shifts are significant and relevant. Thus, isotopic values presented herein indicate various levels of enrichment of each of the chlorinated ethenes. However, the combination of relative magnitude of degradation and variances in subsurface geochemical conditions remains less clear when evaluating identical source contaminants and therefore, must be further explored using a reactive transport model.

Considering the most prevalent mole fractions of chlorinated ethene species in each hydrostratigraphic unit and across the study area, isotopic variability provides additional insight into likely transformative processes (see FIGURE 3-23 through FIGURE 3-25). In the USZ, monitoring wells located at the northern end of Building 3001 source areas have elevated concentrations and $\delta^{13}C$ values characteristic of source

values found in the literature [68]. At these locations, it is concluded that source PCE and TCE likely still exists. In the LSZ, TCE and *cis*-DCE values east of Building 3001 appear to be generally enriched relative to locations underneath and west of Building 3001, suggesting that transformative processes have occurred. These data are supported by isotopically enriched VC and ethene data at the IWTP, as well as generally lower dissolved oxygen [mean DO of 0.56 mg/L for IWTP wells (e.g., 1-11A, 1-49AR, 1-49B, 1-50AR, 1-50BR, and 1-59AR) vs. 1.54 mg/L for others wells] and numerous negative ORP values (e.g., 2-429A, 2-154A, 2-277A, 1-45AR, and 1-12AR) observed during sample collection (TABLE 2-2). However, PCE $\delta^{13}C$ values at monitoring wells 1-49B, 1-11A, and 1-1A appear very similar to assumed PCE source $\delta^{13}C$ values of -30.8 ‰. In the LLSZ, *cis*-DCE and TCE isotopic values are nearly consistently isotopically enriched relative to the USZ and LSZ across the study area. These data are again supported by isotopically enriched VC and ethene results, which leads us to conclude that significant transformation is occurring in the LLSZ. Finally, PCE $\delta^{13}C$ values at monitoring wells 35C and 1-11C in the LLSZ appear isotopically consistent with those results reported in samples from 35BR and 1-11A in the LSZ indicating potential vertical migration of source contaminant, which is an expected possibility considering the history of poorly-installed monitoring wells. Considering the suspected source locations and observed flow dynamics of the northeast quadrant of Tinker AFB, coupled with the isotopic variability across the site (beyond those wells discussed above) provides reasonable evidence of potential plume mixing points in the LSZ and the general nature of the comingled plume. This information will be used to guide the development of the conceptual model, leading to the construction of the 3D reactive transport model.

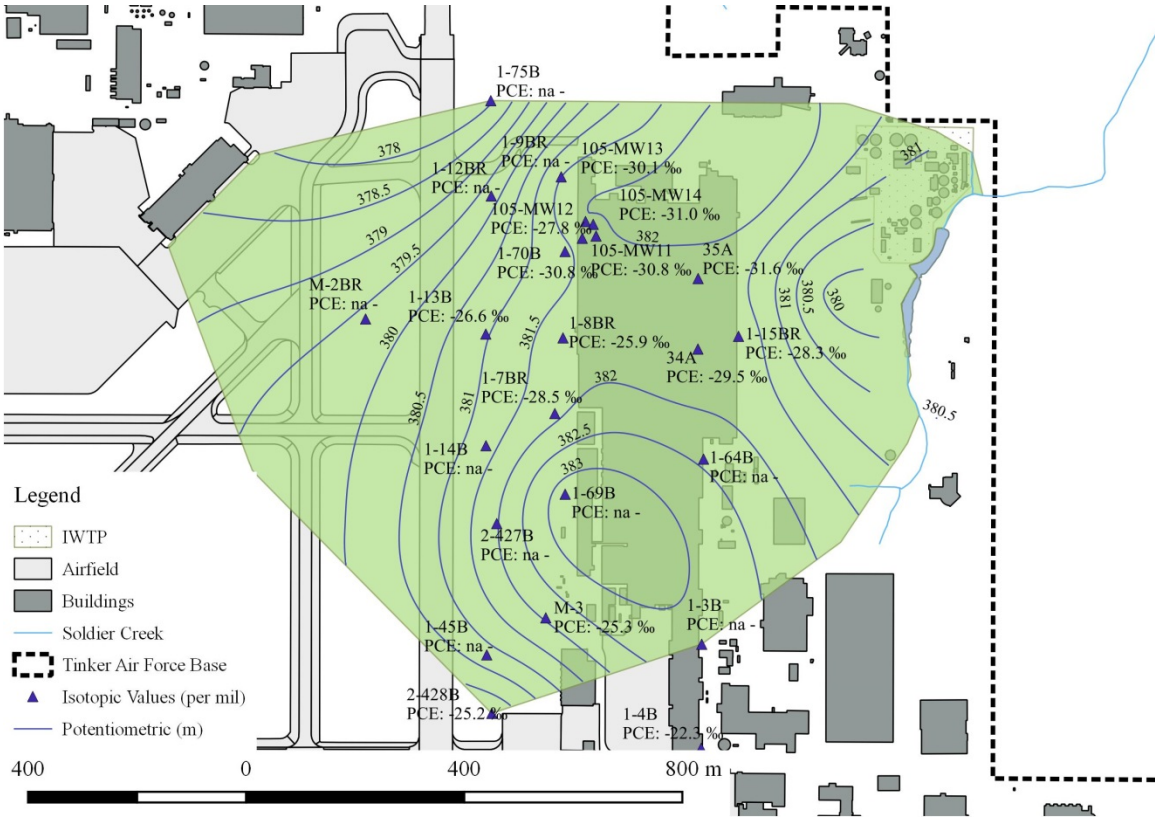

FIGURE 3-29: USZ potentiometric surface and PCE isotopic composition, 2008
Map illustrating groundwater potentiometric surface and PCE isotope results in the USZ within the study area.

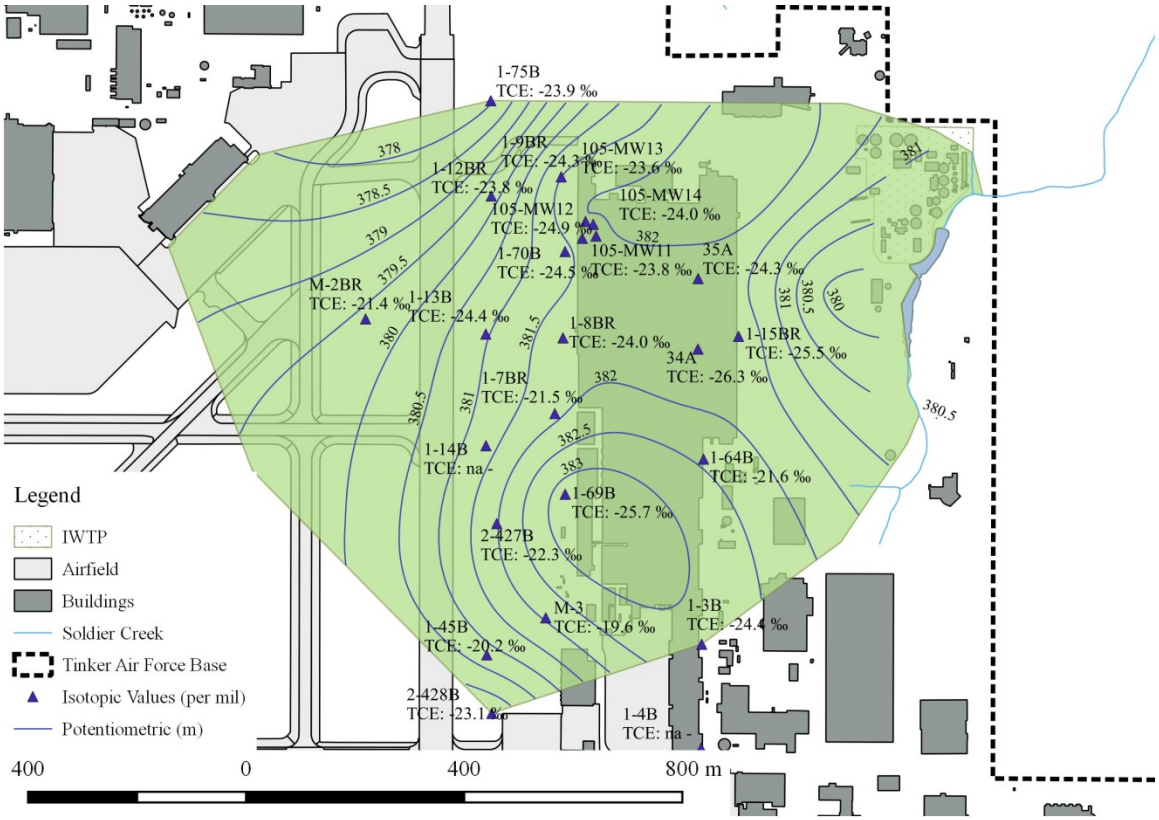

FIGURE 3-30: USZ potentiometric surface and TCE isotopic composition, 2008
Map illustrating groundwater potentiometric surface and TCE isotope results in the USZ within the study area.

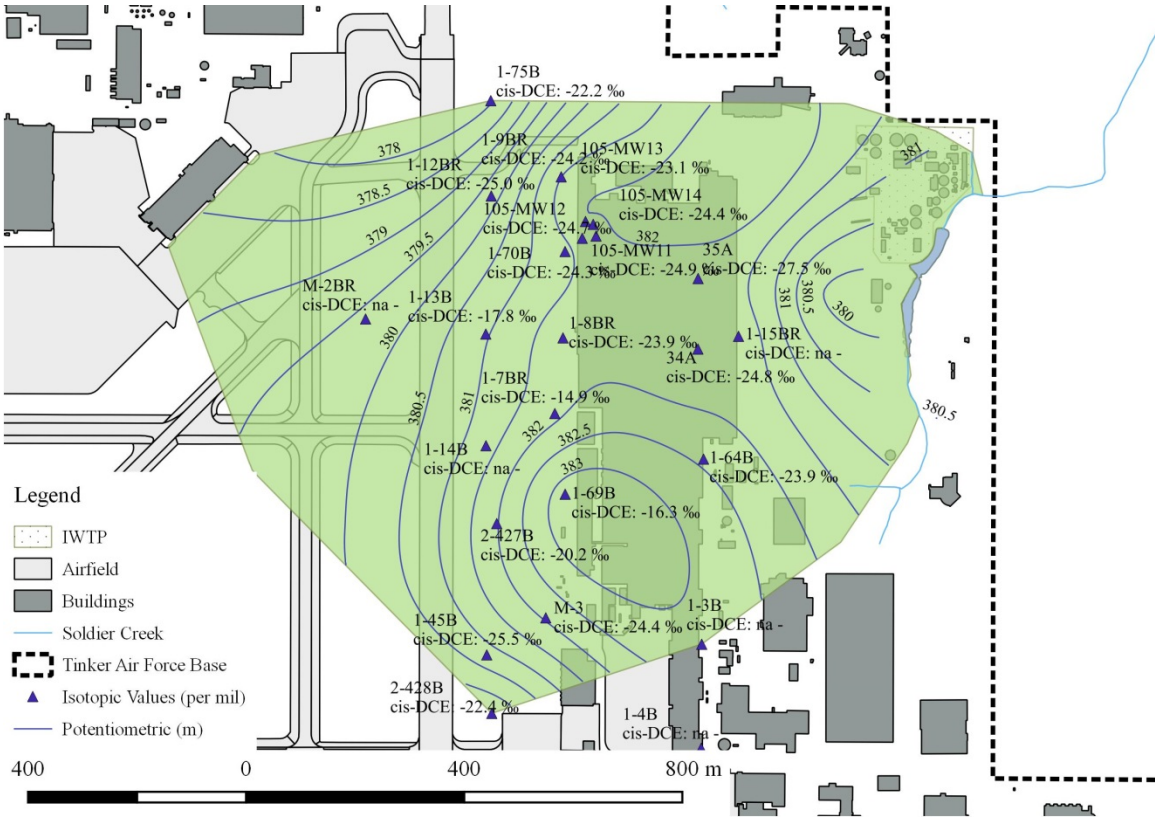

FIGURE 3-31: USZ potentiometric surface and *cis*-DCE isotopic composition, 2008
Map illustrating groundwater potentiometric surface and *cis*-DCE isotope results in the USZ within the study area.

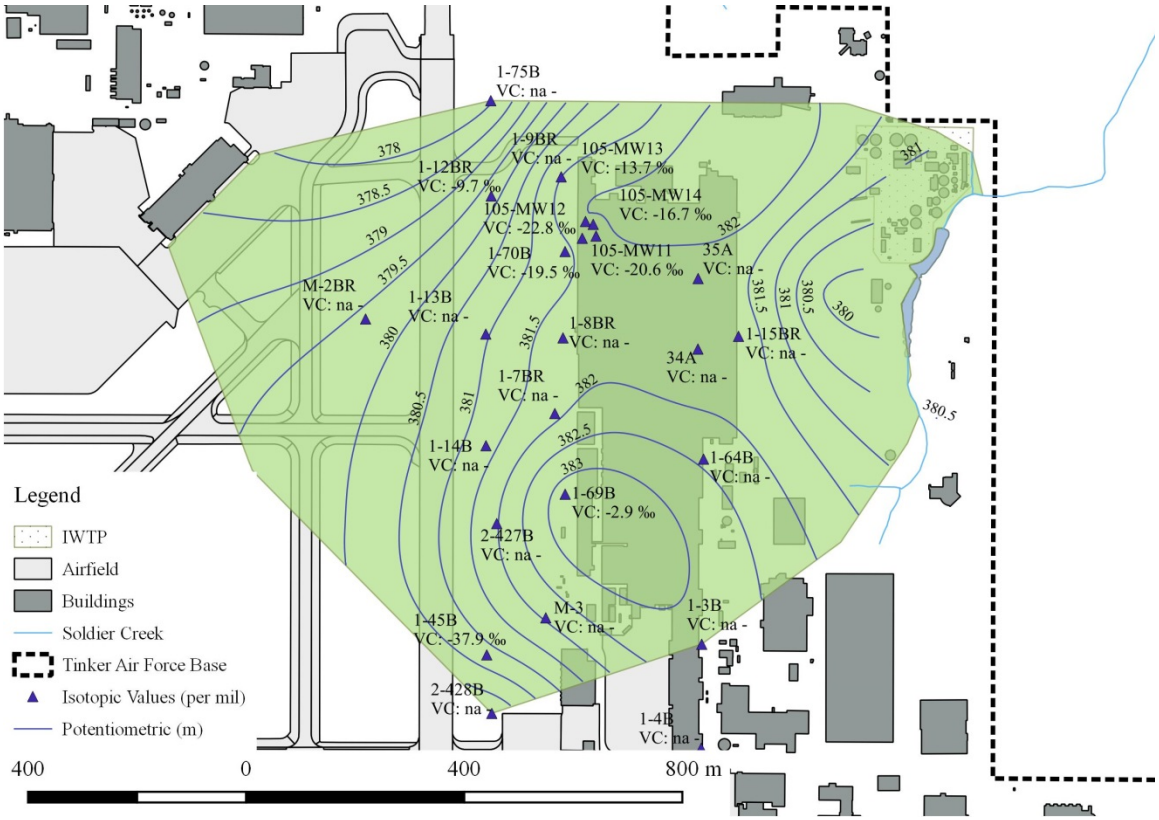

FIGURE 3-32: USZ potentiometric surface and VC isotopic composition, 2008
Map illustrating groundwater potentiometric surface and VC isotope results in the USZ within the study area.

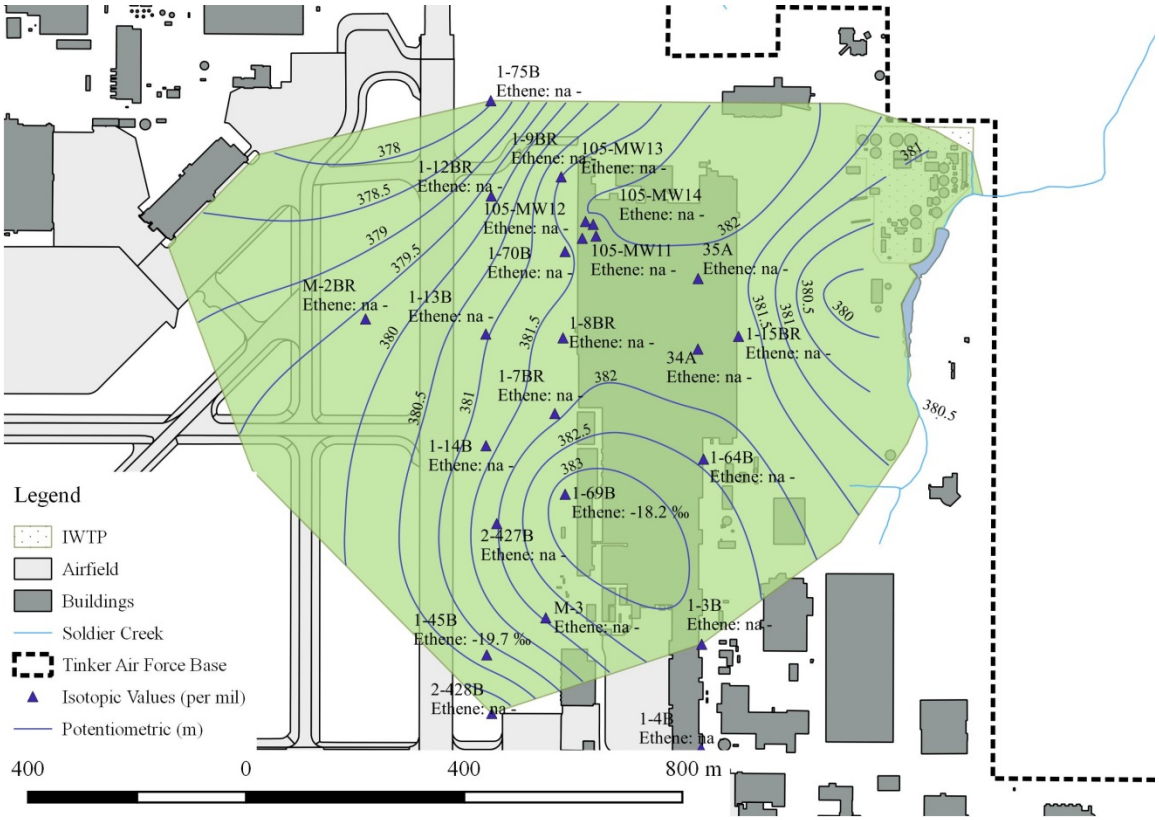

FIGURE 3-33: USZ potentiometric surface and ethene isotopic composition, 2008
Map illustrating groundwater potentiometric surface and ethene isotope results in the USZ within the study area.

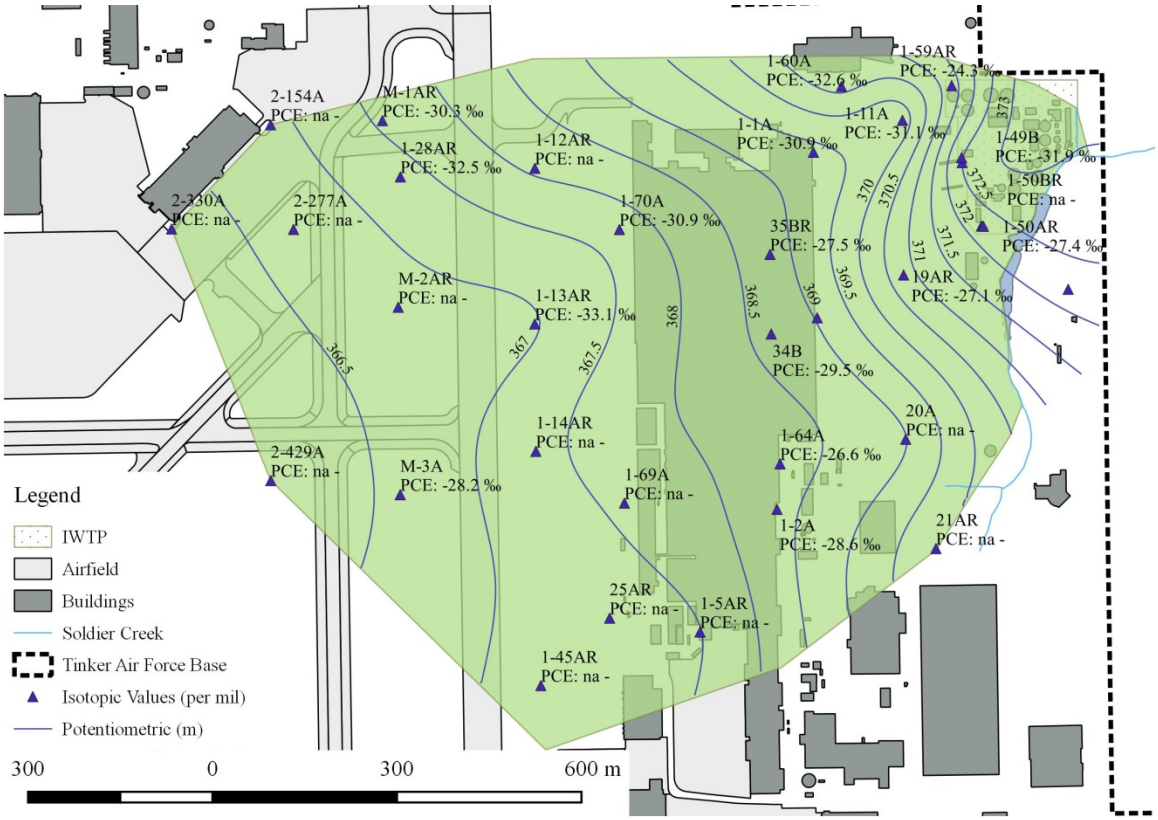

FIGURE 3-34: LSZ potentiometric surface and PCE isotopic composition, 2008
Map illustrating groundwater potentiometric surfaces and PCE isotope results in the LSZ within the study area.

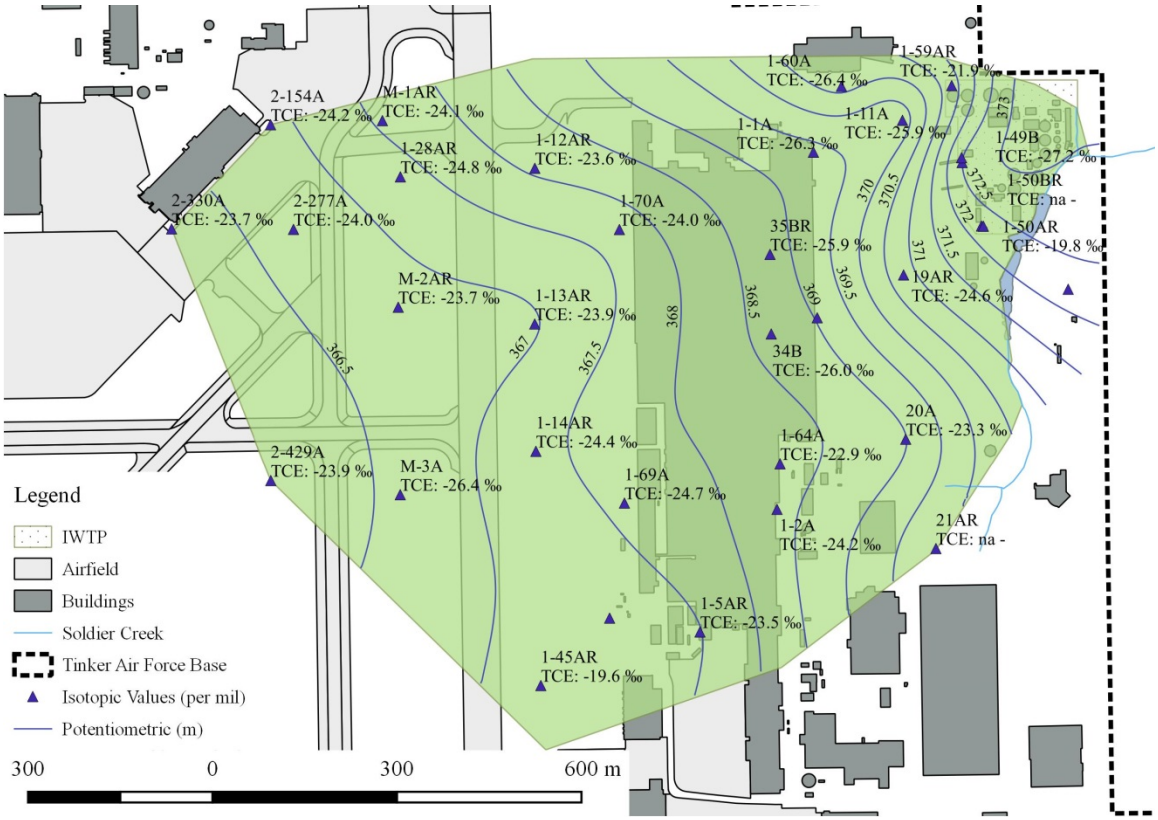

FIGURE 3-35: LSZ potentiometric surface and TCE isotopic composition, 2008
Map illustrating groundwater potentiometric surfaces and TCE isotope results in the LSZ within the study area.

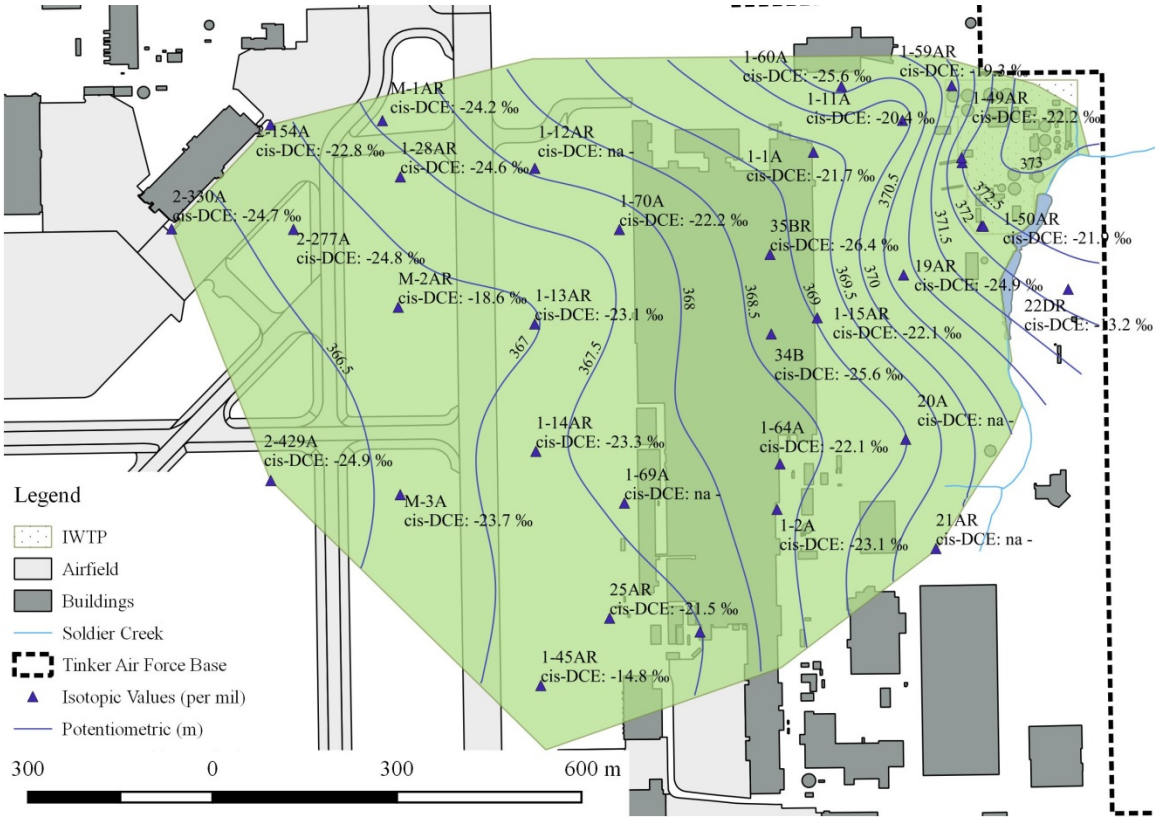

FIGURE 3-36: LSZ potentiometric surface and *cis*-DCE isotopic composition, 2008
Map illustrating groundwater potentiometric surfaces and *cis*-DCE isotope results in the LSZ within the study area.

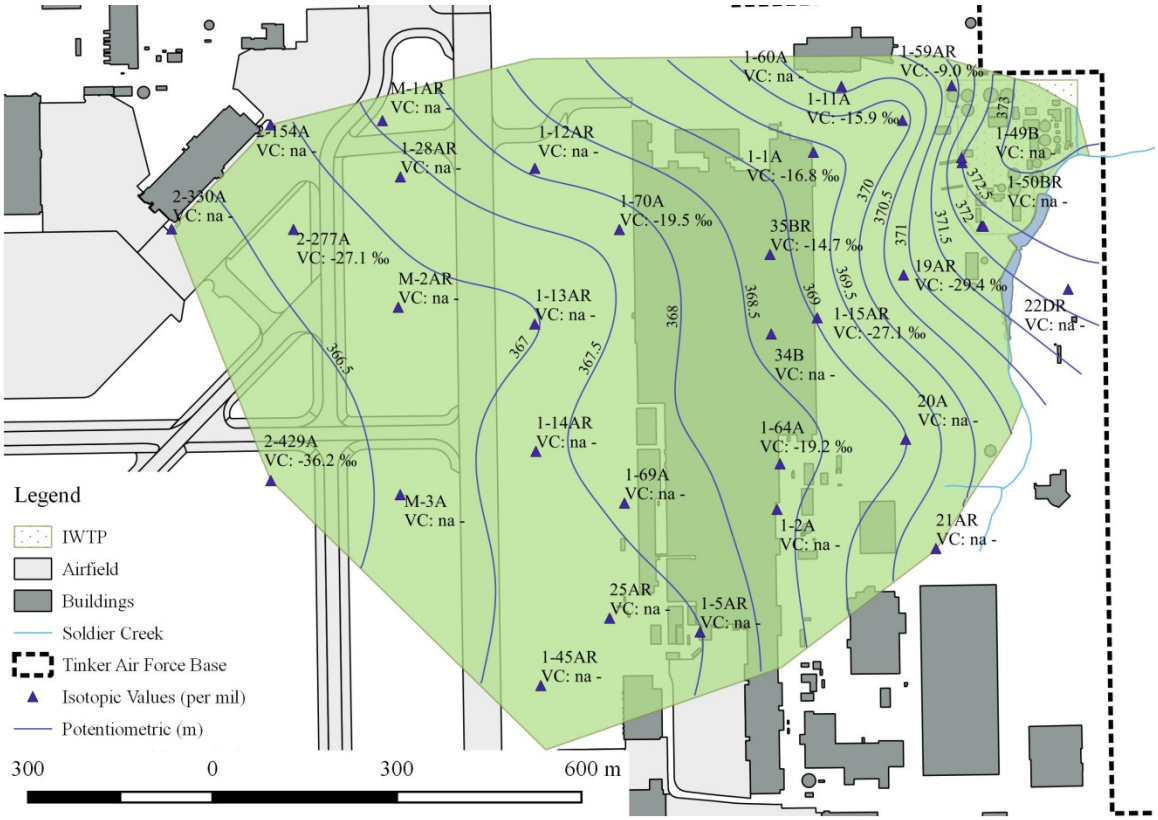

FIGURE 3-37: LSZ potentiometric surface and VC isotopic composition, 2008
Map illustrating groundwater potentiometric surfaces and VC isotope results in the LSZ within the study area.

FIGURE 3-38: LSZ potentiometric surface and ethene isotopic composition, 2008
Map illustrating groundwater potentiometric surfaces and ethene isotope results in the LSZ within the study area.

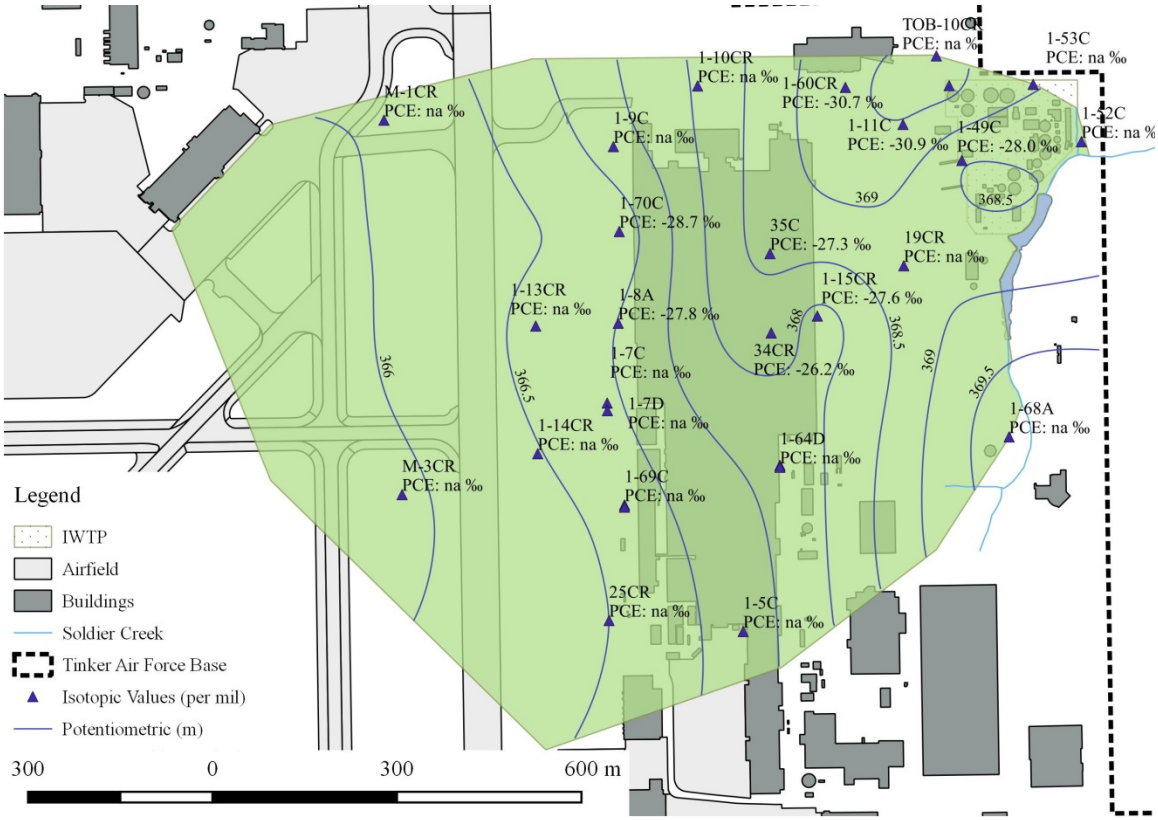

FIGURE 3-39: LLSZ potentiometric surface and PCE isotopic composition, 2008
Map illustrating groundwater potentiometric surfaces and PCE isotope results in the LLSZ within the study area.

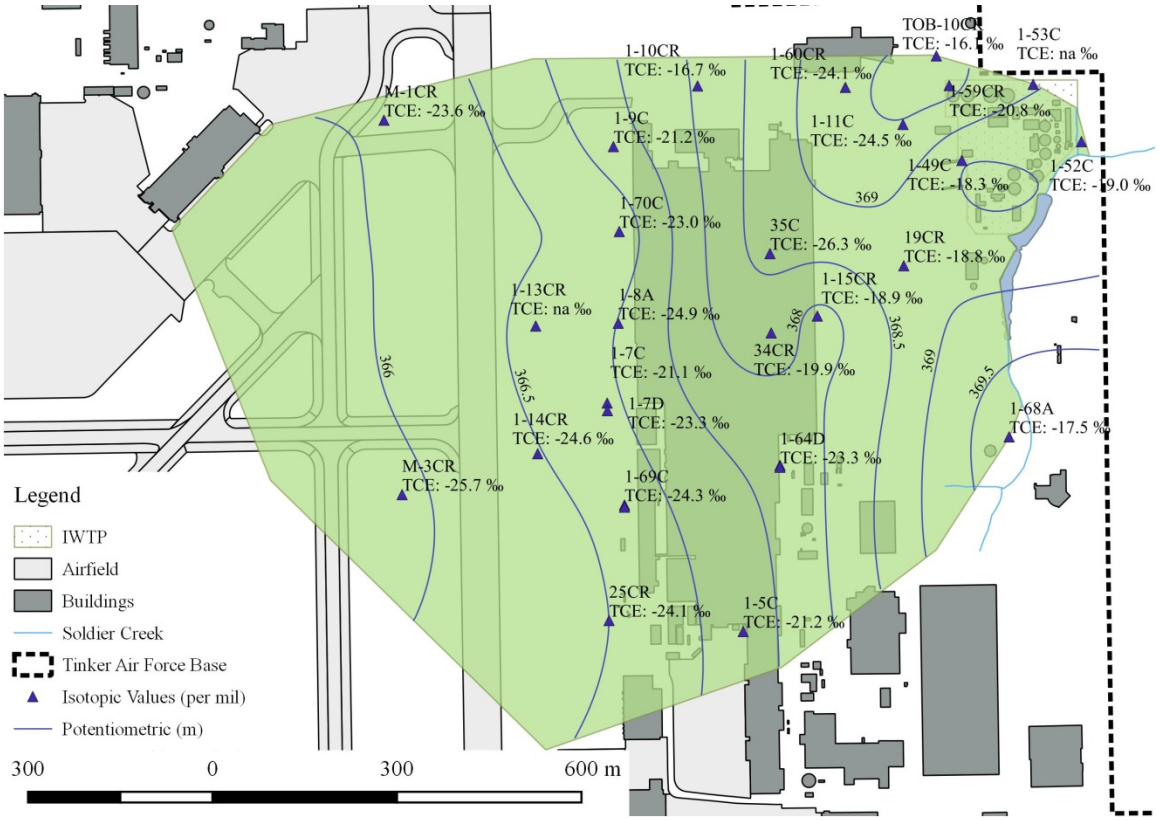

FIGURE 3-40: LLSZ potentiometric surface and TCE isotopic composition, 2008
Map illustrating groundwater potentiometric surfaces and TCE isotope results in the LLSZ within the study area.

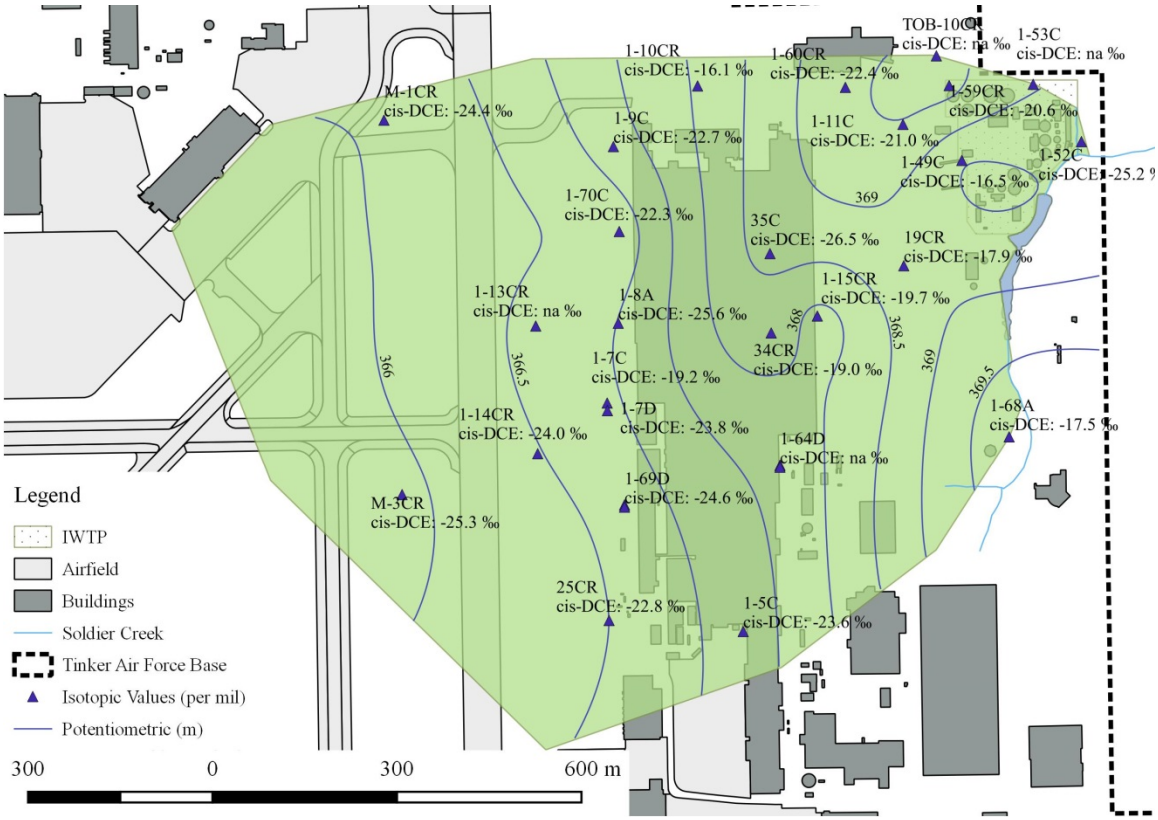

FIGURE 3-41: LLSZ potentiometric surface and *cis*-DCE isotopic composition, 2008
Map illustrating groundwater potentiometric surfaces and *cis*-DCE isotope results in the LLSZ within the study area.

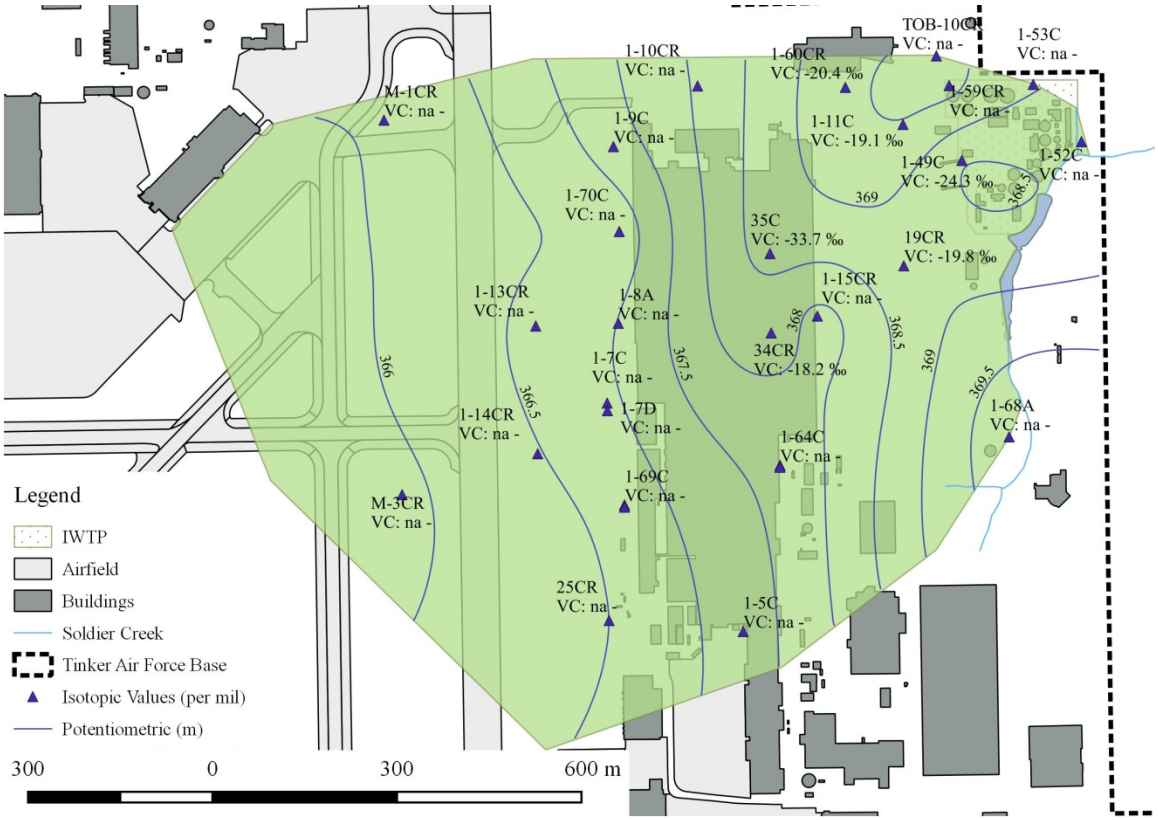

FIGURE 3-42: LLSZ potentiometric surface and VC isotopic composition, 2008
Map illustrating groundwater potentiometric surfaces and VC isotope results in the LLSZ within the study area.

FIGURE 3-43: LLSZ potentiometric surface and ethene isotopic composition, 2008
Map illustrating groundwater potentiometric surfaces and ethene isotope results in the LLSZ within the study area.

CHAPTER 4: FATE AND TRANSPORT MODELING

4.1. Introduction

Traditional subsurface contaminant concentration investigations are common among industry professionals and researchers, as they are helpful in providing valuable information used to justify site contaminant attenuation or remediation. However, meaningful information about source contribution can be more challenging at mixed-plume sites, when the sources contribute identical or nearly identical contaminants. CSIA has proven to be a valuable tool for providing degradative and transformative information, specific to target contaminants, beyond what is observed during traditional investigations. These data can be useful at sites with a single contaminant or where sources contribute different contaminants. While transformative data are important, attributing source contribution at comingled plume sites requires more complex investigative techniques.

Three dimensional reactive transport models provide a mechanism to explore complex comingled plumes, beyond the traditional investigation, including those where CSIA are performed. During model development and calibration, input parameters can be estimated and adjusted until an agreeable fit between field observations and model outcomes are achieved. This allows for researchers to use calibrated models to predict

future behavior of the modeled system. However, one should be aware that, because model input parameters are estimated from small-scale observations (or calculations) often meant to represent large-scale complex heterogeneous subsurface conditions, model solutions are inherently non-unique [69]. By coupling traditional techniques with CSIA in a 3D reactive transport model, source contribution can be more accurately quantified. In the following chapter, the methodology and computational codes used to develop and calibration a 3D reactive transport model, along with the predictive model simulations for the study site are provided. Both conceptual and numerical reactive transport models were developed and calibrated in support of this effort.

4.1.1. Setting / Hydrogeologic Framework

High concentrations of chlorinated ethenes were discovered in the late 1980's emanating from two primary source areas in the northeast corner of TAFB; those source areas are at the northern end of Building 3001 and the IWTP, which lies adjacent to Soldier Creek. Thousands of soil, sediment, and groundwater samples have been collected from numerous wells installed through those source areas. The monitoring wells, often nested, are installed at various depths, primarily in the hydrostratigraphic units known as the USZ, LSZ, and LLSZ. These three water-bearing units overlie an aquiclude, which forms a barrier between the contaminated aquifers and the deeper local production aquifer. The USZ, LSZ, and LLSZ are composed of clays and clayey silts that are interbedded with thin, clayey sand layers and lenticular and interbedded sandstone, shale, and siltstone. The USZ, LSZ, and LLSZ are separated by semi-confining layers, known as the UCL and LCL. The USZ has been eroded away in the vicinity of Soldier Creek.

Aside from years when a pump-and-treat system operated at the site, groundwater surfaces are generally similar from year to year. Groundwater in the unconfined USZ is directed by a groundwater mound that exists underneath Building 3001. The dominant groundwater flow trend for the LSZ and LLSZ throughout the project area is to the southwest. Dissolved-phase chlorinated ethene sources at waste pits in Building 3001 contributed contaminants directly into the USZ, while those sources at the IWTP contributed contaminants directly to the LSZ. During several brief years of pump-and-treat system operation, the USZ was dewatered locally, which accelerated the spread of contaminants from the USZ to the LSZ. Improperly-constructed wells were often the conduit for contaminant migration; however, all suspected poor wells have since been replaced. Groundwater surfaces observed during this work were compared to pre-remediation surfaces and found to be similar, suggesting a return to natural flow conditions.

4.2. Preliminary Conceptual Model Parameter Identification

To quantify potential comingled chlorinated ethene plumes in the subsurface, a preliminary conceptual flow model was established to assist in determining data requirements for numerical simulations of flow and chemical fate and transport. The preliminary conceptual flow model integrated constituent concentrations, stable isotope values and presumed fate and transport of selected constituents. Development of the conceptual flow model consisted of identifying model layers, and water balance components and flow conditions associated with each layer. Conceptual model development for chemical fate and transport consisted of identifying sources areas, parent

chemicals released, expected intermediate chemical species, and intrinsic processes that act on the chemical species.

During the early stages of the investigation, the preliminary conceptual site model consisted of an approximately 1,000 m by 1,800 m rectangular model domain with the long axis oriented 30 degrees north of east. The domain boundary encompassed that area of the northeast quadrant where groundwater has been impacted by known or suspected contaminant releases at Building 3001 and the former wastewater treatment plant. The depth interval of the domain extended from the shallow water table in the Upper Saturated Zone (USZ) to the base of the confining layer underlying the Lower Saturated Zone (LSZ), which included the ULSZ and the LLSZ. Thus the four units comprising the domain from top to bottom were: the USZ, the shale unit separating the USZ and LSZ, the LSZ, and the shale unit below the LSZ. The Production Zone (PZ) was underneath the domain. The top of the PZ coincided with the lower boundary of the model domain.

The preliminary model domain was discretized into 3,164 triangular finite elements in the horizontal plane. These triangular finite elements, known as a mesh, were refined around the two source areas where the density of elements was about twice that in the surrounding area with a coarser mesh. Nodes are points in space that represent one corner of a three-dimensional (tetrahedral in this case) finite element. A slice is a collection of nodes that defines the three-dimensional surface (or contact) separating two layers of finite elements. A layer is the collection of finite elements between two slices and usually represents aquifers, confining units, etc. (e.g., the USZ, UCL, LSZ, etc.). The number of elements of each layer varies. The model domain was divided into layers between each aquifer so that specific hydraulic conductivities could be assigned between

and within units. The USZ and LSZ were further subdivided into five and ten layers, respectively, to provide the requisite discretization for simulating vertical flow and transport and to allow variation in hydraulic conductivity within the LSZ. Each of the resulting 15 layers was horizontal with a constant thickness of approximately 4 meters, totaling 16 horizontal slices. Following further evaluation of site hydrogeology and contaminant data, and in an effort to simplify the model in a way that makes it only as complex as necessary, the layer structures of the preliminary conceptual model were simplified and the horizontal scale was expanded to the domain described below.

4.3. Conceptual Model

The conceptual model for the northeast quadrant is a qualitative description of groundwater flow and chemical fate and transport at the site, and is useful for establishing data requirements for the numerical simulation of flow and chemical fate and transport. Development of the conceptual flow model consists of identifying the model layers, and the water balance components and flow conditions associated with each layer. The conceptual model development for chemical fate and transport consists of identifying the sources areas, the chemicals released, the anticipated intermediate chemical species, and the intrinsic processes that act on the chemical species. For this study, the horizontal extent of northeast quadrant is illustrated on FIGURE 4-1. This boundary also defines the horizontal extent of the conceptual and numerical models.

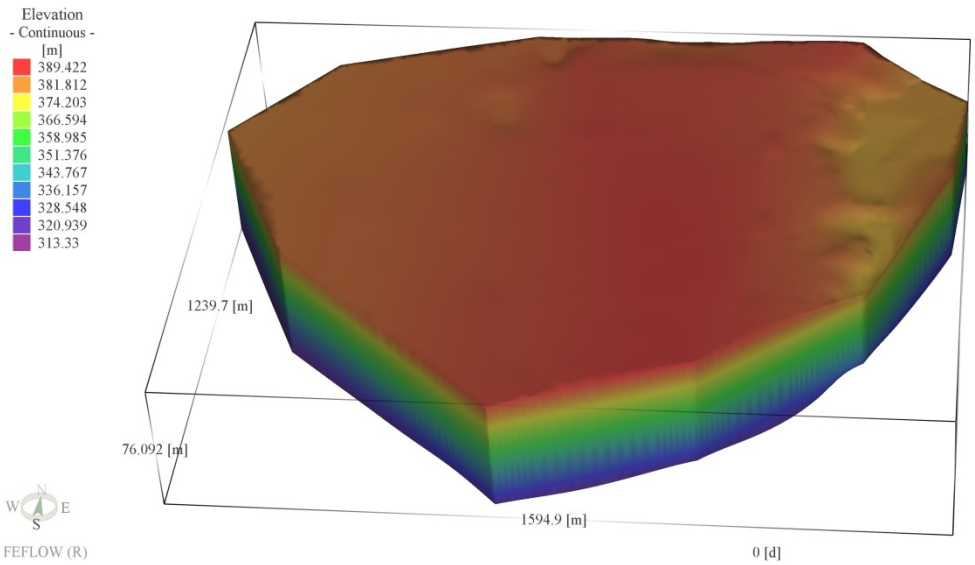

FIGURE 4-1: Elevation of three dimensional finite element model domain
This figure presents the elevation of the three dimensional finite element model domain. Six layers and seven slices are not shown here so elevation can be clearly presented; those layers and slices are shown on FIGURE 4-12.

The conceptual model layers, which correspond to the hydrostratigraphic units (HSUs) of the northeast quadrant, are identified by correlating both lithologic logs of borings and measured water levels at defined depth intervals in the form of hydrogeologic cross sections. Initial estimates of hydraulic parameters are made based on the lithologic descriptions of borings at various locations and depths. Water balance components of the conceptual model are compiled as sources and sinks inside its boundary and the mechanisms for water movement across its boundary. Source areas for chemical species are identified on the basis of past and current chemical species plume maps and historical accounts of chemical species releases in the northeast quadrant. Identification of intermediate chemical species and the physical, chemical, and biological processes acting on them is also based on plume maps combined with an analysis of geochemical indicators of biotransformation mechanisms.

4.3.1. Conceptual Model Layers

Six HSUs have been identified based on the hydrogeologic cross sections developed for this study. From uppermost to lowermost, the HSUs are the upper saturated zone (USZ), the upper confining layer (UCL), the lower saturated zone (LSZ), the lower confining layer (LCL), the lower-lower saturated zone (LLSZ), and the aquiclude (AQ). The USZ, LSZ, and LLSZ are considered to be aquifers based on their predominately sandstone composition. They are separated by the UCL and the LCL which act as semi-confining units due to their predominately shale composition. The thick shale layer that underlies the LLSZ is considered to be an aquiclude. It separates the LLSZ from the production zone (PZ) below and represents the bottom of the conceptual model.

Each aquifer HSU contains lenses of less permeable material (primarily shale) that are not continuous across the horizontal extent of the respective HSU or model area. Potentiometric head variations do not indicate hydraulic separation with vertical position within each HSU due to the low permeability lenses. Therefore, the one-to-one correspondence between model layers and HSUs has been maintained. The conceptual model for the northeast quadrant consists of layers 1 (uppermost) to 6 (lowermost) which correspond directly to these six HSUs.

4.3.1.1. Extent and Thickness of Model Layers

Layer 1 (USZ) consists of the Hennessey Formation and unconsolidated alluvium and fill materials. Layer 1 is an unconfined, water table aquifer present throughout most of the northeast quadrant. The saturated thickness decreases to zero in the eastern portion of the northeast quadrant. The top of the layer at ground surface ranges in elevation

between 377 and 389 m MSL with a mean elevation of about 383 m MSL (FIGURE 4-2). The base of layer 1 ranges in elevation between 367 and 382 m MSL with an average elevation of about 375 m MSL (FIGURE 4-3). The thickness of layer 1 ranges from 0 m to 12 m with an average thickness of about 8 m. The USZ thickness is zero in the vicinity of Soldier Creek where it has been removed by erosion. Layer 1 thickens to the west due to the regional west-southwest dip of the underlying Garber Formation.

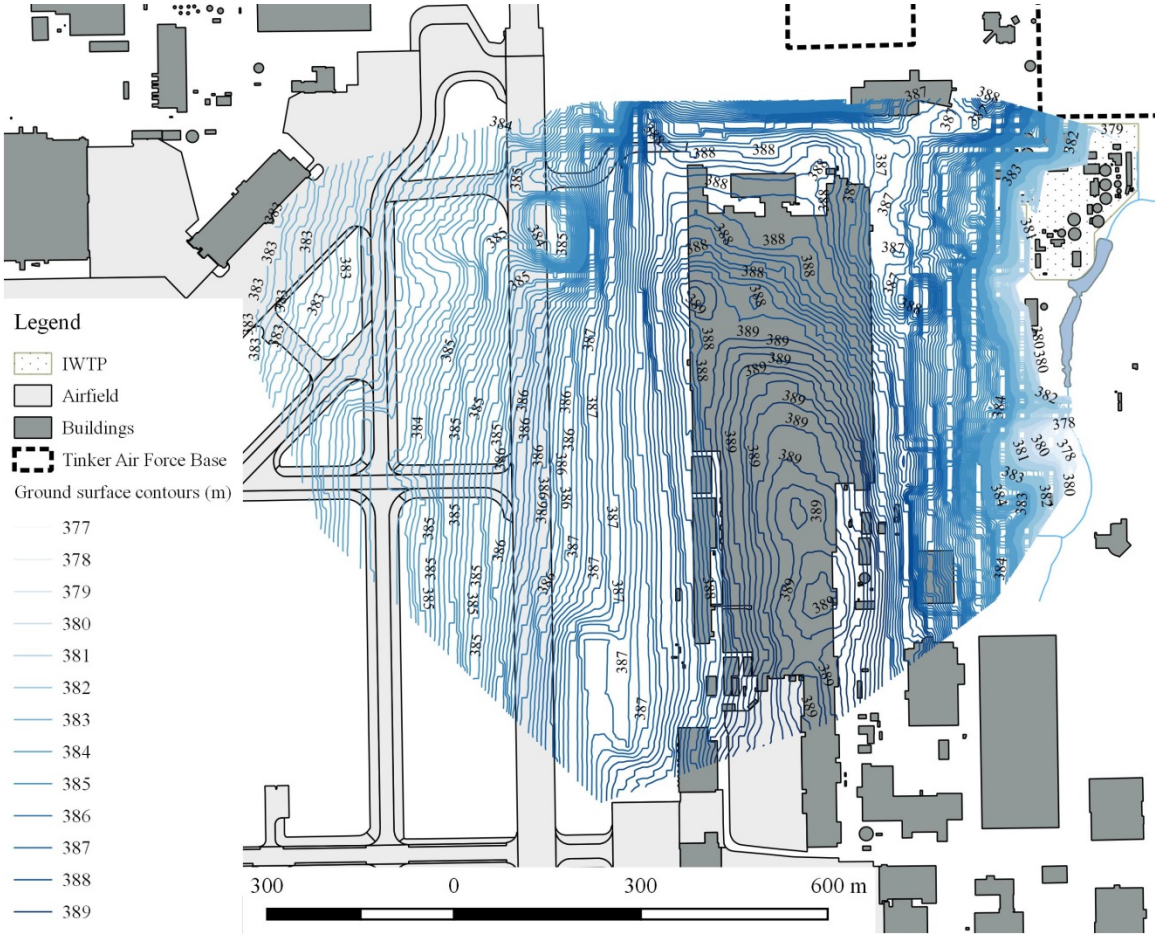

FIGURE 4-2: Elevation of the ground surface, top of Layer 1 (USZ)
The map illustrates the actual elevation of the ground surface in meters. These data also represent Slice 1, which is the top of Layer 1 of the model domain.

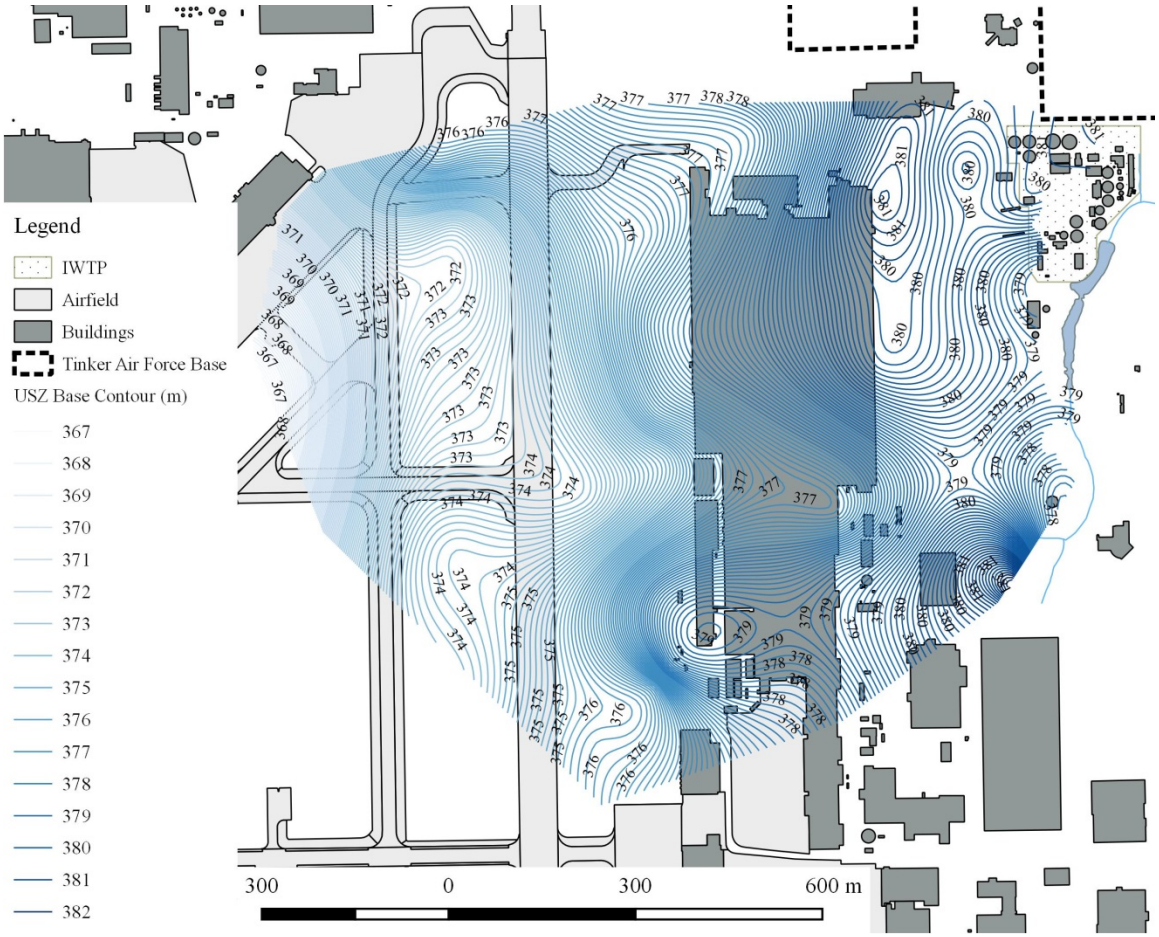

FIGURE 4-3: Elevation of the base of Layer 1 (USZ)
The map illustrates the elevation of the base of Layer 1 (USZ) in meters. These data also represent Slice 2, which is the top of Layer 2 (UCL) of the model domain.

Layer 2 (UCL) is the upper shale layer immediately below the USZ. Locally, layer 2 perches groundwater above the lower aquifer (the LSZ). The effectiveness of the UCL to restrict vertical groundwater flow is locally reduced due to discontinuities, facies changes, and possible man-made conduits that exist within this layer. As the UCL approaches ground surface to the east, its thickness decreases to zero in the vicinity of Soldier Creek where it has been removed by erosion. Additional leakage is likely to occur along this margin due to edge effects including erosional channels and increased weathering. The top of the UCL corresponds to the base of the USZ where it exists. The

base of the layer ranges in elevation between 363 and 378 m MSL with an average elevation of about 371 m MSL (FIGURE 4-4). The thickness of the layer 2 ranges from 0 m to 7 m with an average thickness of 4 m. Layer 2 thickens to the west with a mound occurring in the western half of the quadrant.

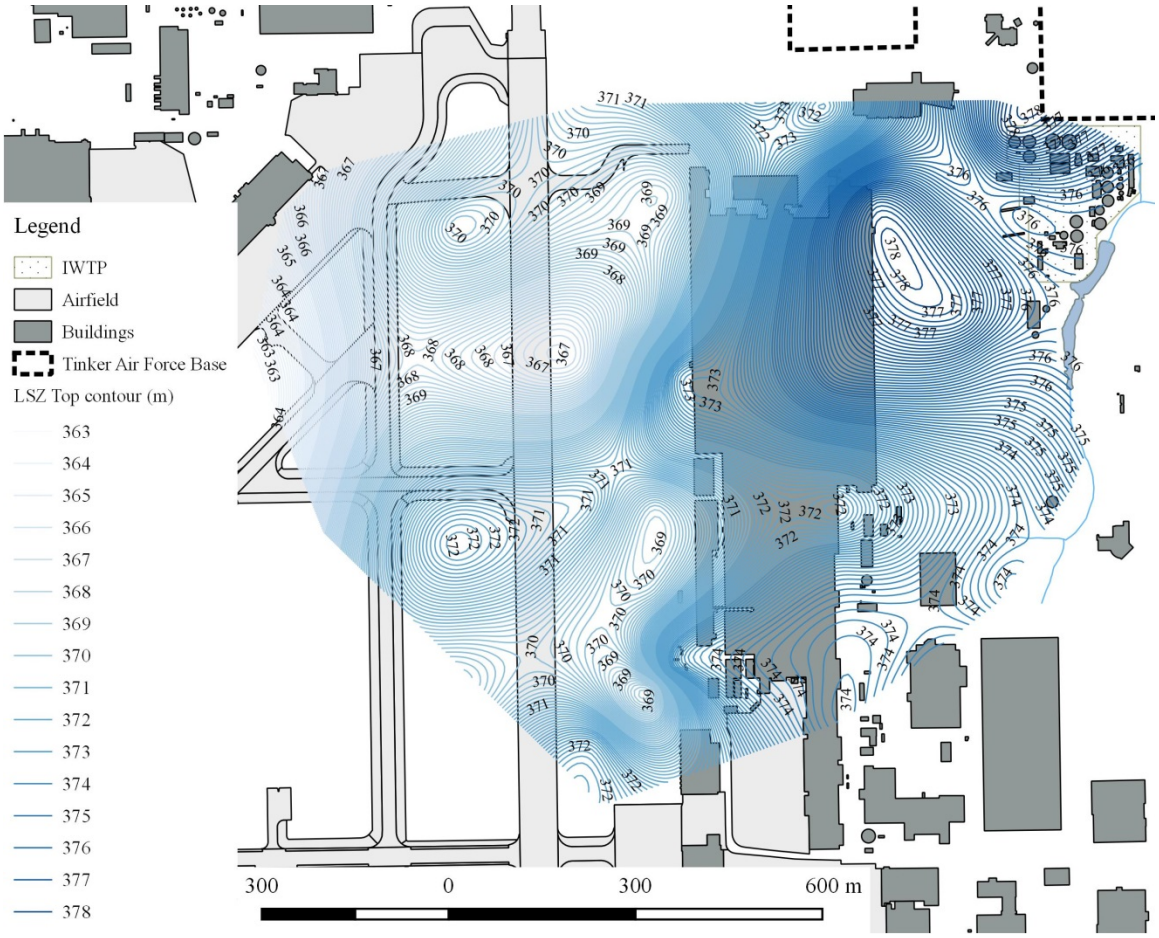

FIGURE 4-4: Elevation of the base of Layer 2 (UCL)
The map illustrates the elevation of the base of Layer 2 (UCL) in meters. These data also represent Slice 3, which is the top of Layer 3 (LSZ) of the model domain.

Layer 3 (LSZ) is a water table aquifer over the northeast quadrant. It becomes confined by the UCL beyond the western boundary of the northeast quadrant. The top of the LSZ corresponds to the base of the UCL where it exists. In the vicinity of Soldier

Creek where the USZ and UCL have been removed by erosion, the top of the LSZ is the ground surface. The base of the layer ranges in elevation from 353 m to 365 m MSL with an average elevation of about 357 m MSL (FIGURE 4-5). The thickness of the layer ranges from 9 m to 24 m with an average thickness of about 16 m. In general, the LSZ thickness decreases from east to west, with a mound and trough occurring in the middle southeastern and southwestern sectors of the quadrant, respectively.

Layer 4 (LCL) is the lower shale layer immediately below the LSZ. It acts as a semi-confining unit for layer 5 below. The base of the layer ranges in elevation from 348 m to 359 m MSL with an average elevation of about 353 m MSL (FIGURE 4-6). The thickness of the layer ranges from 3 m to 6 m with an average thickness of about 4 m. The LCL thickens toward the southwest corner of the northeast quadrant.

Layer 5 (LLSZ) is a confined aquifer over the northeast quadrant. The base of the layer ranges in elevation from 320 m to 337 m MSL with an average elevation of about 328 m MSL (FIGURE 4-7). The thickness of the layer ranges from 19 m to 30 m with an average thickness of about 23 m. The LLSZ thickens to the west with a mound and ridge occurring in the western sector and a trough occurring in the eastern sector of the quadrant. The base of the LLSZ is considered to be a no-flow boundary for the northeast quadrant conceptual model.

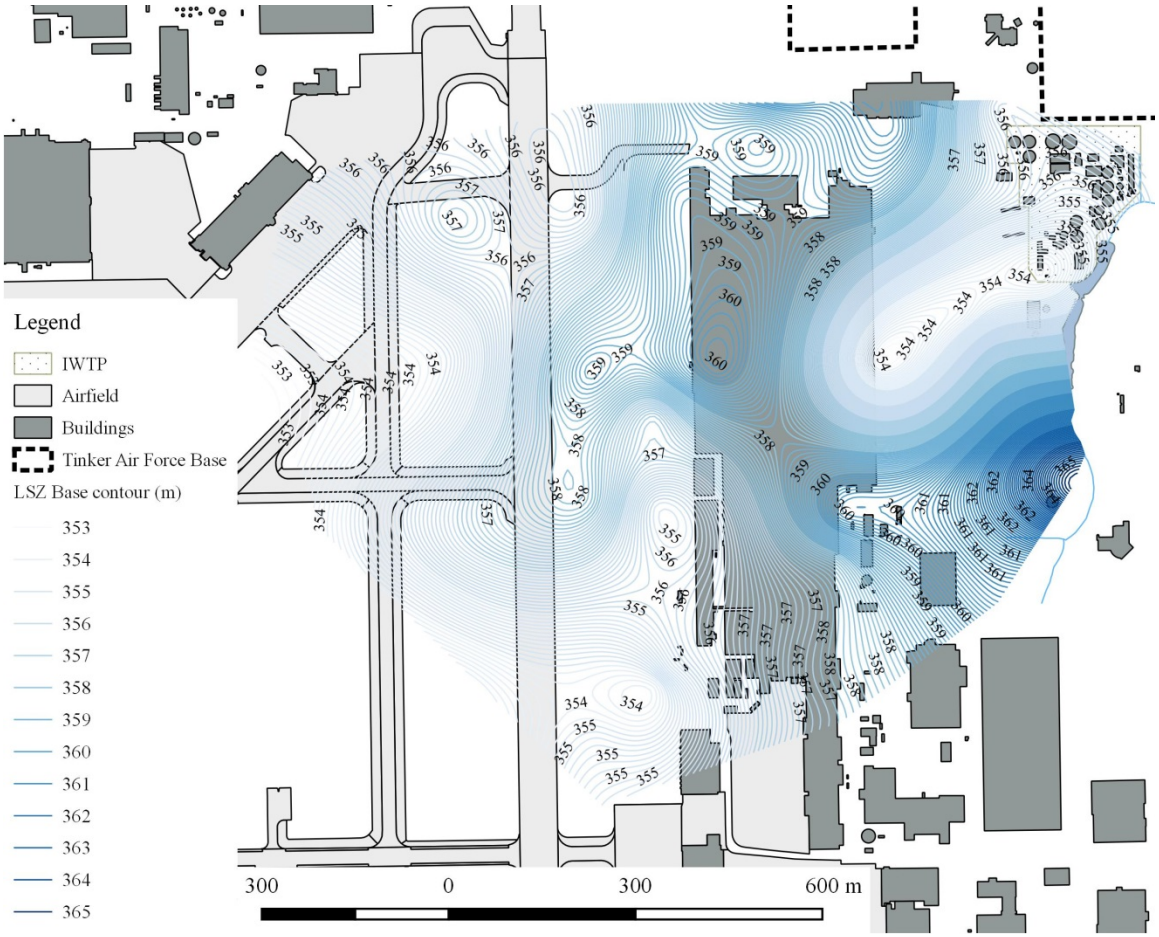

FIGURE 4-5: Elevation of the base of Layer 3 (LSZ)
The map illustrates the elevation of the base of Layer 3 (LSZ) in meters. These data also represent Slice 4, which is the top of Layer 4 (LCL) of the model domain.

Layer 6 (AQ) is the lower shale layer immediately below the LLSZ. It acts as a confining unit for the PZ below. The base of the layer ranges in elevation from 313 m to 333 m MSL with an average elevation of about 322 m MSL (FIGURE 4-8). The thickness of the layer ranges from 3 m to 6 m with an average thickness of about 4 m. The LCL thickens toward the southwest corner of the northeast quadrant.

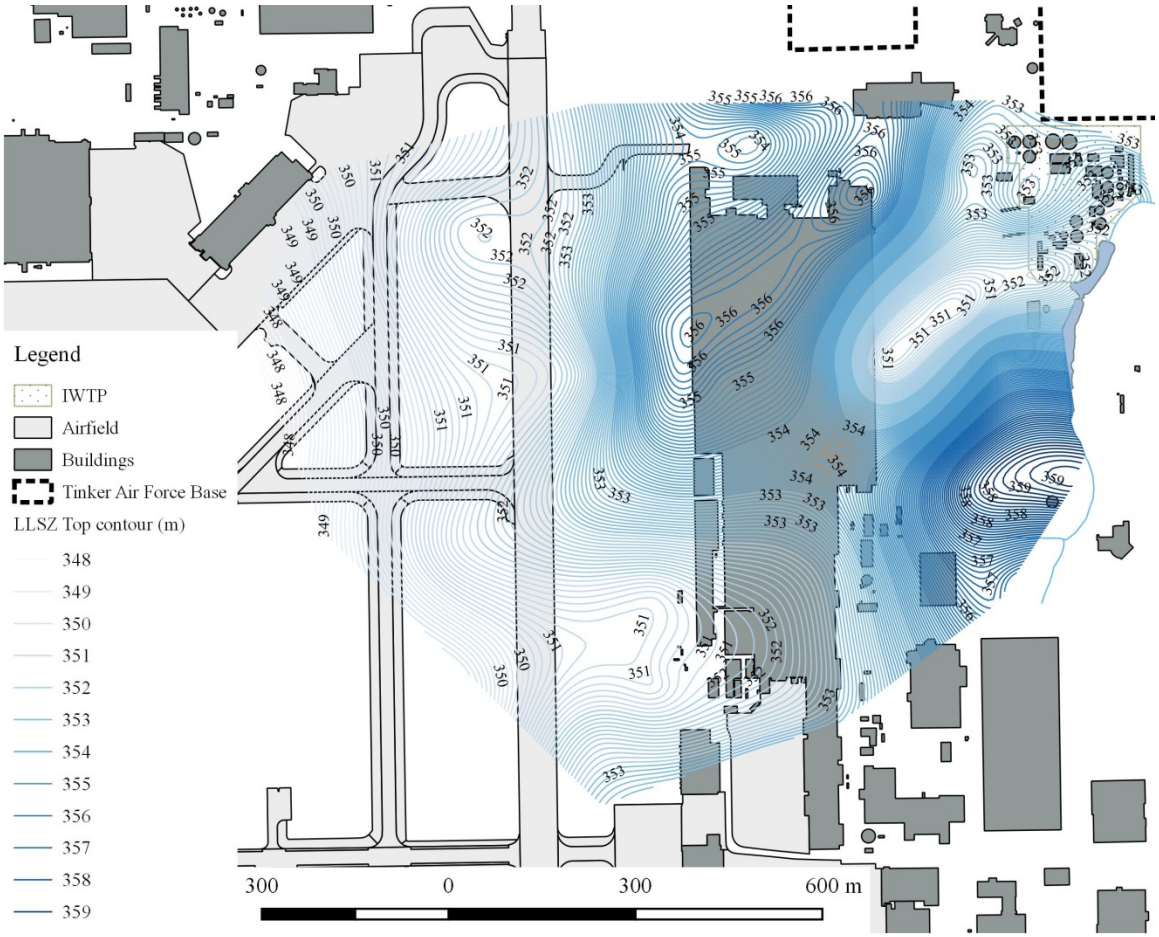

FIGURE 4-6: Elevation of the base of Layer 4 (LCL)
The map illustrates the elevation of the base of Layer 4 (LCL) in meters. These data also represent Slice 5, which is the top of Layer 5 (LLSZ) of the model domain.

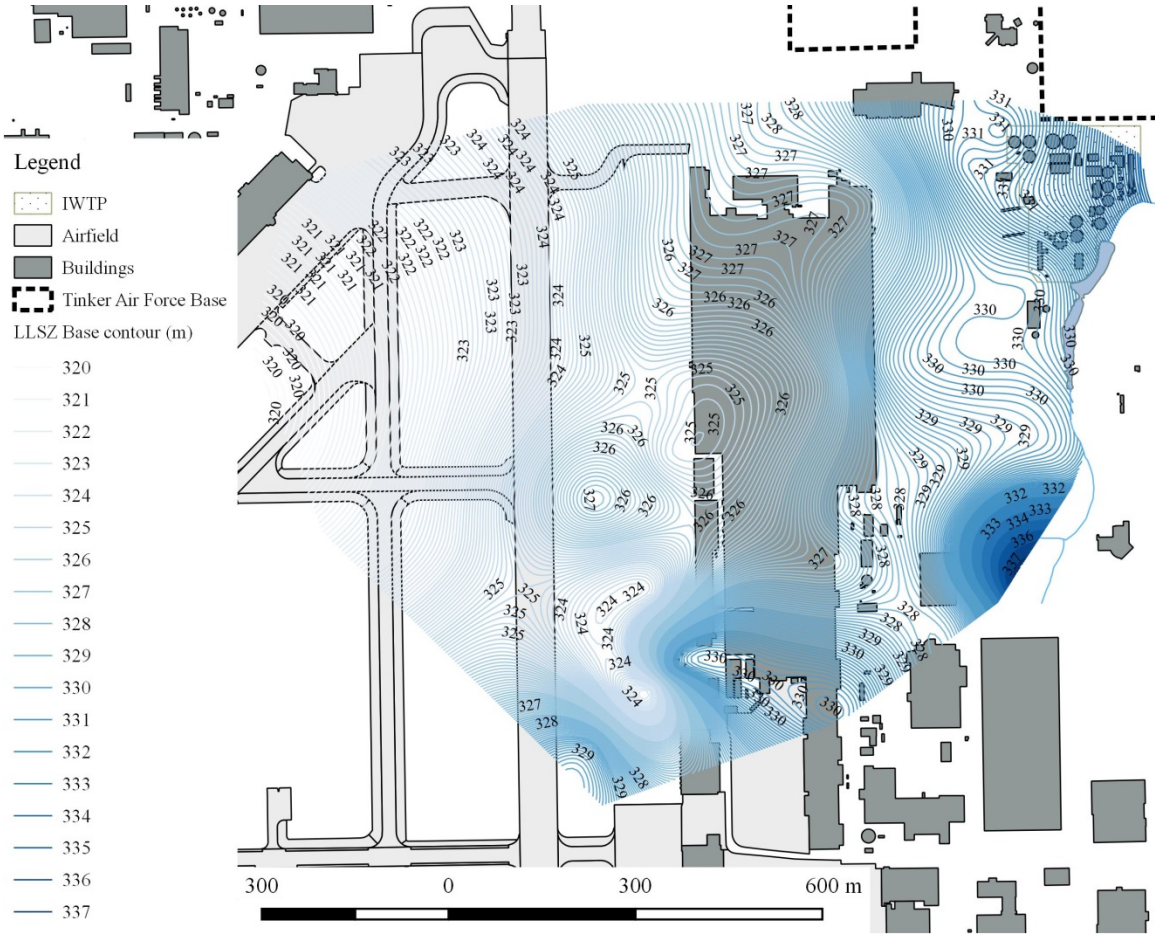

FIGURE 4-7: Elevation of the base of Layer 5 (LLSZ)
The map illustrates the elevation of the base of Layer 5 (LLSZ) in meters. These data also represent Slice 6, which is the top of Layer 6 (AQ) of the model domain.

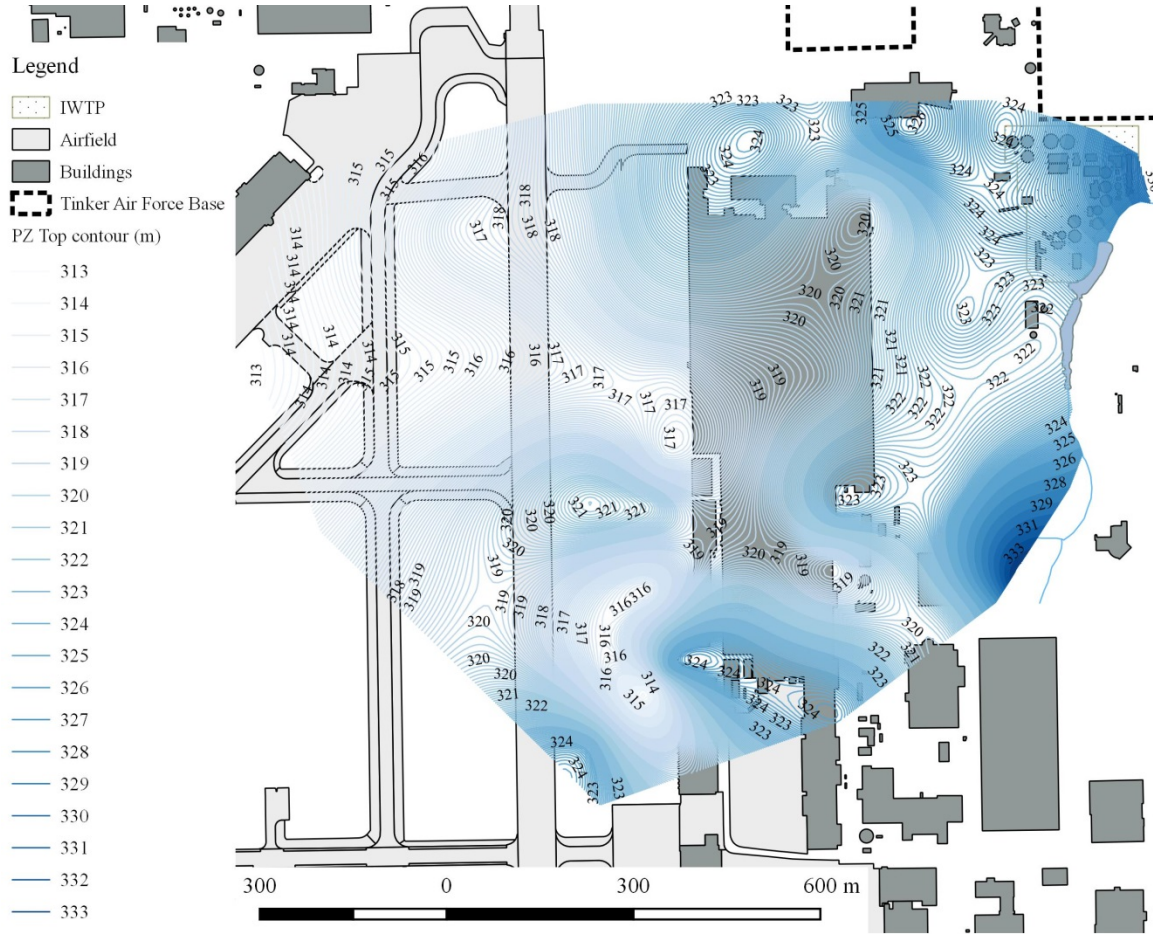

FIGURE 4-8: Elevation of the base of Layer 6 (AQ)
The map illustrates the elevation of the base of Layer 6 (AQ) in meters. These data also represent Slice 7, which is the base of the model domain.

4.3.1.2. Groundwater Flow

Water-level measurements at the northeast quadrant were examined on an intermittent and less than comprehensive basis prior to 1992 [70]. Since that time, numerous quadrant-wide, concurrent rounds of water-level measurements have been taken in support of various remedial efforts at the site. Most of the individual rounds of data are influenced in some way by active groundwater extraction. These data cannot be used to evaluate natural or steady-state groundwater flow conditions. Comprehensive water level measurements were made during a brief period in July 1993 with the specific

purpose of capturing an accurate representation of potentiometric surfaces; those measurements are considered to be the best-available historic representation of steady-state conditions at the site. This data set was later modified in an effort to extend the areal coverage and increase accuracy [70, 71]. Measurements with questionable validity based on well construction were eliminated. Estimated data from locations that were not part of the original set were based on trend analysis. In support of the present study, a complete round of water-level measurements at wells in and around the northeast quadrant was taken in February 2009. The modified July 1993 data and the February 2009 data were compared to characterize steady-state flow conditions in the northeast quadrant. The February 2009 data are the basis for the present discussion of current groundwater flow conditions, and the numerical flow model boundary conditions and calibration.

In addition, transducers were installed from July 2008 to September 2008 in a subset of the wells later measured in February 2009. As discussed in Section 3.1, continuous hydrographs of water levels from these wells were examined for short-term water level variations under natural conditions.

4.3.1.2.1. Layer 1 USZ

The USZ is an unconfined, water-table aquifer throughout most of the northeast quadrant. Where the water table exists in the USZ, it is perched above the LSZ by the UCL. The maximum thickness of the USZ vadose zone is about 7 m along a northwest-southeast trend in the western half of the northeast quadrant. The potentiometric (water table) surface of the USZ indicates a groundwater mound/ridge along a northeast-southwest trend in the middle-western portion of the northeast quadrant (FIGURE 4-9).

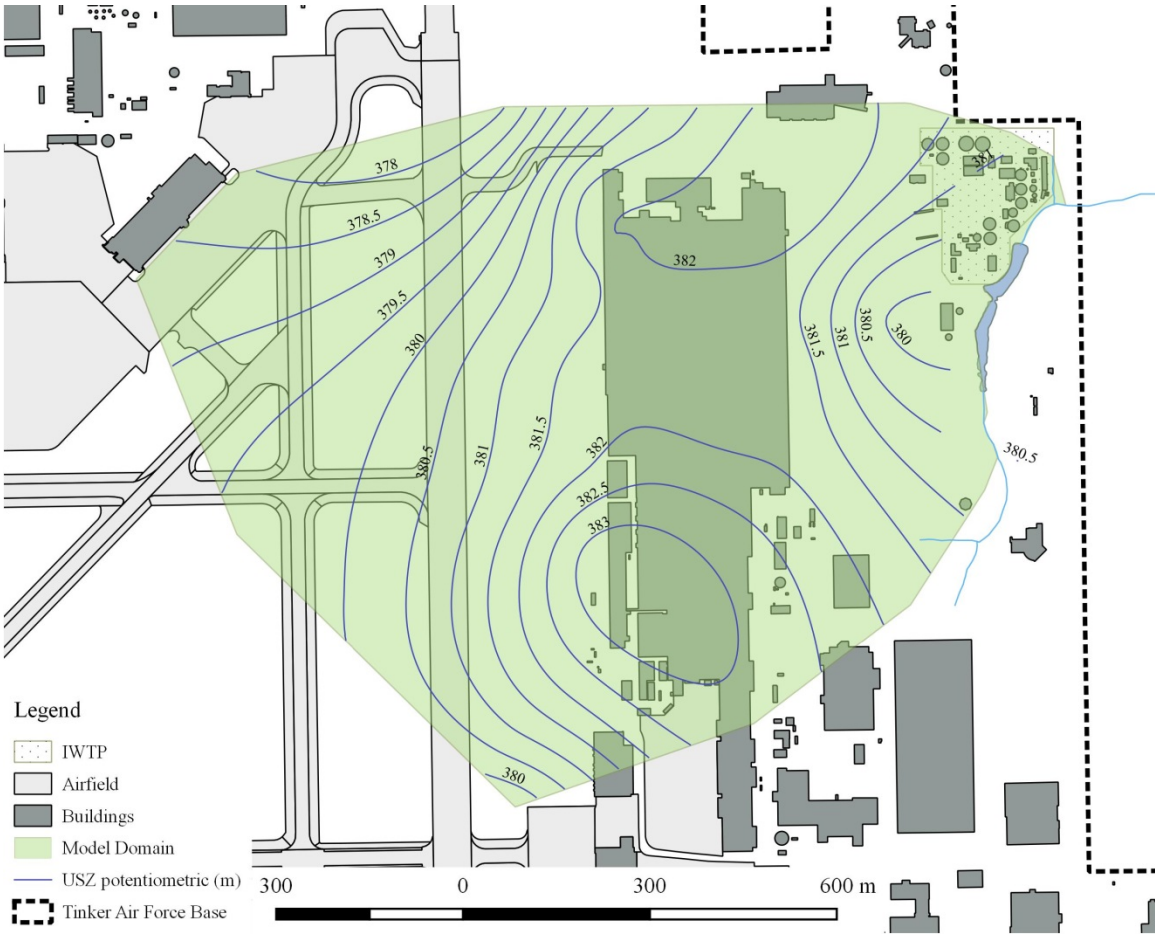

FIGURE 4-9: Potentiometric surface in the USZ, 2008
This figure illustrated the potentiometric surface of the water table aquifer in the USZ.

The mound/ridge may be due in part to discharges from storm drains and utility leakage from Building 3001. The maximum saturated thickness of the USZ is about 6 m in the southwest corner of the northeast quadrant. To the northwest, the saturated thickness decreases to 2 m. To the east, in the vicinity of Soldier Creek, the saturated thickness decreases to zero. No drainage to the surface or direct discharge to Soldier Creek is known to occur. Therefore, the eastern limit to the saturated zone represents a lateral flow boundary, and groundwater flowing east of the mound must move vertically downward through the UCL. Groundwater flowing to the west and northwest of the

mound either continues to move in those directions laterally in the USZ or vertically downward primarily through leakage and/or conduits through the underlying UCL shale.

4.3.1.2.2. Layer 3 LSZ

The LSZ is also an unconfined water-table aquifer throughout the northeast quadrant. In the vicinity of Soldier Creek where the LSZ crops out at the surface, a vadose zone exists above the uppermost saturated zone in the LSZ. The thickness of the unsaturated zone of the LSZ ranges from about 1 m to 8 m, and is thickest in the center of the northeast quadrant. The unsaturated zone is dependent upon the spatial variation of leakage entering from above and leaving below, and the contours of the base of the LSZ layer. The existence of the unsaturated zone below the perched water of the overlying USZ suggests that the UCL effectively limits vertical groundwater flow from above. The potentiometric (water table) surface of the LSZ indicates a general, west-southwest trend in groundwater flow with a suggestion of a moderate mound/ridge in the north-central portion of the quadrant (FIGURE 4-10). Like the unsaturated zone thickness, local variations in the potentiometric (water table) surface are due in part to the spatial variation of leakage entering from above and leaving to below, and the basal formation contours. LSZ groundwater originating as infiltration from above or entering from lateral flow through the upgradient LSZ boundary either continues to move laterally to the west northwest in the LSZ or vertically downward through the underlying shale of the LCL.

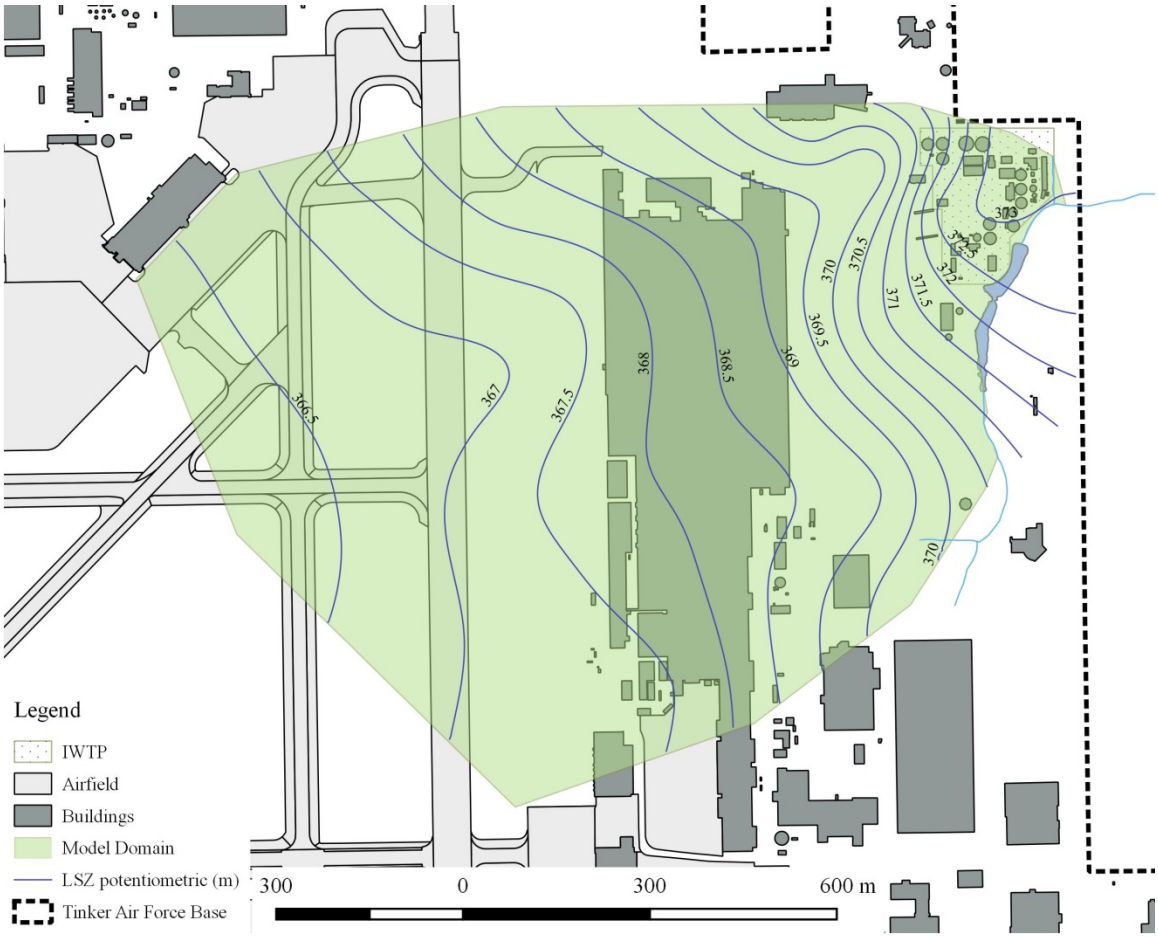

FIGURE 4-10: Potentiometric surface in the LSZ, 2008
This figure illustrated the potentiometric surface of the water table aquifer in the LSZ.

4.3.1.2.3. Layer 5 LLSZ

The LLSZ is a confined aquifer throughout the northeast quadrant. Local mounds in the potentiometric surface produce a groundwater flow divide that trends north to southeast in the eastern sector of the quadrant (FIGURE 4-11). In the western sector of the quadrant, groundwater flow is to the west. In the east, there may also be a minor groundwater flow component to the east. Given that the shale unit underlying the LLSZ is essentially an aquiclude, it was concluded that LLSZ groundwater originating as infiltration from above or entering laterally from one of two upgradient LLSZ boundary

segments continues to move laterally exiting through one of three downgradient LLSZ boundary segments.

FIGURE 4-11: Potentiometric surface in the LLSZ, 2008
This figure illustrated the potentiometric surface of the water table aquifer in the LSZ.

4.3.1.3. Hydraulic Parameters

Hydraulic parameter estimates for the HSUs in the northeast quadrant from previous investigations have been summarized in the Feasibility Study Addendum to the Tinker Air Force Base Industrial Wastewater Treatment Plant/Soldier Creek Off-Base Groundwater Operable Units Feasibility Study (SAIC, 2007). Hydraulic conductivities of the USZ, LSZ, and LLSZ are estimated to range from 0.04 to 6.7 ft/day, 0.25 to 8.7

ft/day, and 0.78 to 15.6 ft/day, respectively. In support of the present study, slug tests were performed at selected wells within and in the vicinity of the northeast quadrant. The combined data set provides a basis for the selection of starting values and upper and lower bounds for hydraulic conductivity in the calibration of the numerical flow model.

4.3.1.4. Groundwater Recharge and Discharge

Recharge to groundwater in the northeast quadrant is spatially variable due to a number of factors. Of primary importance are impervious surface cover, injection of stormwater from building collection systems, and lithologic variations. The relationship between those factors and recharge is complex. Groundwater recharge estimates for the Central Oklahoma Aquifer, which includes the northeast quadrant, range from 0.1 to 8 inches/year based on stream-regression analysis [70]. This range provides a basis for the selection of starting values and upper and lower bounds for recharge in the calibration of the numerical flow model. The calibration provides a means for quantifying the variability of recharge without individually evaluating the effect of each of those aforementioned contributing factors.

During the time interval evaluated as part of the current study, groundwater has been withdrawn from the northeast quadrant for potable water supply and as a part of remedial efforts. Potable water withdrawals, which were intended to be from the production zone (PZ) only, likely also occurred from overlying saturated zones due to improper well construction. Withdrawals occurred from the USZ, LSZ, and LLSZ as a part of remedial efforts in 1994 to 2004 [72]. Presently there are no withdrawals for potable water or remediation within the northeast quadrant. Regionally, groundwater withdrawals for water supply or remediation are not believed to influence groundwater

flow within the northeast quadrant. Therefore, for the purposes of the current study, groundwater flow in the northeast quadrant is considered to be naturally occurring.

The east branch of Soldier Creek is the only significant surface water feature in the northeast quadrant. Flow in Soldier Creek is perennial. The minimum thickness of the LSZ vadose beneath Soldier Creek is approximately two meters. Therefore, Soldier Creek must be a losing stream within the northeast quadrant, and baseflows must originate from upgradient sources. In a previous modeling investigation, shallow sediments in the bed of Soldier Creek are assigned a permeability of 0.1 ft/day for reaches overlying sandstone areas such as the LSZ, and the stream bed thickness is assumed to be one foot [73].

4.3.2. Fate and Transport

4.3.2.1. Source Areas

A number of source areas of chemical species which are the subject of the current study have been identified, as described in Sections 2.3 and 3.4. Some areas are identified with a high degree of certainty. Others are characterized as potential sources. Source area characterization in the northeast quadrant is complicated by a number of factors including imprecise knowledge of the history and quantity of the release, close proximity of two or more sources, variations and uncertainty of the source area lithology, and remedial efforts subsequent to selected releases. In this study, source areas are selected for inclusion in the fate-and-transport model based primarily on recently developed plume maps of the chemical species, supported by the previous investigations. Two source areas are indicated in the Building 3001 area; those are at monitoring wells 105-MW12 and 34A. The third source area is selected at the IWTP. These locations are

considered to be “hot spots” based on recent chemical species detections. The Building 3001 sources areas are situated in USZ. The IWTP source area is situated in the LSZ. The chlorinated hydrocarbon species, PCE and TCE, were likely released at each source area, either in the non-aqueous phase, dissolved phase, or in both phases. PCE and TCE concentrations are persistently high possibly due to continuous dissolution of immobile, non-aqueous phase mass from a smear zone associated with each source area, which suggests a Rayleigh model may not fit site data.

4.3.2.2. Advection and Dispersion

Dissolved chemical species are transported by advection and dispersion under natural groundwater flow conditions in the northeast quadrant. Advective transport is a function of the effective porosity of the aquifer zones and confining layers of the northeast quadrant. In a previous modeling study, effective porosities of 0.2 and 0.02 are assigned to sandstones and shales, respectively in the northeast quadrant [70]. Dispersive transport is quantified by the value of the dispersivity assigned to the setting. At the field scale, dispersivity accounts for both micro- and macro-scale dispersion of dissolved species due to variations in the seepage velocity within the medium. In the northeast quadrant, dispersivity in the direction of groundwater flow (longitudinal dispersivity) is estimated to range from 20 to 50 m. Transverse dispersivity is estimated to range from 0.01 to 0.1 of the longitudinal dispersivity. Both estimates are based on empirical relationships from the literature relating dispersivity to observation scale, or the distance between observation points and the source [8, 74, 75]. Dye trace results support the observed heterogeneity of the site and therefore, provide additional justification for longitudinal and transverse dispersivity estimates.

4.3.2.3. Biotransformation and Sorption

Biotransformation of PCE and TCE by reductive dechlorination has occurred to some extent in the northeast quadrant based on the observance of the intermediate species *cis*-DCE, vinyl chloride, and ethene. The rate and extent of the reductive dechlorination of the parent species PCE and TCE requires an adequate number of suitable bacteria, an adequate supply of electron donors, and suitable reducing conditions. The persistence of the intermediates over time in the northeast quadrant may occur under different scenarios. The sources may be leaching the parent species on a more-or-less continuous basis over time, in which case a pseudo steady-state condition exists where reductive dechlorination is on-going due to a continuous supply of reactants. Alternatively, reductive dechlorination may be limited because one or more of the conditions that promote transformation (e.g., shift to aerobic conditions) is less than optimal. A recent analysis of the molar concentrations of chlorinated hydrocarbon parent species and intermediates over time at selected wells near the IWTP that suggests that reductive dechlorination has occurred in the past, but is not on-going at a significant rate. However, the possibility of continued leaching of parent species from source areas at the IWTP makes this conclusion less than certain [71]. It is likely that the persistent distribution of parent species and intermediates in the northeast quadrant is the combined result of both continued source area leaching and rate limiting conditions for reductive dechlorination.

In this study, reductive dechlorination of the stable carbon isotopes of each chlorinated hydrocarbon species is considered to gain further insight into the course of each reaction, in terms of rate and extent, and contribution of chlorinated hydrocarbons

from each source area. This approach is based on the premise that the light carbon isotopes are reductively dechlorinated at slightly higher rates in the same setting [41].

In the northeast quadrant, sorption of chemical species to solids in the matrix of the sandstones and shales results in the retardation of the dissolved phase under transient transport conditions. Linear instantaneous sorption is quantified by the sorption coefficient, which is a function the chemical species and the chemical and physical properties of the solid matrix. Each chemical species will have a characteristic sorption coefficient range for each type of solid matrix. In a previous modeling study, dimensionless sorption coefficients for TCE of 2.30 and 1.36 were assigned to sandstones and shales, respectively, in the northeast quadrant [70]. When compared on the basis of soil sorption coefficients normalized for total organic carbon content in the soil matrix, the chlorinated hydrocarbon species ranking from most sorbed to least sorbed are; PCE, TCE, *cis*-DCE, and vinyl chloride. Also, in a soil matrix with high clay content, sorption to mineral surfaces could be significant relative to sorption to the organic fraction [74].

4.4. Numerical Model

4.4.1. Finite Element Method

Groundwater flow and the fate and transport of chlorinated hydrocarbons in the northeast quadrant were modeled using the software program FEFLOW version 7.6 by DHI Group, Inc. (https://www.mikepoweredbydhi.com/products/feflow), which is based on the finite element method. This method allows greater flexibility in spatial discretization than does the finite difference technique. This capability is important in the northeast quadrant, where refined finite element meshes at source areas are needed to produce stable and accurate results for transient simulations. The finite element method

can also simulate moving boundary conditions such as unconfined water tables. FEFLOW can perform three dimensional simulations for saturated and unsaturated conditions, with one or two free water surfaces. Multi-species reactive transport is supported. FEFLOW has interpolation routines that can generate spatially variable properties such as model layer thicknesses, boundary conditions, and material properties. For transient simulations, FEFLOW has automatic time stepping routines for stability and user-specified error tolerances.

For the steady-state flow simulation, FEFLOW's Euclidean L2 Integral RMS error norm with 0.001 error tolerance is specified. Water levels in dry cells are unconstrained with a residual water depth of 0.5 m for computing transmissivity. For the transient fate and transport simulations, automatic time step control by the Adams-Bashforth/backward trapezoid time integration scheme with 0.001 day initial time step and 200 day maximum time step is used.

4.4.2. Groundwater Flow Model

4.4.2.1. Model Domain and Boundary Conditions

The model domain contains 917,140 finite elements and 178,855 nodes (FIGURE 4-12). The finite element mesh is locally refined (i.e., smaller finite elements) around the monitoring well nests, to provide more realistic flow simulation. The seven model slices, which represent the layer boundaries, are surfaces constructed in FEFLOW by importing data files with x, y, and z coordinates of the contacts between each layer. In the physical domain of the northeast quadrant, layers 1 and 2 (USZ and UCL) do not exist in the vicinity of Soldier Creek. Historically, the pinching out of layers was handled mathematically by reducing the layers to some small thickness, which allowed modelers

to approach meaningful simulations despite the inability to match true site conditions. However, a more recent version of FEFLOW allows for layer pinching using unstructured three dimensional tetrahedral meshes. When partially or fully unstructured meshes are employed, FEFLOW requires that models be run with the unsaturated/variably saturated flow option using Richards' equation. FEFLOW scales the transmissivity of elements within phreatic layers for head and flow calculations based on the relative thickness of the unsaturated interval. Layers 2, 4, and 5 are considered to be confined. They are specified as the fixed type, or fully saturated with non-moving top and bottom slices.

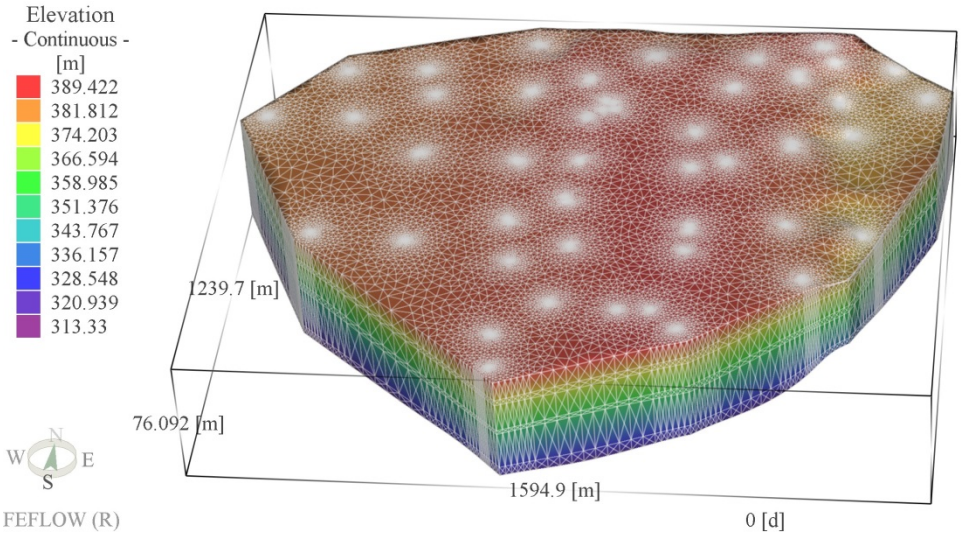

FIGURE 4-12: Three dimensional finite element model domain
This figure presents the three dimensional finite element model domain, including the six layers and seven slices, showing elements and nodes. Nodes are refined around monitoring well nests.

Fixed-head boundary conditions are applied along the northeastern and southwestern borders of all slices. Fixed-head boundaries are applied along the border of slices one and two where the USZ and the UCL exist. The fixed nodal heads are

FEFLOW interpolations of potentiometric surfaces based on measured water levels from February 2009. Northern and southeastern borders are generally perpendicular to groundwater flow; boundary conditions are unassigned and thus, are assumed to be no flow boundaries.

4.4.2.2. Flow Model Calibration

4.4.2.2.1. Methodology

The numerical flow model of the northeast quadrant simulates groundwater flow under steady-state conditions. Groundwater flow within the model domain and through its boundaries is constant with respect to time. Hydraulic heads within the domain and at its boundaries are constant over time as well. Known quantities relevant to the flow model calibration are concurrent water level observations taken at various locations and depths within and around the model domain. Estimated ranges of both hydraulic conductivities for model layers and infiltration due to precipitation are available. The objective of the calibration is to estimate the spatial distribution of hydraulic conductivity within the model domain and the areal distribution of infiltration into the upper domain boundary such that model-generated water levels are in reasonably good agreement with measured water levels at the observation points. The calibrated distributions of hydraulic conductivity and infiltration should be within expected ranges. The resulting flow regime also must meet reasonable expectations with regard to groundwater travel times within the domain.

4.4.2.2.2. Parameter Estimation

Given that the actual parameters of the natural system are infinite and observational data sets are limited, inverse modeling is a widely-used parameter

estimation technique that seeks to minimize the differences between the model output and the observational data set. Benefits of inverse modeling include: (1) clear determination of parameter values that produce the best possible fit to the available observations; (2) diagnostic statistics that quantify the quality of calibration and data shortcomings and needs; (3) inferential statistics that quantify reliability of parameter estimates and predictions; and (4) identification of issues that are easily overlooked during non-automated calibration. However, inverse modeling can be problematic with respect to insensitivity, non-uniqueness, and instability issues [76].

Since some parameters are estimated, there is an inherent level of input uncertainty, so model outcomes also contain uncertainty. Sources of uncertainty include poor characterization or knowledge of the distribution of actual system parameters, mathematical inadequacies of models simulating complex natural systems, and multiple sets of model results that compare well with site observations [77]. To understand the model results in the context of the more global investigative questions, these uncertainties must be assessed. One method of measuring uncertainty in parameter estimates is through the objective function (Φ), a scalar that represents the goodness-of-fit of observations calculated using a given parameter set. Φ equals the sum of squares of the weighted residuals between calculated and measured observations. Minimization of the objective function indicates the best likely estimates of model parameters. Widely-used software packages that attempt to minimize the objective function and are designed to integrate with model codes include PEST [78] and UCODE [79].

PEST is a numerically robust software package that uses a nonlinear estimation technique known as the Gauss-Marquardt-Levenberg (GML) method (Gallagher and

Doherty, 2007). The GML method is a frequentist approach, meaning that unknown parameters are treated as fixed values, which the software attempts to estimate through calibration with an observational data set. This approach is different than another commonly used (Bayesian) approach, where unknown parameters are conceptualized as randomly distributed and software would attempt to refine the probability distribution of the parameters relative to measured observation during the calibration process [77].

A modified version of the "pilot point" methodology (see Section 4.4.2.2.3) described by Doherty (2003) was used within FePEST in conjunction with nonlinear parameter estimation techniques to estimate the spatial distribution of hydraulic conductivity within the model domain and the areal distribution of infiltration into the upper domain boundary such that model-generated water levels are in reasonably good agreement with measured water levels at the observation points by minimizing an "objective function" known as Φ [78, 80]. The objective function is the weighted sum of squared differences between model-generated observation values and those actually measured in the laboratory or field [78]. The numerical model simulates groundwater flow under steady-state conditions. Groundwater flow through domain boundaries and hydraulic heads within the domain are constant over time. Concurrent water level observations taken at various locations and depths were used as known quantities. Hydraulic conductivities for model layers and infiltration due to precipitation ranges are estimated.

4.4.2.2.3. FePEST Methodology

The model was calibrated using an inverse modeling approach through the FePEST software; FePEST is a software package integrated within FEFLOW that

facilitates the proper creation of PEST files. As described earlier, PEST estimates parameters by taking a GML approach that minimizes the objective function (Φ). The model was considered calibrated when the Φ value was sufficiently reduced and calibrated parameters were deemed realistic and reasonable. The numerical model simulates groundwater flow under steady-state conditions. Groundwater flow through domain boundaries and hydraulic heads within the domain are constant over time. Concurrent water level observations taken at various locations and depths were used as known quantities. Hydraulic conductivities for model layers and infiltration due to precipitation ranges are estimated.

Potentiometric surfaces for the seven model slices were developed using the observed water levels for the northeast quadrant. Constant head boundaries for each model slice were generated based on these surfaces. FePEST writes a FEFLOW input file for the northeast quadrant model with the constant-head boundaries applied at the slices and initial estimates for the distributions of hydraulic conductivity and infiltration. FePEST uses a pilot point approach to interpolate the distributions of hydraulic conductivity and infiltration. Twenty pilot points, each with an associated hydraulic conductivity, are assigned to each of the six model layers. In addition, zonal infiltration rates were assigned across the entire top model slice. FePEST performs the interpolation and writes the FEFLOW input file. Each FEFLOW run generates an output file with calculated hydraulic heads at observation points. Measured heads at the observations points are obtained from the potentiometric surfaces.

FePEST first quantifies the relationship between the model result and each starting pilot point variable. Incremental changes to the variables are made in a series of

FEFLOW runs. The resulting heads at the observation points provide the basis for determining linearized relationships, or derivatives, between the variables and the model results. New pilot point variables are calculated by applying the derivatives to the difference between observed and modeled heads. This sequence of determining derivatives and calculating new variables is referred to as optimization iterations. It is repeated until a statistical measure of the difference between observed and modeled heads is reduced to an acceptable value. The final set of pilot point variables is then taken as that for the calibrated flow model.

The PEST control file specifies the control data, parameter data, and observation data for the flow model calibration. The control data include settings related to PEST's Marquardt lambda, which scales the parameter upgrade vector in the nonlinear weighted least squares parameter estimation. The initial lambda, lambda adjustment factor, sufficient new/old phi ratio per optimization iteration, and the limiting relative phi reduction between lambdas are set at 9, 1.5, 0.3, 0.1, and 10 respectively, following PEST guidance (Doherty, 2009). PEST's objective function minima phi is the scalar that represents the goodness-of-fit of observations calculated using the parameter set from a PEST iteration. It equals the sum of squares of the weighted residuals between calculated and measured observations.

Pilot point initial parameter values for horizontal hydraulic conductivity were assigned as follows: layer 1 was 8.64E-3 m/day, layers 3 and 5 were 8.64 m/day, and layers 2 and 4 were 8.64E-4 m/day. Initial infiltration was set at 0.006 cm/day. Initial ratios of horizontal to vertical conductivity were 40 for layers 1, 3, and 5, and 50 for layers 2 and 4. The initial phi calculated based on these parameters was 1,151.4. After

30 iterations, the final phi was 123.92. Based on a ranking of relative sensitivities calculated by PEST at termination of the calibration, the ten most sensitive pilot point parameters are the ratio of horizontal to vertical conductivity for layer 2, infiltration (five pilot points), horizontal conductivity for layer 1, the ratio of horizontal to vertical conductivity for layer 1, and horizontal conductivity for layer 2.

The calibrated flow model's goodness-of-fit is ultimately based on a comparison of modeled and measured water levels (FIGURE 4-13). A side-by-side comparison of measured water level data, from the modified July 1993 and February 2009 data sets, and water levels generated by the calibrated model supports two conclusions.

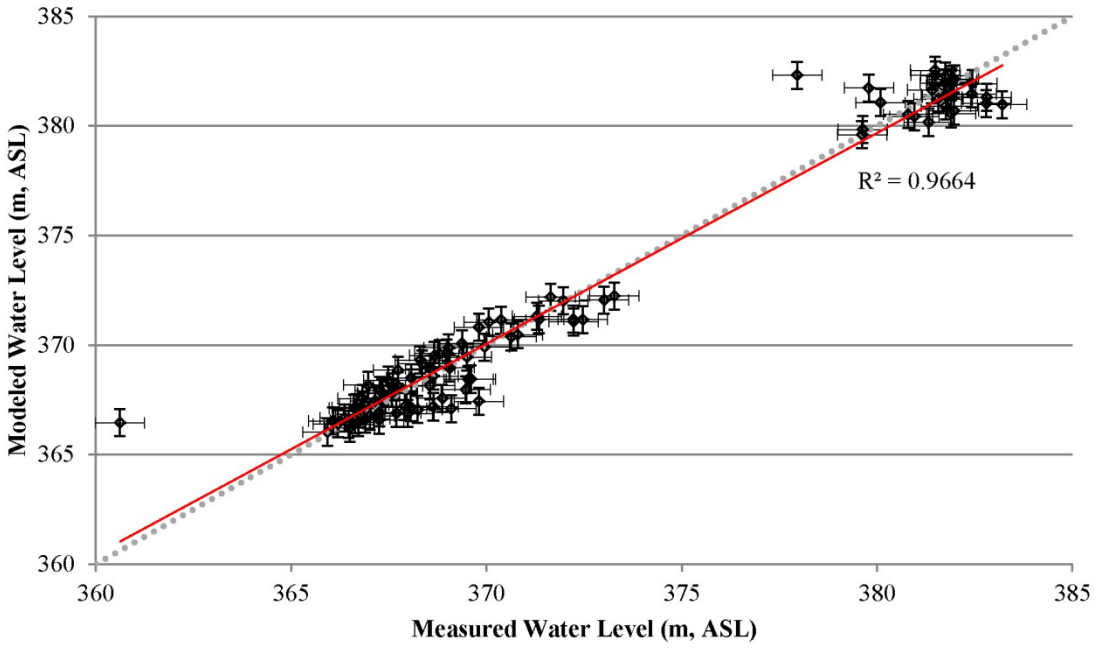

FIGURE 4-13: Measured (2008) versus modeled water levels
Plot illustrates measured water levels (2008) compared to modeled water levels, representing a goodness-of-fit. The gray dotted line represents a 1:1 slope, while the red line represents a trendline for the data, with the measured R^2 of 0.9664.

First, the measured water level data sets from these time periods, 16 years apart, are essentially the same. Therefore, both represent a steady-state flow condition. Second, the calibrated model accurately estimates water levels and groundwater flow for the steady-state condition in the northeast quadrant.

Calibrated infiltration rates range from 3.06E-5 m/day to 3.75E-5 m/day (FIGURE 4-14). The average infiltration rate is about 3.07E-5 m/day. The highest infiltration rates are in the northeast areas of the northeast quadrant, at Soldier Creek.

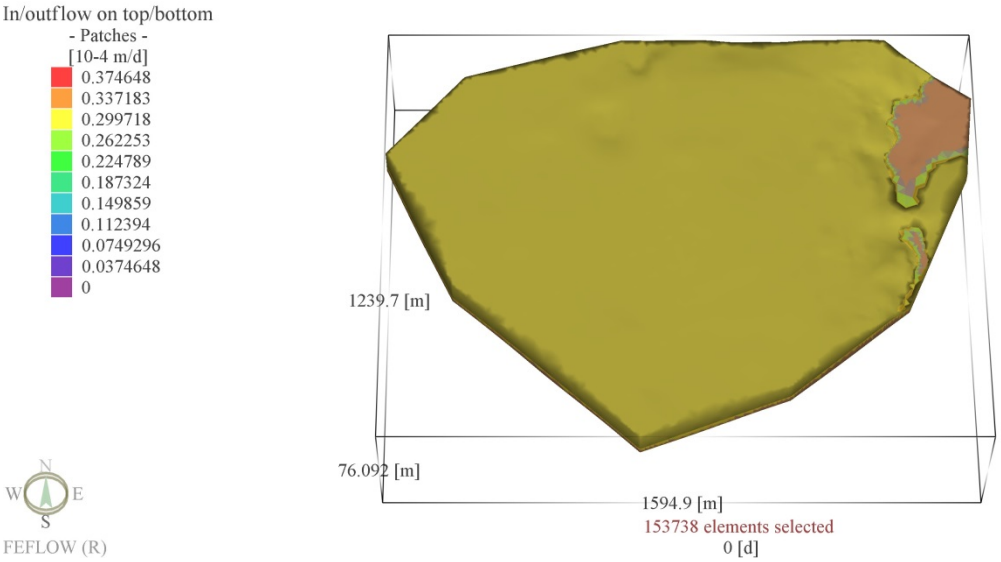

FIGURE 4-14: Calibrated infiltration rates
The figure illustrates the calibrated in/out flow on the top slice of the model domain.

In layer 1, the calibrated horizontal (K_{xx} and K_{yy}) conductivities range from 0.0644 m/day to 0.1250 m/day and 0.0150 m/day to 0.1932 m/day, respectively (FIGURE 4-15). The calibrated vertical (K_{zz}) conductivities range from 2.2E-4 m/day to 2.1E-3 m/day (FIGURE 4-16). The average horizontal (K_{xx} and K_{yy}) and vertical (K_{zz}) conductivities are about 0.0973 m/day, 0.0611 m/day and 0.0014 m/day, respectively.

The highest layer 1 conductivities are in the northwest and southwest areas of the northeast quadrant.

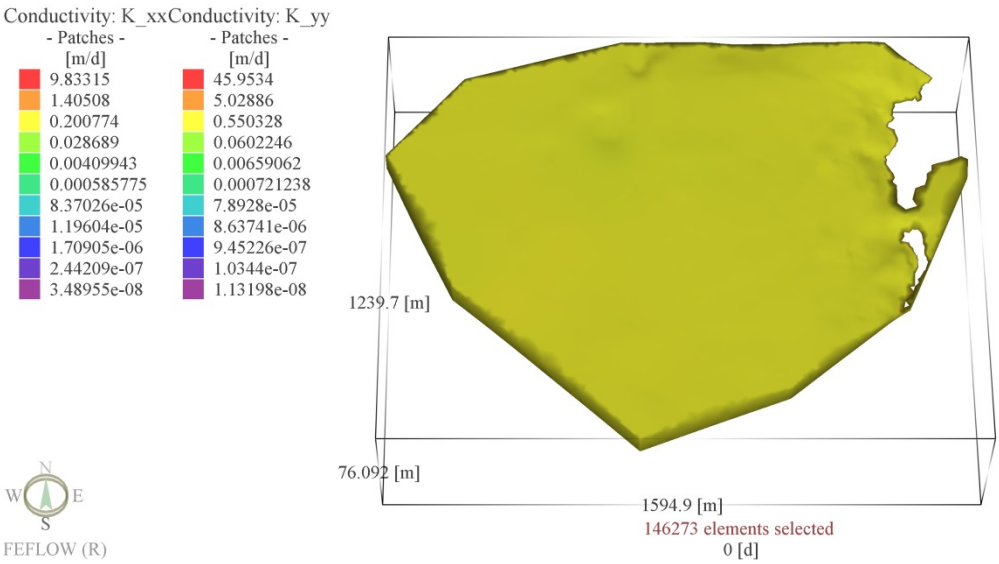

FIGURE 4-15: Calibrated horizontal conductivities (Layer 1)

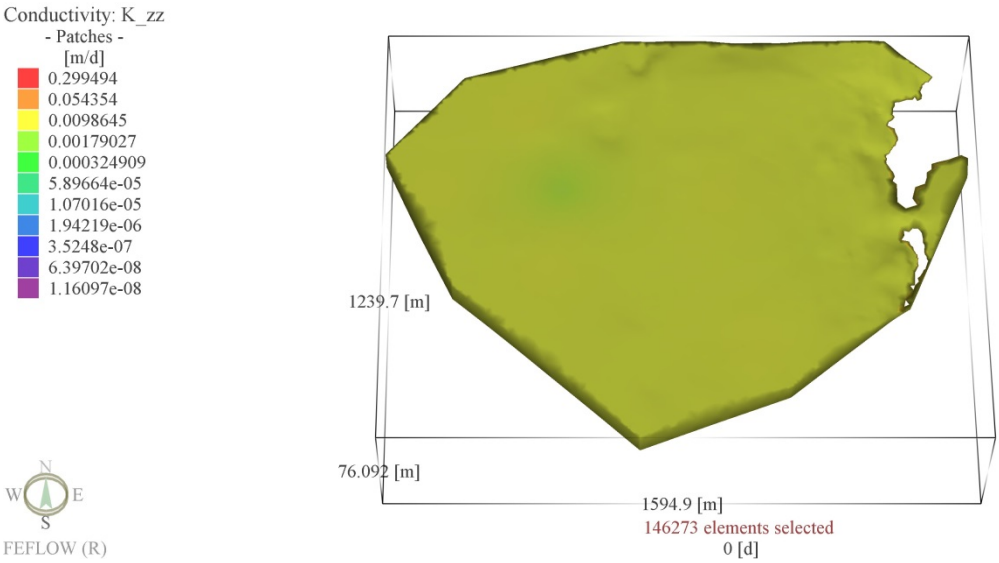

FIGURE 4-16: Calibrated vertical conductivities (Layer 1)

In layer 2, the calibrated horizontal (K_{xx} and K_{yy}) conductivities range from 3.49E-8 m/day to 0.00126 m/day and 1.13E-8 m/day to 9.28E-4 m/day, respectively

(FIGURE 4-17). The calibrated vertical (K_{zz}) conductivities range from 7.37E-6 m/day to 3.42E-5 m/day (FIGURE 4-18). The average horizontal (K_{xx} and K_{yy}) and vertical (K_{zz}) conductivities are approximately 3.94E-4 m/day, 2.23E-4 m/day and 2.16E-5 m/day, respectively. As with layer 1, highest conductivities are in the northwest and southwest areas of the northeast quadrant.

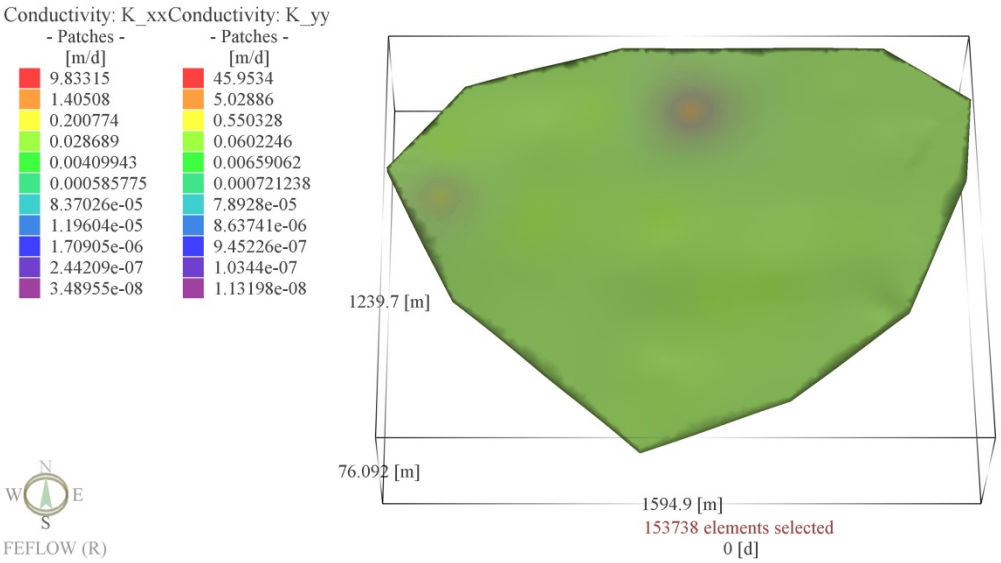

FIGURE 4-17: Calibrated horizontal conductivities (Layer 2)

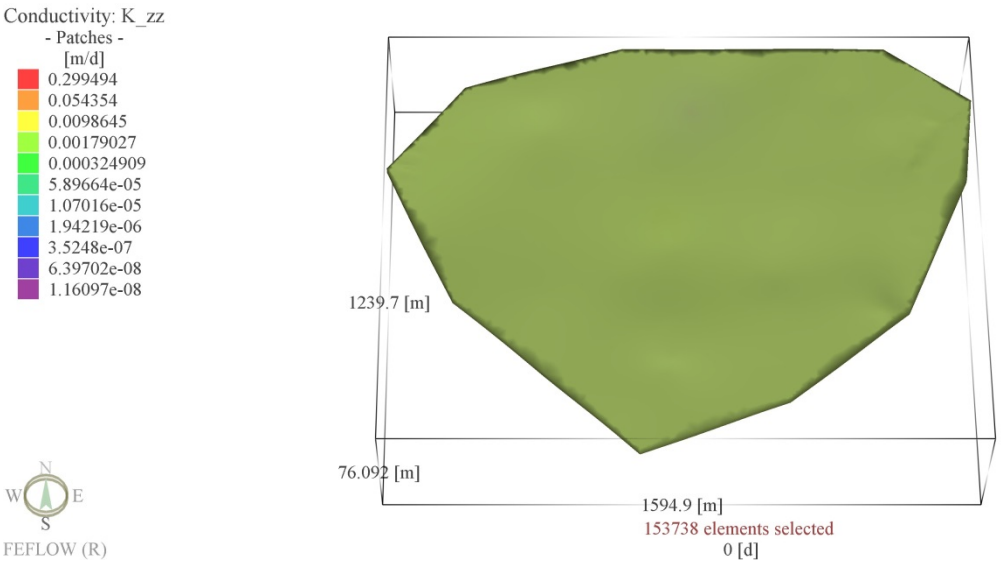

FIGURE 4-18: Calibrated vertical conductivities (Layer 2)

In layer 3, the calibrated horizontal (K_{xx} and K_{yy}) conductivities range from 0.1781 m/day to 7.8691 m/day and 0.4973 m/day to 7.2105 m/day, respectively (FIGURE 4-19). The calibrated vertical (K_{zz}) conductivities range from 0.1185 m/day to 0.2547 m/day (FIGURE 4-20). The average horizontal (K_{xx} and K_{yy}) and vertical (K_{zz}) conductivities are about 3.6635 m/day, 4.8584 m/day and 0.1892 m/day, respectively. The lowest layer 3 conductivities are in the north-central and southeast areas of the northeast quadrant.

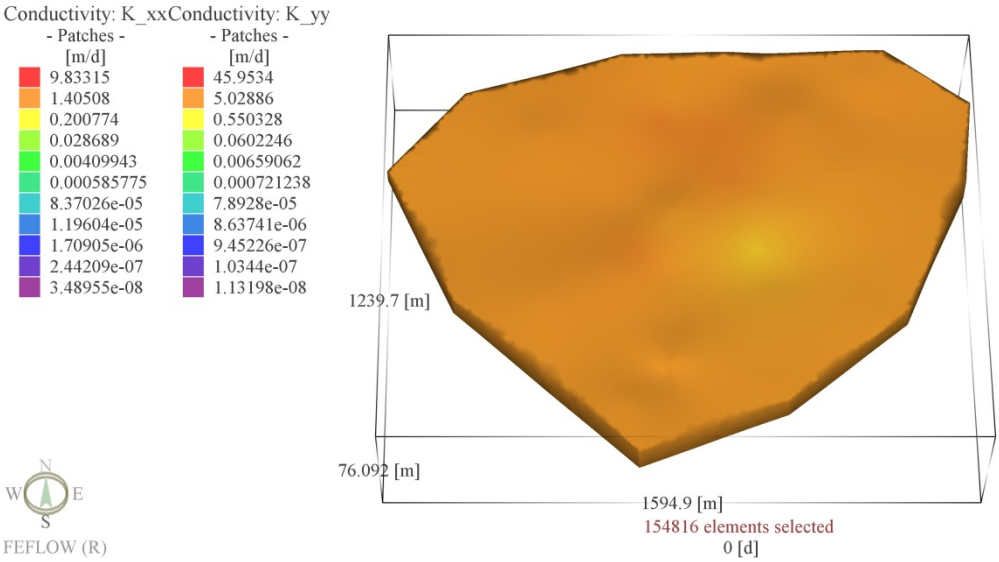

FIGURE 4-19: Calibrated horizontal conductivities (Layer 3)

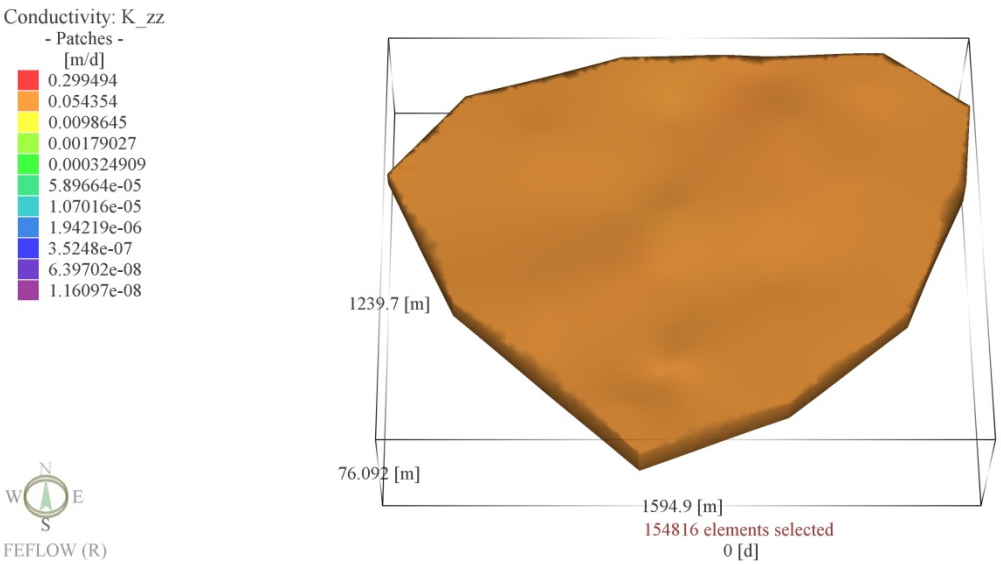

FIGURE 4-20: Calibrated vertical conductivities (Layer 3)

In layer 4, the calibrated horizontal (K_{xx} and K_{yy}) conductivities range from 1.27E-3 m/day to 3.1E-3 m/day and 1.73E-8 m/day to 3.43E-3 m/day, respectively (FIGURE 4-21). The calibrated vertical (K_{zz}) conductivities range from 1.49E-8 m/day to 6.15E-5 m/day (FIGURE 4-22). The average horizontal (K_{xx} and K_{yy}) and vertical (K_{zz}) conductivities are about 2.09E-3 m/day, 7.51E-4 m/day and 2.33E-5 m/day, respectively. The highest layer 4 conductivities are in the north-central and southeast areas of the northeast quadrant.

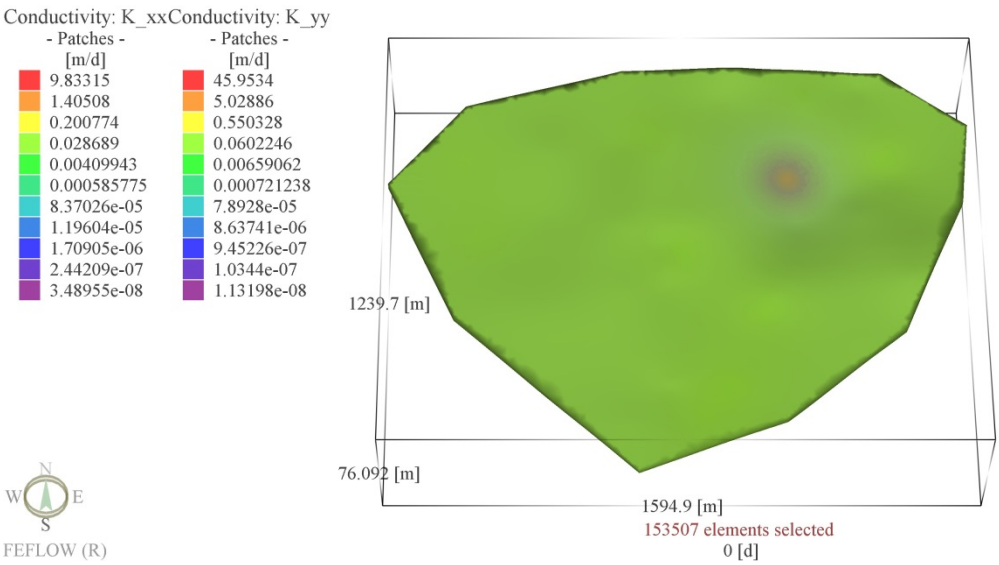

FIGURE 4-21: Calibrated horizontal conductivities (Layer 4)

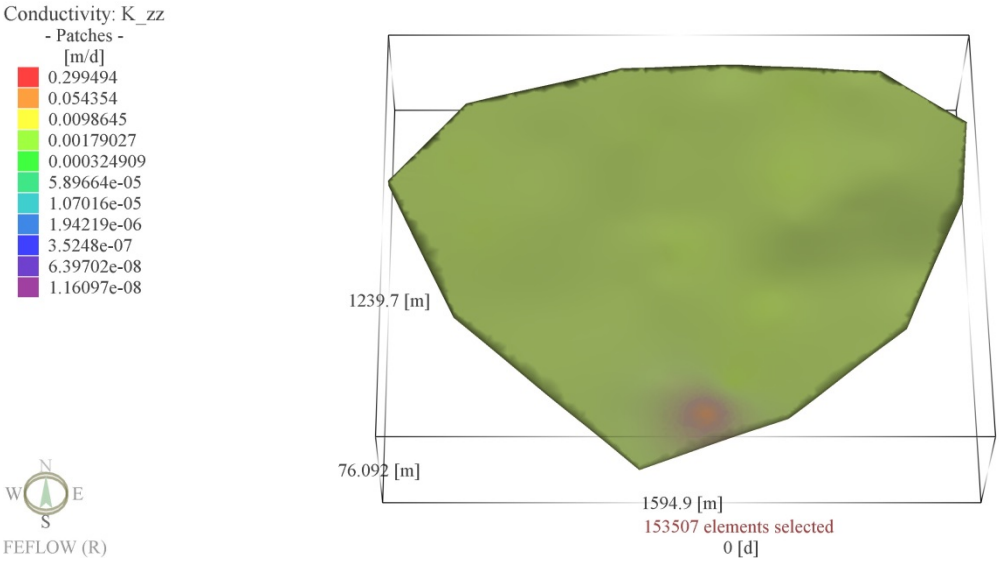

FIGURE 4-22: Calibrated vertical conductivities (Layer 4)

In layer 5, the calibrated horizontal (K_{xx} and K_{yy}) conductivities range from 4.1261 m/day to 9.8332 m/day and 2.6524 m/day to 45.9534 m/day, respectively (FIGURE 4-23). The calibrated vertical (K_{zz}) conductivities range from 1.43E-8 m/day to 0.2995 m/day (FIGURE 4-24). The average horizontal (K_{xx} and K_{yy}) and vertical (K_{zz}) conductivities are about 8.1354 m/day, 10.863 m/day and 0.0954 m/day, respectively.

The highest layer 5 conductivities are in the east-central and southeast areas of the northeast quadrant.

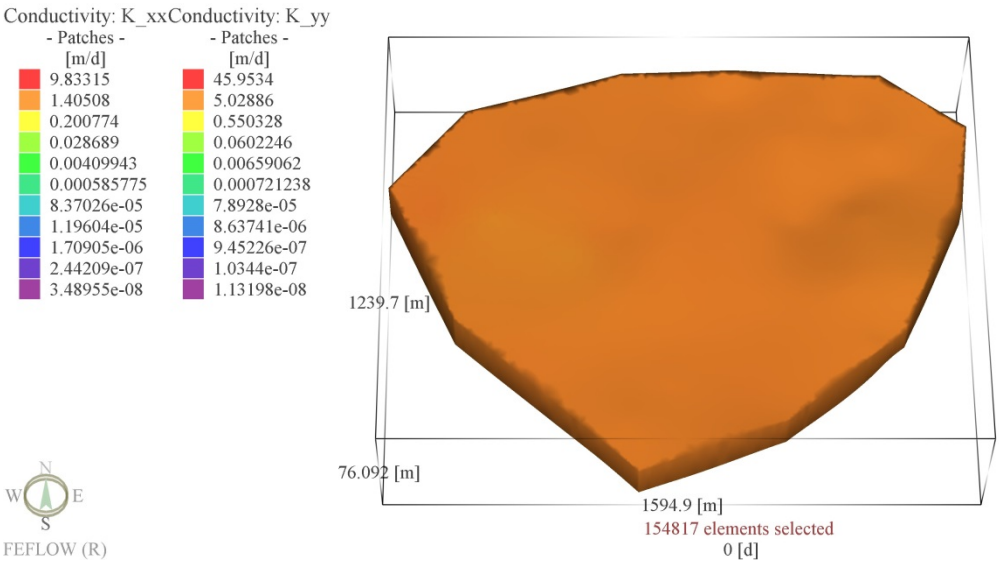

FIGURE 4-23: Calibrated horizontal conductivities (Layer 5)

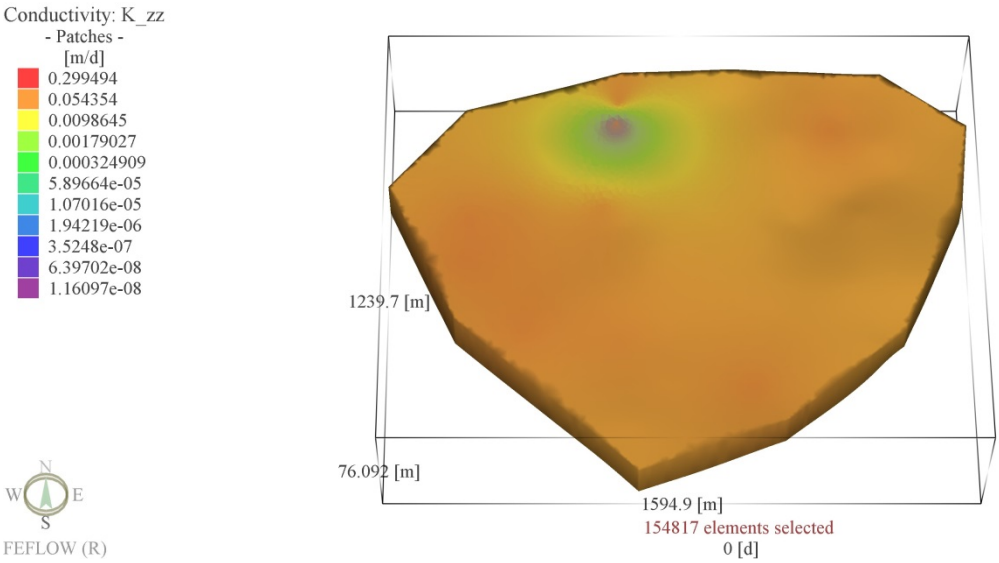

FIGURE 4-24: Calibrated vertical conductivities (Layer 5)

In layer 6, the calibrated horizontal (K_{xx} and K_{yy}) conductivities range from 8.02E-7 m/day to 1.19E-4 m/day and 6.06E-5 m/day to 1.35E-4 m/day, respectively

(FIGURE 4-25). The calibrated vertical (K_{zz}) conductivities range from 1.16E-8 m/day to 1.09E-6 m/day (FIGURE 4-26). The average horizontal (K_{xx} and K_{yy}) and vertical (K_{zz}) conductivities are about 5.49E-5 m/day, 9.19E-5 m/day and 4.12E-7 m/day, respectively. The highest layer 5 conductivities are in the east-central and southeast areas of the northeast quadrant.

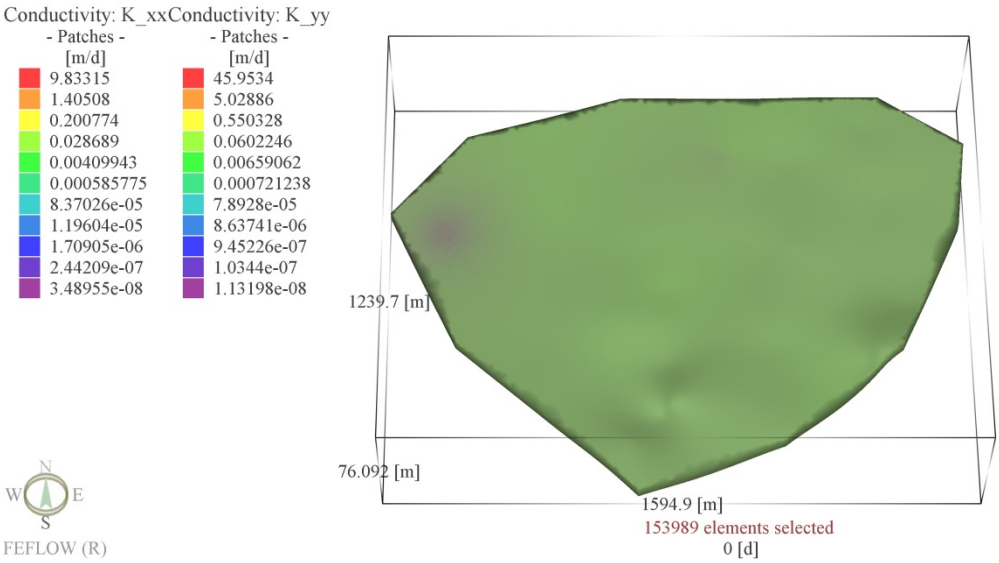

FIGURE 4-25: Calibrated horizontal conductivities (Layer 6)

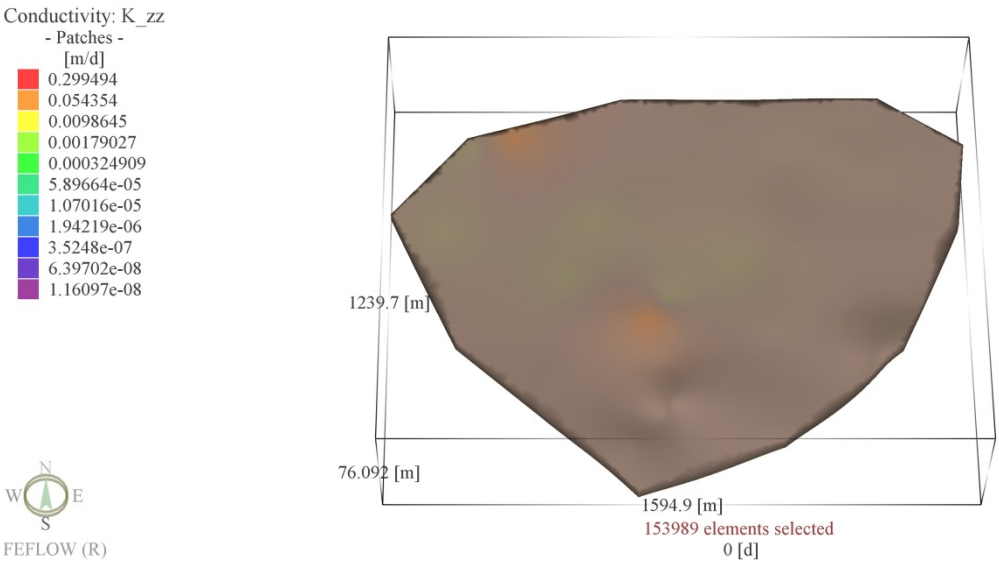

FIGURE 4-26: Calibrated vertical conductivities (Layer 6)

4.4.2.3. Flow Model Simulation

Water enters the northeast quadrant model domain as recharge from infiltrating precipitation and lateral inflow at constant head boundaries. Water exits the northeast quadrant model domain as lateral outflow at constant head boundaries. The infiltration rate, constant head boundary inflow rate, and constant head boundary outflow rate are 41.0 m^3/day, 671.1 m^3/day, and 714.0 m^3/day, respectively, at steady state. A vertical flow component exists in all layers above the basal layer 6. In layers 1, 2, 4, and 6 (USZ, UCL, LCL, and AQ), groundwater flow in the model is primarily vertical. In layers 3 and 5 groundwater flow is primarily lateral to the southwest. Seasonal adjustments are not accounted for in the model.

The modeled potentiometric surface in layer 1 (USZ) is consistent with the northeast-southwest trending groundwater mound which acts as a groundwater divide for lateral flow (FIGURE 4-27). West of the divide, lateral groundwater flow is to the west and northwest. East of the divide, lateral groundwater flow is to the east. No seepage is predicted by the model at the eastern USZ limit. Therefore all groundwater flowing east of the divide eventually becomes vertical, downward flow. For layer 1, rates of infiltration, constant head boundary inflow, and constant head boundary outflow are 40.8 m^3/day, 5.2 m^3/day, and 0.4 m^3/day, respectively, at steady state. The flow rate to the underlying layer 2 (UCL) through the lower interior boundary is 47.9 m^3/day. Unconfined heads in the USZ range from 371 m to 382 m MSL, with an average of 380 m MSL.

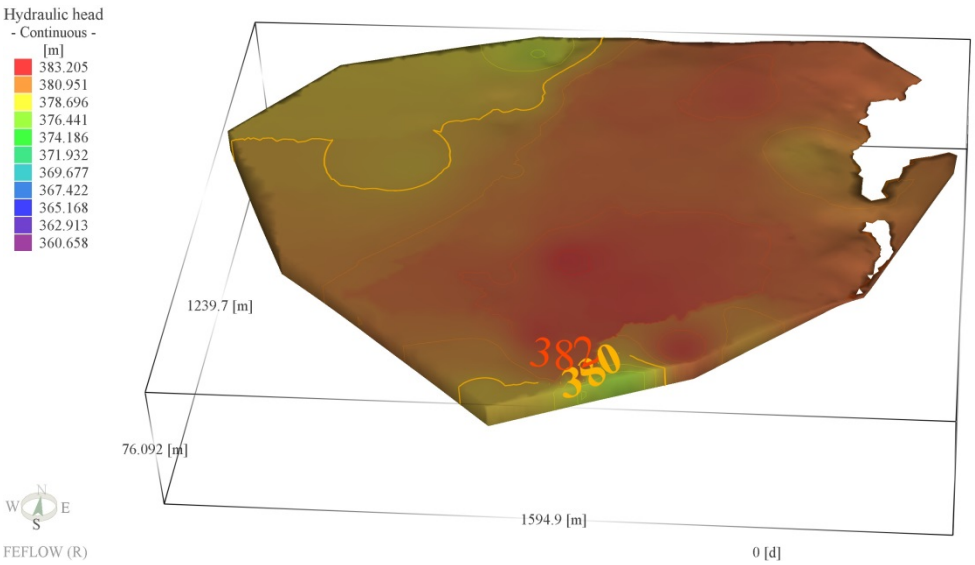

FIGURE 4-27: Modeled potentiometric surface (Layer 1)
Illustrates the modeled potentiometric surface of the layer. Figure contours are illustrated in the native FEFLOW image output file, in meters ASL, in a way that cannot be edited.

The Layer 2 (UCL) potentiometric surface resembles that of the overlying USZ with a groundwater divide for lateral flow near the center of the domain (FIGURE 4-28). For layer 2, rates of constant head boundary inflow and constant head boundary outflow are both very low, 0.03 m^3/day and 2.0 m^3/day, at steady state. Groundwater flow in the UCL is highly refracted due to the contrast of conductivity with layers above and below. The flow rate from the USZ through the upper interior boundary is 159.0 m^3/day. The flow rate exiting through the lower interior boundary to the underlying layer 3 (LSZ) is 1,281.8 m^3/day. Heads in the UCL range from 371 m to 382 m MSL, with an average of about 379 m MSL.

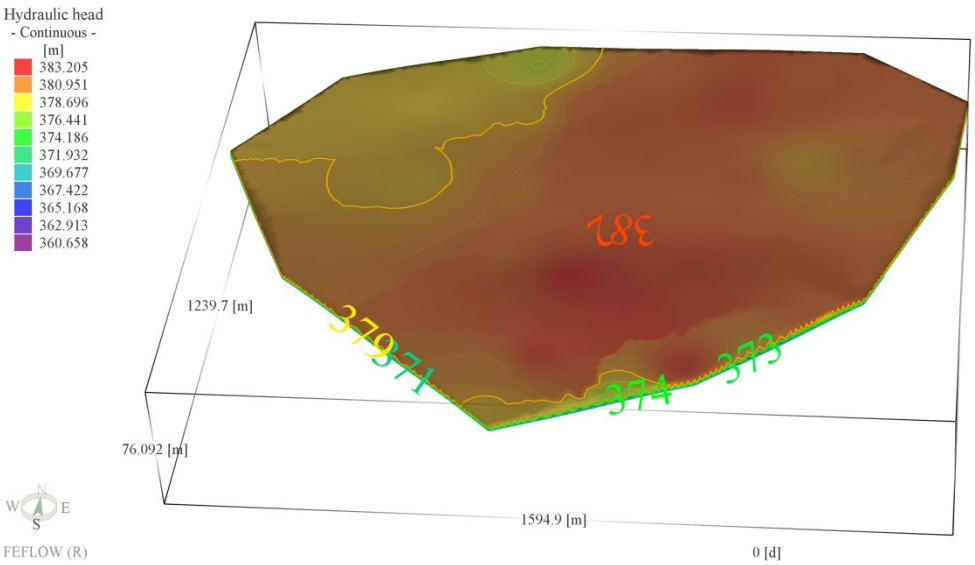

FIGURE 4-28: Modeled potentiometric surface (Layer 2)
Illustrates the modeled potentiometric surface of the layer. Figure contours are illustrated in the native FEFLOW image output file, in meters ASL, in a way that cannot be edited.

The layer 3 (LSZ) potentiometric surface is highest in the vicinity of Soldier Creek due to combined effects of infiltration and lateral inflow from the constant head boundary (FIGURE 4-29). In the western sector, lateral groundwater flow is to the west and southwest. For layer 3, rates of constant head boundary inflow and constant head boundary outflow are 99.1 m^3/day and 127.6 m^3/day, respectively, at steady state. The flow rate from the overlying UCL through the upper interior boundary is 46.6 m^3/day. The flow rate to the underlying LCL through the lower interior boundary is 18.1 m^3/day. Heads in the LSZ range from 367 m to 373 m MSL, with an average of about 370 m MSL.

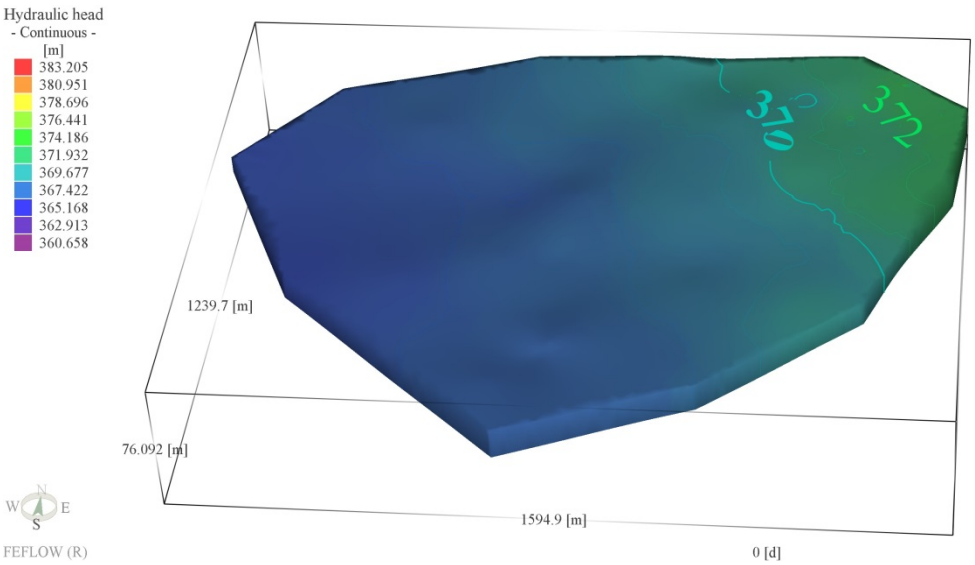

FIGURE 4-29: Modeled potentiometric surface (Layer 3)
Illustrates the modeled potentiometric surface of the layer. Figure contours are illustrated in the native FEFLOW image output file, in meters ASL, in a way that cannot be edited.

The layer 4 (LCL) potentiometric surface resembles that of the overlying LSZ with highest head in the vicinity of Soldier Creek (FIGURE 4-30). To the west, lateral groundwater flow is to the west and southwest. As with the UCL, layer 4 rates of constant head boundary inflow and constant head boundary outflow are very low, 0.014 m^3/day and 0.0.18 m^3/day, respectively, at steady state. Groundwater flow in the LCL is also highly refracted due to the contrast of conductivity with layers above and below. The flow rate from the overlying LSZ through the upper interior boundary is 17.2 m^3/day. The flow rate to the underlying LLSZ through the lower interior boundary is 17.2 m^3/day. Heads in the LCL range from 366 m to 370 m MSL, with an average of about 368 m MSL.

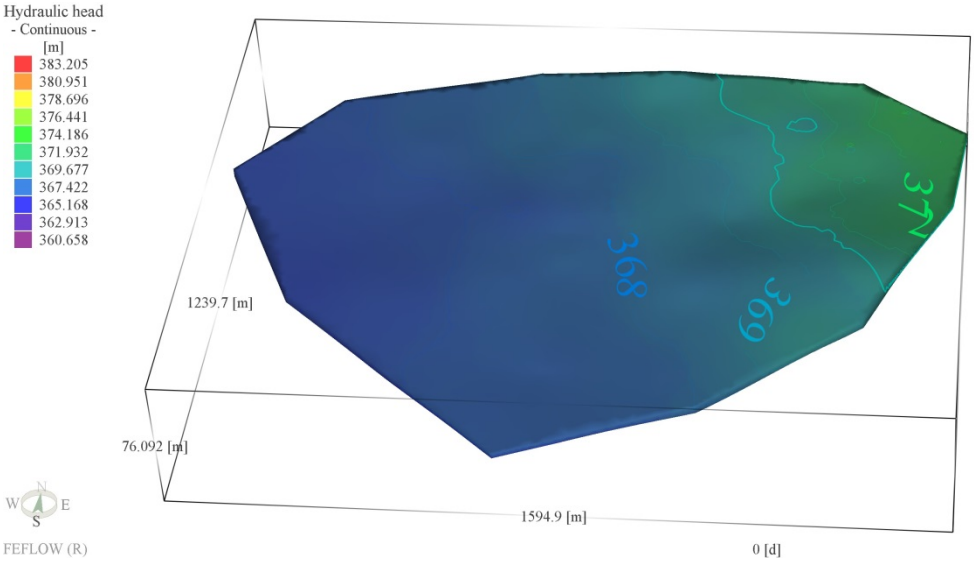

FIGURE 4-30: Modeled potentiometric surface (Layer 4)
Illustrates the modeled potentiometric surface of the layer. Figure contours are illustrated in the native FEFLOW image output file, in meters ASL, in a way that cannot be edited.

The layer 5 (LLSZ) potentiometric surface correctly predicts two local groundwater mounds and a groundwater flow divide that trends north-northwest by south-southeast in the eastern sector of the quadrant (FIGURE 4-31). In the western sector of the quadrant lateral groundwater flow is to the west. In the east, there is a lateral groundwater flow component to the east. For layer 5, rates of constant head boundary inflow and constant head boundary outflow are 566.8 m^3/day and 583.9 m^3/day, respectively, at steady state. The flow rate from the overlying LCL through the upper interior boundary is 25.1 m^3/day. The flow rate to the underlying AQ through the lower interior boundary is 7.9 m^3/day. Heads in the LLSZ range from 366 m to 370 m MSL, with an average of about 368 m MSL.

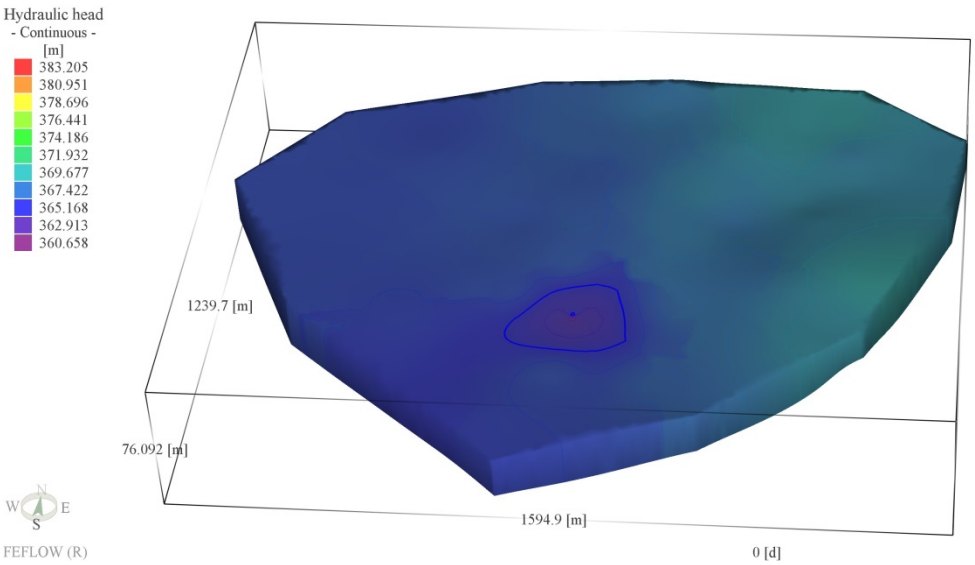

FIGURE 4-31: Modeled potentiometric surface (Layer 5)
Illustrates the modeled potentiometric surface of the layer. Figure contours are illustrated in the native FEFLOW image output file, in meters ASL, in a way that cannot be edited.

The layer 6 (AQ) potentiometric surface resembles that of the overlying LLSZ with two local groundwater mounds and a groundwater flow divide that trends north-northwest by south-southeast in the eastern sector of the quadrant (FIGURE 4-32). In the western sector of the quadrant lateral groundwater flow is to the west. In the east, there is a lateral groundwater flow component to the east. As with the UCL and LCL, layer 6 rates of constant head boundary inflow and constant head boundary outflow are very low, 0.0013 m^3/day and 0.0011 m^3/day, respectively, at steady state. Groundwater flow in the AQ is also highly refracted due to the contrast of conductivity with layers above and below. The flow rate from the overlying LLSZ through the upper interior boundary is 0.002 m^3/day. The base of the AQ is a no-flow boundary. Therefore, all groundwater entering the layer exits as lateral flow through constant-head boundaries.

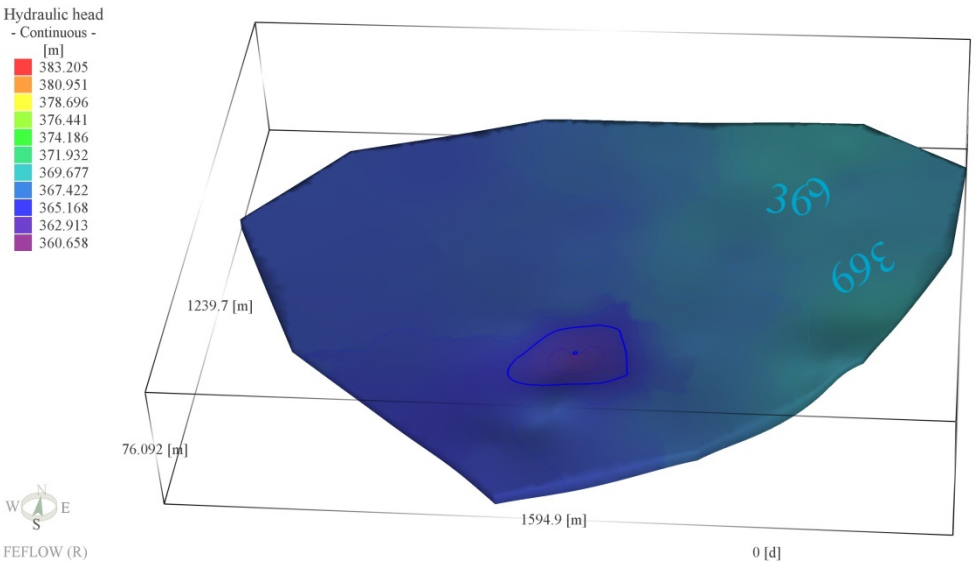

FIGURE 4-32: Modeled potentiometric surface (Layer 6)
Illustrates the modeled potentiometric surface of the layer. Figure contours are illustrated in the native FEFLOW image output file, in meters ASL, in a way that cannot be edited.

4.4.2.4. Soldier Creek

Soldier Creek is simulated as a transfer boundary condition in the northeast quadrant flow model. Constant heads equal to the creek channel elevation plus 0.5 m are assigned along the creek channel on model slices 3 and 4, which are the upper and lower limits, respectively, of layer 3 (LSZ). The sediment thickness of the creek channel is assumed to be 0.5 m with a hydraulic conductivity of 2E-5 m/day, which is the approximate average vertical conductivity of the UCL. The creek channel is higher than LSZ water table below it. Therefore, Soldier Creek is recharging the LSZ in the northeast quadrant. At steady state, the recharge from Soldier Creek is 3 m^3/day or 0.2% of the total inflow to the northeast quadrant model domain. Therefore, the effect of Soldier Creek on groundwater flow in the northeast quadrant is negligible, and its contribution to recharge is not considered in the flow and mass-balance calculations.

4.4.3. Contaminant Fate and Transport Model

The contaminant fate and transport model simulates the release, migration, and biotransformation of PCE and TCE from two source areas in the northeast quadrant model domain. Biotransformation is by sequential reductive dechlorination of the parent compounds and intermediate species in the following order: PCE, TCE, *cis*-DCE, vinyl chloride, and ethene. As described earlier, *cis*-DCE is the primary product of sequential reductive dechlorination of TCE. Thus, *trans*-DCE was not considered within this modeling study.

Light and heavy carbon isotopes, ^{12}C and ^{13}C, of each parent and intermediate are considered separately to simulate the differential biotransformation rates between isotopes of the same species. The simulation begins with the initial releases from each source area which are assumed to occur simultaneously; advection of source contaminants is based on the calibrated flow model. The releases are continuous throughout the duration of the simulation, which ends at the time that represents the current (2008) distribution of chlorinated ethenes in the northeast quadrant. In the present discussion, the term 'overall concentration' refers to a chlorinated ethene parent or intermediate species without regards to its isotopes (i.e., the overall concentration of a species is the sum of its ^{12}C and ^{13}C isotopes).

4.4.3.1. Fate and Transport Calibration

Calibration of the fate and transport model is undertaken by first categorizing input variables as either secondary or primary. Secondary variables are those for which limited site-specific information is available. Detailed specification of secondary variables throughout the model domain is not justifiable. Generally a value is taken from

the literature based on lithologic or geologic site characterizations. Then, a single value of the secondary variable is applied throughout a layer or the entire model domain. Longitudinal and transverse dispersivity, sorption, diffusion, and effective porosity are considered as secondary variables. Modeled species concentrations are sensitive to the primary variables, so their effects on model results are readily quantifiable. Thus, there is a stronger basis for their selection. More guidance from the literature may be available for selected primary variables as well. Overall species source concentrations and overall species biotransformation rates are considered as primary variables. With regards to isotopes, source isotopic ratios ($\delta^{13}C$ ‰) and isotopic fractionation factors (α) are also considered as primary variables. The primary and secondary model variables are adjusted to minimize the difference between measured and modeled concentrations for each isotopic species at selected monitoring wells in the northeast quadrant.

The model calibration for fate and transport is necessarily approximate and subjective due to a number of factors including the heterogeneity of site conditions and the incomplete history of chlorinated ethene releases and subsequent remedial activities. The calibrated model only approximates measured concentrations at some locations. At other locations where the measured and modeled concentrations are significantly different, the limitations of the model are acknowledged. Detailed, location-specific adjustments to model input variables to improve the match between measured and modeled concentrations have limited justification because of the uncertainty associated with those variables. It is believed that such a detailed effort will not significantly improve the overall model quality.

4.4.3.2. Primary Model Variables

The extent of biotransformation of each isotopic species (e.g., $^{12}C_{TCE}$, $^{13}C_{TCE}$, etc.) as it migrates from a source is directly related to four primary model variables; the source concentrations, the overall species biotransformation rate, the isotopic fractionation factor (α), and the source isotopic ratio ($\delta^{13}C$ ‰). Higher sources concentrations will limit the biotransformation extent throughout the plume unless concentrations are at steady state. A higher overall species biotransformation rate will obviously further the extent of isotopic fractionation for the species. The isotopic enrichment factor primarily establishes the differential biotransformation rates of two isotopes of the same species. The fourth primary variable, the source isotope ratio ($\delta^{13}C$ ‰), establishes the source concentration for each isotope for a given overall species concentration. The source isotope ratio is perhaps, the primary determinant of the species isotope ratio away from the source.

In the calibration process, initial trial values for the overall source concentrations, overall biotransformation rates for parent species (i.e., PCE and TCE) are selected to approximate following simulation the corresponding measured concentrations for each parent and intermediate species. Source concentrations for each isotope then are set based on the current, measured source isotope ratios. These source isotope ratios are considered to be constant from the initial release throughout the duration of the simulation. Isotope fractionation factors for the parents are selected from the literature [41], as noted in Section 1.2.1.6; for PCE $\alpha_{initial}$ was 0.9950 and for TCE $\alpha_{initial}$ was 0.9875. They are considered to be constant as well, but can be varied within a relatively narrow range according to the literature. Trial runs determine adjustments that are made

to overall source concentrations and overall parent biotransformation rates to reproduce the measured, parent isotopic concentrations. Subsequently, trial, overall biotransformation rates and literature-based isotope enrichment factors for intermediates are selected for the next series of model runs to approximate the measured, intermediate isotopic concentrations. The intermediate isotopic concentrations are dependent on the parent isotopic concentrations as well. So the source concentrations and parent overall biotransformation rates are adjusted in the final calibration runs if the intermediate biotransformation rates reach the limit of their effect on the modeled result.

The practical ranges for the source concentrations are taken as 10% to 100% of the solubility of PCE or TCE based on the possible occurrence of free product. The model source concentrations are ultimately quantified based on the calibration previously described. Identical source concentrations at the Building 105 and IWTP sources produce acceptable calibration results. The overall source concentrations at the 105, 34A, and IWTP source areas are 60 mg/L and 330 mg/L for PCE and TCE, respectively. The source isotope ratios for PCE and TCE are –33.1 ‰ and –27.1 ‰, respectively. Therefore, the source isotopic concentrations at the 105, 34A, and IWTP source areas are 59.3536 mg/L, 0.6464 mg/L, 326.4233 mg/L, and 3.5767 mg/L for ^{12}C PCE, ^{13}C PCE, ^{12}C TCE, and ^{13}C TCE, respectively. Isotopic source concentrations are applied as continuous, nodal boundary conditions. The 105 and 34A source is applied at nodes on slice 2 at the base of layer 1. The IWTP source is applied at a node on slice 4 at the base of layer 3. Source concentrations are constant throughout the duration of the simulation.

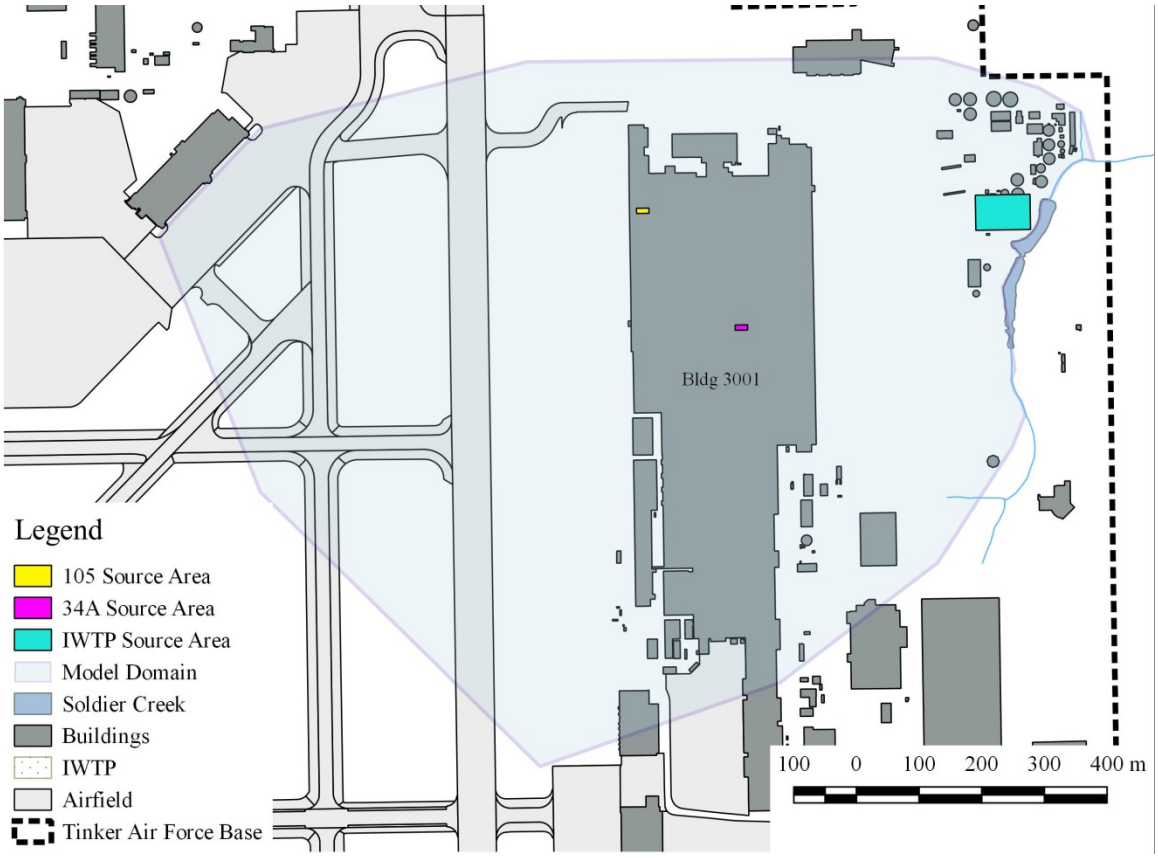

FIGURE 4-33: Simulated source areas
Illustrates the source areas within the model domain. The 105 and 34A sources are applied at nodes on slice 2 at the base of layer 1. The IWTP source is applied at a node on slice 4 at the base of layer 3.

A Monod-type biotransformation rate model is best suited to quantify the reaction kinetics of reductive chlorination [81]. In the field, this equates to zero-order reaction kinetics near source areas where concentrations are high and first-order reaction kinetics away from the source where concentrations are low. In most field studies, first-order reaction kinetics are assumed because either concentrations are in the first-order range or the additional resources required to apply the Monod kinetics model cannot be justified. In the present study, first-order reaction kinetics are assumed throughout the model domain. Although concentrations near source areas are above the first-order range, reaction rates may be limited by conditions for reductive dechlorination that are less than

optimal. Thus the difference between the two rate models, in terms of concentrations and biotransformed mass, is limited as well.

The model calibration suggests that the parent species, PCE and TCE, have different overall first-order reaction rate constants that are applicable in all model layers. The rate constants for PCE and TCE, expressed as equivalent half lives, are 33 years and 40 years, respectively. These half lives are longer than those from another modeling study at the site (i.e., TCE 1.95 to 11 years; [71]). The previous modeling study is based on declines in chlorinated ethene concentration with time in a single well near the IWTP over a period of 10 years. The authors of the previous modeling study suggest that calculated TCE half life represents all attenuation process, including dispersion and dilution, not just transformation and thus, may not be applicable across this study's model domain. The change in measured parent species isotope ratios with distance from the source areas suggests that biotransformation of the parent compounds in the northeast quadrant is minimal; for PCE refer to FIGURE 3-29 (105 area to 1-7BR) and for TCE refer to FIGURE 3-30 (105 area to 1-13B). On the other hand, a comparison of the measured isotope ratios for parent and intermediate species shows that the intermediates are further biotransformed; for *cis*-DCE refer to FIGURE 3-31 (105 area to 1-13B) and for VC refer to FIGURE 3-32 (105 area to 1-12BR). The best fit overall half lives for the intermediate species are 3 years, 0.6 years, and 0.6 years, for *cis*-DCE, vinyl chloride, and ethene, respectively, in all model layers. These half lives are in better agreement with the literature. The implication is that the biotransformation of each intermediate is significantly less limited than that of the parent species.

Isotope fractionation that occurs during reductive dechlorination is quantified by the isotope fraction factor, a compound specific constant that relates the isotope ratio of the instantaneously formed product to the isotope ratio of the reactant [81]. For first order reaction kinetics, the ^{12}C chlorinated ethene species reaction rate is the product of the overall reaction rate and the ^{12}C concentration. The ^{13}C chlorinated ethene species reaction rate is the product of the overall reaction rate, the ^{13}C concentration and the isotope fractionation factor. The model calibration suggests that the appropriate isotope fractionation factors are 0.9915, 0.9900, 0.9898, 0.9735, and 0.9735 for PCE, TCE, *cis*-DCE, vinyl chloride, and ethene, respectively, in all model layers. These values are taken from published ranges [41]. These ranges are relatively narrow, so the degree of fractionation is mainly a function of the source isotope ratios, the overall reaction rates of each chlorinated ethene species, and the extent of biotransformation.

4.4.3.3. Secondary Model Variables

Secondary model variables are selected and set in preliminary model calibration runs. Longitudinal and transverse dispersivities are specified as 20 m and 5 m, respectively. The primary basis for this selection is that the modeled trial-and-error extent of simulated chlorinated ethene plumes at the end of the 20 year simulation approximates the current, measured extent (or scale) of the chlorinated ethene plumes, thus informing us the dispersivity estimates are conservative. Dispersivity estimates for the northeast quadrant based on the literature are lower than these values. However, spreading of the chlorinated ethene plume is known to be influenced by lithologic and geologic heterogeneity at the site based on the dye trace conducted as a part of the present study. In addition, remediation activities at various locations in the northeast quadrant

may have contributed to chlorinated ethene plume spreading. The selected values for dispersivity represent the combined effect of all plume spreading mechanisms. The lack of sensitivity of the simulated chlorinated ethene extent results to species-specific sorption coefficients obtained from the literature is significantly less than that for the primary variables. Therefore, a unitless sorption coefficient of 3 is specified for the isotopes of all parent and intermediate species, which is not significantly different that values selected in a previous study [70]. Diffusion values obtained from the literature, were 8.8e-5, 9.0e-5, 1.0e-4, and 1.2e-4 m^2/d for PCE, TCE, cDCE, and VC, respectively. Effective porosities of 0.25 and 0.05 are specified for the aquifer layers (layers 1, 3, and 5) and the confining layers (layers 2, 4 and 6), respectively. The values are selected based on the literature and the previous modeling study [70]. As with dispersivity, the modeled plumes based on these porosities are reasonably consistent with the current chlorinated ethene plumes at the site.

4.5. Simulation Results

4.5.1. Constituent Concentrations

At the end of the 20 year simulation, the migration from source areas and sequential reductive dechlorination of the ^{12}C parent compounds and intermediates are evidenced by the occurrence of the ^{12}C isotopic forms of PCE (residual reactant), TCE (residual reactant and product), and *cis*-DCE, vinyl chloride and ethene (products) throughout much of the model domain (FIGURE 4-34 through FIGURE 4-48). The distribution of each is a function of the simulated groundwater flow regime, the source area concentrations and locations, and the relative biotransformation rates of each species. The ^{12}C isotopic species ranked in order of concentration from highest to lowest

in the model domain are TCE, PCE, *cis*-DCE, followed by both vinyl chloride and ethene, which have similar concentrations. This ranking is primarily a function of the source areas concentrations, the reaction sequence, and the relative biotransformation rates of each species.

With regard to the transient versus steady state character of the plume, the concentrations of each species away from the source areas beyond 20 years continue to increase, although minimally, suggesting a transient plume that is expanding in the concentration and extent of all species, at a very slow rate. However, the stability of the model beyond 20 years was hampered by model computational limitations, which complicated the production of reliable data. The complete reduction of PCE and TCE to ethene would be indicated in areas where ethene is the dominant species. No such area is readily apparent. The possible conversion of ethene to CO_2 was not considered in this study.

At the end of the 20 year simulation, ^{12}C isotopes of PCE, TCE, *cis*-DCE, vinyl chloride, and ethene from the IWTP source and the 105 / 34A sources are mixed in the LSZ and LLSZ. Analysis of slices through the model domain from the IWTP source to the 105 /34A sources shows that concentrations are highest in the east-central portion of the model domain, lower to the east and west, then steadily decrease to the west with near-zero concentrations in the northwest and southwest corners. For the primary source mass, the slices through the model domain from the IWTP source to the 105 / 34A sources shows ^{12}C TCE concentrations first decreasing, then increasing, moving due west. However, there are very low ^{12}C TCE concentrations in the central part of the

shallow layers of the model domain indicating that plumes from these two sources are not mixing at this depth (FIGURE 4-37).

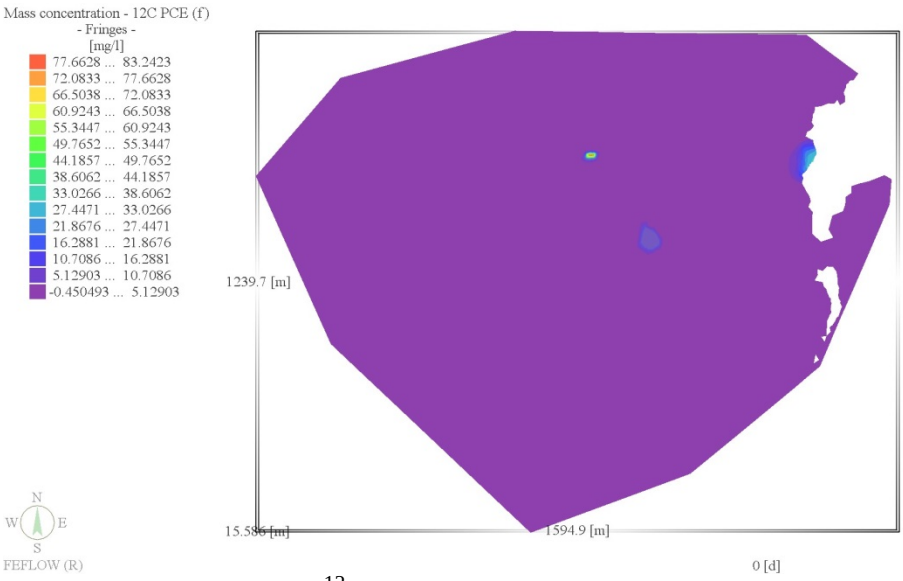

FIGURE 4-34: Modeled ^{12}C PCE mass concentration in the USZ

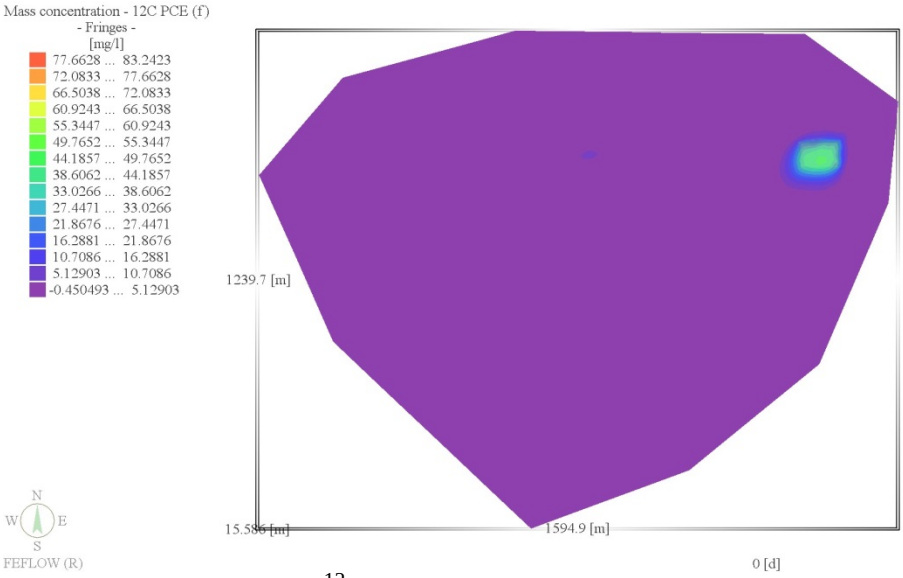

FIGURE 4-35: Modeled ^{12}C PCE mass concentration in the LSZ

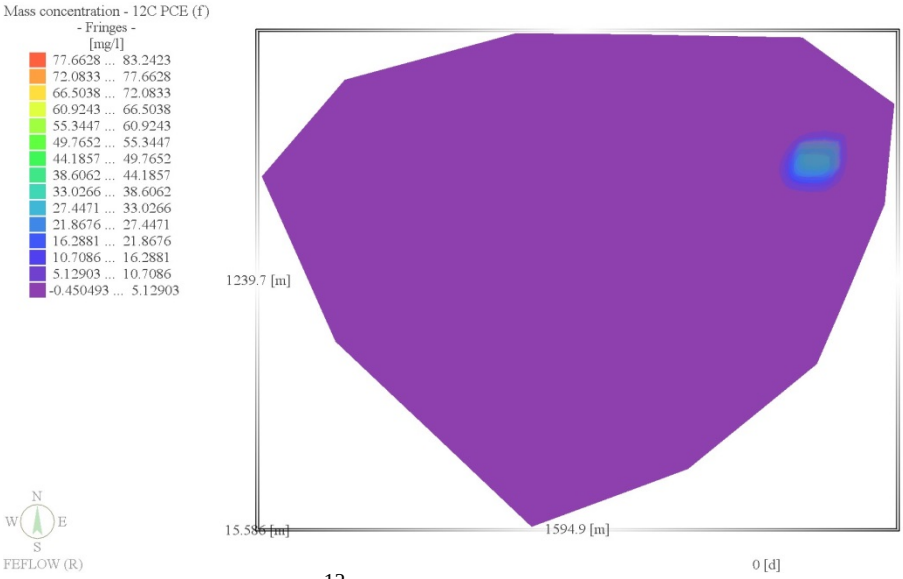

FIGURE 4-36: Modeled ^{12}C PCE mass concentration in the LLSZ

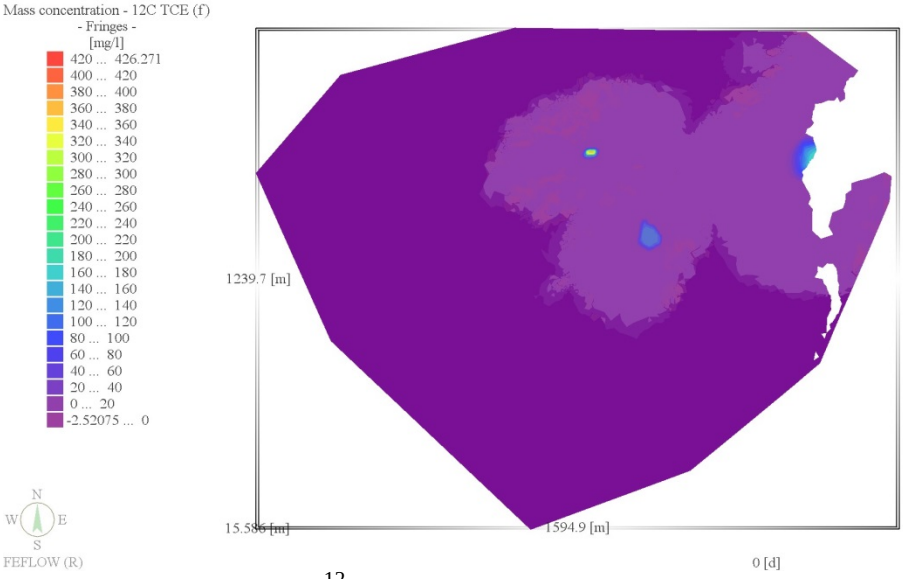

FIGURE 4-37: Modeled ^{12}C TCE mass concentration in the USZ

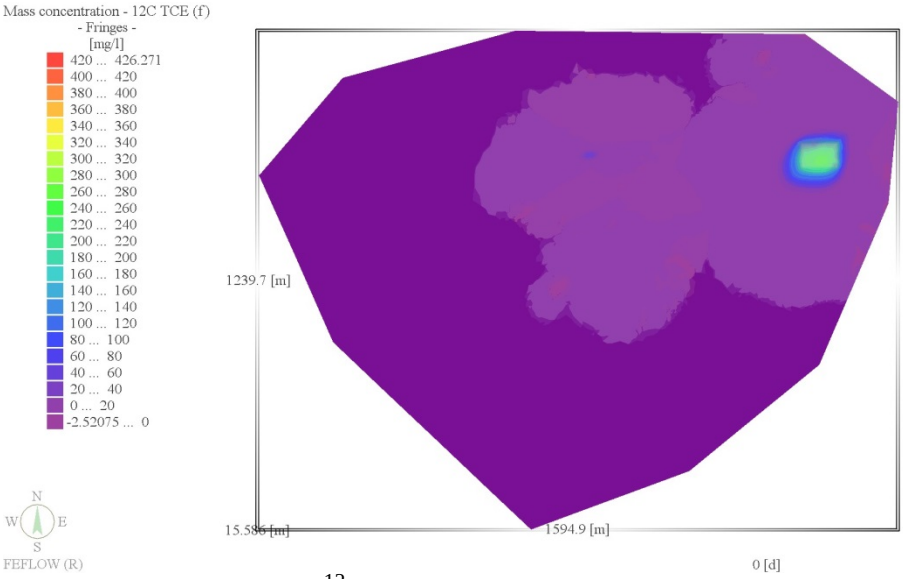

FIGURE 4-38: Modeled ^{12}C TCE mass concentration in the LSZ

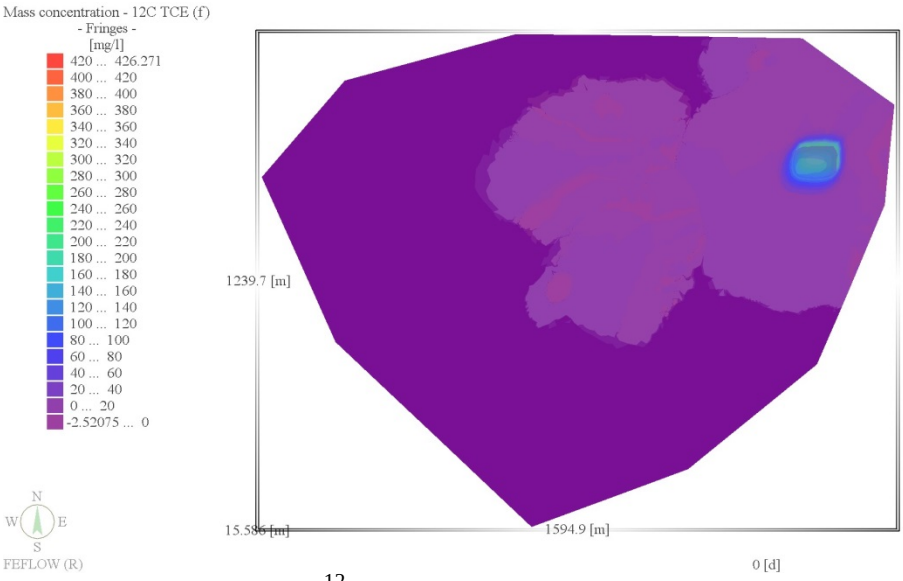

FIGURE 4-39: Modeled ^{12}C TCE mass concentration in the LLSZ

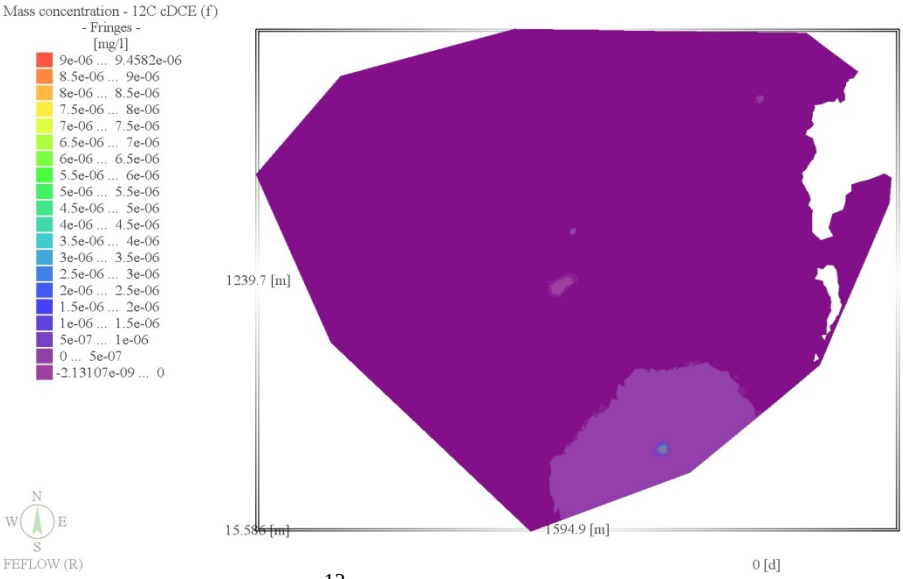

FIGURE 4-40: Modeled ^{12}C cDCE mass concentration in the USZ

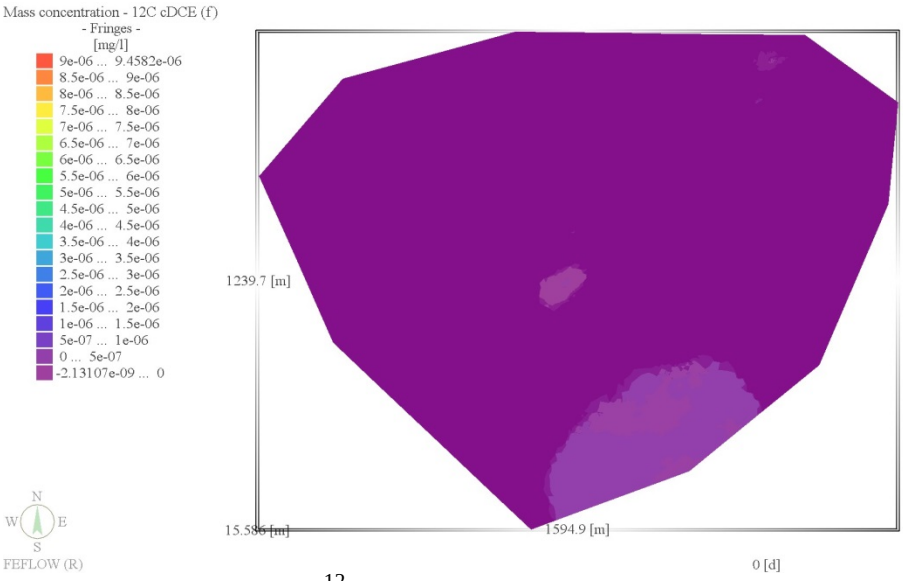

FIGURE 4-41: Modeled ^{12}C cDCE mass concentration in the LSZ

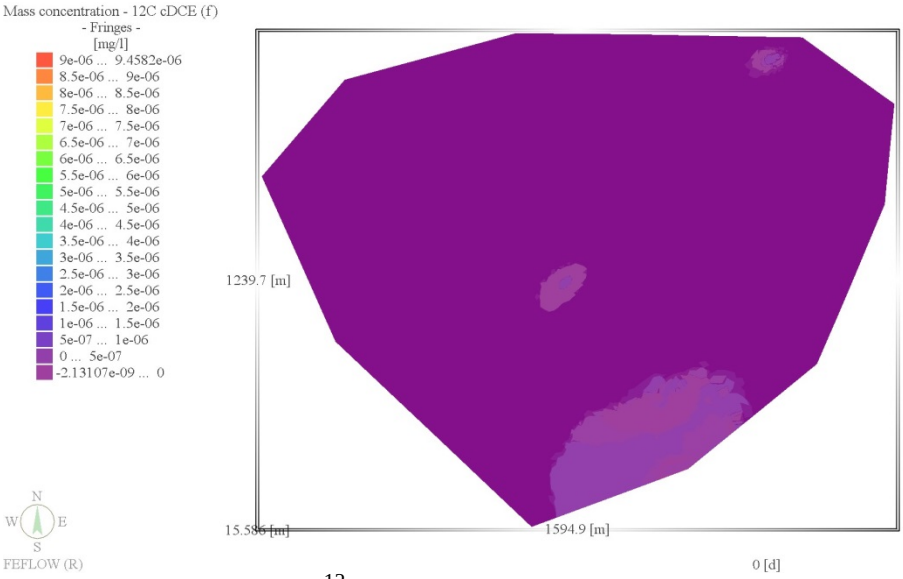

FIGURE 4-42: Modeled ^{12}C cDCE mass concentration in the LLSZ

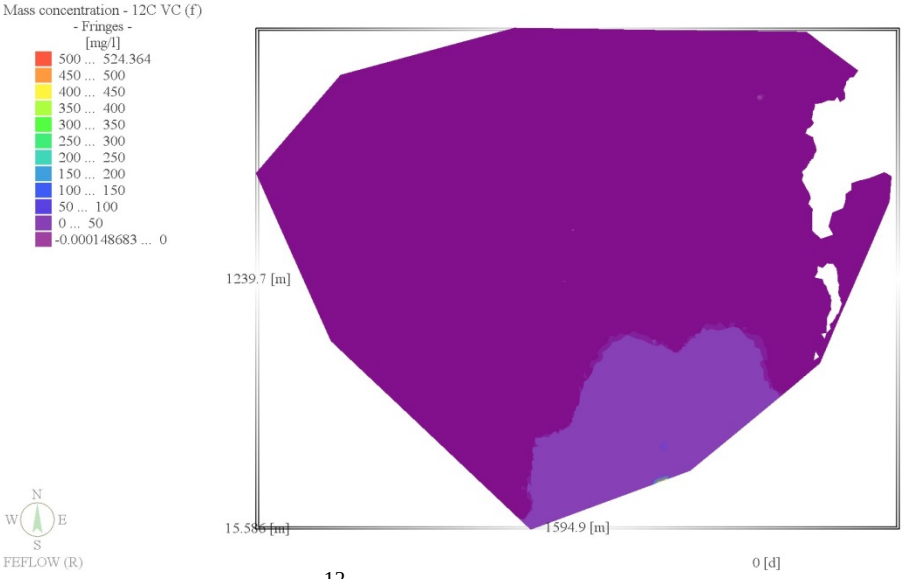

FIGURE 4-43: Modeled ^{12}C VC mass concentration in the USZ

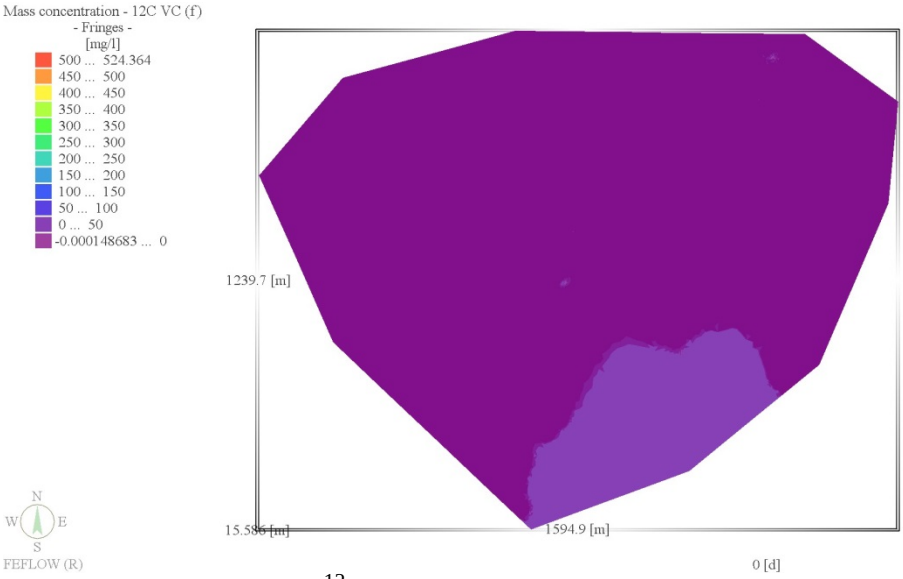

FIGURE 4-44: Modeled ^{12}C VC mass concentration in the LSZ

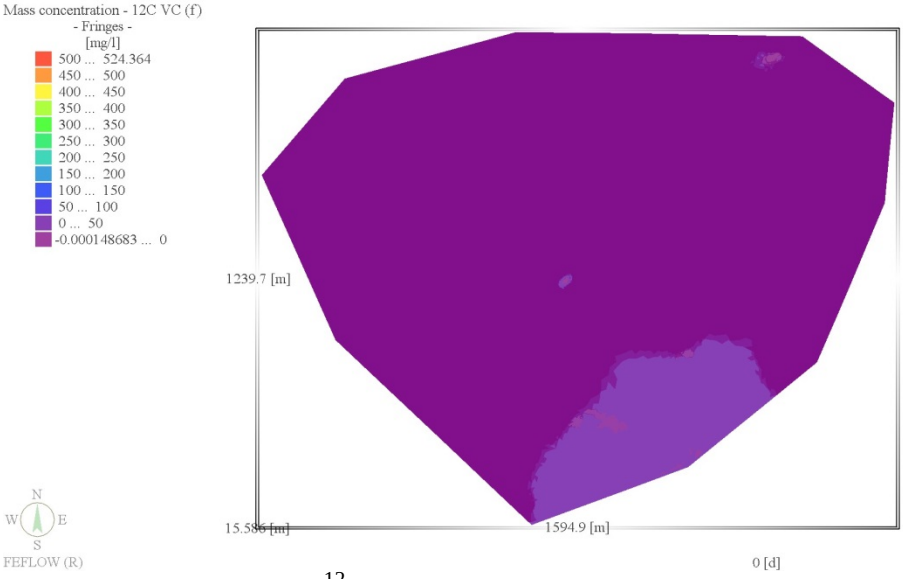

FIGURE 4-45: Modeled ^{12}C VC mass concentration in the LLSZ

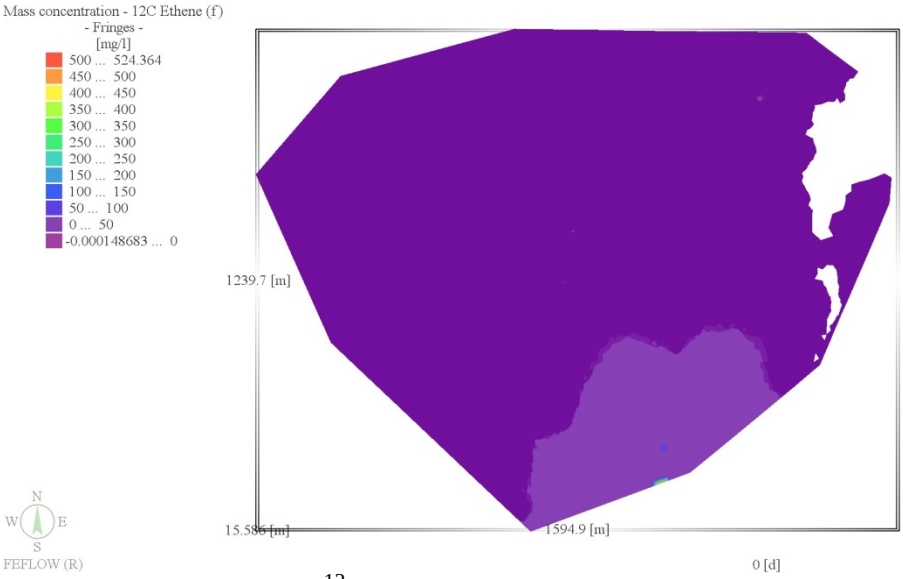

FIGURE 4-46: Modeled ^{12}C ethene mass concentration in the USZ

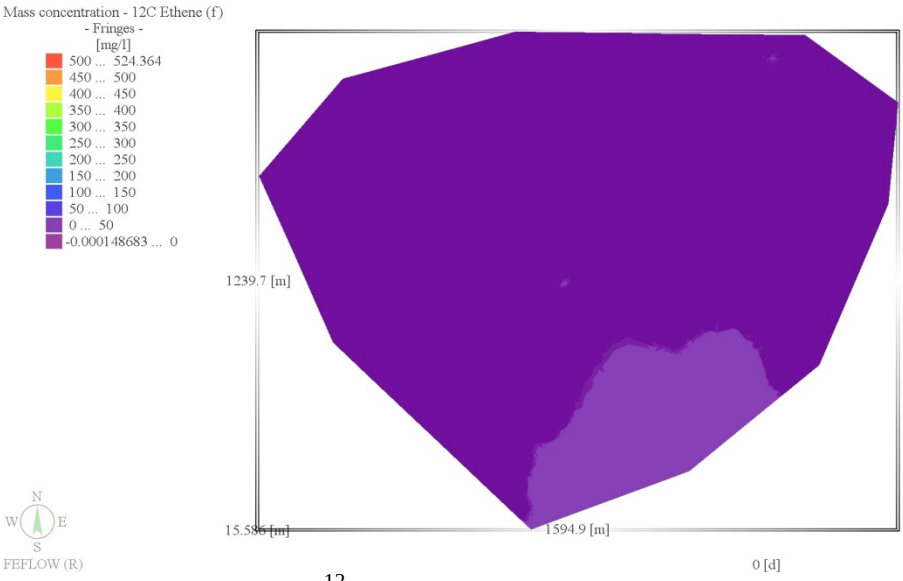

FIGURE 4-47: Modeled ^{12}C ethene mass concentration in the LSZ

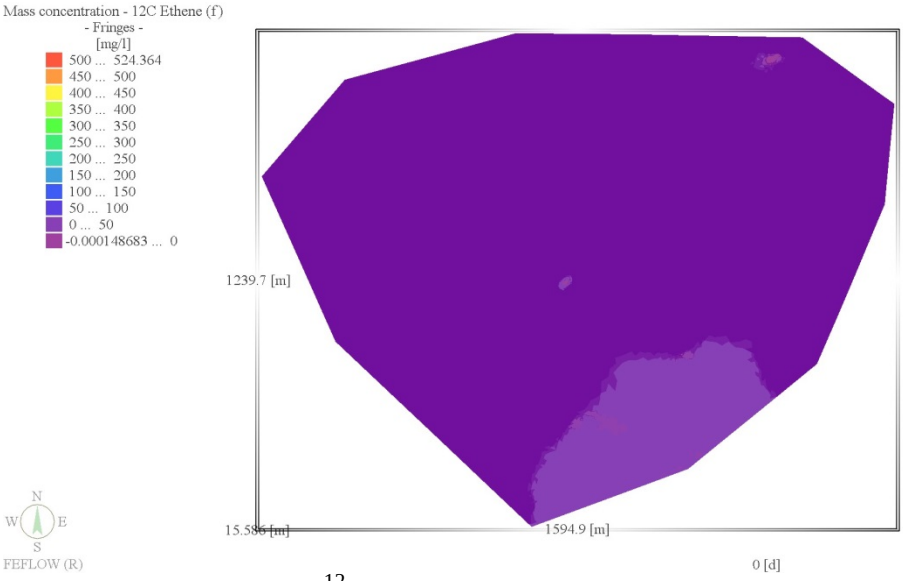

FIGURE 4-48: Modeled ^{12}C ethene mass concentration in the LLSZ

The migration from source areas and sequential reductive dechlorination of the ^{13}C parent compounds and intermediates is qualitatively similar to that for the ^{12}C species albeit at lower concentrations (FIGURE 4-34 through FIGURE 4-63). Likewise, the slices through the model domain from the IWTP source to the 105 / 34A sources shows that concentrations are highest in the east-central portion of the model domain, lower to the east and west, then steadily decrease to the west with near-zero concentrations in the northwest and southwest corners. However the lowest concentrations in this interval may not be measurable. Thus mixing may not be indicated based on measured ^{13}C concentrations.

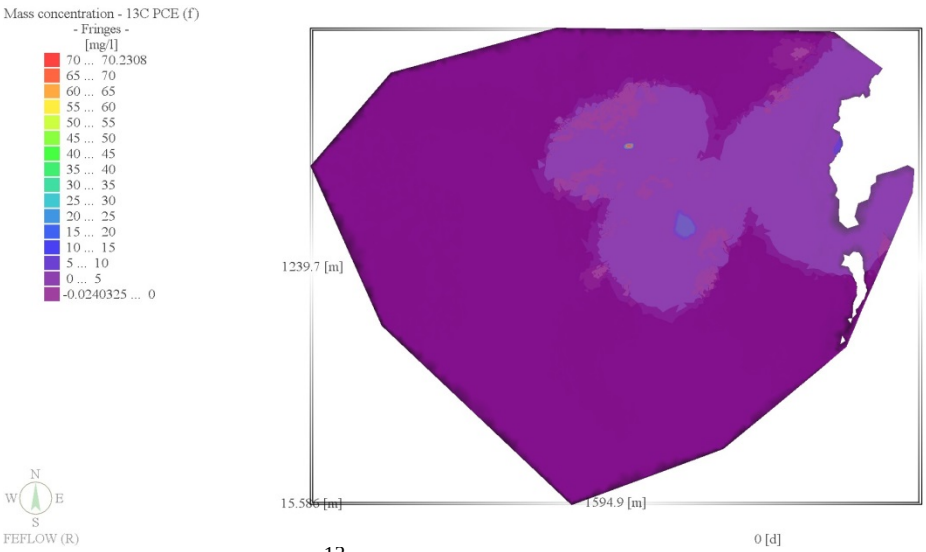

FIGURE 4-49: Modeled ^{13}C PCE mass concentration in the USZ

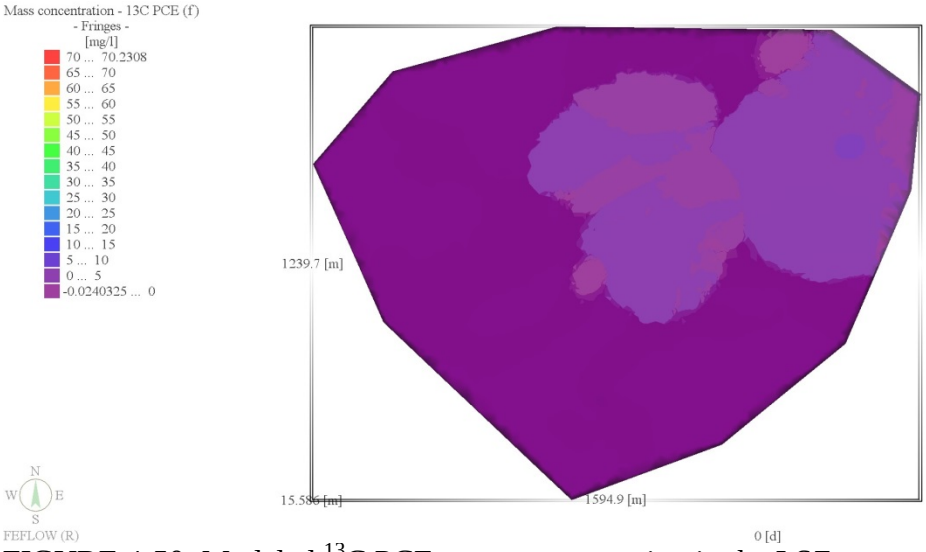

FIGURE 4-50: Modeled ^{13}C PCE mass concentration in the LSZ

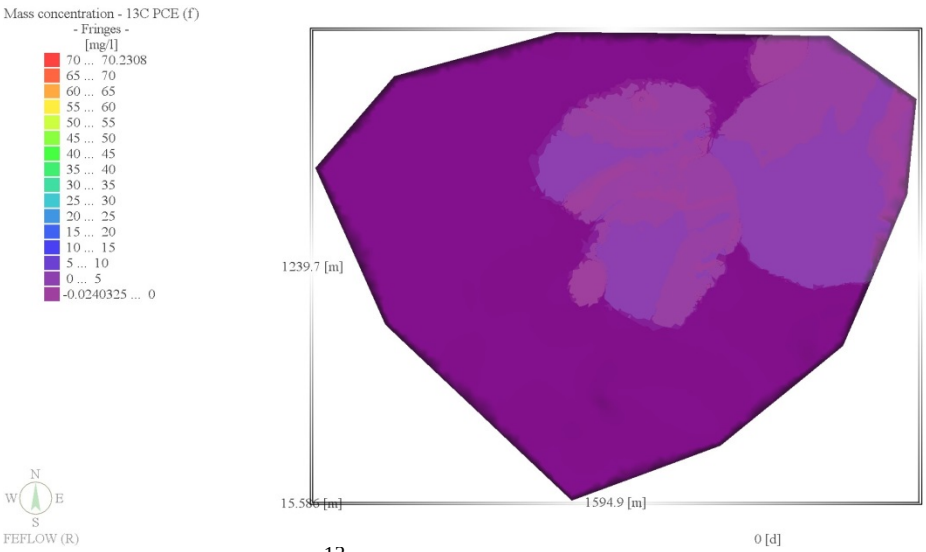

FIGURE 4-51: Modeled ^{13}C PCE mass concentration in the LLSZ

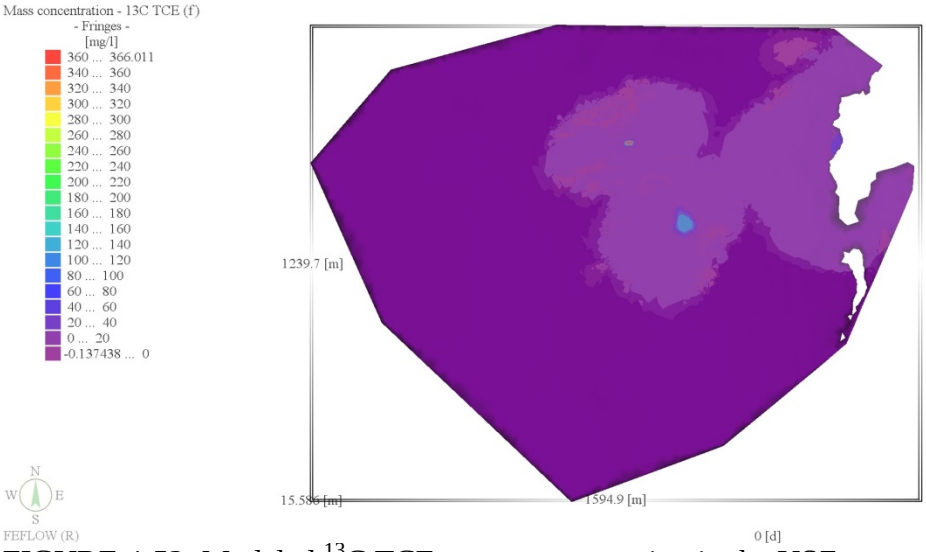

FIGURE 4-52: Modeled ^{13}C TCE mass concentration in the USZ

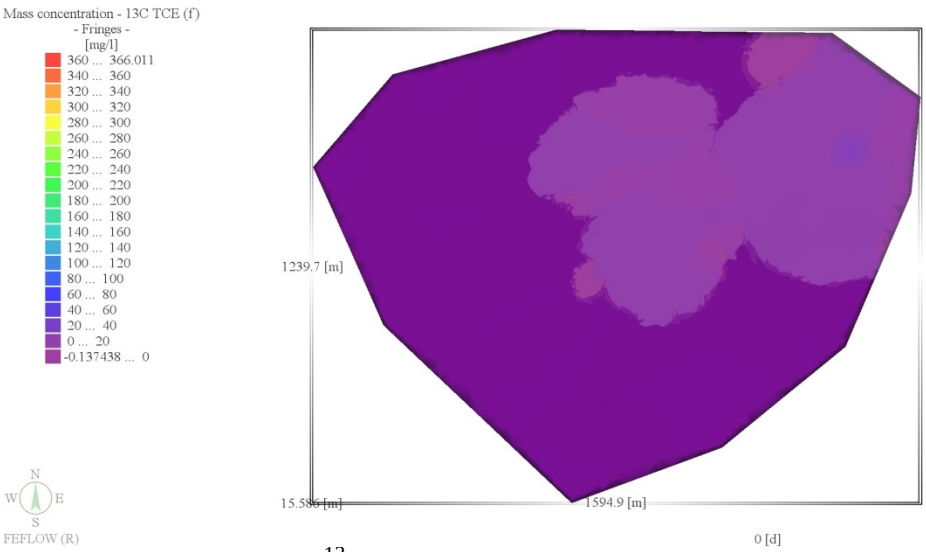

FIGURE 4-53: Modeled ^{13}C TCE mass concentration in the LSZ

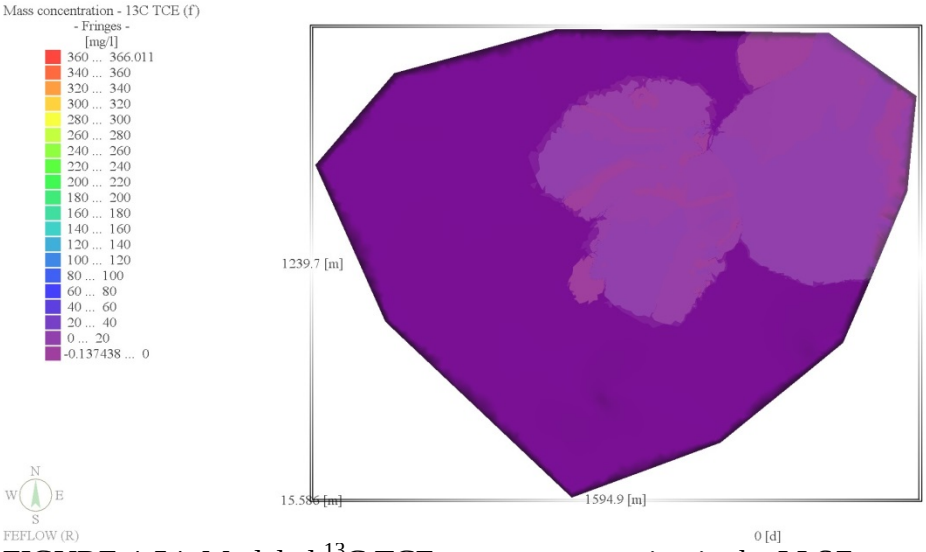

FIGURE 4-54: Modeled ^{13}C TCE mass concentration in the LLSZ

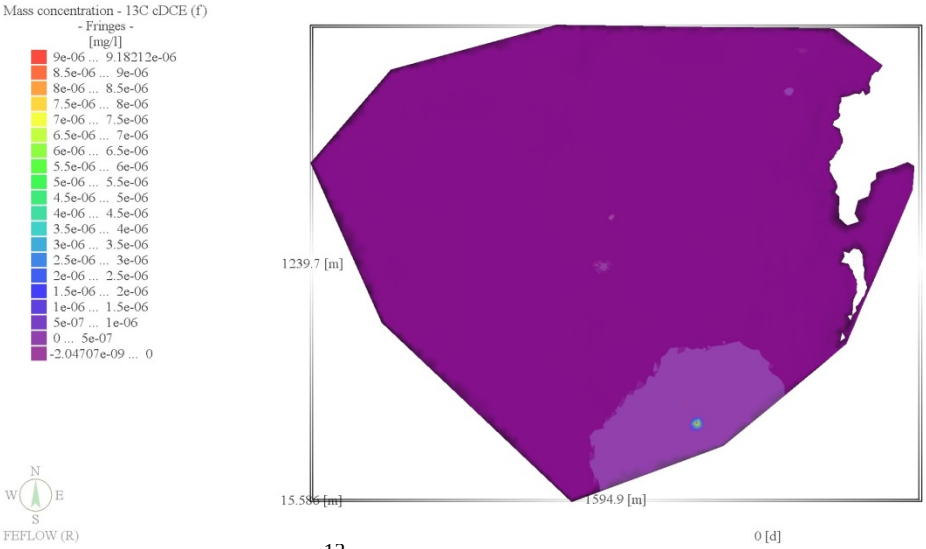

FIGURE 4-55: Modeled ^{13}C cDCE mass concentration in the USZ

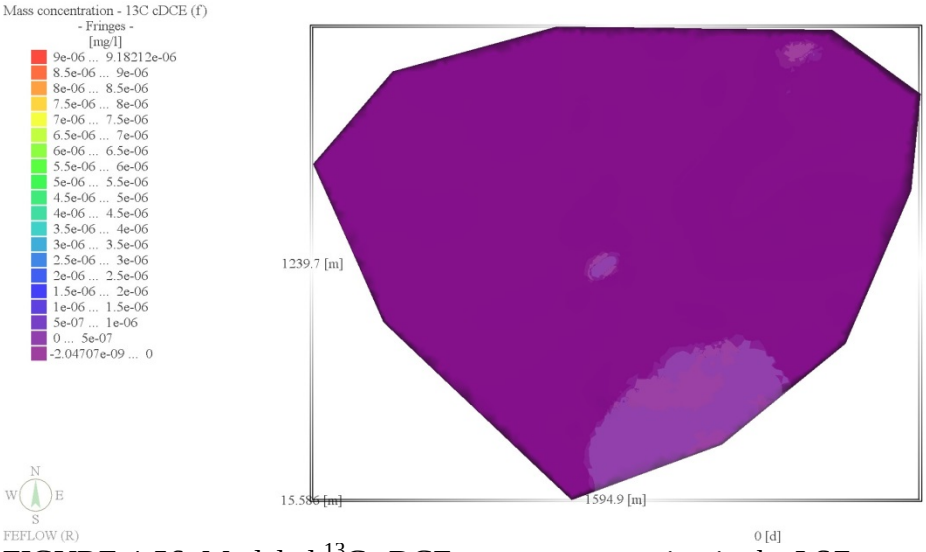

FIGURE 4-56: Modeled ^{13}C cDCE mass concentration in the LSZ

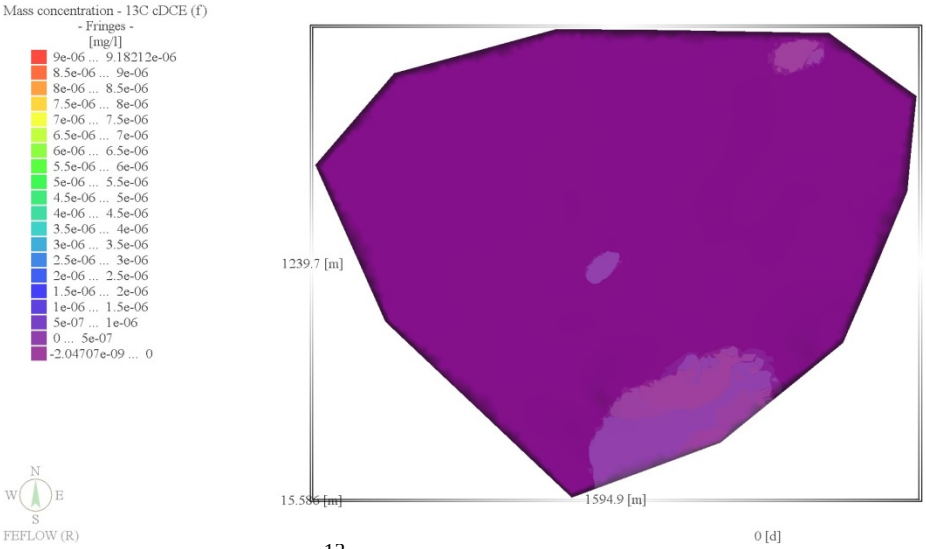

FIGURE 4-57: Modeled ^{13}C cDCE mass concentration in the LLSZ

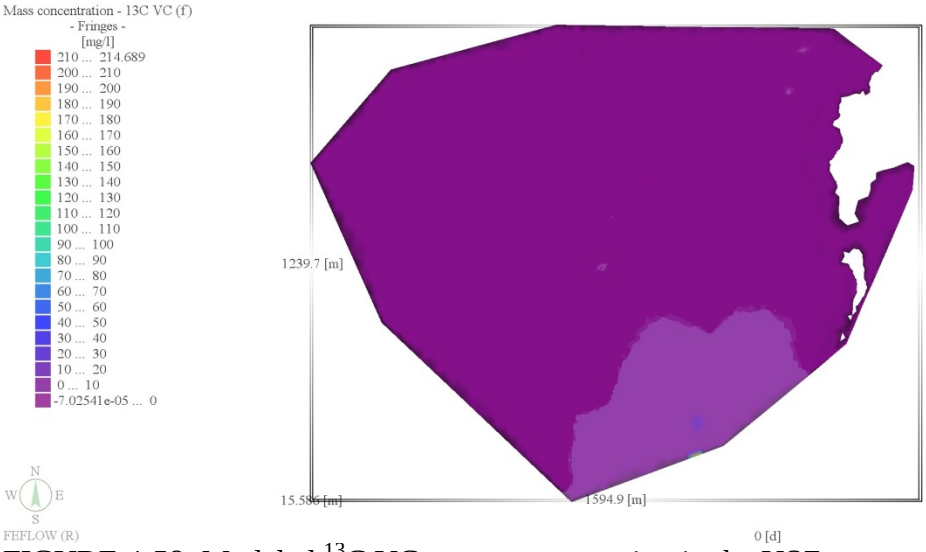

FIGURE 4-58: Modeled ^{13}C VC mass concentration in the USZ

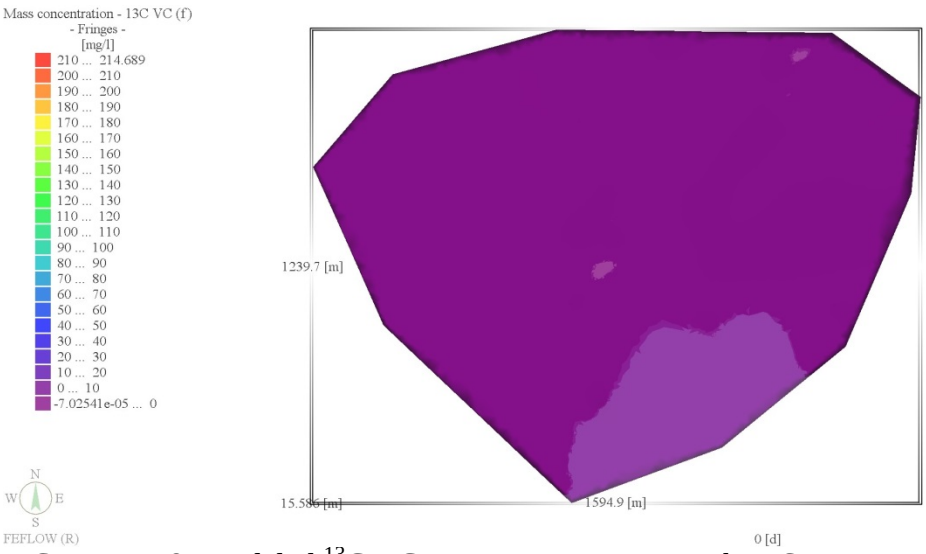

FIGURE 4-59: Modeled ^{13}C VC mass concentration in the LSZ

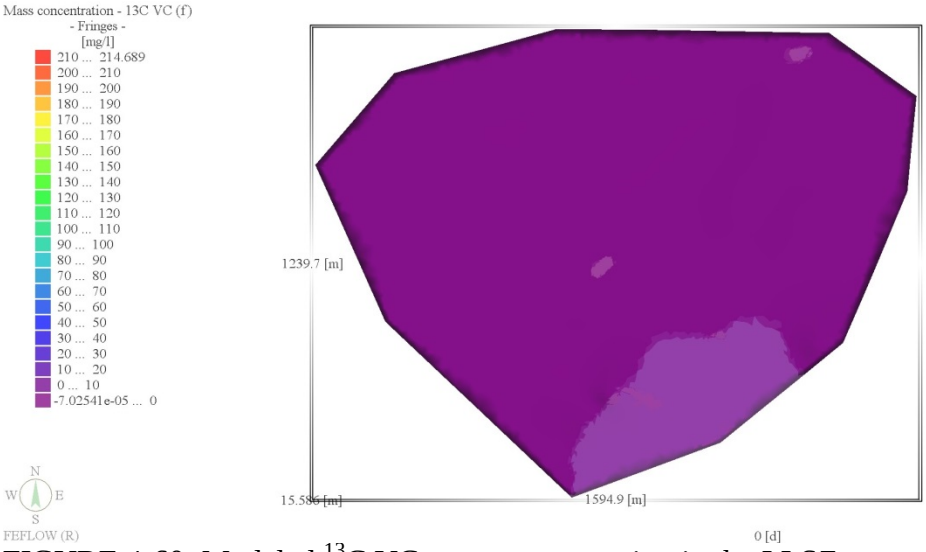

FIGURE 4-60: Modeled ^{13}C VC mass concentration in the LLSZ

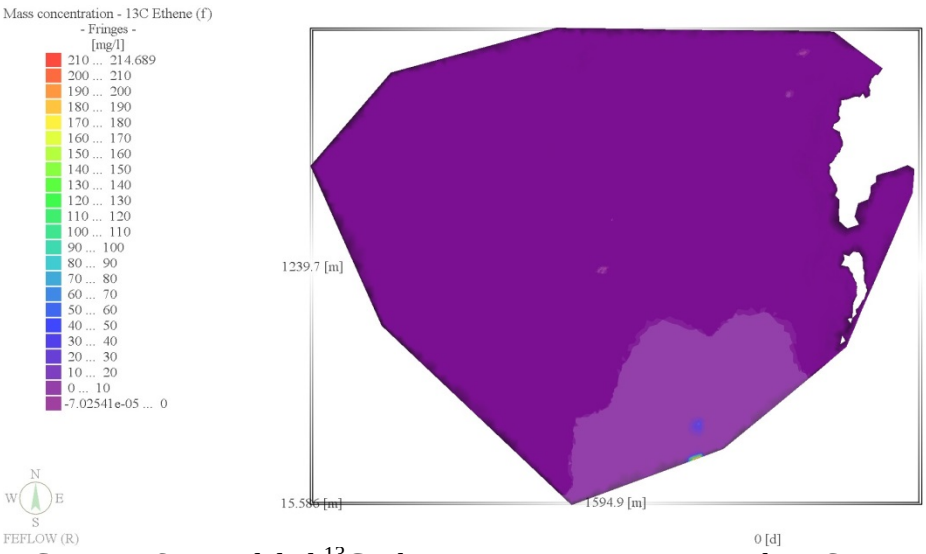

FIGURE 4-61: Modeled ^{13}C ethene mass concentration in the USZ

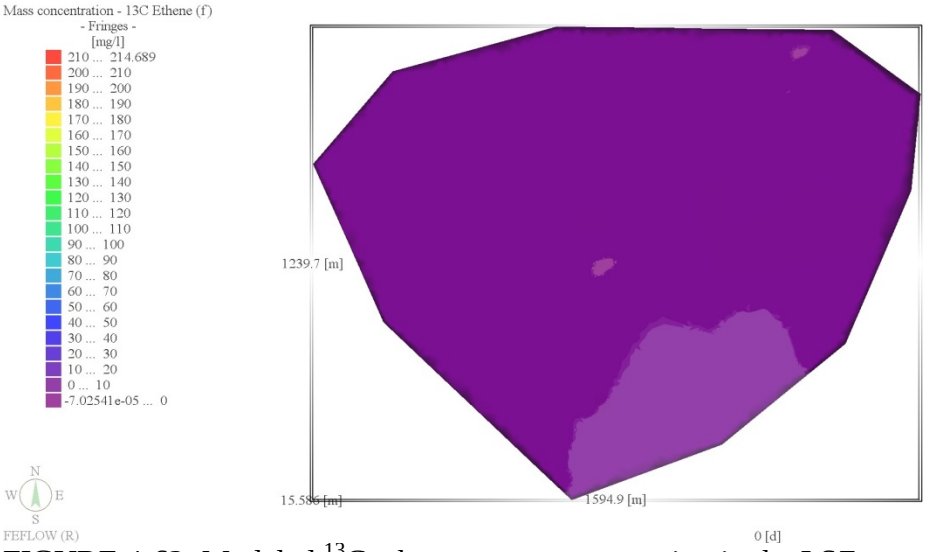

FIGURE 4-62: Modeled ^{13}C ethene mass concentration in the LSZ

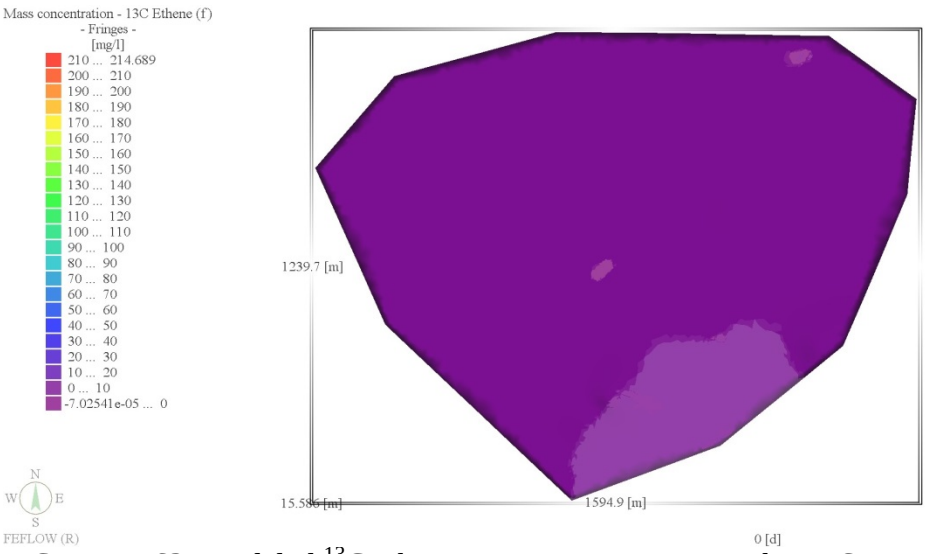

FIGURE 4-63: Modeled ^{13}C ethene mass concentration in the LLSZ

4.5.1.1. ^{12}C Mass Balance

Chlorinated ethenes are entering the model domain by means of the fixed concentration (e.g., constant source release) boundary conditions at each of the two sources. At the end of the 20 year simulation, FEFLOW output indicates ^{12}C PCE is entering the domain on model slice 2 at a rate of 3 grams/day from the 105 source. On model slice 4, ^{12}C PCE is entering the domain at 299 grams/day from the IWTP source. On model slice 2, ^{12}C TCE is entering the domain at a rate of 19 grams/day from the 105 source. On model slice 4, ^{12}C TCE is entering the domain at 1,652 grams/day from the IWTP source.

Chlorinated ethenes are exiting the model domain at the constant head boundary conditions along the border of each model slice. At the end of the 20 year simulation, FEFLOW output indicates the ^{12}C species are exiting the entire model domain at rates of 1 gram/day, 3 grams/day, 1.7e-8 grams/day, 2 grams/day, and 2 grams/day for PCE, TCE, *cis*-DCE, vinyl chloride, and ethene, respectively. The distribution of these rates with depth in the domain is quantified using model calculated rates associated with each

model slice. On a percentage basis (percentage of grams/day being transferred from slice to slice), the rate distributions for individual ^{12}C species are similar with the exception of PCE. The slice pair 1-2 represents layer 1 and the upper half of layer 2 (USZ). The slice pair 3-4 represents lower half of model layer 2, model layer 3, and the upper half of model layer 4 (LSZ). The slice pair 5-6 represents the lower half of model layer 4 and layer 5 (LLSZ). For ^{12}C PCE, the average rate (grams/day) percentages for model slice pairs 1-2, 3-4, and 5-6 are 400%, 5100%, and 50%, respectively. For ^{12}C TCE, the average rate percentages for model slice pairs 1-2, 3-4, and 5-6 are 400%, 4800%, and 50%, respectively. For ^{12}C cDCE, the average rate percentages for model slice pairs 1-2, 3-4, and 5-6 are 78%, 35%, and 25%, respectively. For ^{12}C VC and ethene, the average rate percentages for model slice pairs 1-2, 3-4, and 5-6 are 30%, 50%, and 30%, respectively. These percentages used to describe slice to slice transfer, in turn, are used to quantify layer-associated mass percentages. Like the chlorinated ethene distributions within the domain, these rate distributions are a function of the simulated groundwater flow regime, the source area concentrations and locations, and the relative biotransformation rates of each species. The higher exit rates associated with the middle and lower depth intervals are primarily due to the combined downward and lateral movement of mass from the two modeled source areas.

For the entire model domain, the biotransformation rates are independent of mass transfer rates described above, and for ^{12}C species at the end of the 20 year simulation are: PCE, 1.0 gram/day; TCE, 5.9 grams/day; *cis*-DCE, 4.4 grams/day; vinyl chloride, 4.0 grams/day; and ethene, 3.6 grams/day. For the parent compounds, PCE and TCE, these rates reflect the offsetting effects of high concentrations and lengthy half lives on

the biotransformation rates. For the intermediate compounds, the offsetting effects on biotransformation rates are low concentrations and high biotransformation rates.

The distribution of species-specific biotransformation rates throughout the domain are quantified using model calculated rates associated with each model slice. On a percentage basis (percentage of grams/day being biotransformed from slice to slice), the biotransformation rate (grams/day) distributions for individual ^{12}C species are similar. For all species, the approximate rate percentages for model slice pairs 1-2, 3-4, and 5-6 are 33%, 14%, and 52%, respectively. These percentages, in turn, are used to quantify layer-associated percentages. The relationships are the same as those for the mass transfer rates described above. The slice pair 1-2 represents layer 1 and the upper half of layer 2. The slice pair 3-4 represents lower half of model layer 2, model layer 3, and the upper half of model layer 4. The slice pair 5-6 represents the lower half of model layer 4 and layer 5. The lower rate associated with the middle depth interval can be attributed to the higher relative rate of water and mass movement through the more conductive model layer 3, resulting in lower residence times for biotransformation to take place.

4.5.1.2. ^{13}C Mass Balance

At the end of the 20 year simulation, FEFLOW output indicates ^{13}C PCE is entering the domain on model slice 2 at a rate of 0.1 grams/day from the 105 source. On model slice 4, ^{13}C PCE is entering the domain at 2 grams/day from the IWTP source. On model slice 2, ^{13}C TCE is entering the domain at a rate of 0.1 grams/day from the 105 source. On model slice 4, ^{13}C TCE is entering the domain at 10 grams/day from the IWTP source.

At the end of the 20 year simulation, FEFLOW output indicates the ^{13}C species are exiting the entire model domain at rates of 0.3 grams/day, 1.6 grams/day, 0.1 grams/day, 0.02 grams/day, and 0.02 grams/day for PCE, TCE, *cis*-DCE, vinyl chloride, and ethene, respectively. The distribution of these rates with domain depth is quantified using model calculated rates associated with each model slice. These percentages, like described above for ^{12}C, are used to quantify layer-associated percentages. The slice pairs (described previously) represents the USZ, LSZ and LLSZ. For ^{13}C PCE, the average rate percentages for model slice pairs 1-2, 3-4, and 5-6 are 90%, 300%, and 50%, respectively. For ^{13}C TCE, the average rate percentages for model slice pairs 1-2, 3-4, and 5-6 are 80%, 500%, and 60%, respectively. For ^{13}C cDCE, the average rate percentages for model slice pairs 1-2, 3-4, and 5-6 are 90%, 400%, and 40%, respectively. For ^{13}C VC and Ethene, the average rate percentages for model slice pairs 1-2, 3-4, and 5-6 are 30%, 50%, and 30%, respectively. Like the chlorinated ethene distributions within the domain, these rate distributions are a function of the simulated groundwater flow regime, the source area concentrations and locations, and the relative biotransformation rates of each species. The higher exit rates associated with the middle and lower depth intervals are primarily due to the combined downward and lateral movement of mass from the three source areas.

For the entire model domain, the biotransformation rates for ^{13}C species at the end of the 20 year simulation are: PCE, 0.01 gram/day; TCE, 0.06 gram/day; *cis*-DCE, 0.05 grams/day; vinyl chloride, 0.04 gram/day; and ethene, 0.04 gram/day. For the parent compounds, PCE and TCE, these rates reflect the offsetting effects of high concentrations and lengthy half lives on the biotransformation rates. For the intermediate compounds,

the offsetting effects on biotransformation rates are low concentrations and high biotransformation rates.

The distribution of species-specific biotransformation rates throughout the domain are quantified using model calculated rates associated with each model slice. On a percentage basis, the rate distributions for individual species are similar. For all species, the approximate rate percentages for model slice pairs 1-2, 3-4, and 5-6 are 34%, 15%, and 51%, respectively. These rates, in turn, are used to quantify layer-associated percentages. The relationships are the same as those for the mass exit rates described above. The lower rate associated with the middle depth interval can be attributed to the higher relative rate of water and mass movement through the more conductive model layer 3, resulting in lower residence times for biotransformation to take place.

4.5.2. Constituent Carbon Isotopic, Measured and Modeled

A simple graphical method was developed to evaluate the measured and modeled isotopic results following model iterations (FIGURE 4-64 through FIGURE 4-72). To accomplish this, a subset of monitoring wells within the numerical model domain from the USZ, LSZ and LLSZ was selected. Those monitoring wells were sorted from west to east and plotted along the x-axis. The measured isotopic values for the chlorinated ethenes reported at each well were plotted along the y-axis. Graphs were generated for the measured and modeled data sets. The modeled isotopic values were also plotted against the measured isotopic values. In some cases, the monitoring wells lack isotopic data; they were initially selected during concentration comparisons before the isotopic comparisons began.

In the USZ, 15 key monitoring wells were selected for closer evaluation (FIGURE 4-64 and FIGURE 4-65). Measured isotopic results indicate little to moderate transformation at many of the well locations. In a closed system, as TCE degrades, the *cis*-DCE is initially isotopically depleted relative to the TCE. Upon completion of the transformation, the TCE will no longer exist and the *cis*-DCE isotopic value will be equal to that of the original TCE isotopic value. Given that TCE and *cis*-DCE isotopic signatures are nearly identical at several locations, this is interpreted to indicate that TCE and *cis*-DCE in various stages of dechlorination are mixing. Also note that VC exists at six locations with isotopic values that indicate enrichment. These data indicate *cis*-DCE and VC are both likely degrading. However, the VC isotopic values indicate that any *cis*-DCE being transformed to VC is then being transformed into ethene. Recall that the $\delta^{13}C$ ‰ for PCE and TCE used as model input were -30.8 ‰ and -24.9 ‰, respectively. Monitoring wells closest to the source locations (e.g., 105-MW11 through 105-MW14) had the highest modeled concentrations and most source-like isotopic values following the model run. Comparison of the measured isotopic data to the modeled isotopic data reveals results with an acceptable match (FIGURE 4-66). If the measured and modeled data were identical, the data would plot along a trend line with a slope equal to one. Further refinement of model parameters, particularly the isotope fractionation factor, may provide a better overall match. However, for the purposes of this discussion, this match has met the threshold criteria.

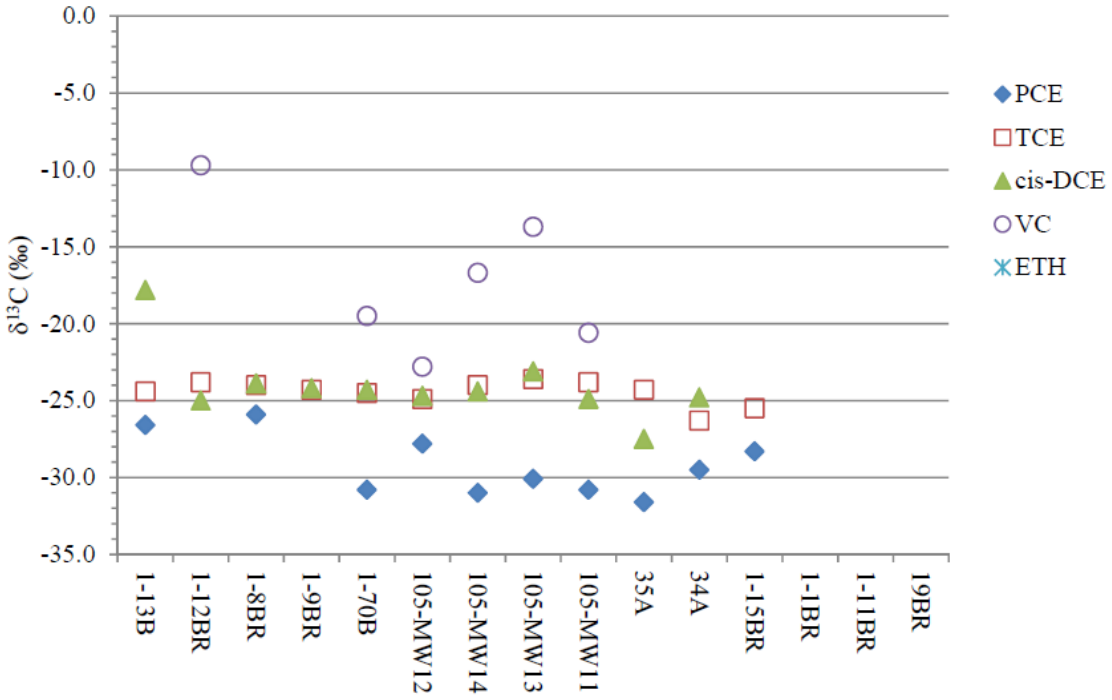

FIGURE 4-64: Measured $\delta^{13}C$ chlorinated ethenes in the USZ, 2008

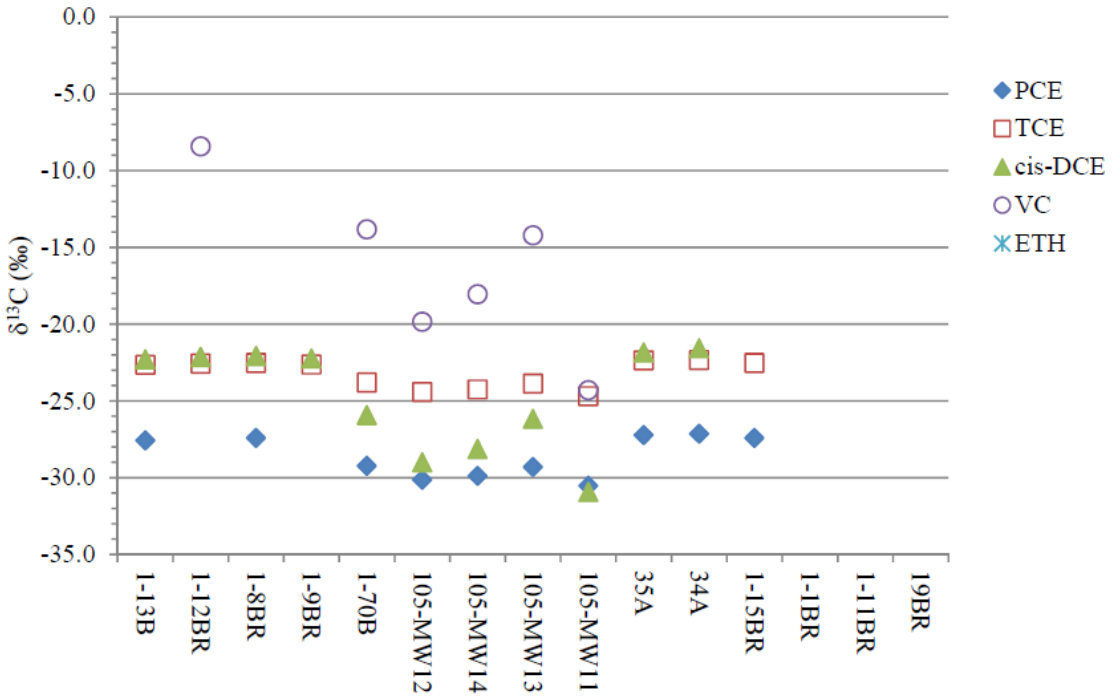

FIGURE 4-65: Modeled $\delta^{13}C$ chlorinated ethenes in the USZ

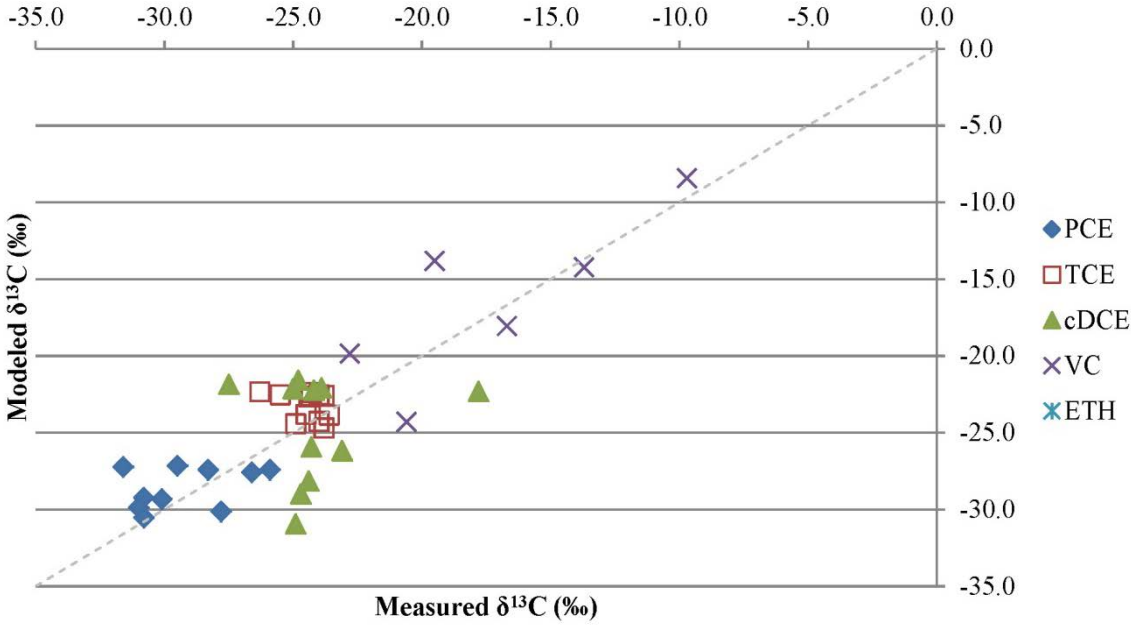

FIGURE 4-66: Measured (2008) vs. modeled $\delta^{13}C$ chlorinated ethenes in the USZ

In the LSZ, 14 key monitoring wells were selected for closer evaluation (FIGURE 4-67 and FIGURE 4-68). Measured isotopic results indicate moderate to advanced transformation. An initial observation of the measured versus modeled data might reveal dissimilar results. A closer inspection may clarify the apparent discrepancies in the data, particularly for monitoring wells 1-15AR, 1-11A, 19AR, and 1-50BR.

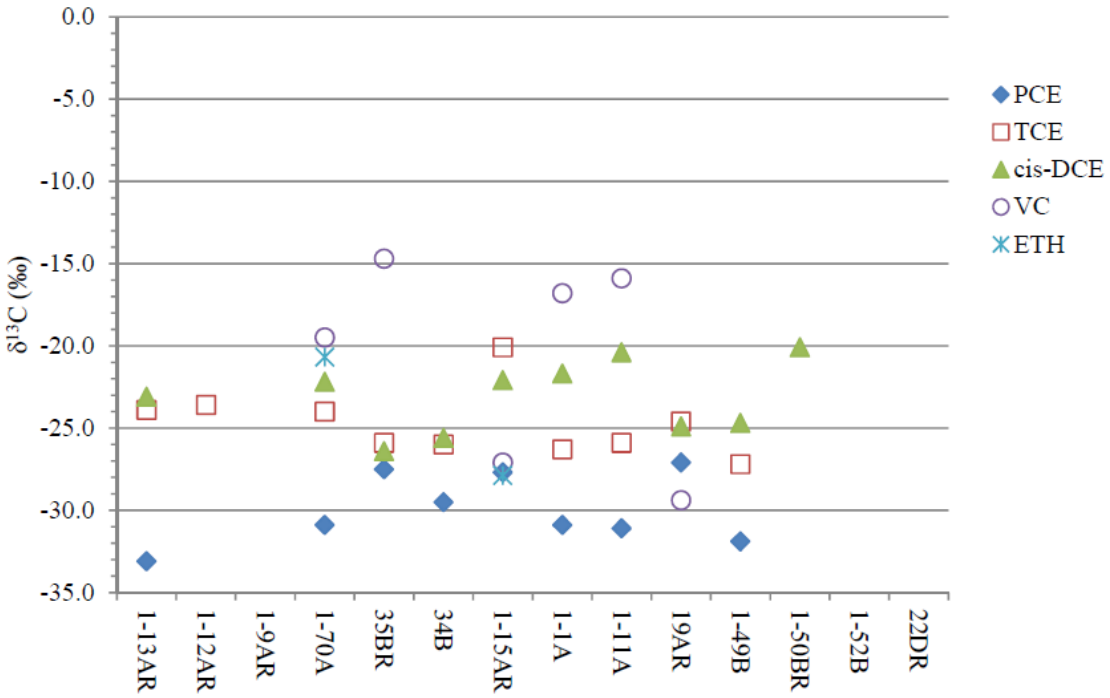

FIGURE 4-67: Measured $\delta^{13}C$ chlorinated ethenes in the LSZ, 2008

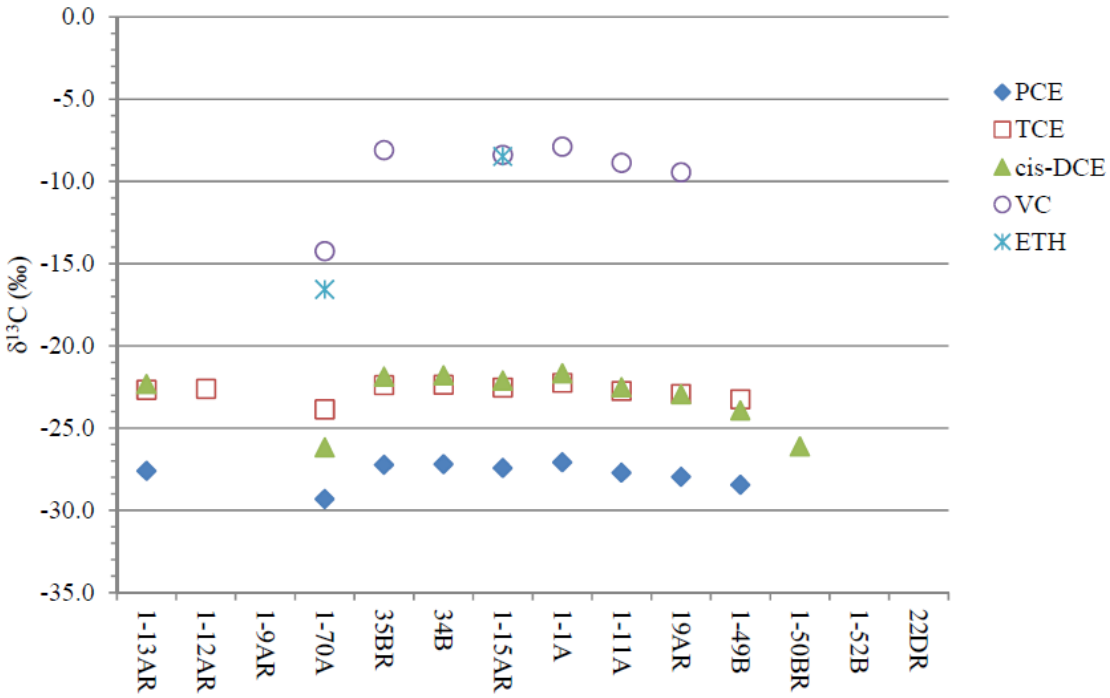

FIGURE 4-68: Modeled $\delta^{13}C$ chlorinated ethenes in the LSZ

Each of these four wells has chlorinated ethene concentrations that are significant. Modeled isotopic values for VC and ethene at 1-15AR and VC at 19AR appear to be too enriched relative to measured isotopic values. Modeled isotopic values for *cis*-DCE at 1-50BR appear to be more depleted than the measured isotopic value for *cis*-DCE, which is strange considering the proximity of this well to the source at the IWTP. Modeled isotopic values for *cis*-DCE and VC at monitoring well 1-11A are depleted and enriched, respectively. As a test during modeling, location-specific criteria were assigned for any monitoring well location within the model domain, which forced the parameters to generate modeled results that were nearly identical to measured results. Therefore, it is speculated that location-specific properties like heterogeneity, dissolved oxygen, and oxidation/reduction potential or fluid properties like dispersivity that differ from the regional subsurface conditions may be the cause of the apparent isotopic mismatches noted by data plotted off of an ideal trend line (i.e., slope equal to one) (FIGURE 4-69).

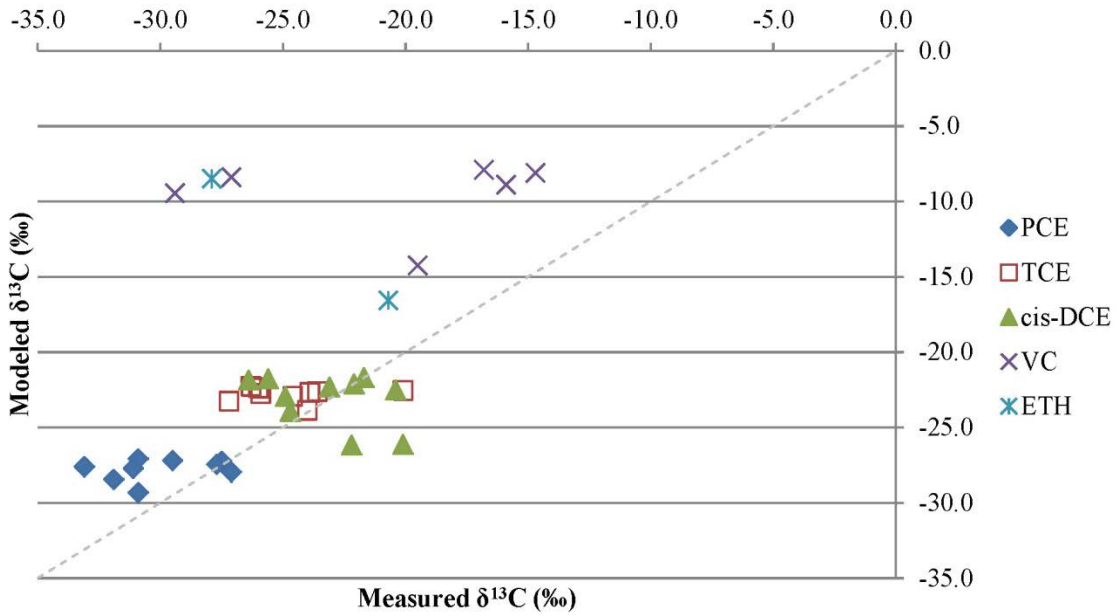

FIGURE 4-69: Measured (2008) vs. modeled $\delta^{13}C$ chlorinated ethenes in the LSZ

In the LLSZ, 11 key monitoring wells were selected for closer evaluation (FIGURE 4-70 and FIGURE 4-71). Measured isotopic results indicate moderate transformation. Similar to the isotopic comparisons in the LSZ, there appear to be conflicting measured and modeled results. Monitoring well 1-52C is upgradient of the source location and is likely affected by dispersivity assumptions. Modeled isotopic results for TCE and *cis*-DCE at monitoring wells 1-15CR, 19CR, and 1-49C appear to be depleted with respect to measured isotopic values. It is also evident that modeled isotopic values for VC and ethene are too enriched relative to measured isotopic values. It is suspected that variations in assumed kinetic reaction rates (faster for TCE and *cis*-DCE and slower for VC and ethene) would explain the apparent isotopic differences noted by data plotted off of an ideal trend line (i.e., slope equal to one) (FIGURE 4-72). It is also possible that VC and ethene are products of reactants not included in this study.

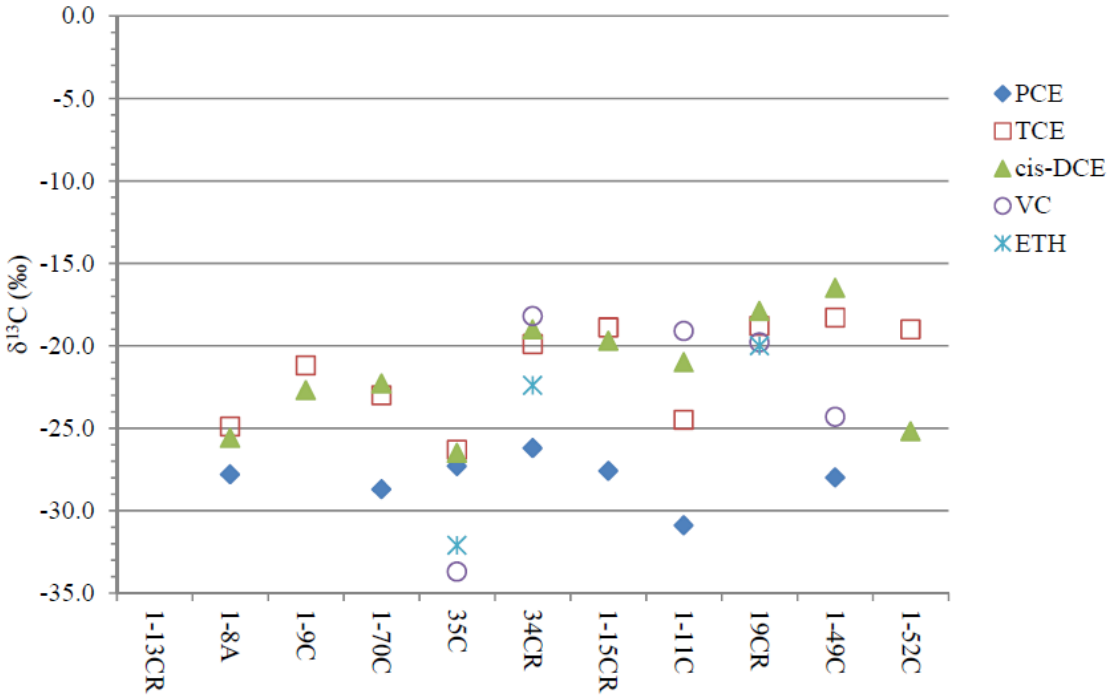

FIGURE 4-70: Measured $\delta^{13}C$ chlorinated ethenes in the LLSZ, 2008

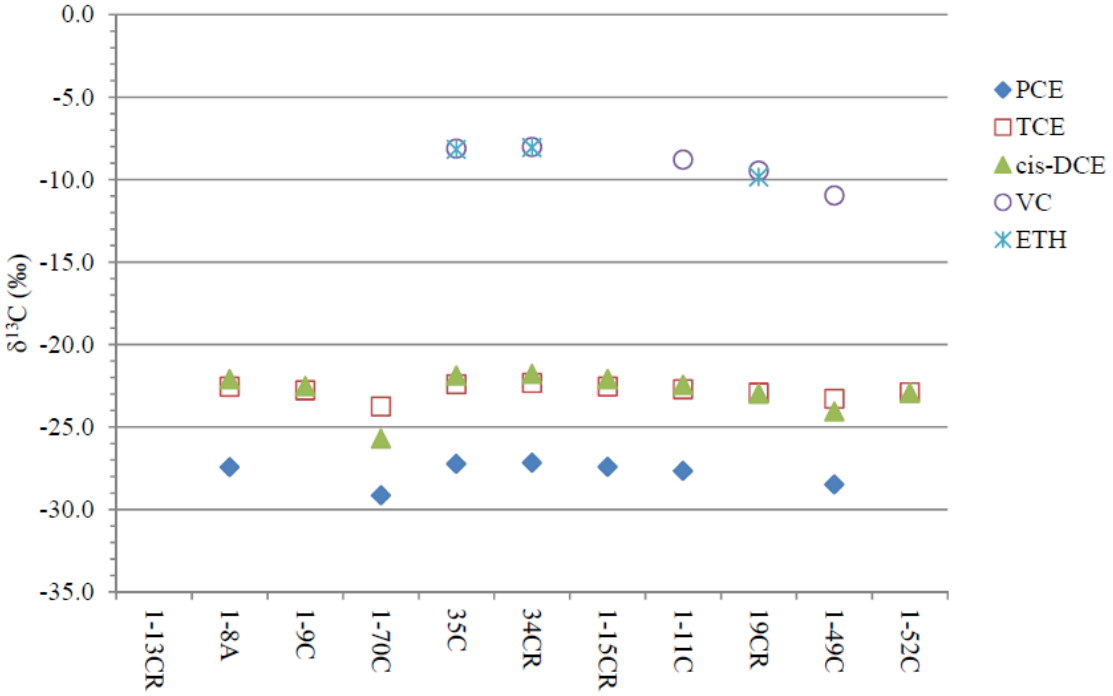

FIGURE 4-71: Modeled $\delta^{13}C$ chlorinated ethenes in the LLSZ

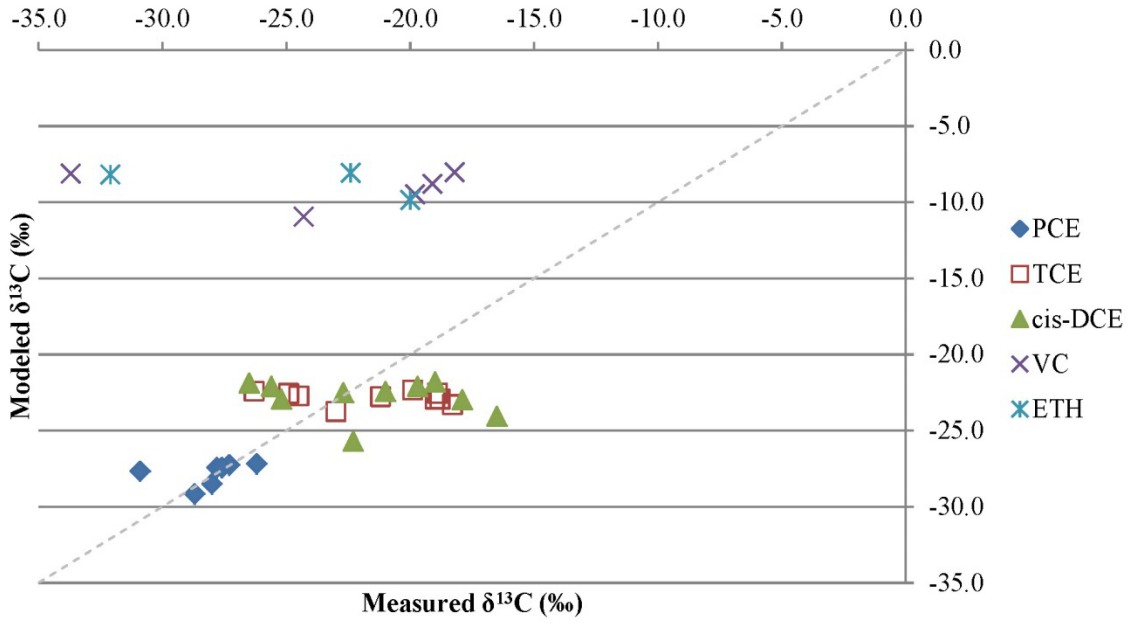

FIGURE 4-72: Measured (2008) vs. modeled $\delta^{13}C$ chlorinated ethenes in the LLSZ

4.6. Summary

Based on the hydraulic, chemical, and isotopic data collected in the study area, key parameters required to successfully develop and calibrate a 3D reactive transport model capable of providing a quantitative mass contribution assessment of comingled chlorinated ethene plumes were identified.

To quantify mass contribution of comingled chlorinated ethene plumes using traditional techniques, vast amounts of site-specific data are required. Those data include physical characteristics of the subsurface environment, biogeochemical conditions of both contaminant and host environment, and temporal or spatial variations of those factors. The type and quantity of data necessary to gain a complete understanding of a site is often cost prohibitive.

The large quantity and spatial extent of data accumulated at Tinker AFB, along with complexities of the site, provided a unique setting for us to develop the modeling framework. At other similar sites, fiscal constraints may not allow for such an investigation. It is believed that utilizing CSIA and a 3D reactive transport model rather than a traditional labor-intensive and expensive investigation may allow investigators to collect less site-specific data and reach similar conclusions.

All of the required data for three dimensional modeling was closely evaluated, in order to establish a framework for modeling efforts at the study area and other sites. As with any reactive model construction, infrastructure, lithologic, hydraulic and analytical data are required to build the hydrostratigraphic and potentiometric layers, slices and boundaries. When adequate data are not available, these components will be conceptual in nature. Depending on the resources available, some effort should be made to extend

the model beyond the conceptual design using site-specific data; the overall results will be more meaningful if the model is calibrated and verified. Hydraulic parameters are important for smaller scale sites and should be determined, if possible. However, for large and/or homogeneous sites, these values can be approximated (e.g., empirically deriving dispersivity values based on scale). Water balance components are required for the model; these can be estimated using local input (e.g., precipitation) data. Boundary flux is often a difficult component of the model to resolve with great confidence but, if the model domain is large enough to cover the area of interest, flux assumptions become less crucial. Finally, the success of being able to determine the extent of transformation of comingled chlorinated plumes as they migrate from a source area within a 3D reactive transport model is directly related to four primary model variables; source concentrations, overall species biotransformation rates, isotope fractionation factors (α), and source isotopic ratios ($\delta^{13}C$ ‰). Contaminant source locations should be established based on site history and contaminant concentration data, if available. The data suggest that source concentration assumptions for overall mass and light and heavy isotope composition for each of the chemical constituents are critical to providing meaningful results. Biotransformation rates are generally site-specific; estimates should be made based on close inspection of subsurface geochemical conditions and the presence/absence of source degradation products. Ideally, the isotope fractionation factor would be determined using isotopic results and making assumptions about the percentage of source mass remaining. Without those data, fractionation factors can be estimated initially and then adjusted within the model until a satisfactory model result is obtained. Light and heavy carbon isotopes, ^{12}C and ^{13}C, of each source and intermediate contaminant should

be considered separately to simulate differential biotransformation rates between isotopes of the same species.

CHAPTER 5: DISCUSSION AND CONCLUSIONS

Herein, a framework for integration of CSIA along with standard chemical and hydraulic information into a 3D reactive fate and transport model is presented. Chlorinated ethene concentrations and compound-specific isotope data, along with other traditional field measurements are coupled into a reactive finite element fate and transport model.

5.1. Isotopic Variability

For PCE and TCE, a source isotopic value of -30.8 ‰ and -24.9 ‰, respectively, was selected based on conservative estimates of the apparent source locations (i.e., isotopic values at monitoring wells with high constituent concentrations). As described previously, isotopic shifts in the less negative direction (i.e., -30 ‰ to -20 ‰) indicate $\delta^{13}C$ enrichment. While non-degradative process can cause minor isotopic shifts, enrichment primarily occurs when chlorinated ethenes degrade. For example, Hunkeler et al. (2008) note that for highly chlorinated hydrocarbons such as PCE and TCE, little biodegradation occurs as long as oxygen is present and the redox potential is elevated and the relevance of biodegradation can be evaluated by characterizing redox conditions [41].

Furthermore, groundwater velocities are low, which indicates that spatial isotopic variation is as important as temporal variation. In other words, the isotopic variation across the site (in three dimensions) were taken at face value and assumed that isotopic shifts are significant. Thus, the isotopic values presented herein indicate various levels

of enrichment of each of the chlorinated ethenes. It is clear based on the presence of transformation products and the apparent isotopic shifts that degradative processes are occurring within the project site subsurface. However, the relative magnitude of the degradation and location of the favorable degradative (microbially-active, anaerobic) environment remains less clear.

Considering the most prevalent mole fractions of chlorinated ethene species in each HSU and across the model domain, the isotopic variability provides additional insight into likely transformative (or lack thereof) processes. In the USZ, groundwater samples from monitoring wells located at the 105 and 34 sources areas have $\delta^{13}C$ values characteristic of source values found in the literature [68]. Because TCE (in addition to PCE) was used in degreasing pits at these locations, it is reasonable to assume that source TCE likely exists. In the LSZ, TCE and *cis*-DCE values east of Building 3001 appear to be generally enriched relative to locations underneath and west of Building 3001, further suggesting transformative processes. These data are supported by isotopically enriched VC and ethene data at the IWTP, as well as generally lower dissolved oxygen and ORP values. However, PCE $\delta^{13}C$ values at monitoring wells 1-49B, 1-11A, and 1-1A appear very similar to the assumed PCE source $\delta^{13}C$ values. In the LLSZ, *cis*-DCE and TCE isotopic values are nearly consistently isotopically enriched relative to the USZ and LSZ across the model domain, suggesting these reactants have undergone reductive dechlorination. These data are again supported by isotopically enriched VC and ethene results. Finally, PCE $\delta^{13}C$ values at monitoring wells 35C and 1-11C in the LLSZ appear isotopically consistent with those results reported in samples from 35BR and 1-11A in the LSZ.

5.2. Sensitivity Analysis

Sensitivity analysis provides insight into the effects of uncertainty in model variables, the responsiveness of the model to changes in variables, and the relative importance of model variables. It is acknowledged that there is a degree of subjectivity associated with model variable selection that should be quantified. In the present study, consideration of isotopes adds another dimension to the traditional sensitivity analysis of fate and transport models, especially with regards to the extent of biotransformation of parent and intermediate chlorinated ethene species. The sensitivities of three variables from the fate and transport model are considered; overall biotransformation half life, dispersivity, and source concentration. Model variable values from the aforementioned calibration are considered to be the base case. One variable is increased by 20 % or reduced by 20 % from its base value in each of six pairs of ^{12}C and ^{13}C model runs. Results are considered at two locations in the model domain corresponding to monitoring wells 1-15AR and 1-70A. These wells are screened in model layer 3 (LSZ) at some distance from the three sources. Therefore, their concentrations are determined by on-going subsurface reactions along the flowpath from the sources. Overall biotransformation half lives are varied as a group, including parent and intermediate species, in the ^{12}C and ^{13}C sensitivity runs. The isotope fractionation factors are not varied from the base case.

At well 1-15AR, higher biotransformation half lives or lower biotransformation rates produce higher overall concentrations (over their respective base case values) and more negative (lighter) $\delta^{13}C$ values. For concentrations, a positive increase denotes higher concentrations. For $\delta^{13}C$ values, a positive value denotes a shift toward greater

^{13}C depletion. The molar sum of overall chlorinated ethene concentrations is higher (4.3 %) than the base case, as expected.

TABLE 5-1: Results of higher biotransformation half lives at well 1-15AR

	PCE	TCE	*cis*-DCE	VC	Ethene
Concentrations	+6.4 %	+4.2 %	+1.9 %	+1.3 %	+0.6 %
$\delta^{13}C$	+1.6 %	+1.3 %	+3.3 %	+10.8 %	+13.3 %

Abbreviations: PCE – tetrachloroethene, TCE – trichloroethene, *cis*-DCE – *cis*-1,2-dichloroethene, VC – vinyl chloride

At well 1-70A, higher biotransformation half lives yield both higher and lower overall concentrations and more negative (lighter) $\delta^{13}C$ values. The molar sum of overall concentrations is 1.8 % higher than the base case.

TABLE 5-2: Results of higher biotransformation half lives at well 1-70A

	PCE	TCE	*cis*-DCE	VC	Ethene
Concentrations	+3.2 %	+2.1 %	–4.0 %	–5.7 %	–7.8 %
$\delta^{13}C$	+0.9 %	+0.8 %	+3.1 %	+9.7 %	+12.4 %

Abbreviations: PCE – tetrachloroethene, TCE – trichloroethene, *cis*-DCE – cis-1,2-dichloroethene, VC – vinyl chloride

At both locations, the percent change in overall chlorinated ethene concentration decreases with each step in the reaction sequence, becoming negative for the intermediate species at well 1-70A. This trend is consistent with the rate change being applied at each step in the sequence together with the intermediate species' higher biotransformation rates. At well 1-70A, where overall chlorinated ethene concentrations are about two orders of magnitude higher, the effect of the intermediate species' higher biotransformation rates is more pronounced. At both locations, the $\delta^{13}C$ values indicate each species is more depleted than the base case, as expected. The percent change in

$\delta^{13}C$ increases with each step in the reaction sequence. The more enriched intermediate species exhibit a greater response to the rate change because relatively more of the ^{13}C species is available in the base case to drive the first order reaction at their higher biotransformation rates.

At well 1-15AR, lower biotransformation half lives or higher biotransformation rates produce lower overall concentrations and more positive (heavier) $\delta^{13}C$ values. The molar sum of overall concentrations is 6.1 % lower than the base case.

TABLE 5-3: Results of lower biotransformation half lives at well 1-15AR

	PCE	TCE	*cis*-DCE	VC	Ethene
Concentrations	–8.7 %	–5.9 %	–4.3 %	–3.9 %	–3.4 %
$\delta^{13}C$	–2.6 %	–2.4 %	–4.2 %	–12.1 %	–14.0 %

Abbreviations: PCE – tetrachloroethene, TCE – trichloroethene, *cis*-DCE – *cis*-1,2-dichloroethene, VC – vinyl chloride

At 1-70A, lower biotransformation half lives produce both lower and higher overall concentrations and more positive (heavier) $\delta^{13}C$ values. The molar sum of overall concentrations is 2.7 % lower than the base case. These trends and conclusions drawn are essentially the reverse of those observed for the higher half lives, confirming that the model responds as expected.

TABLE 5-4: Results of lower biotransformation half lives at well 1-70A

	PCE	TCE	*cis*-DCE	VC	Ethene
Concentrations	–4.5 %	–3.0 %	+3.2 %	+5.0 %	+7.3 %
$\delta^{13}C$	–1.2 %	–1.1 %	–3.8 %	–10.8 %	–13.4 %

Abbreviations: PCE – tetrachloroethene, TCE – trichloroethene, *cis*-DCE – *cis*-1,2-dichloroethene, VC – vinyl chloride

At well 1-15AR, higher dispersivities produce higher overall concentrations and more negative (lighter) $\delta^{13}C$ values. The molar sum of overall concentrations is 86.5 % higher than the base case.

TABLE 5-5: Results of higher dispersivities at well 1-15AR

	PCE	TCE	*cis*-DCE	VC	Ethene
Concentrations	+87.3 %	+86.6 %	+85.0 %	+84.5 %	+84.1 %
$\delta^{13}C$	+0.4 %	+0.4 %	+0.9 %	+2.8 %	+3.4 %

Abbreviations: PCE – tetrachloroethene, TCE – trichloroethene, *cis*-DCE – *cis*-1,2-dichloroethene, VC – vinyl chloride

The significantly higher overall concentrations suggest that well 1-15AR is offset from the center of the plume where concentrations are highest. The higher dispersivities may have expanded the chlorinated ethene distribution transversely toward 1-15AR. The percent change in $\delta^{13}C$ increases with each step in the reaction sequence. The more enriched species exhibit a greater response to the higher concentration because relatively more of the ^{13}C species is available in the base case to drive the first-order reaction at their higher biotransformation rates.

At well 1-70A, higher dispersivities produce both higher and lower overall concentrations and more negative (lighter) $\delta^{13}C$ values. The molar sum of overall concentrations is 0.4 % lower than the base case.

TABLE 5-6: Results of higher dispersivities at well 1-70A

	PCE	TCE	*cis*-DCE	VC	Ethene
Concentrations	+0.1 %	–0.3 %	–3.0 %	–3.8 %	–4.7 %
$\delta^{13}C$	+0.3 %	+0.2 %	+1.0 %	+3.3 %	+4.1 %

Abbreviations: PCE – tetrachloroethene, TCE – trichloroethene, *cis*-DCE – *cis*-1,2-dichloroethene, VC – vinyl chloride

The overall chlorinated ethene results suggest that well 1-70A is close to the center of the plume where concentrations are highest. The higher dispersivities may have shifted the concentrations distribution longitudinally where the extent of the complete PCE-to-ethene reaction is slightly further along. This interpretation is supported by the decreased intermediate concentrations together with increased $\delta^{13}C$ values.

At well 1-15AR, lower dispersivities produce lower overall concentrations and more positive (heavier) $\delta^{13}C$ values. The molar sum of overall concentrations is 58.6 % lower than the base case.

TABLE 5-7: Results of lower dispersivities at well 1-15AR

	PCE	TCE	*cis*-DCE	VC	Ethene
Concentrations	–58.8 %	–58.6 %	–58.2 %	–58.1 %	–58.0 %
$\delta^{13}C$	–0.6 %	–0.6 %	–1.2 %	–3.8 %	–4.7 %

Abbreviations: PCE – tetrachloroethene, TCE – trichloroethene, *cis*-DCE – *cis*-1,2-dichloroethene, VC – vinyl chloride

These results, which are expected based on those for higher dispersivities, suggest well 1-15AR is offset from the center of the plume and the lower dispersivities may have resulted in the chlorinated ethene distribution moving transversely away from it. Except for PCE, the percent change in $\delta^{13}C$ decreases with each step in the reaction sequence. The more enriched species exhibit a greater response to the lower concentration because relatively more of the ^{13}C species is available to drive the first order reaction at their higher biotransformation rates.

At well 1-70A, lower dispersivities produce higher overall concentrations and more positive (heavier) $\delta^{13}C$ values. The molar sum of overall concentrations is 0.9 % higher than the base case.

TABLE 5-8: Results of lower dispersivities at well 1-70A

	PCE	TCE	*cis*-DCE	VC	Ethene
Concentrations	+0.2 %	+0.7 %	+3.9 %	+4.8 %	+5.9 %
$\delta^{13}C$	–0.4 %	–0.3 %	–1.2 %	–4.0 %	–5.0 %

Abbreviations: PCE – tetrachloroethene, TCE – trichloroethene, *cis*-DCE – *cis*-1,2-dichloroethene, VC – vinyl chloride

These results, which are expected based on those for higher dispersivities, suggest that well 1-70A is close to the center of the plume and the lower dispersivities may have shifted the concentrations distribution longitudinally where the extent of the complete PCE-to-ethene reaction is slightly less farther along. This interpretation is supported by the increased intermediate concentrations together with decreased $\delta^{13}C$ values.

At both wells 1-15AR and 1-70A, higher source concentrations produce overall concentrations that are 20 % higher for all species. At well both 1-15AR and 1-70A, $\delta^{13}C$ values are more negative (lighter).

TABLE 5-9: Results of higher source concentrations

	PCE	TCE	*cis*-DCE	VC	Ethene
$\delta^{13}C$ (1-15AR)	+53.0 %	+66.8 %	+69.3 %	+172.4 %	+167.0 %
$\delta^{13}C$ (1-70A)	+2.3 %	+3.1 %	+3.6 %	+7.0 %	+6.5 %

Abbreviations: PCE – tetrachloroethene, TCE – trichloroethene, *cis*-DCE – *cis*-1,2-dichloroethene, VC – vinyl chloride

The linear response of the overall concentrations suggests that quasi-steady state conditions exist for the base case and the increased source concentrations. However, the $\delta^{13}C$ results imply a significant shift to more depleted conditions for all species. The more enriched species exhibit a greater response to the higher concentration because relatively more of the ^{13}C species is available in the base case to drive the first-order

reaction at their higher biotransformation rates. The greater response at well 1-15AR in terms of $\delta^{13}C$ may be a dispersive effect, in which the more depleted plume at higher concentrations has expanded at this location.

At both wells 1-15AR and 1-70A, lower source concentrations produce overall concentrations that are 20 % lower for all species. At well 1-15AR and 1-70A, $\delta^{13}C$ values more positive (heavier). These trends and conclusions drawn are essentially the reverse of those observed for the higher source concentrations, confirming that the model responds as expected.

TABLE 5-10: Results of lower source concentrations

	PCE	TCE	*cis*-DCE	VC	Ethene
$\delta^{13}C$ (1-15AR)	–0.5 %	–0.8 %	–0.8 %	–1.9 %	–1.9 %
$\delta^{13}C$ (1-70A)	–0.1 %	–0.4 %	–0.4 %	–0.7 %	–0.6 %

Abbreviations: PCE – tetrachloroethene, TCE – trichloroethene, *cis*-DCE – *cis*-1,2-dichloroethene, VC – vinyl chloride

5.3. Source Differentiation Discussion

The calibrated model of ^{12}C and ^{13}C chlorinated ethene isotopes can be used to characterize and quantify the fractional contributions of different chlorinated ethene sources at specific locations in mixed chlorinated ethene plumes. This is a potentially valuable tool for site characterization, environmental forensics, and remedial design. The concept is applied in the present study by starting with a calibrated “base case” model and varying source concentrations individually for each of two of the three source areas; IWTP and 34A. PCE and TCE concentrations at one source are increased by 50 % or reduced by 50 % from their base values in each of four pairs of ^{12}C and ^{13}C model runs. Results are presented for one central location in the model domain corresponding to

monitoring well 1-15AR; this well was selected because it is located in model layer 3 (LSZ) in between and at some distance from the two sources. The same conceptual approach could be used for source areas 105 and ITWP, with a different well screened in the LSZ.

At well 1-15AR, higher IWTP source concentrations produce higher overall chlorinated ethene concentrations (over their respective base case values) and more positive (heavier) $\delta^{13}C$ values. The molar sum of overall chlorinated ethene concentrations is 37.4 % higher than the base case.

TABLE 5-11: Results of higher IWTP source concentrations at well 1-15AR

	PCE	TCE	*cis*-DCE	VC	Ethene
Concentrations	+36.8 %	+37.4 %	+38.5 %	+38.7 %	+39.0 %
$\delta^{13}C$	–0.20 %	–0.16 %	–0.72 %	–2.50 %	–3.30 %

Abbreviations: PCE – tetrachloroethene, TCE – trichloroethene, *cis*-DCE – *cis*-1,2-dichloroethene, VC – vinyl chloride

The quasi-linear response of the overall chlorinated ethene concentrations suggests that steady-state conditions may exist for the base case and the increased IWTP source concentrations. The $\delta^{13}C$ results imply a slight shift to more enriched conditions for all species. The more enriched intermediate species exhibit a greater response to the higher concentration because relatively more of the ^{13}C species is available to drive the first-order reaction at their higher biotransformation rates. The greater enrichment at well 1-15AR with higher IWTP source concentrations suggests that the IWTP contribution to the plume at this location is more enriched relative to contributions from other sources. At well 1-15AR, lower IWTP source concentrations produce lower overall chlorinated ethene concentrations and more negative (lighter) $\delta^{13}C$ values. The molar sum of overall

chlorinated ethene concentrations is 37.3 % lower than the base case. These results and conclusions drawn are essentially the reverse of those observed for the higher IWTP source concentrations.

TABLE 5-12: Results of lower IWTP source concentrations at well 1-15AR

	PCE	TCE	*cis*-DCE	VC	Ethene
Concentrations	–36.7 %	–37.3 %	–38.5 %	–38.8 %	–39.1 %
$\delta^{13}C$	+0.31 %	+0.10 %	+1.34 %	+4.97 %	+6.85 %

Abbreviations: PCE – tetrachloroethene, TCE – trichloroethene, *cis*-DCE – *cis*-1,2-dichloroethene, VC – vinyl chloride

At well 1-15AR, higher 34A source concentrations produce higher overall chlorinated ethene concentrations and more negative (lighter) $\delta^{13}C$ values. The molar sum of overall chlorinated ethene concentrations is 12.7 % lower than the base case.

TABLE 5-13: Results of higher 34A source concentrations at well 1-15AR

	PCE	TCE	*cis*-DCE	VC	Ethene
Concentrations	+13.3 %	+12.7 %	+11.5 %	+11.2 %	+10.9 %
$\delta^{13}C$	+0.78 %	+0.53 %	+1.23 %	+3.96 %	+4.95 %

Abbreviations: PCE – tetrachloroethene, TCE – trichloroethene, *cis*-DCE – *cis*-1,2-dichloroethene, VC – vinyl chloride

The quasi-linear response of the overall chlorinated ethene concentrations suggests that steady-state conditions may exist for the base case and the increased 34A source concentrations. The $\delta^{13}C$ results imply a slight shift to more depleted conditions for all species. The more depleted intermediate species exhibit a greater response to the higher concentration because relatively more of the ^{13}C species is available in the base case to drive the first-order reaction at their higher biotransformation rates. The greater depletion at well 1-15AR with higher 34A source concentrations suggests that the 34A

contribution to the plume at this location is more depleted relative to contributions from other sources. At well 1-15AR, lower 34A source concentrations produce lower overall chlorinated ethene concentrations and more positive (heavier) $\delta^{13}C$ values. The molar sum of overall chlorinated ethene concentrations is 12.6 % lower than the base case.

TABLE 5-14: Results of lower 34A source concentrations at well 1-15AR

	PCE	TCE	*cis*-DCE	VC	Ethene
Concentrations	–13.2 %	–12.6 %	–11.5 %	–11.3 %	–11.0 %
$\delta^{13}C$	–1.48 %	–1.91 %	–2.80 %	–8.06 %	–9.16 %

Abbreviations: PCE – tetrachloroethene, TCE – trichloroethene, *cis*-DCE – *cis*-1,2-dichloroethene, VC – vinyl chloride

These results and conclusions drawn are essentially the reverse of those observed for the higher 34A source concentrations. When contributions to 1-15AR from the 105 source area was modeled (as above), results indicate that the 105 source contributes insignificant chlorinated ethenes to the 1-15AR location. Therefore, based on the IWTP and 34A source modeling analyses, the relative chlorinated ethene contributions to the central well 1-15AR location from the IWTP and 34A sources are ~75 % and ~25 %, respectively.

5.4. Conclusions

The primary objective of this research was to develop a framework for integration of CSIA along with standard chemical and hydraulic information into a 3D reactive fate and transport model in order to quantify the mass contribution of chlorinated ethenes to a comingled plume from multiple source locations. The intent was to extend the traditional investigative processes used to describe contaminant characteristics by incorporating environmental forensic techniques, in this case, compound-specific isotope analysis, into

a reactive finite element fate and transport model. To achieve the objective, numerous tasks were required; those tasks included 1) identifying the appropriate information needed to prepare for future on-site actions, 2) determination of the most efficient investigative processes, 3) utilization and documentation of conventional soil and groundwater sampling methods, 4) calibration of the three-dimensional finite-element model using empirical data, and 5) quantitatively demonstrate source delineation.

These goals were accomplished using a combination of classical investigative techniques, complex modeling and environmental forensics (i.e., compound-specific isotope analysis). Information needed to prepare for future on-site activities includes historical site information, subsurface physical characteristics and analytical data. This work provides a template for collection of these necessary data in an efficient and effective manner. Neither conventional concentration nor non-conventional isotopic data alone are sufficient to achieve a comprehensive understanding of contaminant movement and transformation. Convention concentration data provide an understanding of where chlorinated ethene mass resides, and how that mass changes if samples are collected over time. Hydraulic flow data help investigators understand how mass may move within the site domain. Isotopic data are instrumental in providing insight into the transformation processes taking place within the site domain. When these investigative features are combined, as there have been in this study, using off-the-shelf software (e.g., FEFLOW and FePEST) to assist in modeling development, calibration, and simulation, a fundamental approach for source differentiation is realized.

Thus, a process has been demonstrated which Department of Defense environmental personnel (in the case of this site) can use to develop a more robust

understanding of comingled chlorinated ethene plumes. With sufficient data and accurate plume delineation, source differentiation and contribution appears to be possible. While it is recognized collecting vast amounts of data and constructing advanced three-dimensional models are expensive, it has been shown that major steps can be taken toward understanding plume commingling with moderate funding. It is believed that no one has combined the investigative techniques included herein as has been done. For that reason, it is concluded that this methodology represents a novel approach to site investigation of comingled chlorinated ethene plumes.

It should be noted, there is room for improvement on this research. Integration of the light and heavy isotopes herein was accomplished using chlorinated ethene isotopologues, which were either modeled as ^{12}C:^{12}C molecules or ^{13}C:^{13}C molecules. This was done to simplify the incorporation of each of those isotopologues into the fate and transport model. Chlorinated ethene isotopologues composed of ^{13}C:^{13}C molecules are quite rare, essentially because of the naturally low abundance of ^{13}C (1.11%) [82]. The isotopologue complication could be explored by future researchers by examining more closely the method by which modeled $\delta^{13}C$ values are calculated from independently modeled chlorinated ethene isotopologue.

This work also used both PCE and TCE as source contaminants, which may have complicated the interpretation of the results. Assumptions regarding TCE as a source may be refuted (i.e., TCE may be primarily a product of PCE degradation). Choosing another site, where source contaminant parameters are well-constrained in historical data, and preferably a site where TCE is the only source, would clearly simplify much of the

approach described herein, might also elucidate the evolution of degradation product fate and transport, and may likely provide more compelling results.

Another key advancement that could be considered by future researchers is the incorporation of chlorine and hydrogen isotopes, in addition to carbon isotopes, into the modeling process. These additional isotopes would greatly improve the understanding of the transformation mechanisms and help constrain the carbon enrichment factors, thus improving the construction (and likely simulations) of the fate and transport model, leading to more confident quantification of source contribution.

REFERENCES

1. USEPA, Cleaning Up the Nation's Waste Sites: Markets and Technology Trends, O.o.S.W.a.E. Response, Editor. 2004, U. S. Environmental Protection Agency.

2. Blessing, M., et al., Delineation of Multiple Chlorinated Ethene Sources in an Industrialized Area -- A Forensic Field Study Using Compound-Specific Isotope Analysis. Environmental Science & Technology, 2009. 43(8): p. 2701-2707.

3. Pooley, K.E., et al., Aerobic Biodegradation of Chlorinated Ethenes in a Fractured Bedrock Aquifer: Quantitative Assessment by Compound-Specific Isotope Analysis (CSIA) and Reactive Transport Modeling. Environmental Science & Technology, 2009. 43(19): p. 7458-7464.

4. Hunkeler, D., R. Aravena, and E. Cox, Carbon isotopes as a tool to evaluate the origin and fate of vinyl chloride: Laboratory experiments and modeling of isotope evolution. Environmental Science & Technology, 2002. 36(15): p. 3378-3384.

5. Nijenhuis, I., et al., Assessment of the natural attenuation of chlorinated ethenes in an anaerobic contaminated aquifer in the Bitterfeld/Wolfen area using stable isotope techniques, microcosm studies and molecular biomarkers. Chemosphere, 2007. 67(2): p. 300-311.

6. Wilson, J.T., X. Lu, and D.H. Kampbell, Evaluation of the Role of Dehalococcoides Organisms in the Natural Attenuation of Chlorinated Ethylenes in Ground Water, N.R.M.R. Laboratory, Editor. 2006, United States Environmental Protection Agency, National Risk Management Research Laboratory: Cincinnati, Ohio.

7. Hunkeler, D., R. Aravena, and B.J. Butler, Monitoring microbial dechlorination of tetrachloroethene (PCE) in groundwater using compound-specific stable carbon isotope ratios: Microcosm and field studies. Environmental Science & Technology, 1999. 33(16): p. 2733-2738.

8. Clement, T.P., et al., Natural attenuation of chlorinated ethene compounds: model development and field-scale application at the Dover site. Journal of Contaminant Hydrology, 2000. 42(2-4): p. 113-140.

9. Blessing, M., et al. Aerobic biodegradation of chlorinated ethenes in a fractured bedrock aquifer: quantitative assessment by compound-specific isotope analysis. in EGU General Assembly. 2008.

10. Chartrand, M.M.G., et al., Compound specific hydrogen isotope analysis of 1,2-dichloroethane: potential for delineating source and fate of chlorinated hydrocarbon contaminants in groundwater. Rapid Communications in Mass Spectrometry, 2007. 21(12): p. 1841-1847.

11. Aulenta, F., et al., Field study of in situ anaerobic bioremediation of a chlorinated solvent source zone. Industrial & Engineering Chemistry Research, 2007. 46(21): p. 6812-6819.

12. Abe, Y. and D. Hunkeler, Does the Rayleigh equation apply to evaluate field isotope data in contaminant hydrogeology? Environmental Science & Technology, 2006. 40(5): p. 1588-1596.

13. Morrill, P.L., et al., Quantifying chlorinated ethene degradation during reductive dechlorination at Kelly AFB using stable carbon isotopes. Journal of Contaminant Hydrology, 2005. 76(3-4): p. 279-293.

14. Lollar, B.S., et al., Stable carbon isotope evidence for intrinsic bioremediation of tetrachloroethene and trichloroethene at area 6, Dover Air Force Base. Environmental Science & Technology, 2001. 35(2): p. 261-269.

15. Slater, G.F., et al., Variability in carbon isotopic fractionation during biodegradation of chlorinated ethenes: Implications for field applications. Environmental Science & Technology, 2001. 35(5): p. 901-907.

16. Vieth, A., et al., In-situ biodegradation of tetrachloroethene and trichloroethene in contaminated aquifers monitored by stable isotope fractionation. Isotopes in Environmental and Health Studies, 2003. 39(2): p. 113-124.

17. Sorenson, K.S., et al. Assessing Enhanced Anaerobic and Intrinsic Aerobic Biodegradation of Trichloroethene. 2001.

18. Bloom, Y., et al., Carbon isotope fractionation during microbial dechlorination of trichloroethene, cis-1,2-dichloroethene, and vinyl chloride: Implications for assessment of natural attenuation. Environmental Science & Technology, 2000. 34(13): p. 2768-2772.

19. Lollar, B.S., et al., Contrasting carbon isotope fractionation during biodegradation of trichloroethylene and toluene: Implications for intrinsic bioremediation. Organic Geochemistry, 1999. 30(8A): p. 813-820.

20. Dayan, H., et al., Carbon isotopic fractionation during reductive dehalogenation of chlorinated ethenes by metallic iron. Organic Geochemistry, 1999. 30(8A): p. 755-763.

21. Darlington, R., et al., Biotic and Abiotic Anaerobic Transformations of Trichloroethene and cis-1,2-Dichloroethene in Fractured Sandstone. Environmental Science & Technology, 2008. 42(12): p. 4323-4330.

22. Liang, X., et al., Distinguishing abiotic and biotic transformation of tetrachloroethylene and trichloroethylene by stable carbon isotope fractionation. Environmental Science & Technology, 2007. 41(20): p. 7094-7100.

23. Van Breukelen, B.M., Extending the Rayleigh equation to allow competing isotope fractionating pathways to improve quantification of biodegradation. Environmental Science & Technology, 2007. 41(11): p. 4004-4010.

24. Song, D.L., et al., Stable carbon isotope fractionation during enhanced in situ bioremediation of trichloroethene. Environmental Science & Technology, 2002. 36(10): p. 2262-2268.

25. Rangsivek, R. and M.R. Jekel, Removal of dissolved metals by zero-valent iron (ZVI): Kinetics, equilibria, processes and implications for stormwater runoff treatment. Water Research, 2005. 39(17): p. 4153-4163.

26. Hirschorn, S.K., et al., Pathway dependent isotopic fractionation during aerobic biodegradation of 1,2-dichloroethane. Environmental Science & Technology, 2004. 38(18): p. 4775-4781.

27. Arnold, W.A. and A.L. Roberts, Pathways and Kinetics of Chlorinated Ethylene and Chlorinated Acetylene Reaction with Fe(0) Particles. Environmental Science & Technology, 2000. 34(9): p. 1794-1805.

28. Sun, Y.W., et al., Effect of reaction kinetics on predicted concentration profiles during subsurface bioremediation. Journal of Contaminant Hydrology, 1998. 31(3-4): p. 359-372.

29. Davis, J.H., Fate and Transport Modeling of Selected Chlorinated Organic Compounds at Hanger 1000, U.S. Naval Air Station, Jacksonville, Florida, U.S.D.o.t. Interior, Editor. 2003: Tallahassee, Florida.

30. Wilson, J.T., et al., Evaluation of the Protocol for Natural Attenuation of Chlorinated Solvents: Case Study at the Twin Cities Army Ammunition Plant, N.R.M.R. Laboratory, Editor. 2001, United States Environmental Protection Agency: Cincinnati, Ohio.

31. Hunkeler, D., B.M. Van Breukelen, and M. Elsner, Modeling chlorine isotope trends during sequential transformation of chlorinated ethenes. Environ Sci Technol, 2009. 43(17): p. 6750-6.

32. Aeppli, C., et al., Quantifying in situ transformation rates of chlorinated ethenes by combining compound-specific stable isotope analysis, groundwater dating, and carbon isotope mass balances. Environ Sci Technol, 2010. 44(10): p. 3705-11.

33. Elsner, M., et al., Current challenges in compound-specific stable isotope analysis of environmental organic contaminants. Analytical and Bioanalytical Chemistry, 2012. 403(9): p. 2471-2491.

34. Wiegert, C., et al., Dual carbon-chlorine stable isotope investigation of sources and fate of chlorinated ethenes in contaminated groundwater. Environ Sci Technol, 2012. 46(20): p. 10918-25.

35. Jin, B., S.B. Haderlein, and M. Rolle, Integrated carbon and chlorine isotope modeling: applications to chlorinated aliphatic hydrocarbons dechlorination. Environ Sci Technol, 2013. 47(3): p. 1443-51.

36. Kuder, T., et al., 3D-CSIA: Carbon, Chlorine, and Hydrogen Isotope Fractionation in Transformation of TCE to Ethene by a Dehalococcoides Culture. Environ. Sci. Technol., 2013. 477(17).

37. Lutz, S.R. and B.M. Van Breukelen, Combined Source Apportionment and Degradation Quantification of Organic Pollutants with CSIA: 1. Model Derivation. Environmental Science & Technology, 2014. 48(11): p. 6220-6228.

38. Pankow, J.F. and J.A. Cherry, Dense Chlorinated Solvents and Other DNAPLs in Groundwater: History, Behavior, and Remediation. 1996, Portland, Oregon: Waterloo Press.

39. Parsons, Principles and Practices of Enhanced Anaerobic Bioremediation of Chlorinated Solvents. 2004, Parsons Engineering Science, Inc.

40. Clark, I.D. and P. Fritz, Environmental Isotopes in Hydrogeology. 1997, Boca Raton, FL: CRC Press/Lewis Publishers. 328.

41. Hunkeler, D., et al., A Guide for Assessing Biodegradation and Source Identification of Organic Ground Water Contaminants using Compound Specific Isotope Analysis (CSIA), O.o.R.a. Development, Editor. 2008, USEPA: Ada, Oklahoma. p. 82.

42. Faure, G., Principles and Applications of Inorganic Geochemistry: a Comprehensive Textbook for Geology Students. 1991, New York: Macmillan, Inc.

43. Scott, K.M., et al., Optimal methods for estimating kinetic isotope effects from different forms of the Rayleigh distillation equation. Geochimica Et Cosmochimica Acta, 2004. 68(3): p. 433-442.

44. Mariotti, A., et al., Experimental Determination of Nitrogen Kinetic Isotope Fractionation - Some Principles - Illustrations for the Denitrification and Nitrification Processes. Plant and Soil, 1981. 62(3): p. 413-430.

45. Hunkeler, D., et al., Effect of source variability and transport processes on carbon isotope ratios of TCE and PCE in two sandy aquifers. Journal of Contaminant Hydrology, 2004. 74(1-4): p. 265-282.

46. Christ, J.A., et al., Coupling aggressive mass removal with microbial reductive dechlorination for remediation of DNAPL source zones: a review and assessment. Environ Health Perspect, 2005. 113(4): p. 465-77.

47. Loffler, F.E., J.M. Tiedje, and R.A. Sanford, Fraction of electrons consumed in electron acceptor reduction and hydrogen thresholds as indicators of halorespiratory physiology. Applied and Environmental Microbiology, 1999. 65(9): p. 4049-4056.

48. Maymo-Gatell, X., et al., Isolation of a bacterium that reductively dechlorinates tetrachloroethene to ethene. Science, 1997. 276(5318): p. 1568.

49. Hunkeler, D., et al., Assessment of degradation pathways in an aquifer with mixed chlorinated hydrocarbon contamination using stable isotope analysis. Environmental Science & Technology, 2005. 39(16): p. 5975-5981.

50. ITRC, Overview of In situ Bioremediation of Chlorinated Ethene DNAPL Source Zones. 2005, Interstate Technology & Regulatory Council, Bioremediation of Dense Nonaqueous Phase Liquids (Bio DNAPL) Team: Washington, D.C.

51. Yang, Y. and P.L. McCarty, Biologically Enhanced Dissolution of Tetrachloroethene DNAPL. Environmental Science & Technology, 2000. 34(14): p. 2979-2984.

52. Radian, Installation Restoration Program, Phase II - Field Evaluation, Stage 1 Draft Final Report. 1984, Radian Corporation: Austin, TX.

53. Radian, Installation Restoration Program, Phase II - Confirmation/Quantification, Stage 2 Final Report. 1985, Radian Corporation: Austin, TX.

54. Parsons, Tinker Air Force Base, Remedial Investigation Report, Soldier Creek/Off-Base Groundwater Operable Unit. 1995, Parsons Engineering Science, Inc.: Austin, TX.

55. USAF. Tinker AFB History. Available from: http://www.tinker.af.mil/.

56. Parkhurst, D., S. Christenson, and G.N. Breit, Groundwater Quality Assessment of the Central Oklahoma Aquifer, Oklahoma, Geochemical and Geohydrologic Investigation, Open File Report 92-642. 1993, United States Geological Survey.

57. USEPA, Innovations in Site Characterization: Geophysical Investigation at Hazardous Waste Sites. 2000, Office of Solid Waste and Emergency Response: Washington, D.C.

58. Bingham, R.H. and R.L. Moore, Reconnaissance of the Water Resources of the Oklahoma City Quadrangle, Central Oklahoma, in Oklahoma Geological Survey, Hydrogeologic Atlas 4. 1975, Oklahoma Geological Survey: Norman, OK.

59. Battelle, Final Report on Development of 3D Site Stratigraphy for the Northeast Quadrant. 1995, Battelle Memorial Institute: Columbus, Ohio.

60. USACE, Final Report for Building 3001 (NPL Site) Supplemental Remedial Investigations. 1990, U.S. Army Corps of Engineers, Tulsa District: Tulsa, OK.

61. Hvorslev, M.J., Time lag and soil permeability in ground-water observations. 1951, US Army Corps of Engineers, Waterways Experiment Station: Vicksburg, MS. p. 50.

62. Klingel, E.J., J.E. Shiflet, and T. Aley, Fluorescent dye tracing for defining chlorinated ethene plume remediation targets. Remediation Journal, 2010. 20(3): p. 111-119.

63. USEPA, Method 8260B Volatile Organic Compounds by Gas Chromatography/Mass Spectrometry (GC/MS), Revision 2. 1996.

64. Kuder, T., P. Philp, and J. Allen, Effects of Volatilization on Carbon and Hydrogen Isotope Ratios of MTBE. Environmental Science & Technology, 2009. 43(6): p. 1763-1768.

65. Parsons, North Tank Area Focused Remedial Investigation Report. 1994, Parsons Engineering Science, Inc.

66. Chu, K.H., et al., Stable carbon isotope fractionation during aerobic biodegradation of chlorinated ethenes. Environmental Science & Technology, 2004. 38(11): p. 3126-3130.

67. Chartrand, M.M.G., et al., Carbon isotopic fractionation during aerobic vinyl chloride degradation. Environmental Science & Technology, 2005. 39(4): p. 1064-1070.

68. van Warmerdam, E.M., et al., Stable chlorine and carbon isotope measurements of selected chlorinated organic solvents. Applied Geochemistry, 1995. 10: p. 547-552.

69. Doherty, J.E. and R.J. Hunt, Approaches to highly parameterized inversion: a guide to using PEST for groundwater-model calibration. 2010: US Department of the Interior, US Geological Survey.

70. Battelle, Draft Report for Groundwater Flow and Solute Transport Modeling. 1995, Battelle Memorial Institute: Columbus, Ohio.

71. SAIC, Final Addendum to Tinker Air Force Base, Industrial Wastewater Treatment Plant/Soldier Creek Off-Base Groundwater Operable Units Feasibility Study. 2007, Science Applications International Corporation: Midwest City, OK.

72. Parsons, Draft Annual Report for the System Shutdown and Rebound Sampling Program in Support of the Technical Impracticability Evaluation for Operable Unit 1 Groundwater at the Building 3001 NPL Site, Tinker Air Force Base, Oklahoma. 2005, Parsons Engineering Science, Inc.

73. Battelle, Final Letter Report for Soldier Creek Influent/Effluent Study. 1995, Battelle Memorial Institute: Columbus, Ohio.

74. Weidemeier, T.H., et al., Technical Protocol for Evaluating Natural Attenuation of Chlorinated Solvents in Ground Water. 1998, United States Environmental Protection Agency: Office of Research and Development.: Washington, D.C.

75. Stenback, G.A., et al., Impact of transverse and longitudinal dispersion on first-order degradation rate constant estimation. J Contam Hydrol, 2004. 73(1-4): p. 3-14.

76. Mary C. Hill, R.L.C.D.W.P., A Controlled Experiment in Ground Water Flow Model Calibration. Ground Water, 1998. 36(3): p. 520-535.

77. Gallagher, M. and J. Doherty, Parameter estimation and uncertainty analysis for a watershed model. Environmental Modelling & Software, 2007. 22(7): p. 1000-1020.

78. Doherty, J., Manual (5th Edition) and Addendum for PEST: Model-Independent Parameter Estimation. 2009, Watermark Numerical Computing: Corinda, Australia.

79. Poeter, E.P., et al., UCODE_2005 and Six Other Computer Codes for Universal Sensitivity Analysis, Calibration, and Uncertainty Evalutation. 2005, U.S. Geological Survey. p. 283.

80. Doherty, J., Ground Water Model Calibration Using Pilot Points and Regularization. Ground Water, 2003. 41(2): p. 170-177.

81. van Breukelen, B.M., D. Hunkeler, and F. Volkering, Quantification of sequential chlorinated ethene degradation by use of a reactive transport model incorporating isotope fractionation. Environmental Science & Technology, 2005. 39(11): p. 4189-4197.

82. Coplen, T.B., et al., Isotope-Abundance Variations of Selected Elements. Pure and Applied Chemistry, 2002. 74(10): p. 1987-2017.